

TOTAL SYNTHESIS OF A BICYCLO[1.1.0]BUTANE FATTY ACID AND  
BIOSYNTHETICALLY EMPOWERED INVESTIGATION OF THE BIOLOGICAL  
ACTIVITY OF APOPTOLIDIN

By

Sean Michael DeGuire

Dissertation

Submitted to the Faculty of the Graduate School of

Vanderbilt University in partial fulfillment of

the requirements for the degree of

DOCTOR OF PHILOSOPHY

In

Chemistry

May, 2013

Nashville, Tennessee

Approved:

Dr. Gary A. Sulikowski

Dr. Brian O. Bachman

Dr. Craig W. Lindsley

Dr. Ned A. Porter

## ACKNOWLEDGEMENTS

First, I would like to thank my research advisor Prof. Gary A. Sulikowski for his invaluable direction during my graduate studies. Dr. Sulikowski's extensive knowledge of both synthetic chemistry and chemical biology was critical in the development of syntheses and biological studies. Moreover, I would like to express my upmost appreciation of Dr. Sulikowski's enthusiasm and support in my desire to work at the interface of chemistry and biology. I would also like to thank my committee members Dr. Brian O. Bachmann, Dr. Ned A. Porter and Dr. Craig W. Lindsley for valuable advice and conversations about projects, science and the future.

I would also like to thank the past and present members of the Sulikowski research group for promoting an ideal environment for work and study. Specifically, I would like to thank Dr. Bruce J. Melancon who worked next to me throughout my graduate studies and helped to develop my synthetic skills and chemical intuition. I would also like to thank Dr. Darren Engers and Dr. Jesse Teske for valuable discussions and opinions on strategies and data interpretation.

I would also like to thank the various collaborators that have contributed to my projects. Dr Alan Brash and Bill Boeglin were critical for advice on purification of the final bicyclobutane product. Dr. Sunphil Choi and his advisor Dr. Zaher Nahle introduced me to techniques used in cell culture for apoptolidin biological studies. I would also like to thank Dr. Larry J. Marnett for offering his cell culture facility for me to perform biological experiments as well as providing advice on project goals. Dr. Alessandro

Ustione, Brenda Crews, Jashim Uddin and Cristina Daniel provided critical help in biological and fluorescence microscopy experiments. I would also like to thank Dr. Don Stec for help with NMR experiments.

Finally, I would like to thank my loving family for their continued support of my pursuit of knowledge. From an early age, I was inspired by my parents' knowledge and abilities in what seemed like everything to a young and curious child. Through our constant conversations of science and medicine, they encouraged me to continue to study and learn more. Growing up in the woods and fields of Kentucky and the mountains of North Carolina instilled in me a life long appreciation for the miraculous beauty and complexity of the natural world. Work around our farm including building fences, barns, and roofs or planting and caring for gardens and fields not only gave me an appreciation for a hard day of work but also taught me that the complex things in the world (a building or a human cell) arose from careful control over the simple things (a well placed nail or chemical bond). Without the influence and support of my family, I have no doubt that I would not ever have chosen to pursue a doctorate much less have been able to achieve it.

## TABLE OF CONTENTS

<b>ACKNOWLEDGEMENTS .....</b>	<b>ii</b>
<b>LIST OF TABLES .....</b>	<b>vii</b>
<b>LIST OF SCHEMES .....</b>	<b>viii</b>
<b>LIST OF FIGURES .....</b>	<b>x</b>
<b>LIST OF SPECTRA .....</b>	<b>xii</b>
<b>CHAPTER I Total Synthesis of a Novel Bicyclobutane Fatty Acid.....</b>	<b>1</b>
Background Information.....	1
A Unique Fatty Acid Metabolite from Cyanobacteria .....	1
Chemistry of Bicyclo[1.1.0]butanes.....	8
Synthetic Strategy.....	12
Synthesis of a Bicyclobutane Fatty Acid.....	15
Model Study .....	15
Preparation of a Substrate for the Stereocontrolled Cascade Reaction .....	22
Cascade Cyclization Investigation and Completion of the Synthesis .....	30
Experimental Methods .....	34
References.....	52
Spectra Relevant to Chapter 1.....	57
<b>CHAPTER II Structural Diversification of Apoptolidins Through Mutasynthesis. 82</b>	
Background Information.....	82
Isolation of Apoptolidin .....	82
Synthesis of Apoptolidins.....	85
Biosynthesis of Apoptolidin: Type 1 PKS .....	90

Genetic Manipulation of Apoptolidin Biosynthesis .....	93
Identifying the Apoptolidin Biosynthetic Gene Cluster .....	93
Genetic Knockouts .....	96
Experimental Methods .....	104
References.....	110
Spectra Relevant to Chapter 2.....	113
<b>CHAPTER III Apoptolidin Biological Activity Studies .....</b>	<b>124</b>
Background: Previous Reports on Biological Activity.....	124
A Cell Selective Cytotoxic Polyketide Natural Product.....	124
Known Mechanisms of Apoptosis Induction .....	130
Metabolic Reprogramming.....	133
F <sub>0</sub> F <sub>1</sub> ATPase: A Target of Apoptolidin? .....	137
Structure Activity Relationships of Apoptolidins .....	139
Results: Investigations in the Sulikowski Lab .....	143
Cytotoxicity of Apoptolidins.....	143
Toxicity Through Apoptosis or Necrosis .....	150
Experimental Methods .....	153
References.....	157
<b>CHAPTER IV Probing the Role of Apoptolidin Deoxy Sugars .....</b>	<b>162</b>
Fluorescent Apoptolidin Probe Syntheses .....	162
Mitochondrial Co-localization and Transport Experiment Plan .....	163
Synthesis and Biological Evaluation of Azido Apoptolidin A and H.....	164
First Generation “Click” Fluorophore: Terminal Alkyne .....	166
Second Generation “Click” Fluorophore: Cyclooctyne .....	171
Third Generation “Click” Fluorophore: Bicyclononyne .....	173
Cyanine Apoptolidin Conjugate Microscopy Studies.....	180
Cy3 Conjugate Treatment Conditions .....	180

Cy3 Confocal Microscopy: Subcellular Localization .....	182
Current Studies: Depolarization and Non-cationic Fluorophores.....	185
Mitochondrial Decoupling Strategy .....	186
Fourth Generation “Click” Fluorophores: Non-cationic Fluorophores.....	187
Conclusions and Future Studies.....	192
Experimental Methods.....	193
References.....	207
Spectra Relevant to Chapter Four .....	210
<b>CHAPTER V Conclusions and Future Directions for Apoptolidin Biological Target Studies .....</b>	<b>225</b>
Ongoing Investigations of the Biological Target of Apoptolidin .....	225
Measuring Inhibition of $F_1F_0$ ATPase .....	225
Identifying Novel Targets of Apoptolidin.....	227
Overview of Apoptolidin Project Results.....	230
Experimental Methods.....	231
References.....	235
Spectral Data Relevant to Chapter 5.....	236

## LIST OF TABLES

<b>Table I-1:</b> Strain energies of select cyclic hydrocarbons.....	8
<b>Table I-2:</b> NMR shifts comparison of model bicyclo[1.1.0]butane <b>1.15</b> with natural product <b>1.1</b> .....	21
<b>Table II-1:</b> $^{13}\text{C}$ (150 MHz) and $^1\text{H}$ (600 MHz) NMR shifts for apoptolidin H <b>2.11</b> and isoapoptolidin H <b>2.23</b> .....	103
<b>Table III-1</b> Apoptolidin structure activity relationships ( $^*$ H292 Human Lung Carcinoma, $^\dagger$ 1A9 Human Ovarian Carcinoma, $^\ddagger$ AD12-3Y1) .....	141

## LIST OF SCHEMES

<b>Scheme I-1:</b> Allene oxide biosynthesis .....	2
<b>Scheme I-2:</b> Proposed biosynthetic mechanism.....	7
<b>Scheme I-3:</b> Examples of reactivity of bicyclo[1.1.0]butanes .....	10
<b>Scheme I-4:</b> Examples of previous bicyclo[1.1.0]butane syntheses .....	11
<b>Scheme I-5:</b> Cyclization reactions .....	13
<b>Scheme I-6:</b> Cyclization/epoxidation cascade .....	14
<b>Scheme I-7:</b> Retrosynthetic analysis .....	15
<b>Scheme I-8:</b> Cyclopropanation of <i>Z</i> -2-pentenol <b>1.20</b> .....	16
<b>Scheme I-9:</b> Failed epoxide forming reactions .....	17
<b>Scheme I-10:</b> Failed epoxide opening cyclization .....	18
<b>Scheme I-11:</b> Phenyl carbamate model cuprate cyclization .....	19
<b>Scheme I-12:</b> Preparation of vinyl epoxide <b>1.36</b> .....	20
<b>Scheme I-13:</b> Model cyclization .....	21
<b>Scheme I-14:</b> Alkyne addition route .....	23
<b>Scheme I-15:</b> Alkylation of azeleic acid monomethylester <b>1.18</b> .....	24
<b>Scheme I-16:</b> Sulfur ylide couplings.....	25
<b>Scheme I-17:</b> Keto-Darzens reaction .....	25
<b>Scheme I-18:</b> Horner-Wadsworth-Emmons coupling.....	26
<b>Scheme I-19:</b> Basic epoxidations.....	27
<b>Scheme I-20:</b> Hydroxyl directed epoxidations.....	28
<b>Scheme I-21:</b> Dimethyl dioxirane epoxidation .....	28



<b>Scheme I-22:</b> Stereochemical analysis of epoxy alcohol products <b>1.47</b> .....	29
<b>Scheme I-23:</b> Mesylate formation.....	30
<b>Scheme I-24:</b> Application of model cyclization conditions.....	31
<b>Scheme I-25:</b> Reducing nucleophilicity.....	32
<b>Scheme I-26:</b> Cyclization cascade to complete the synthesis of <b>1.1</b> .....	33
<b>Scheme II-1:</b> Biosynthesis of polyketides .....	92
<b>Scheme IV-1:</b> Synthesis of azido apoptolidin A <b>4.1</b> and H <b>4.2</b> .....	165
<b>Scheme IV-2:</b> Synthesis of Rhox-alkyne <b>4.6</b> .....	167
<b>Scheme IV-3:</b> First generation fluorescent apoptolidin synthesis .....	168
<b>Scheme IV-4:</b> Synthesis of cyclooctyne amine <b>4.11</b> .....	171
<b>Scheme IV-5:</b> Cyclooctne Rhox conjugate <b>4.12</b> .....	172
<b>Scheme IV-6:</b> Unsuccessful cyclooctyne “click” reaction .....	173
<b>Scheme IV-7:</b> Synthesis of bicyclononyne amine <b>4.22</b> .....	176
<b>Scheme IV-8:</b> Preparation of Cy3 bicyclononyne conjugate <b>4.24</b> .....	177
<b>Scheme IV-9:</b> Preparation of Cy3 Apoptolidin A and H Conjugates .....	179
<b>Scheme IV-10:</b> Cy3 acid <b>4.27</b> at physiological pH.....	184
<b>Scheme IV-11:</b> Preparation of AMCA bicyclononyne conjugate <b>4.29</b> .....	188
<b>Scheme IV-12:</b> Preparation of AMCA apoptolidin A and H conjugates <b>4.30</b> and <b>4.31</b> .....	190
<b>Scheme IV-13:</b> Alexafluor 568 BCN Synthesis .....	191
<b>Scheme V-1:</b> The pyruvate kinase coupled ATPase assay .....	226
<b>Scheme V-2:</b> Preparation of biotinyl bicyclononyne conjugate\ .....	227
<b>Scheme V-3:</b> Preparation of biotinyl apoptolidin A <b>5.3</b> .....	229

## LIST OF FIGURES

<b>Figure I-1:</b> Bicyclo[1.1.0]butane product <b>1.1</b> and leukotriene like product <b>1.2</b> .....	4
<b>Figure I-2:</b> Oxylipins with interesting biological functions .....	5
<b>Figure I-3:</b> Bicyclo[1.1.0]butane fatty acid fragments .....	12
<b>Figure II-1:</b> Structure of natural apoptolidins.....	83
<b>Figure II-2:</b> Nicolaou's apoptolidin analogues .....	87
<b>Figure II-3:</b> Sulikowski's apoptolidin analogues.....	88
<b>Figure II-4:</b> Semisynthetic apoptolidin analogues.....	89
<b>Figure II-5:</b> Genetic organisation of the apoptolidin gene cluster in <i>Nocardiosis</i> sp. FU40 .....	95
<b>Figure II-6:</b> Overview of the proposed biosynthetic pathway for apoptolidin.....	96
<b>Figure II-7:</b> Mass selective (1146.5 m/z) LCMS trace of FU40 wt and FU40ΔApoS8..	98
<b>Figure II-8:</b> Mass selective (858.5 m/z) LCMS trace of FU40ΔApoGT2.....	100
<b>Figure II-9:</b> Mass selective (1002.6 and 1146.5 m/z) LCMS trace FU40ΔApoM3 .....	101
<b>Figure II-10:</b> HPLC trace of apoptolidin A/isoapoptolidin A purification .....	107
<b>Figure II-11:</b> HPLC trace for apoptolidin H/isoapoptolidin H purification .....	109
<b>Figure III-1:</b> NCI-60 cell line screening results for apoptolidin A .....	126
<b>Figure III-2:</b> Cytotoxic macrocycles .....	127
<b>Figure III-3:</b> Known mechanisms for mitochondrial apoptosis initiation.....	132
<b>Figure III-4:</b> Glucose Metabolism Pathways .....	134
<b>Figure III-5:</b> Preliminary data from apoptolidin testing.....	144
<b>Figure III-6:</b> Apoptolidin cell density assay.....	145

<b>Figure III-7:</b> Apoptolidin A and H H292 cell viability assay .....	146
<b>Figure III-8:</b> Oligomycin cell density requirement .....	147
<b>Figure III-9:</b> PK-M2 allosteric activators.....	148
<b>Figure III-10:</b> PKM2 activator co treatment results .....	149
<b>Figure III-11:</b> Annexin V-FITC (X-axis) and propidium iodide (Y-axis) FACS results from 100 nM treatment with apoptolidin A and H for two and three days .....	152
<b>Figure IV-1:</b> Azido apoptolidin A and H H292 cell viability assay .....	166
<b>Figure IV-2:</b> Initial confocal microscopy results with compound <b>4.7</b> .....	170
<b>Figure IV-3:</b> Highly reactive cyclooctynes for “click” chemistry.....	174
<b>Figure IV-4:</b> Cy3 apoptolidin A and H H292 cell viability assay .....	178
<b>Figure IV-5:</b> Treatment of H292 cells for 15 or 60 minutes with 200 nM Cy3 Apoptolidin A or H with or without washout as indicated. ....	181
<b>Figure IV-6:</b> H292 cells stained with <b>4.25</b> (top left), <b>4.26</b> (top right), <b>4.27</b> (bottom left) and <b>4.24</b> (bottom right) and with Mitotracker Green FM. Cy3 fluorescence is shown in red, Mitotracker in green.....	183
<b>Figure IV-7:</b> Protonophore mitochondrial decouplers.....	186
<b>Figure IV-8:</b> AMCA apoptolidin A and H H292 cell viability assay.....	189
<b>Figure V-1:</b> Biotinyl apoptolidin A H292 cell viability assay.....	228

## LIST OF SPECTRA

<b>Spectra I-1:</b> The 400 MHz $^1\text{H}$ and 125 MHz $^{13}\text{C}$ NMR spectra of <b>1.21</b> in $\text{CDCl}_3$ . .....	57
<b>Spectra I-2:</b> The 400 MHz $^1\text{H}$ and 125 MHz $^{13}\text{C}$ NMR spectra of <b>1.22</b> in $\text{CDCl}_3$ . .....	58
<b>Spectra I-3:</b> The 400 MHz $^1\text{H}$ and 125 MHz $^{13}\text{C}$ NMR spectra of <b>1.23</b> in $\text{CDCl}_3$ . .....	59
<b>Spectra I-4:</b> The 400 MHz $^1\text{H}$ and 125 MHz $^{13}\text{C}$ NMR spectra of <b>1.24</b> in $\text{CDCl}_3$ . .....	60
<b>Spectra I-5:</b> The 400 MHz $^1\text{H}$ and 125 MHz $^{13}\text{C}$ NMR spectra of <b>1.27</b> in $\text{CDCl}_3$ . .....	61
<b>Spectra I-6:</b> The 400 MHz $^1\text{H}$ and 125 MHz $^{13}\text{C}$ NMR spectra of <b>1.32</b> in $\text{CDCl}_3$ . .....	62
<b>Spectra I-7:</b> The 400 MHz $^1\text{H}$ and 125 MHz $^{13}\text{C}$ NMR spectra of <b>1.33</b> in $\text{CDCl}_3$ . .....	63
<b>Spectra I-8:</b> The 400 MHz $^1\text{H}$ spectra of <b>1.34</b> in $\text{CDCl}_3$ . .....	64
<b>Spectra I-9:</b> The 400 MHz $^1\text{H}$ and 100 MHz $^{13}\text{C}$ NMR spectra of <b>1.19</b> in $\text{CDCl}_3$ . .....	65
<b>Spectra I-10:</b> The 600 MHz $^1\text{H}$ and 150 MHz $^{13}\text{C}$ NMR spectra of <b>1.36</b> in $\text{C}_6\text{D}_6$ . .....	66
<b>Spectra I-11:</b> The 400 MHz $^1\text{H}$ and 100 MHz $^{13}\text{C}$ DEPT135 NMR spectra of <b>1.15</b> in $\text{C}_6\text{D}_6$ . .....	67
<b>Spectra I-12:</b> The 400 MHz $^1\text{H}$ and 100 MHz $^{13}\text{C}$ NMR spectra of <b>1.38</b> in $\text{CDCl}_3$ . .....	68
<b>Spectra I-13:</b> The 400 MHz $^1\text{H}$ and 100 MHz $^{13}\text{C}$ NMR spectra of <b>1.40</b> in $\text{CDCl}_3$ . .....	69
<b>Spectra I-14:</b> The 400 MHz $^1\text{H}$ and 100 MHz $^{13}\text{C}$ NMR spectra of <b>1.41</b> in $\text{CDCl}_3$ . .....	70
<b>Spectra I-15:</b> The 400 MHz $^1\text{H}$ and 100 MHz $^{13}\text{C}$ NMR spectra of <b>1.43</b> in $\text{CDCl}_3$ . .....	71
<b>Spectra I-16:</b> The 400 MHz $^1\text{H}$ and 100 MHz $^{13}\text{C}$ NMR spectra of <b>1.44</b> in $\text{CDCl}_3$ . .....	72
<b>Spectra I-17:</b> The 400 MHz $^1\text{H}$ and 125 MHz $^{13}\text{C}$ NMR spectra of <b>1.51</b> in $\text{CDCl}_3$ . .....	73
<b>Spectra I-18:</b> The 400 MHz $^1\text{H}$ and 125 MHz $^{13}\text{C}$ NMR spectra of <b>1.46</b> in $\text{CDCl}_3$ . .....	74
<b>Spectra I-19:</b> The 500 MHz $^1\text{H}$ and 125 MHz $^{13}\text{C}$ NMR spectra of <i>syn</i> - <b>1.47a</b> in $\text{CDCl}_3$ . .....	75

<b>Spectra I-20:</b> The 500 MHz $^1\text{H}$ and 125 MHz $^{13}\text{C}$ NMR spectra of <i>syn</i> - <b>1.47b</b> in $\text{CDCl}_3$ .	76
<b>Spectra I-21:</b> The 400 MHz $^1\text{H}$ and 150 MHz $^{13}\text{C}$ NMR spectra of <i>anti</i> - <b>1.47a</b> in $\text{CDCl}_3$ .	77
<b>Spectra I-22:</b> The 400 MHz $^1\text{H}$ and 150 MHz $^{13}\text{C}$ NMR spectra of <i>anti</i> - <b>1.47b</b> in $\text{CDCl}_3$ .	78
<b>Spectra I-23:</b> The 400 MHz $^1\text{H}$ and 125 MHz $^{13}\text{C}$ NMR spectra of <b>1.57</b> in $\text{CDCl}_3$ .	79
<b>Spectra I-24:</b> The 400 MHz $^1\text{H}$ and 125 MHz $^{13}\text{C}$ NMR spectra of <b>1.53</b> in $\text{CDCl}_3$ .	80
<b>Spectra I-25:</b> The 600 MHz $^1\text{H}$ and 150 MHz $^{13}\text{C}$ NMR spectra of <b>1.1</b> in $\text{C}_6\text{D}_6$ .	81
<b>Spectra II-1:</b> The 600 MHz $^1\text{H}$ and 150 MHz $^{13}\text{C}$ NMR spectra of <b>2.7</b> in $\text{CD}_3\text{OD}$ .	113
<b>Spectra II-2:</b> The 600 MHz $^1\text{H}$ and 150 MHz $^{13}\text{C}$ NMR spectra of <b>2.11</b> in $\text{CD}_3\text{OD}$ .	114
<b>Spectra II-3:</b> The 400 MHz COSY NMR of <b>2.11</b> in $\text{CD}_3\text{OD}$ .	115
<b>Spectra II-4:</b> The 400 MHz HSQC NMR spectrum of <b>2.11</b> in $\text{CD}_3\text{OD}$ .	116
<b>Spectra II-5:</b> The 400 MHz HMBC NMR spectrum of <b>2.11</b> in $\text{CD}_3\text{OD}$ .	117
<b>Spectra II-6:</b> The 400 MHz NOESY NMR spectrum of <b>2.11</b> in $\text{CD}_3\text{OD}$ .	118
<b>Spectra II-7:</b> The 600 MHz $^1\text{H}$ and 150 MHz $^{13}\text{C}$ NMR of <b>2.23</b> in $\text{CD}_3\text{OD}$ .	119
<b>Spectra II-8:</b> The 400 MHz COSY NMR spectrum of <b>2.23</b> in $\text{CD}_3\text{OD}$ .	120
<b>Spectra II-9:</b> The 400 MHz HSQC NMR spectrum of <b>2.23</b> in $\text{CD}_3\text{OD}$ .	121
<b>Spectra II-10:</b> The 400 MHz HMBC NMR spectrum of <b>2.23</b> in $\text{CD}_3\text{OD}$ .	122
<b>Spectra II-11:</b> The 400 MHz NOESY NMR spectrum of <b>2.23</b> in $\text{CD}_3\text{OD}$ .	123
<b>Spectra IV-1:</b> The 600 MHz $^1\text{H}$ and 150 MHz $^{13}\text{C}$ NMR spectra of <b>2.1</b> in $\text{CD}_3\text{OD}$ .	210
<b>Spectra IV-2:</b> The 500 MHz HSQC NMR spectrum of <b>4.1</b> in $\text{CD}_3\text{OD}$ .	211
<b>Spectra IV-3:</b> The 500 MHz CIGAR HMBC NMR spectrum of <b>4.1</b> in $\text{CD}_3\text{OD}$ .	212

<b>Spectra IV-4:</b> The 600 MHz $^1\text{H}$ and 150 MHz $^{13}\text{C}$ NMR spectra of <b>4.2</b> in $\text{CDCl}_3$ , .....	213
<b>Spectra IV-5:</b> The 600 MHz COSY NMR spectrum of <b>4.2</b> in $\text{CDCl}_3$ , .....	214
<b>Spectra IV-6:</b> The 600 MHz HSQC NMR spectrum of <b>4.2</b> in $\text{CDCl}_3$ , .....	215
<b>Spectra IV-7:</b> The 600 MHz HMBC NMR spectrum of <b>4.2</b> in $\text{CDCl}_3$ , .....	216
<b>Spectra IV-8:</b> The 600 MHz CIGAR HMBC NMR spectrum of <b>4.2</b> in $\text{CDCl}_3$ , .....	217
<b>Spectra IV-9:</b> The 600 MHz $^1\text{H}$ and 150 MHz $^{13}\text{C}$ NMR spectra of <b>4.24</b> in $\text{CD}_3\text{OD}$ , ..	218
<b>Spectra IV-10:</b> The 600 MHz COSY NMR spectrum of <b>4.24</b> in $\text{CD}_3\text{OD}$ , .....	219
<b>Spectra IV-11:</b> The 600 MHz $^1\text{H}$ NMR spectrum of <b>4.25</b> in $\text{CD}_3\text{OD}$ , .....	220
<b>Spectra IV-12:</b> The 600 MHz $^1\text{H}$ and 150 MHz $^{13}\text{C}$ NMR spectra of <b>4.26</b> in $\text{CD}_3\text{OD}$ , ..	221
<b>Spectra IV-13:</b> The 600 MHz $^1\text{H}$ and 150 MHz $^{13}\text{C}$ NMR spectra of <b>4.29</b> in $\text{CDCl}_3$ , ..	222
<b>Spectra IV-14:</b> The 600 MHz $^1\text{H}$ NMR spectrum of <b>4.30</b> in $\text{CD}_3\text{OD}$ , .....	223
<b>Spectra IV-15:</b> The 600 MHz $^1\text{H}$ NMR spectrum of <b>4.31</b> in $\text{CD}_3\text{OD}$ , .....	224
<b>Spectra V-1:</b> The 400 MHz $^1\text{H}$ and 100 MHz $^{13}\text{C}$ NMR spectra of <b>5.2</b> in $\text{CDCl}_3$ , .....	236
<b>Spectra V-2:</b> The 600 MHz $^1\text{H}$ NMR spectrum of <b>5.3</b> in $\text{CD}_3\text{OD}$ , .....	237

## CHAPTER I

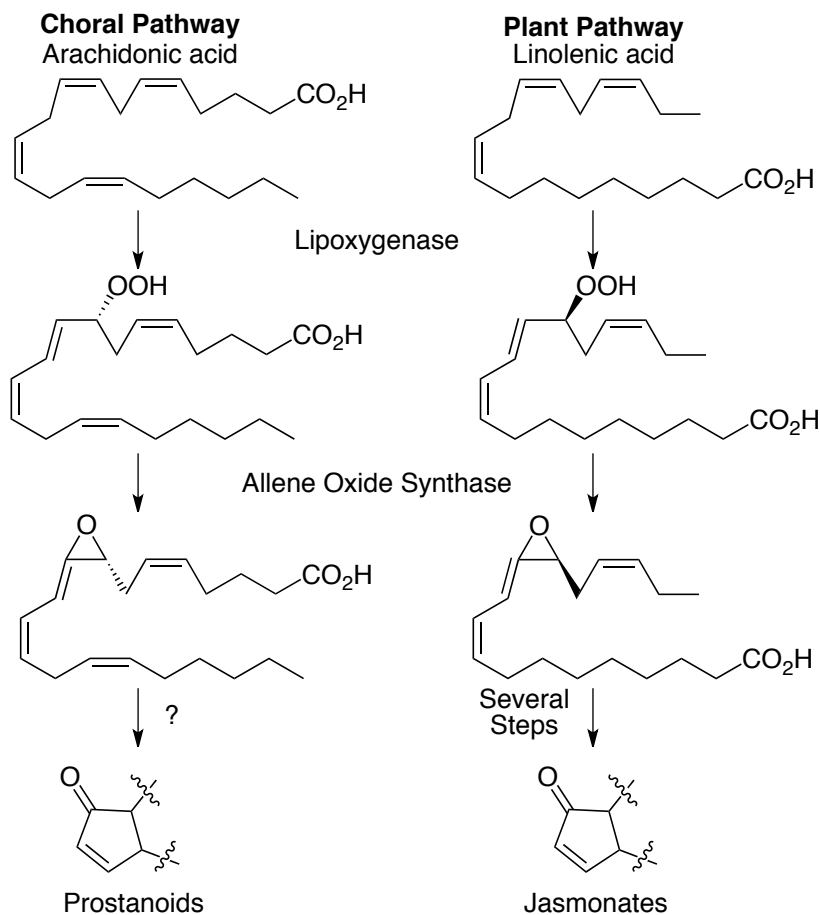
### Total Synthesis of a Novel Bicyclobutane Fatty Acid

#### **Background Information**

##### *A Unique Fatty Acid Metabolite from Cyanobacteria*

Fatty acid metabolites are known to have important functions in controlling biological processes of many organisms. Since their initial discovery, the biosynthesis of prostaglandins has been the focus of significant research due to their role as secondary signaling molecules governing pain and inflammation in mammals.<sup>1</sup> When it was discovered that these fatty acid metabolites were also produced in the Caribbean sea whip coral *Plexaura homomalla*, further study was initiated to determine the biosynthetic pathway leading to such molecules in lower organisms. In mammals, prostaglandin biosynthesis is initiated by the reaction of arachadonic acid with cyclooxygenases. It was hypothesized that in *Plexaura homomalla* these natural products were produced, not by homologous cyclooxygenase enzymes, but by a pathway similar to that used by plants for the conversion of linolenic acid to the jasmonic acid involving lipoxygenase and allene oxide synthase enzymes (**Scheme I-1**).<sup>2</sup> While searching the genome of *Plexaura homomalla* for lipoxygenases involved in this proposed pathway, Brash and co-workers identified a gene encoding a novel peroxidase-lipoxygenase fusion protein.<sup>3</sup> The peroxidase domain of this fusion protein functions similarly to an allene oxide synthase (AOS), converting hydroperoxy-fatty acids to an allene oxide. In the plant pathway, the

hemo-proteins that catalyze this reaction are members of the cytochrome P450 superfamily. The AOS domain of the coral fusion protein contains no sequence homology to cytochrome P450 proteins and, instead, contains a modified catalase active site. Unlike typical catalase domains, the coral protein's active site is able to accept hydroperoxy-fatty acids instead of only hydrogen peroxide. While it has now been determined that coral species contain COX isoforms that are used for the biosynthesis of prostaglandins,<sup>4</sup> the search for a lipoxygenase pathway resulted in the identification of this novel class of fusion protein involved in fatty acid metabolism.

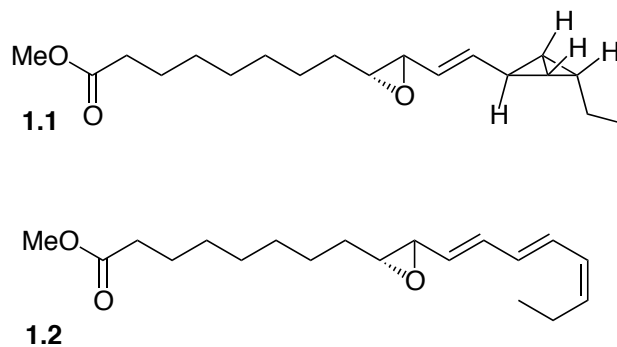


**Scheme I-1:** Allene oxide biosynthesis



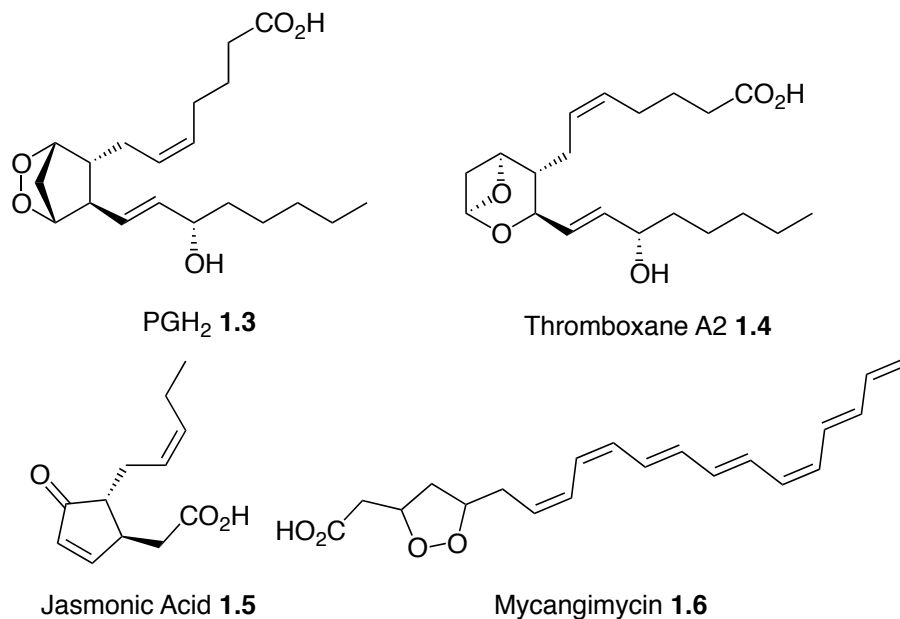
Intrigued by this new class of catalase enzyme, Brash and coworkers next performed BLAST searches on other known genomes to identify similar genes in other species. High sequence homology was found in a gene of the cyanobacterium *Anabaena* sp. strain PCC 7120. Characterization and expression of this gene's product revealed a fusion protein containing a catalase-related domain and a lipoxygenase domain, similar to that of the coral protein. Studies on the lipoxygenase revealed that it was an active lipoxygenase that converted C18 polyunsaturated fatty acids into the corresponding 9R-hydroperoxides. The catalase-related domain was found to convert the 9R-hydroperoxylinolenic acid product of the lipoxygenase domain into a variety of products including triols, diols, and epoxides. It was hypothesized that many of these products arrived from the decomposition of a single unstable product.<sup>5</sup>

To determine the structure of this hypothetical unstable intermediate, the gene encoding the fusion-protein was cloned, expressed in *E. coli* and purified using a histidine tag. The purified protein was treated with the product of the lipoxygenase domain, 9R-hydroperoxylinolenic acid. The products of this reaction were then immediately extracted with cold hexanes and converted to the methyl ester by immediate treatment with diazomethane. Two products were isolated from this process and spectral characterization revealed both to incorporate a vinyl epoxide functional group. Further analysis determined the minor product to be a triene epoxide **1.2**, while the major product was found to incorporate a unique strained bicyclo[1.1.0]butane ring **1.1** (**Figure I-1**).<sup>5</sup>



**Figure I-1:** Bicyclo[1.1.0]butane product **1.1** and leukotriene like product **1.2**

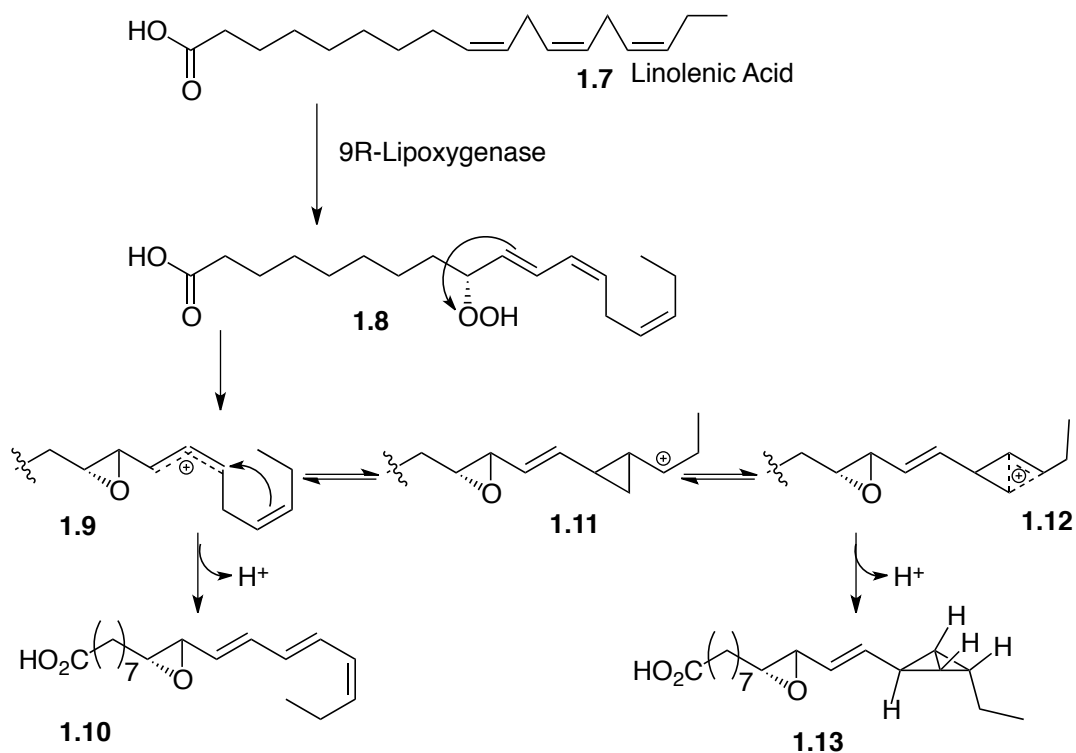
The structure of the bicyclobutane containing product was solved using data from several NMR spectroscopy experiments. The  $^1\text{H}$  NMR and COSY spectra show that the major product contains only one double bond. HRMS data show that the compound has an identical mass to the known triene epoxide product **1.2**, and therefore must contain two carbon rings to account for the unsaturation. After determining the general connectivity of the molecule through HSQC and HMBC experiments, DEPT experiments were key in determining the location of the rings and establishing them as a bicyclo[1.1.0]butane. Four consecutive carbons (C-13–C-16) were determined to each be bound to a single proton and three carbons based on the chemical shifts and DEPT experiments. Strong coupling was observed in the COSY experiments between H-14, H-15 and H-16 but H-13 was found to only couple to H-12, suggesting a dihedral angle near  $90^\circ$  between the pair. H-13 is therefore on the endo face. Finally, NOESY through space correlations confirmed the structure of the product to be methyl 9-R-10-R-*trans*-epoxyoctadeca-11-*trans*-(13,14,15,16-bicyclo[1.1.0]butyl)-enoate **1.1**.<sup>5</sup>



**Figure I-2:** Oxylipins with interesting biological functions

Because fatty acids play many important roles in all living cells, both their biological functions and biosynthesis have been the focus of much study. Apart from being the major component of cellular and organelle membranes and storage lipids, many fatty acids and their derivatives act as important signaling molecules (**Figure I-2**). One of the primary reactions that takes place in fatty acid metabolism is the oxidation of polyunsaturated fatty acids (PUFAs) to a general class of secondary metabolites called oxylipins.<sup>6</sup> While many of the known oxidations are initiated by lipoxygenase enzymes (LOX), a few noteworthy examples exist of PUFA oxidation by cyclooxygenases (COX), also known as prostaglandin H synthases (PGHS). COX enzymes catalyze the conversion of arachidonic acid to prostaglandin H<sub>2</sub> (PGH<sub>2</sub>, **1.3**). In mammals, depending on the tissue in which PGH<sub>2</sub> is generated, PGH<sub>2</sub> is further metabolized to diverse secondary signaling molecules. In platelets, PGH<sub>2</sub> is converted to thromboxane A<sub>2</sub> **1.4**, which acts

as a vasoconstrictor and promotes platelet aggregation. In other tissues, PGH<sub>2</sub> is converted to one of several prostaglandins that mediate many systemic responses including pain, inflammation and fever generation.<sup>1</sup> In plants, LOXs initiate the first step in the synthesis of jasmonic acid **1.5**, an oxylipin that serves as a phytohormone by regulating plant development and acting as a transcription factor generated locally in response to physical damage.<sup>7</sup> In fungi, LOX have been reported to generate oxylipins that play roles in growth and development,<sup>8</sup> quorum sensing,<sup>9</sup> pathogenesis,<sup>10</sup> and regulation of sexual and asexual spore development.<sup>11</sup> In algae, oxylipins have been implicated in signaling responses to pathogenic or mechanical attack.<sup>12</sup> Compared to eukaryotes, relatively little is known about oxylipin biosynthesis and function in prokaryotes.<sup>13</sup> Indeed, the first prokaryotic LOX enzymes were not identified until 2001.<sup>14</sup> Characterization of these enzymes has revealed products common to other life forms as well as novel products such as the bicyclobutane fatty acid **1.13**, but little is known about the biological function of these molecules in bacteria. One exception is mycangimycin **1.6**, an oxylipin isolated from an actinomycete that lives in symbiosis with the fungus *Entomocorticium* sp. A.<sup>15</sup> This fungus is part of a second symbiotic relationship with the southern pine beetle, *Dendroctonus frontalis*, which carries the fungus as a nutrient source for its larvae. Mycangimycin's selective antifungal activity against the competing fungus, *O. minus*, protects the host beetle from this competing pathogenic fungus. With such diverse biological roles ascribed to oxylipin natural products, it is intriguing to wonder what function the unique bicyclobutane fatty acid **1.13** could have either directly or as an intermediate in further oxylipin biosynthesis.



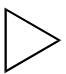

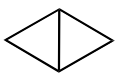
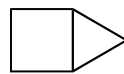
**Scheme I-2:** Proposed biosynthetic mechanism

While the biosynthetic pathways for the production of many oxylipins are well characterized, the bicyclo[1.1.0]butane **1.13** isolated from cyanobacterium represents a novel structure for any natural molecule. Brash *et al* proposed a mechanism for its formation involving a series of carbocation rearrangements that represents an unusual productive pathway in the chemistry of carbocations (**Scheme I-2**).<sup>5</sup> By the proposed route, the 9R-LOX domain of the fusion protein converts linolenic acid **1.7** into 9R-hydroperoxylinolenic acid **1.8** through a standard mechanism. The modified catalase domain then catalyzes the conversion of **1.8** into an epoxy allyl cation **1.9**. Deprotonation at this step leads to the minor triene epoxide product **1.10**. Alternatively, as it is also homoallylic, **1.9** can rearrange to form the cyclopropyl carbinyl cation **1.11**. Sigma

hyperconjugation of the C-14–C-15 bond of the cyclopropane results in the formation of the nonclassical bicyclobutonium cation **1.12**. Deprotonation at C14 leads to the bicyclobutane product **1.13**. Typically, rearrangements of homoallylic carbocations result in the formation of cyclopropyl, cyclobutyl and homoallyl products. This mechanism, if correct, represents a novel pathway from such carbocations to bicyclobutane products. It is suspected that a high degree of control in the enzyme active site results in the stabilization of the proposed bicyclobutonium ion to promote deprotonation by a basic site on the protein. Evidence for such a constrained active site is supported by the fact that no cyclopropane products arriving from the deprotonation of **1.11** are observed.<sup>5</sup>

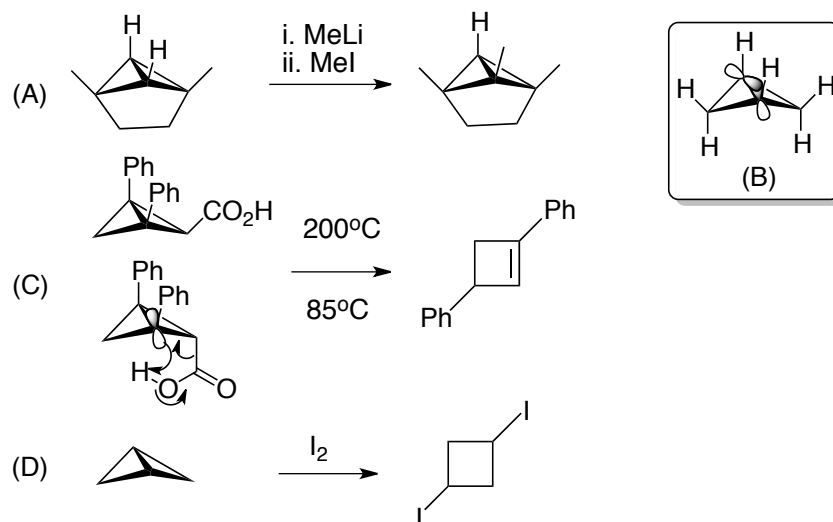
While we were intrigued to learn why evolution would have selected for an enzyme to produce this unusual, highly strained structure, the small quantities of **1.13** available from *in vitro* enzymatic production prevented such investigations. The important roles of many oxidized fatty acid natural products in biology, the unique structure and the synthetic challenges that the molecule presented attracted our lab to design a synthesis of this bicyclobutane oxylipin natural product.

#### *Chemistry of Bicyclo[1.1.0]butanes*

Structure				
Strain Energy (kcal/mol)	27	26	64	51

**Table I-1:** Strain energies of select cyclic hydrocarbons<sup>16</sup>

The challenge in designing a synthesis of this unique fatty acid metabolite lies primarily in the formation of the highly strained bicyclo[1.1.0]butane ring. As the smallest possible bicyclic ring system, bicyclo[1.1.0]butanes are expected to have a large amount of ring strain. The strain energies of a few small cyclic hydrocarbons are shown in **Table I-1**. A comparison to the next largest bicyclic ring system, bicyclo[2.1.0]pentane reveals that the ring strain of the bicyclo[1.1.0]butane is even larger than would be predicted. The ring strain of bicyclo[2.1.0]pentane is essentially the sum of its constituent rings, while that of bicyclo[1.1.0]butane is significantly more than double that of cyclopropane. This instability is attributed to a very high amount of torsional strain necessary to form the highly compact structure. IR and Raman spectral data have led to the assignment of the structure of bicyclobutane as essentially two equilateral triangles fused with a  $126^\circ$  interplanar angle and the C-C-H bond angle centered at the bridgehead carbon is estimated to be  $163^\circ$ .<sup>17</sup> While the side bond angles are similar to those of cyclopropane, the bridging bond is greatly distorted from the ideal  $109.5^\circ$  bond angle of an  $sp^3$  carbon. The thermal instability of these molecules resulting from this great torsional strain has been observed in reactions and even exploited in ring expansion methodologies.<sup>18</sup>

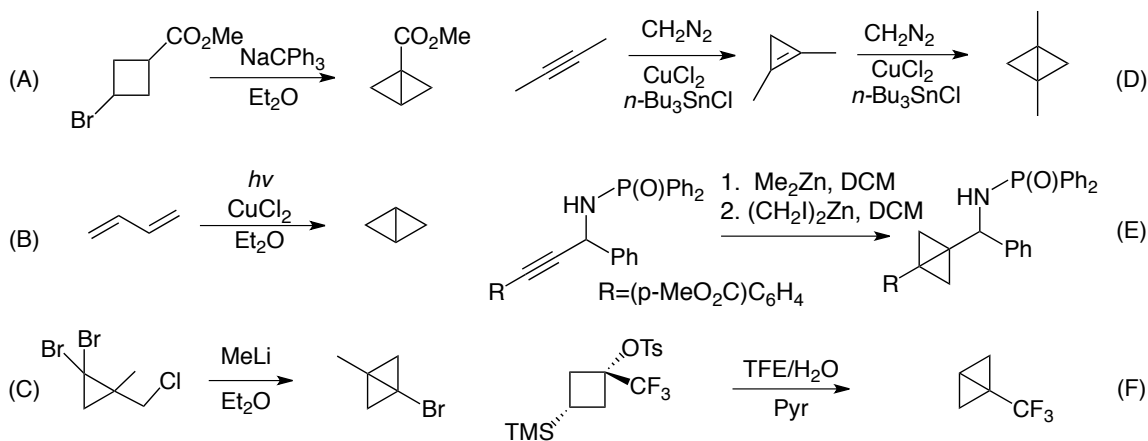


**Scheme I-3:** Examples of reactivity of bicyclo[1.1.0]butanes

Molecular orbital calculations have led to an interesting bond model for the central carbon-carbon bond of the bicyclo[1.1.0]butane ring that helps to explain its reactivity. Bicyclo[1.1.0]butane is known to be reactive towards a variety of reagents including acids, bases, carbenes, and halogens.<sup>16</sup> Calculations based on  $^{13}\text{C}$ - $^1\text{H}$  coupling constants estimate that the C-H bond of the bridgehead carbon is hybridized between  $\text{sp}^2$  and  $\text{sp}$ , giving it a near acetylenic ( $\text{sp}$  hybrid) character.<sup>19</sup> This estimation is supported by ready deprotonation of the bridgehead carbon upon treatment with methyllithium (**Scheme I-3, A**).<sup>20</sup> Many degradation pathways of bicyclobutanes involve breaking the central C-C bond. Molecular orbital calculations suggest that this bond is likely formed as a bent  $\sigma$  bond of unhybridized p-orbitals, giving it electron density above the molecule as well as to the sides (**Scheme I-3, B**).<sup>21</sup> This model is supported by the relative ease of decarboxylation of exo over endo 2,4-diphenylbicyclo[1.1.0]butane carboxylate (**Scheme I-3, C**).<sup>22</sup> The exo face of the bond is sterically inaccessible, while the endo face is



readily protonated at the external lobe of the central bond. The p-character of this bond also helps to explain the UV-absorbance of 1,3-diphenylbicyclo[1.1.0]butane at 270 nm indicative of a conjugated biphenyl system.<sup>23</sup> Electrophilic halogens are able to add across the central bond giving *cis* products, suggesting a four centered transition state (**Scheme I-3, D**).<sup>16</sup> As these examples illustrate, attempting synthetic transformations on a substrate containing a bicyclo[1.1.0]butane moiety poses a significant challenge due to the unique bonding and reactivity of the molecule.

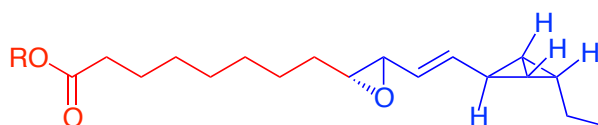


**Scheme I-4:** Examples of previous bicyclo[1.1.0]butane syntheses

While no other natural products have been reported to date that contain a bicyclo[1.1.0]butane previously, several syntheses of bicyclo[1.1.0]butanes have been reported. The first confirmed synthesis of a bicyclo[1.1.0]butane was described by Wiberg and Ciula in 1959. Wiberg employed a transannular alkylation reaction of methyl 3-bromocyclobutanecarboxylate to form the key central C-C bond (**Scheme I-4, A**).<sup>24</sup> Since this publication, a few other methods have been developed for access to the

bicyclo[1.1.0]butane structure with various functional group substitutions. One interesting method is the photochemical mediated cyclization of butadiene to provide the parent bicyclo[1.1.0]butane hydrocarbon (**Scheme I-4, B**).<sup>25</sup> The most frequently employed method to access the fused ring system is the intramolecular displacement of a leaving group by a cyclopropyl anion derived from a lithium-halogen exchange reaction (**Scheme I-4, C**).<sup>26</sup> Other methods utilize various methods of cyclopropanation. One such example is a double carbene addition to an alkyne using an excess of the carbene reagent (**Scheme I-4, D**).<sup>27</sup> Wipf has employed this method in the formation of bridgehead substituted bicyclobutanes using the Simmons-Smith reagent (**Scheme I-4, E**).<sup>28</sup> Recently, Tilley and co-workers generated a bicyclobutane by the hydrolysis of a cyclobutyl sulfonate, employing  $\beta$ -silyl stabilization of the intermediate carbocation (**Scheme I-4, F**).<sup>29</sup>

### *Synthetic Strategy*

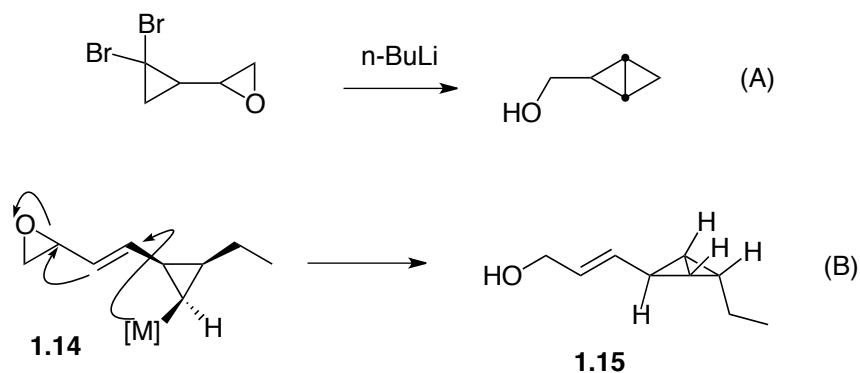


R= H or Me

**Figure I-3:** Bicyclo[1.1.0]butane fatty acid fragments

In contemplating a synthesis of bicyclo[1.1.0]butane fatty acid **1.13**, we identified two distinct fragments of the molecule of differing complexity (**Figure I-3**). The first fragment contains the eight carbon alkyl chain and terminal carboxylic acid incorporating

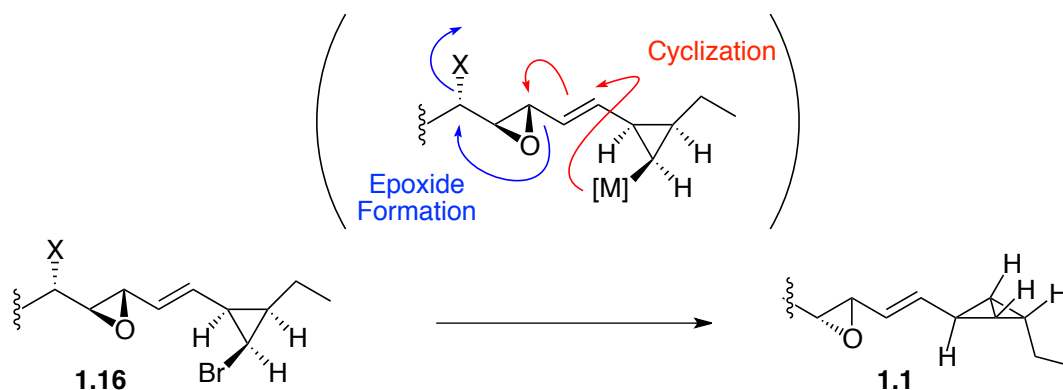
no stereogenic centers or other functionality. The carboxylic acid moiety must emerge as the methyl ester for spectral comparison with the literature as well as the known instability of the parent acid. The second fragment contains the reactive bicyclo[1.1.0]butane, two stereogenic centers and a vinyl epoxide. While the isolated bicyclo[1.1.0]butane moiety is achiral due to its symmetry, attention must be paid to the exo and endo orientation of the alkenyl and ethyl groups, respectively. To address this stereocontrolled assembly of the core bicyclobutane we elected to conduct a simple model study to identify an appropriate reaction substrate and conditions.



**Scheme I-5:** Cyclization reactions

We chose to pursue a cyclization reaction similar to that developed by Bentley, that utilized an intermolecular epoxide opening by an in situ formed cyclopropyl anion (**Scheme I-5, A**).<sup>30</sup> After investigating several substrates, we arrived at the extension of such a reaction to an  $S_N2'$  epoxide opening that, if performed on an all cis substituted cyclopropane **1.14**, would provide us with the requisite relative stereochemistry of the bicyclo[1.1.0]butane ring **1.15** (**Scheme I-5, B**). Furthermore, we proposed that the

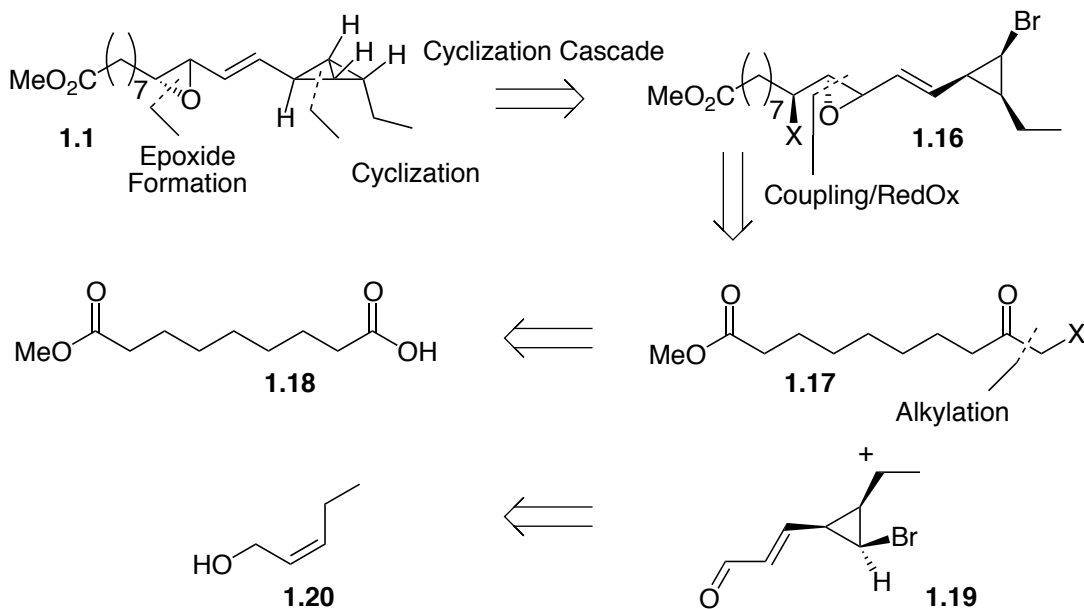
alcohol group of **1.15** could be used to elaborate this intermediate to the target molecule, should the bicyclobutane prove stable to reaction conditions.



**Scheme I-6:** Cyclization/epoxidation cascade

Ultimately, the key to our synthesis was the placement of the bicyclobutane forming cyclization as the final step. We hypothesized that if we were to carry out the  $S_N2'$  epoxide opening cyclization on an substrate such as **1.16** that, under the basic reaction conditions, the resulting alkoxide could displace a leaving group strategically placed adjacent to the epoxide to form not only the bicyclo[1.1.0]butane ring but also the vinyl epoxide in a single step (**Scheme I-6**). To arrive selectively at the desired *trans* epoxide product of the proposed cascade reaction, we needed only to ensure that the leaving group in substrate **1.16** was installed *anti* to the epoxide. Substrate **1.16** could be formed through one of several strategies coupling aldehyde **1.19** with a derivative of azelaic acid monomethyl ester **1.18** including a Keto-Darzens reaction, sulfur ylide

epoxidations and olefination reactions. Aldehyde **1.19** could be prepared from *Z*-2-pentenol **1.20** (Scheme I-7).

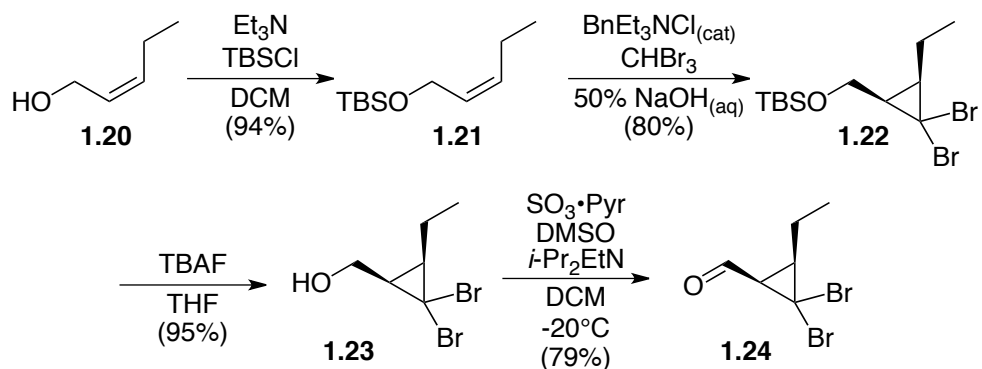


**Scheme I-7:** Retrosynthetic analysis

### Synthesis of a Bicyclobutane Fatty Acid

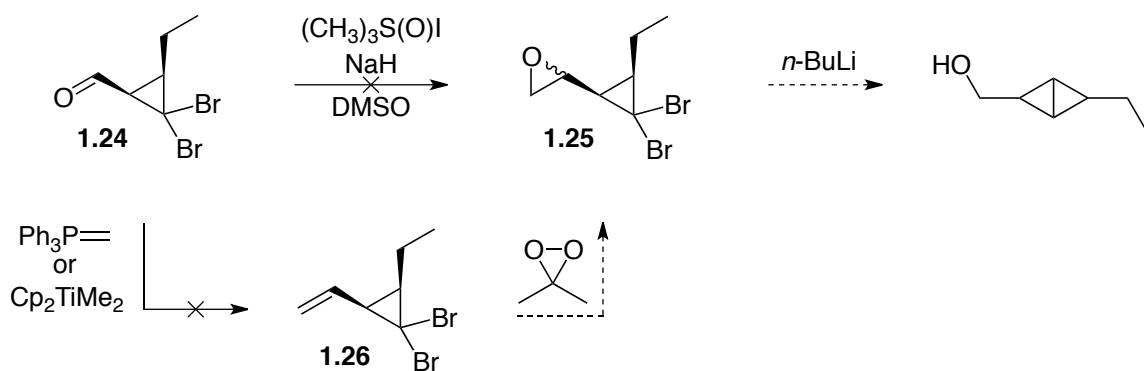
#### *Model Study*

Our model study investigation began with assembly of *cis*-dibromocyclopropane **1.24** starting from *cis*-2-pentenol **1.20** (Scheme I-8). To this end, protection of the primary alcohol of *cis*-2-pentenol **1.20** as a TBS ether **1.21** followed by dibromocarbene addition under phase transfer conditions provided the cyclopropane **1.22** in good yield (Scheme I-8). Deprotection of the silyl ether followed by oxidation of the resulting primary alcohol under Parikh-Doering conditions<sup>31</sup> gave cyclopropyl aldehyde **1.24**.



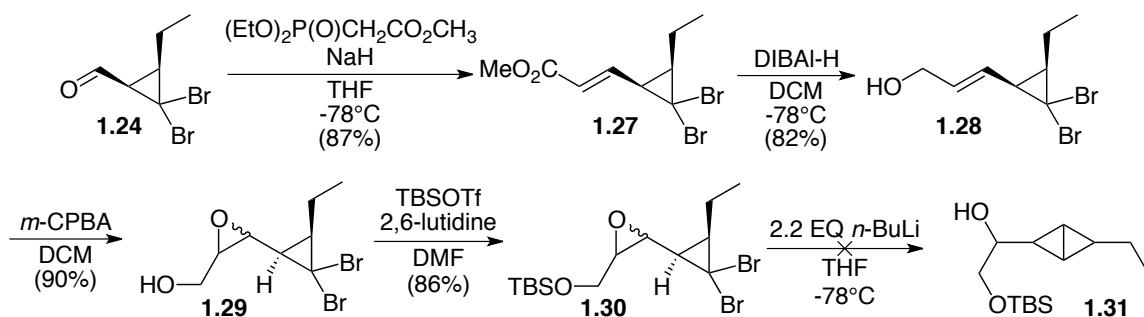
**Scheme I-8:** Cyclopropanation of *Z*-2-pentenol **1.20**

Having been inspired by the work of Bentley (**Scheme I-5**, A), we first investigated the possibility of bicyclo[1.1.0]butane formation from the intermolecular opening of a terminal epoxide (**Scheme I-9**). However, direct conversion of aldehyde **1.24** to the epoxide **1.25** by treatment with dimethylsulfoxonium ylide<sup>32</sup> was unsuccessful. Surprisingly, both Wittig olefination and treatment with dimethyl titanocene also failed to provide olefin **1.26** for epoxidation to the desired substrate **1.25**.



**Scheme I-9:** Failed epoxide forming reactions

Thinking that perhaps terminal epoxide **1.25** and vinyl cyclopropane **1.26** were too unstable for isolation via chromatographic purification, we next turned our attention to the preparation of a more substituted epoxide. Gratifyingly, olefination of aldehyde **1.24** using a Horner-Wadsworth-Emmons olefination proceeded in high yield to afford  $\alpha,\beta$ -unsaturated ester **1.27** (Scheme I-10). Reduction of **1.27** followed by peracid epoxidation of the resultant allylic alcohol **1.28** yielded the epoxy alcohol **1.29** as a mixture of diastereomers. Protection of the alcohol as the silyl ether **1.30** allowed for facile chromatographic separation of the two diastereomers. Unfortunately, treatment of either isomer with excess *n*-BuLi resulted only in lithium/halogen exchange and the desired cyclization to bicyclo[1.1.0]butane **1.31** was not observed.

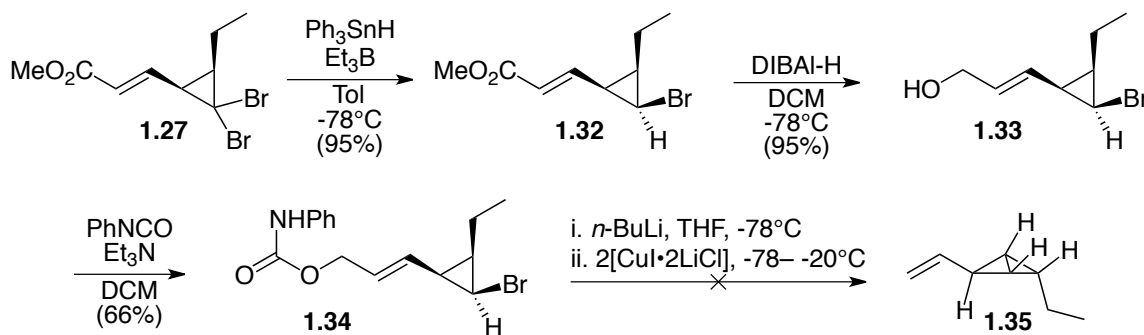


**Scheme I-10:** Failed epoxide opening cyclization

Our failure to affect intramolecular epoxide opening led us to investigate other electrophilic substituents. To test our idea of an intermolecular  $S_N2'$  cyclization that would install the vinyl group, we sought to prepare a substrate for a cuprate cyclization utilizing a phenyl carbamate leaving group. To ensure that only the cis cyclopropyl cuprate was being generated, we developed reaction conditions to selectively reduce the sterically less hindered trans bromo group. While standard  $Bu_3SnH$ -AIBN (benzene at reflux) was effective in non-stereoselective monobromination, Oshima's low temperature variation ( $Ph_3SnH$  and  $Et_3B$  in the presence of molecular oxygen) was found to provide the desired stereoselectivity.<sup>33</sup> We hypothesize that, while the cyclopropyl radical intermediate formed is planar, strong steric repulsion between the cyclopropyl substituents of **1.27** and the very bulky triphenyl stanane hydrogen source lead to the observed high selectivity, resulting in a 95% isolated yield of the desired all cis cyclopropylbromide **1.32** (Scheme I-11). Subsequent reduction followed by treatment of the resultant alcohol **1.33** with phenylisocyanate resulted in the formation of the phenyl carbamate **1.34**. Lithium halogen exchange followed by *in situ* formation of the organocuprate resulted in consumption of the starting material. In one experiment, LCMS



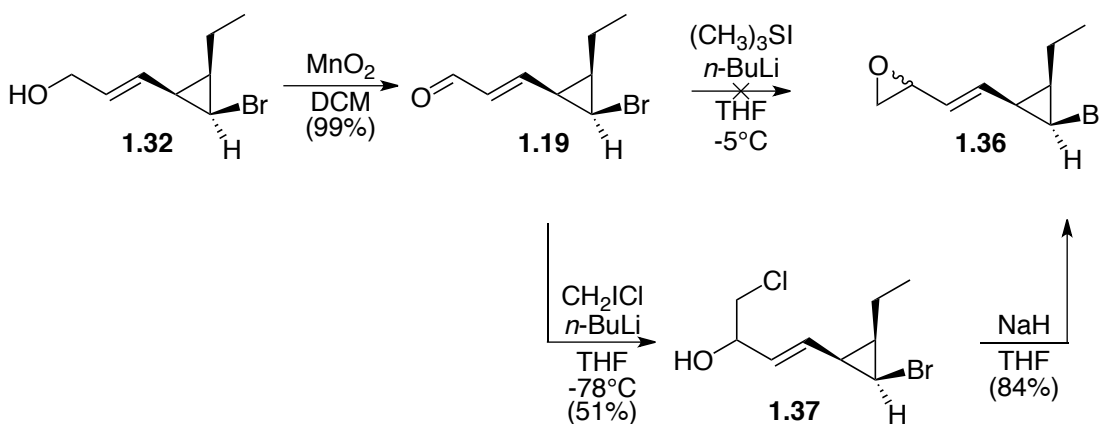
analysis of the reaction mixture showed an ion corresponding to the desired product **1.35**. However, NMR analysis of the crude reaction mixture as well as multiple attempts at chromatographic purification never revealed further evidence of bicyclo[1.1.0]butane formation. The low molecular weight and compact structure of the predicted product **1.35** made us suspect that the compound could be highly volatile and consequently evaporate during the reaction work-up. Attempts at direct distillation of the reaction mixture were also unsuccessful in delivering the desired product.



**Scheme I-11:** Phenyl carbamate model cuprate cyclization

In order to avoid product volatility, we combined our previous strategies by generating a cuprate for for an  $S_N2'$  epoxide opening. To that end, allylic alcohol **1.32** was oxidized in high yield to aldehyde **1.19** using  $MnO_2$  (**Scheme I-12**). Isolation of the desired terminal epoxide **1.36** was unsuccessful under a variety of conditions using sulfur ylide additions to the aldehyde. The instability of terminal vinyl epoxides to  $SiO_2$  chromatography had been previously observed by Matteson, who developed a two-step procedure for converting aldehydes to epoxides.<sup>34</sup> With this method, lithium/iodine

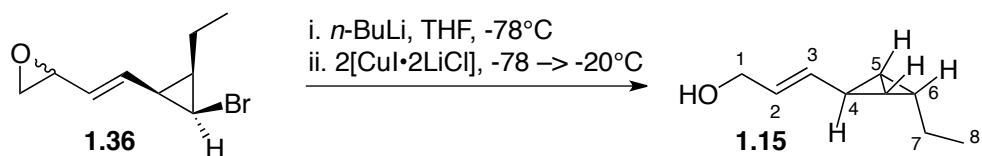
exchange of chloriodomethane generated chloromethylithiate in situ. The resultant addition provided chlorohydrin **1.37** in modest yield, which was easily purified on SiO<sub>2</sub>. Treatment of **1.37** with sodium hydride followed by aqueous work-up revealed the epoxide **1.36** in good yield as an inconsequential mixture of diastereomers without further purification.



**Scheme I-12:** Preparation of vinyl epoxide **1.36**

Gratifyingly, treatment of this mixture of epoxides **1.36** with *n*-BuLi followed by transmetallation to the organocuprate produced the desired bicyclo[1.1.0]butane alcohol **1.15** (**Scheme I-13**). <sup>1</sup>H, <sup>13</sup>C, and <sup>13</sup>C DEPT NMR analysis of the reaction mixture after aqueous workup showed a surprisingly clean spectrum of the desired bicyclo[1.1.0]butane. Indicative NMR shifts in the natural product and the model bicyclo[1.1.0]butane are shown in **Table I-2**. Attempts to purify the product using flash chromatography or chilled normal or reversed phase HPLC resulted in rapid decomposition of the bicyclo[1.1.0]butane; no desired product was isolated from these

experiments. This observed instability led us to pursue the cascade cyclization that places the bicyclo[1.1.0]butane forming cyclization as the final step of the synthesis.



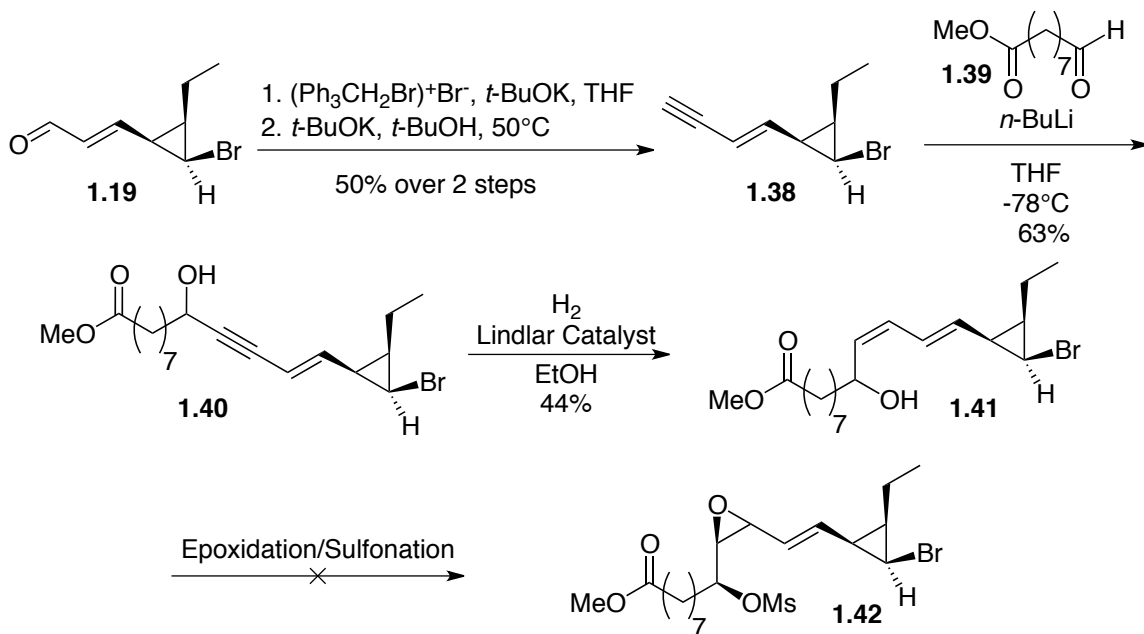
**Scheme I-13:** Model cyclization

C#	$\delta$ <sup>1</sup> H(model)	$\delta$ <sup>13</sup> C(model)	$\delta$ <sup>1</sup> H(lit)	$\delta$ <sup>13</sup> C(lit)
2	5.67 (ddd, <i>J</i> = 15.2, 5.6, 5.2 Hz)	129.3	5.34(dd, <i>J</i> = 15.4, 8.1 Hz)	128
3	5.27 (dd, <i>J</i> = 15.6, 9.2 Hz)	129.4	5.39(dd, <i>J</i> = 15.5, 8.2 Hz)	133
4	2.44 (d, 8.8 Hz)	44.8	2.36 (d, 8.2 Hz)	44.73
5	1.40 (m)	9.18	1.31/1.34 (m)	9.32/9.23
6	1.91 (m)	45.9	1.91 (m)	45.8

**Table I-2:** NMR shifts comparison of model bicyclo[1.1.0]butane **1.15** with natural product **1.1**

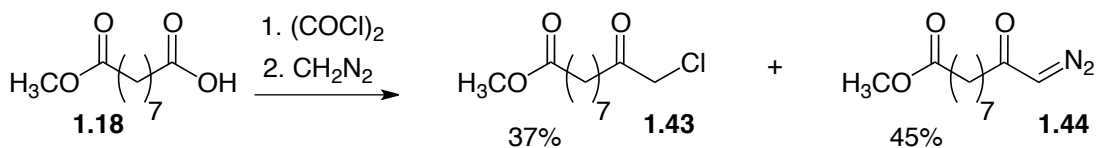
### *Preparation of a Substrate for the Stereocontrolled Cascade Reaction*

Having identified reaction conditions whereby a bicyclo[1.1.0]butane product with the desired substitution could be formed, we turned our attention to the investigation of an optimal route to incorporate the remaining alkyl chain in a substrate for the proposed bis-cyclization reaction. Initially, aldehyde **1.19** was converted to alkyne **1.38** in two steps and modest yield (**Scheme I-14**). Deprotonation of **1.38** at low temperature generated an intermediate alkynyllithium, which was added to aldehyde **1.39** (accessed in 3 steps from *cis*-cyclooctyne)<sup>35</sup> to form advanced intermediate **1.40**. Extensive investigation into conditions for the semihydrogenation to dieneol **1.41** resulted in a 44% yield of **1.41** with poor reproducibility. Subsequent attempts at sulfonation of **1.41** were unsuccessful using a variety of reagents (TsCl, Ts<sub>2</sub>O, MsCl and Ms<sub>2</sub>O) and reaction conditions. Furthermore, treatment of **1.41** under either metal-catalyzed or peracid epoxidation conditions failed to provide the desired epoxide products leading instead to either a mixture of products or decomposition. The low yield of this route hindered our ability to find acceptable conditions to afford the desired *anti*-epoxy sulfonates, therefore a more efficient route was pursued.



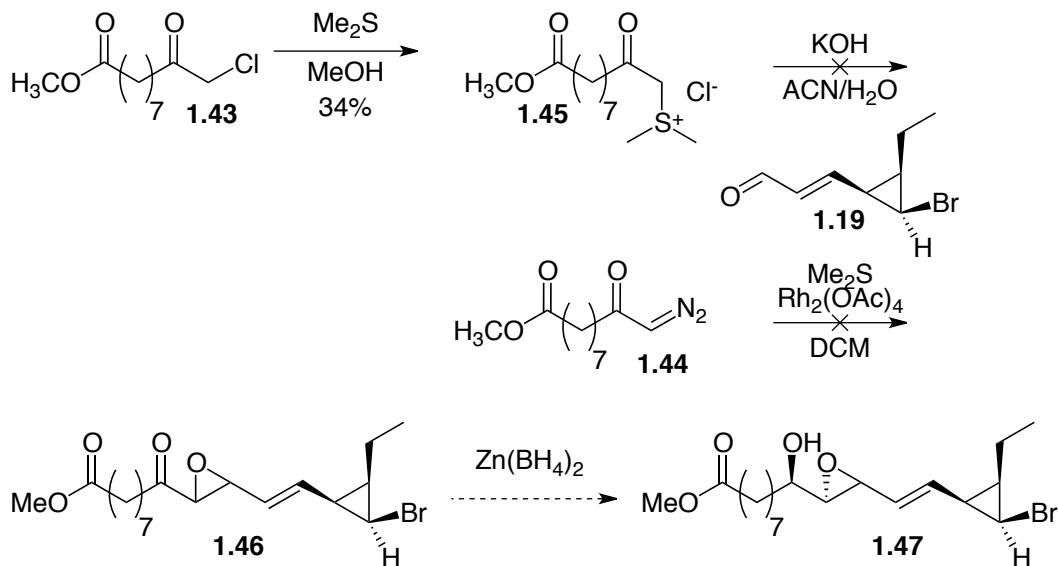
**Scheme I-14:** Alkyne addition route

With the observed difficulty in the preparation and oxidation of substrates such as **1.41**, we next investigated reactions that would not only couple the saturated alkyl fragment with our cyclopropane but also simultaneously install the elusive epoxide. Variations of the Corey-Chaykovsky reaction have been developed by Aggarwal utilizing sulfur ylide condensation with aldehydes to provide direct access to 2,3 epoxyketones.<sup>36</sup> While such reactions had not been demonstrated to be effective in coupling two aliphatic substrates, we prepared the substrates to investigate this as a route to our target molecule. Azelaic acid monomethylester **1.18** was converted to the acid chloride, then treated with diazomethane to provide a separable mixture of  $\alpha$ -chloro ketone **1.43** and  $\alpha$ -diazoketone **1.44** (Scheme I-15). First,  $\alpha$ -chloroketone **1.43** was converted to the sulfonium salt **1.45**



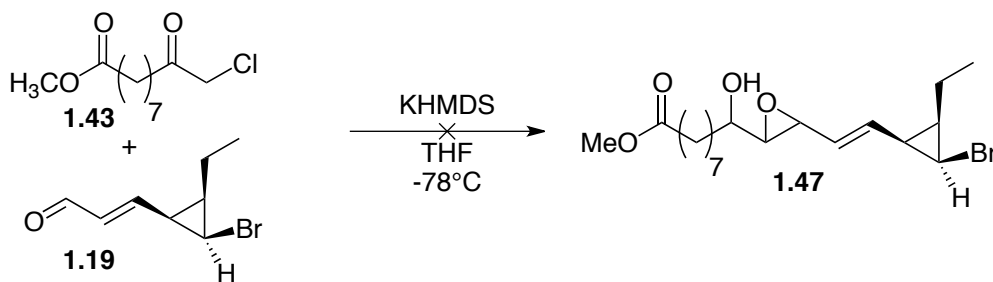
**Scheme I-15:** Alkylation of azeleic acid monomethylester **1.18**

by treatment with methyl sulfide (**Scheme I-16**). Attempts at condensation of aldehyde **1.19** with an in situ generated ylide under Aggarwal's conditions failed to affect the desired condensation to epoxy ketone **1.47**.<sup>37</sup> Ylide generation was also attempted by the formation of a rhodium carbene from diazoketone **1.44** followed by treatment with dimethyl sulfide.<sup>38</sup> These conditions were also unsuccessful at producing the desired epoxyketone **1.48**. In both of these reactions, the strong change in color reported to accompany ylide formation was not observed under the conditions examined.



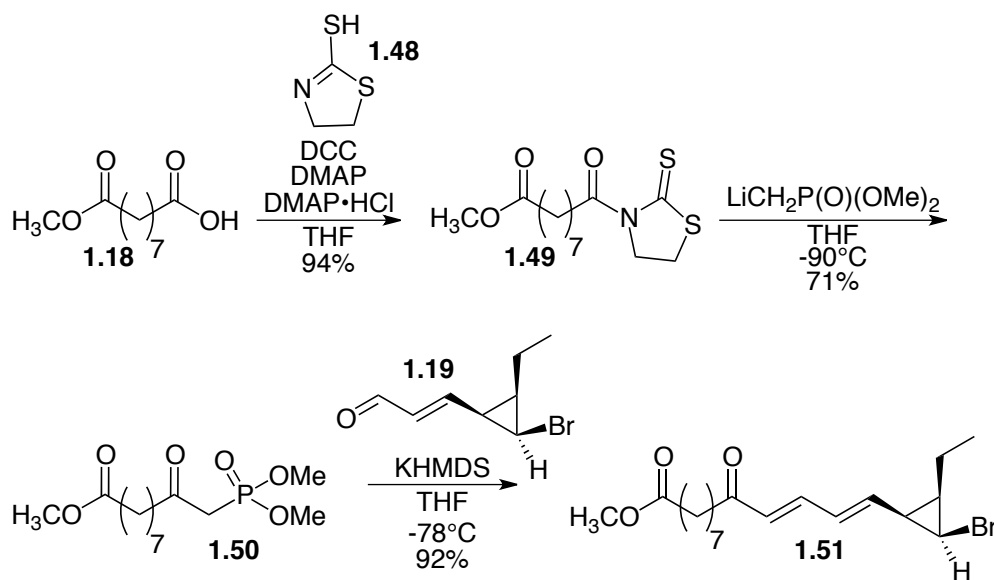
**Scheme I-16:** Sulfur ylide couplings

Next, we investigated the use of a keto-Darzens<sup>39</sup> reaction to couple aldehyde **1.19** with  $\alpha$ -chloroketone **1.43** to provide the epoxy alcohol **1.47** (Scheme I-17). Unfortunately, under a variety of conditions, only decomposition of  $\alpha$ -chloroketone **1.43** was observed, accompanied by recovery of aldehyde **1.19**.



**Scheme I-17:** Keto-Darzens reaction

Knowing from previous experiments that aldehyde **1.19** was reactive to olefination with phosphorous ylides, we next pursued a Horner-Wadsworth-Emmons strategy (**Scheme I-18**). Azeleic acid monomethylester **1.18** was coupled to 2-mercaptothiazole **1.48** to give amide **1.49**. Treatment of this amide with the lithiate of methyl dimethylphosphonate afforded the  $\beta$ -ketophosphonate ester **1.50** in good yield.<sup>40</sup> Condensation of this product with **1.19** afforded dieneone **1.51** in 91% yield.

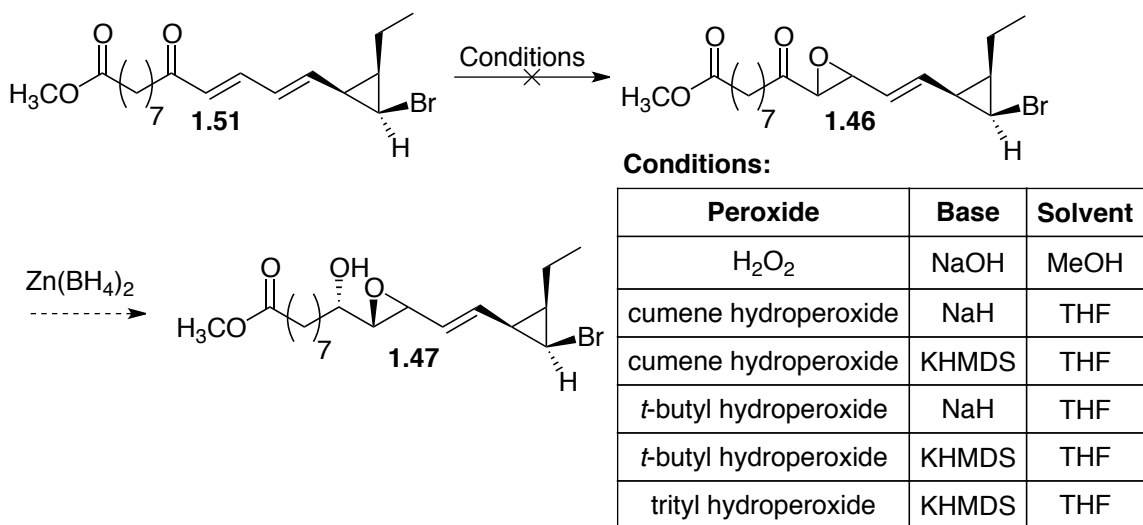


**Scheme I-18:** Horner-Wadsworth-Emmons coupling

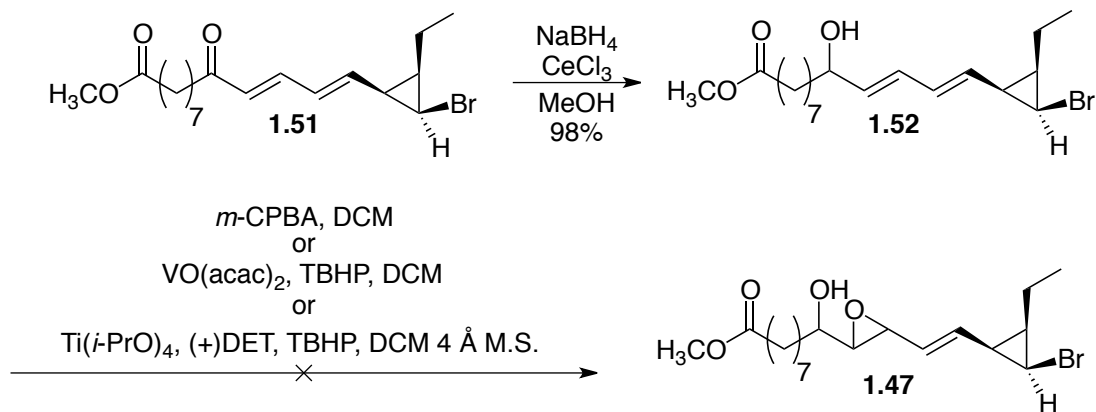
From dienone **1.51** we could investigate multiple methods for conversion to the desired *anti*-epoxysulfonate. First, we attempted basic epoxidation of the vicinal olefin to give epoxy ketone **1.46** (**Scheme I-19**). Using  $\text{Zn}(\text{BH}_4)_2$ , such a ketone could be selectively reduced to the required *anti*-epoxy alcohol.<sup>41</sup> However, **1.51** proved unreactive to all combinations of base and peroxide assayed. While basic epoxidations



are common with  $\alpha,\beta$ -unsaturated ketones, very few examples exist with  $\alpha,\beta,\gamma,\delta$ -unsaturated ketones. Extensive delocalization of  $\pi$ -electrons within both the diene and the cyclopropane likely contributes to the poor reactivity of **1.51** to basic epoxidation. Luche reduction<sup>42</sup> of **1.51** afforded dieneol **1.52**, which was subjected to various hydroxyl directed epoxidation methods (**Scheme I-20**). Treatment with peroxyacid epoxidation conditions resulted in no reaction. Metal catalyzed hydroxyl directed epoxidations using either  $\text{VO}(\text{acac})_2$  or  $\text{Ti}(i\text{-PrO})_4$  were unreactive at low temperature and provided a complex mixture of products upon warming.

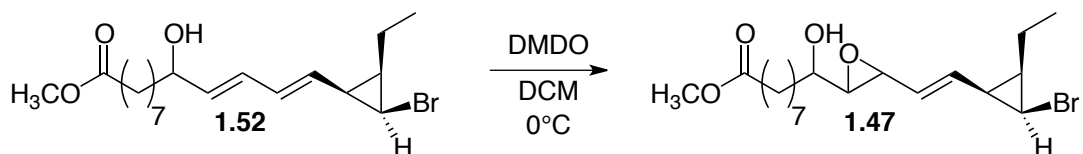


**Scheme I-19:** Basic epoxidations



**Scheme I-20:** Hydroxyl directed epoxidations

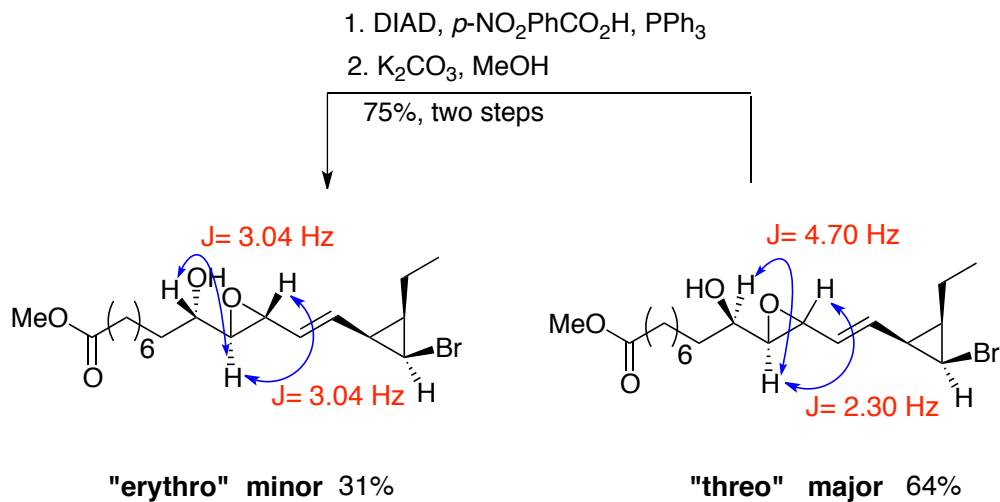
Having had no success with hydroxyl-directed epoxidations, we next investigated dimethyl dioxirane (DMDO), a reagent occasionally reported to be hydroxyl directed.<sup>43-44</sup> Treatment of alcohol **1.52** with DMDO at 0°C resulted in the regio-selective epoxidation of the vicinal double bond (**Scheme I-21**).



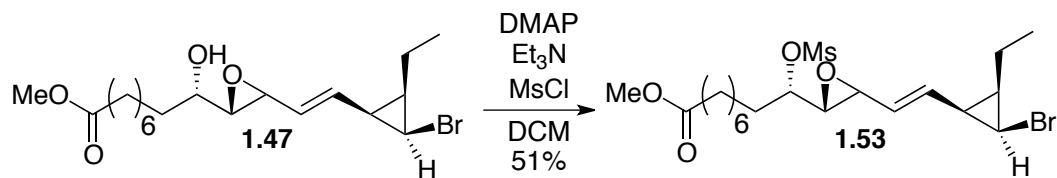
**Scheme I-21:** Dimethyl dioxirane epoxidation

Separation of the four diastereomeric epoxide products of **1.47** on NP-HPLC allowed for a tentative assignment of the relative stereochemistry of the epoxyalcohols based upon  $^1\text{H}$ - $^1\text{H}$  coupling constants (**Scheme I-22**).<sup>45,46</sup> The reaction showed a slight (~2:1) selectivity for the undesired *threo* or *syn* epoxyalcohol products. The desired *anti*

epoxy alcohol products could be separated from the *syn* diastereomers by flash chromatography. As the proposed cascade cyclization was diastereo-convergent by design, the *anti* epoxy alcohol products were taken forward as a mixture of diastereomers. Using the Mitsunobu reaction, the *syn* epoxy alcohol products could be easily converted to the *anti* in 75% yield over two steps. Treatment of **1.47** with MsCl provided mesylate **1.54** in modest yield (Scheme I-23). With this compound in hand, we could finally investigate the proposed cascade reaction.



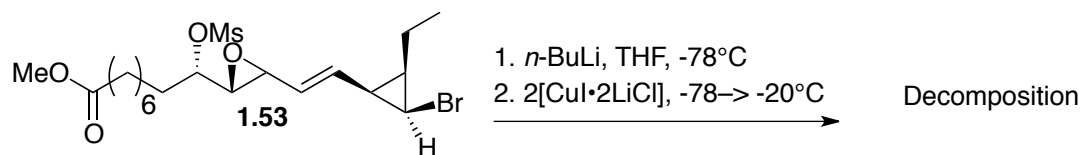
**Scheme I-22:** Stereochemical analysis of epoxy alcohol products **1.47**



**Scheme I-23:** Mesylate formation

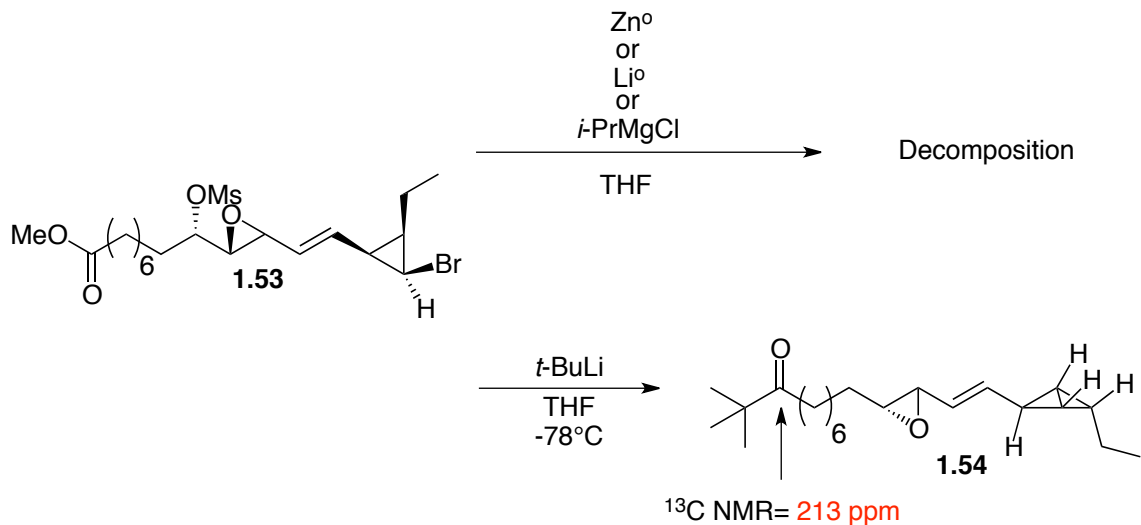
### *Cascade Cyclization Investigation and Completion of the Synthesis*

Initially, we attempted to apply the conditions that had been successful for the cyclization reaction in our model system. However, low temperature treatment of **1.53** with *n*-BuLi to affect a lithium/halogen exchange followed by transfer to a cold solution of CuI•2LiCl afforded neither the desired product nor any recoverable starting material as determined by <sup>1</sup>H NMR analysis of the crude reaction mixture and attempts at chromatographic purification (**Scheme I-24**). To determine if the lithium/halogen exchange was successful and selective, we next treated **1.53** with *n*-BuLi alone. After aqueous workup of this reaction mixture, we expected to observe debromination of **1.53**. However, we were intrigued to discover that the resultant cyclopropyllithiate intermediate had subsequently cyclized to a bicyclo[1.1.0]butane-containing product, as indicated by <sup>1</sup>H NMR analysis. While purification of this product was unsuccessful, it was also clear from the <sup>1</sup>H NMR data that the *n*-BuLi had also reacted with the methyl ester moiety. Furthermore it was unclear if the desired epoxide forming displacement had occurred.



**Scheme I-24:** Application of model cyclization conditions

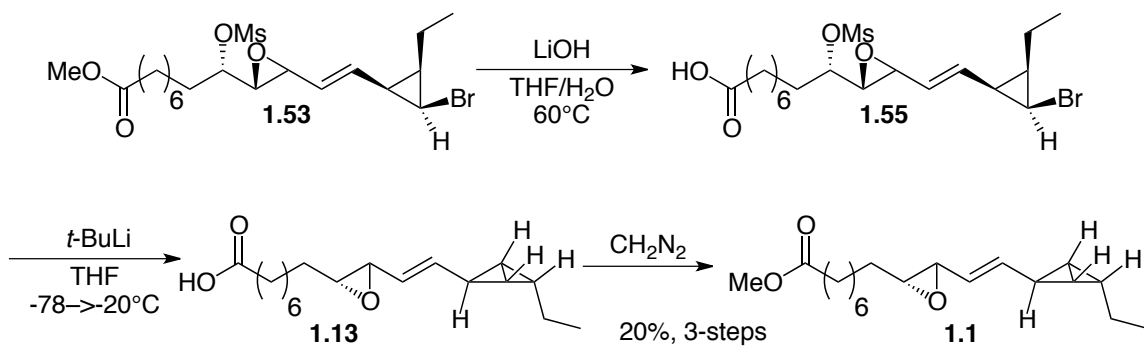
We recognized the possibility of *n*-BuLi acting as a nucleophile on the electrophilic methyl ester group and next surveyed other reagents capable of metal/halogen exchange that would be less nucleophilic (**Scheme I-25**). Sterically hindered Grignard reagents have shown success in metal/halogen exchange for previously reported cyclizations, however treatment of **1.53** with such reagents lead only to decomposition. Certain lithium/halogen exchange reactions have been successful and selective using high surface area lithium metal sources such as lithium sand, however treatment of **1.53** with this reagent afforded no reaction at low temperatures and rapid decomposition upon warming. Similar results were obtained using various non-nucleophilic zinc sources including activated Zinc dust or Rieke Zinc. We next turned back to alkyl lithium reagents, and treated **1.53** with excess *t*-BuLi. Gratifyingly, <sup>1</sup>H NMR analysis of this reaction mixture indicated a very clean conversion to a single bicyclobutane product. Furthermore, 1D TOCSY analysis of this mixture indicated the successful formation of the desired epoxide moiety confirming the success of the cascade reaction. However, it was again evident that the methyl ester was no longer present and <sup>13</sup>C NMR data indicated that instead, the *t*-butylketone **1.54** had been formed.



**Scheme I-25:** Reducing nucleophilicity

Having failed in our attempts to attenuate the nucleophilicity of the lithiating reagent, we sought a strategy that would instead alter the substrate to remove the electrophilic site. To this end, ester **1.53** was hydrolyzed by treatment with LiOH to provide the carboxylic acid **1.55** (Scheme I-26). Rapid isolation of this compound followed by treatment with an excess of  $t\text{-BuLi}$  resulted first in deprotonation of the acid followed by lithium/halogen exchange. The resulting dianion then cyclized to the bicyclo[1.1.0]butane and formed the desired epoxide intercepting the natural product **1.13**. After warming to  $-20^\circ\text{C}$ , the reaction mixture was treated with diazomethane to afford methyl ester **1.1** in a clean conversion. HPLC purification under conditions identical to those used in the original isolation resulted in a 20% yield of **1.1**. Spectral data was in agreement with that reported in the literature, confirming our success in synthesizing the product.<sup>47</sup> The acid **1.13** proved unstable and all attempts at its isolation from the reaction

mixture were unsuccessful. Indeed, NMR analysis of the crude reaction mixture revealed no evidence of a bicyclo[1.1.0]butane when treatment with diazomethane was forgone.



**Scheme I-26:** Cyclization cascade to complete the synthesis of **1.1**

A route to this unique fatty acid natural product was developed that employs a cyclization/epoxidation cascade reaction as the key step to deliver the product in 3.06% yield over 13 linear steps as a racemate. Studies aimed at determining the biological role of this unusual metabolite can now be investigated with this synthetic material. Brash reported that the enzymatic production of this compound leads to the isolation of a variety of downstream products. With a pure source of **1.1**, it is now possible to determine which of these products arise from its degradation as opposed to those from triene epoxide **1.2**. Furthermore, we hypothesize that the vinyl oxirane and bicyclobutane may act as an electrophile, perhaps used to modify macromolecules. Preparation of a labeled derivative of **1.1** could allow this hypothesis to be tested.

## Experimental Methods

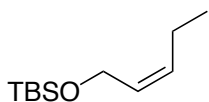
**General procedure:** All non-aqueous reactions were performed in flame-dried or oven-dried round-bottomed flasks under an atmosphere of argon. Where necessary (so noted) solutions were deoxygenated by alternate freeze (liquid nitrogen)/evacuation/argon-flush/thaw cycles (FPT, three iterations) or degassed by purging with argon for several minutes. Stainless steel syringes or cannulae were used to transfer air- and moisture-sensitive liquids. Reaction temperatures were controlled using a thermocouple thermometer and analog hotplate stirrer. Reactions were conducted at room temperature (rt, approximately 23 °C) unless otherwise noted. Flash column chromatography was conducted as described Still et. al. using silica gel 230-400 mesh.<sup>48</sup> Where necessary, silica gel was neutralized by treatment of the silica gel prior to chromatography with the eluent containing 1% triethylamine. Analytical thin-layer chromatography (TLC) was performed on E. Merck silica gel 60 F254 plates and visualized using UV, ceric ammonium molybdate, potassium permanganate, and anisaldehyde stains. Yields were reported as isolated, spectroscopically pure compounds.

**Materials.** Solvents were obtained from either a MBraun MB-SPS solvent system or freshly distilled (tetrahydrofuran was distilled from sodium-benzophenone; toluene was distilled from calcium hydride and used immediately; dimethyl sulfoxide was distilled from calcium hydride and stored over 4Å molecular sieves). Commercial reagents were used as received with the following exceptions. The molarity of *n*-butyllithium and *tert*-butyllithium solutions were determined by titration using diphenylacetic acid as an indicator (average of three determinations).



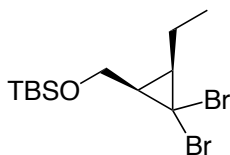
**Instrumentation.** Reverse phase HPLC was conducted on a Varian ProStar HPLC system using a Phenomenex Luna 5u C18(2) 100A Axia 50 x 30.00 mm column unless otherwise noted. Infrared spectra were obtained as thin films on NaCl plates using a Thermo Electron IR100 series instrument and are reported in terms of frequency of absorption ( $\text{cm}^{-1}$ ).  $^1\text{H}$  NMR spectra were recorded on Bruker 300, 400, 500, or 600 MHz spectrometers and are reported relative to deuterated solvent signals. Data for  $^1\text{H}$  NMR spectra are reported as follows: chemical shift ( $\delta$  ppm), multiplicity (s = singlet, d = doublet, t = triplet, q = quartet, p = pentet, m = multiplet, br = broad, app = apparent), coupling constants (Hz), and integration.  $^{13}\text{C}$  NMR spectra were recorded on Bruker 75, 100, 125, or 150 MHz spectrometers and are reported relative to deuterated solvent signals. LC/MS was conducted and recorded on an Agilent Technologies 6130 Quadrupole instrument. High-resolution mass spectra were obtained from the Department of Chemistry and Biochemistry, University of Notre Dame using either a JEOL AX505HA or JEOL LMS-GCmate mass spectrometer.

### Compound Preparation

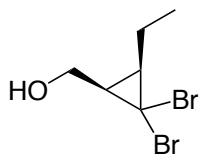


**Silyl ether 1.21** To a solution of cis-2-penten-1-ol (**1.20**) (1.0 mL, 9.75 mmol) in dichloromethane (19.5 mL) at 0 °C was added triethylamine (2.04 mL, 14.63 mmol) and the resulting solution was maintained at 0 °C for 10 min, tert-butyldimethylchlorosilane (TBSCl) (1.76g, 11.70 mmol) in DMF (4.0 mL) was added. The resulting solution was warmed to rt and maintained at that temperature for 4 h. Water (20 mL) was added to the reaction mixture and the aqueous

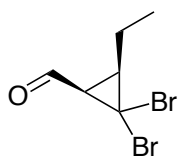
layer was extracted with dichloromethane (3 × 20 mL). The combined organic extracts were dried (MgSO<sub>4</sub>) and concentrated in vacuo. The resulting residue was purified by flash chromatography (20:1 hexane-EtOAc) to afford 1.84 g (94%) of **1.21** as a colorless oil: *R<sub>f</sub>* = 0.63 (10:1 hexane-EtOAc); IR (neat) 2958, 1463 cm<sup>-1</sup>; <sup>1</sup>H NMR (500 MHz, CDCl<sub>3</sub>) δ 5.49-5.41 (m, 2H), 4.23 (d, *J* = 6.0 Hz, 2H), 2.06-2.03 (m, 2H), 0.97 (t, *J* = 7.5 Hz, 3H), 0.90 (s, 9H), 0.07 (s, 6H); <sup>13</sup>C NMR (125 MHz, CDCl<sub>3</sub>) δ; 132.7, 129.1, 59.6, 26.3, 21.1, 18.6, 14.4, -4.9; MS (ESI) *m/z* 199.1512 (M + H)<sup>+</sup> (199.1513 calcd for C<sub>11</sub>H<sub>23</sub>OSi).



**Dibromide 1.22** To a solution of silyl ether **1.21** (1.0 g, 5.0 mmol) and benzyltriethylammonium chloride (BnNEt<sub>3</sub>Cl) (20.0 mg, 0.1 mmol) in bromoform (2.85 mL, 17.5 mmol) was added a solution of NaOH (1.42 g, 35.4 mmol) in water (1.42 mL) over 1 h. The reaction mixture was stirred for 16 h. The mixture was diluted with water (50 mL) and filtered through a plug of Celite, washed with dichloromethane (150 mL). The aqueous layer was extracted with dichloromethane (3 x 30 mL). The combined organic extracts were dried (MgSO<sub>4</sub>) and concentrated in vacuo. The resulting residue was purified by flash chromatography (hexane) to afford 1.49 g (80%) of **1.22** as a colorless oil: *R<sub>f</sub>* = 0.48 (20:1 hexane-EtOAc); IR (neat) 2957, 1463, 1255cm<sup>-1</sup>; <sup>1</sup>H NMR (500 MHz CDCl<sub>3</sub>) δ 3.80 (dd, *J* = 11.15, 6.55 Hz, 1H), 3.58 (dd, *J* = 11.5, 7.24 Hz, 1H), 1.88 (dt, *J* = 11.00, 6.85 Hz, 1H), 1.63 (dt, *J* = 11.00, 7.30 Hz, 1H), 1.52-1.40 (m, 2H), 1.08 (t, *J* = 7.35 Hz, 3H), 0.91 (s, 9H), 0.09 (s, 3H), 0.08 (s, 3H); <sup>13</sup>C NMR (125 MHz, CDCl<sub>3</sub>) δ; 61.4, 35.6, 35.0, 34.3, 26.1, 20.8, 18.5, 13.1, -5.0, -5.1; MS (ESI) *m/z* 392.9858 (M + Na)<sup>+</sup> (392.9855 calcd for C<sub>12</sub>H<sub>24</sub>Br<sub>2</sub>NaOSi).

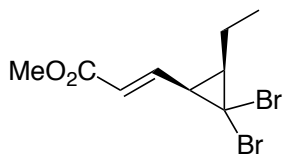


**Alcohol 1.23** To a solution of dibromide **1.22** (2.18 g, 5.8 mmol) in THF (58.0 mL) was added a solution of tetrabutylammonium (TBAF) (8.2 mL, 1.0 M in THF, 8.2 mmol). After 30 min, the solution was diluted with ethyl acetate (30 mL) and washed with 1 M aqueous HCl (50 mL). The aqueous layer was extracted with ethyl acetate (3 × 30 mL) and the combined organic extracts were dried (MgSO<sub>4</sub>) and concentrated in vacuo. The resulting residue was purified by flash chromatography (8:1 hexane-EtOAc) to afford 1.42 g (95%) of **1.23** as a light yellow oil:  $R_f$  = 0.27 (4:1 hexane-EtOAc); IR (neat) 3351, 2967, 2931, 1460, cm<sup>-1</sup>; <sup>1</sup>H NMR (500 MHz CDCl<sub>3</sub>) δ 3.75-3.66 (m, 2H), 1.96-1.91 (m, 2H), 1.69-1.64 (m, 1H), 1.56-1.40 (m, 2H), 1.06 (t,  $J$  = 7.38 Hz, 3H); <sup>13</sup>C NMR (125 MHz, CDCl<sub>3</sub>) δ 61.2, 36.0, 34.9, 34.2, 20.9, 13.1; MS (EI)  $m/z$  255.9080 (M + H)<sup>+</sup> (255.9098 calcd for C<sub>6</sub>H<sub>10</sub>Br<sub>2</sub>O).

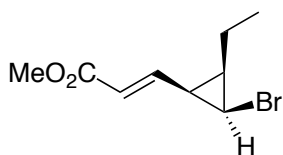


**Aldehyde 1.24** To a solution of alcohol **1.23** (2.48 g, 9.63 mmol) in dichloromethane (40 mL) and DMSO (10 mL) at -15 °C was added N,N-diisopropylethylamine (5.02 mL, 28.84 mmol). The resulting solution was maintained for 10 min at -15 °C and SO<sub>3</sub>·Pyr (4.59 g, 28.84 mmol) in DMSO (10 mL) was added dropwise. The resulting solution was maintained at -15 °C for 1 h and warmed to rt. After dilution with Et<sub>2</sub>O (75 mL) the solution was washed sequentially with water (2 x 30 mL), brine (1 x 30 mL), 15% NaHCO<sub>3</sub> (1 x 30 mL) and saturated aqueous CuSO<sub>4</sub> (2 x 30 mL). The organic layer was then dried (MgSO<sub>4</sub>) and concentrated in vacuo. The residue was purified by flash chromatography (8:1 hexane-EtOAc) to afford 1.94 g (79%) of **1.24** as a light yellow oil:  $R_f$  = 0.58 (4:1 hexane-EtOAc); IR (neat) 2969, 2874, 1707 cm<sup>-1</sup>; <sup>1</sup>H NMR (500 MHz CDCl<sub>3</sub>) δ 9.31 (d,  $J$  = 5.55 Hz, 1H), 2.40 (dd,  $J$  = 10.90, 5.55 Hz, 1H), 2.14-2.08 (m, 1H), 1.97-1.89 (m, 1H), 1.80-1.71 (m, 1H), 1.12 (t,  $J$

= 7.35 Hz, 3H);  $^{13}\text{C}$  NMR (125 MHz,  $\text{CDCl}_3$ )  $\delta$  198.3, 41.6, 40.2, 29.1, 21.5, 13.0; MS (ESI)  $m/z$  255.0, (M + H) (254.90 calcd for  $\text{C}_6\text{H}_9\text{Br}_2\text{O}$ ).

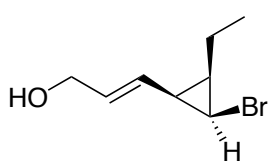


**Enoate 1.27** To a solution of methyl 2-(diethoxyphosphoryl)acetate (3.18 g, 18.17 mmol) in THF (90 mL) at 0 °C was added NaH (392 mg, 16.35 mmol) in 5 portions over 2 min. The resulting solution was maintained at 0 °C for 10 min then warmed to rt. Neat aldehyde **1.24** was added to the solution dropwise. The resulting reaction mixture was stored for 4 h then diluted with  $\text{Et}_2\text{O}$  (100 mL). The ethereal solution was then washed with 1 M NaOH (50 mL). The organic layer was separated and the aqueous layer was extracted with  $\text{Et}_2\text{O}$  (3 x 75 mL). The combined organic extracts were dried ( $\text{MgSO}_4$ ) and concentrated in vacuo. The residue was purified by flash chromatography (10:1 hexane-EtOAc) to afford 2.45 g (87%) of **1.27** as a light yellow oil:  $R_f$  = 0.58 (4:1 hexane-EtOAc); IR (neat) 2968, 2933, 2875, 1708,  $\text{cm}^{-1}$ ;  $^1\text{H}$  NMR (400 MHz,  $\text{CDCl}_3$ )  $\delta$  6.60 (dd,  $J$  = 15.6, 10.0 Hz, 1H), 6.13 (d,  $J$  = 15.6 Hz, 1H), 3.75 (s, 3H), 2.42 (t,  $J$  = 10.4 Hz, 1H), 1.93 (ddd,  $J$  = 10.7, 7.5, 7.5 Hz, 1H), 1.72-1.63 (m, 1H), 1.54-1.47 (m, 1H), 1.06 (t,  $J$  = 7.6 Hz, 3H);  $^{13}\text{C}$  NMR (125 MHz,  $\text{CDCl}_3$ )  $\delta$  166.0, 143.3, 125.1, 51.7, 39.9, 35.7, 35.1, 21.7, 12.5; MS (ESI)  $m/z$  332.9114 (M + Na) $^+$  (332.9096 calcd for  $\text{C}_9\text{H}_{12}\text{Br}_2\text{NaO}_2$ ).



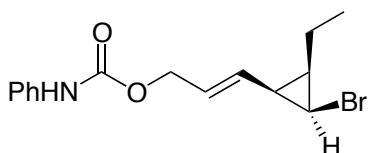
**Cyclopropylbromide 1.32** To a solution of enoate **1.27** (6.45 g, 19.73 mmol) in toluene (79 mL) at -78 °C was added triphenylstannane (6.93 mL, 19.73 mmol) and a solution of triethylborane (5.92 mL, 1 M in hexanes, 5.92 mmol). The reaction flask was fitted with a drying tube and the solution was maintained at -78 °C for 4 h. The reaction mixture was warmed to room temperature and poured into a saturated solution of potassium fluoride

(100 mL) and the resulting mixture was stirred for an additional 3 h. The solution was then passed through a plug of Celite and washed with Et<sub>2</sub>O (150 mL). The resulting solution was extracted with Et<sub>2</sub>O (3 x 75mL) The combined organics were dried (MgSO<sub>4</sub>) and concentrated to ~80 mL in vacuo (toluene not removed). The resulting solution was filtered through a long plug of silica gel first with hexanes (500 mL) then with Et<sub>2</sub>O (500 mL). The ethereal fractions were combined and concentrated in vacuo. The residue was purified by flash chromatography (10:1 hexane-Et<sub>2</sub>O) to afford 4.37 g (95%) of **1.32** as a light yellow oil: *R<sub>f</sub>*= 0.50 (4:1 hexane-EtOAc); IR (neat) 2968, 1732, 1645, 1435 cm<sup>-1</sup>; <sup>1</sup>H NMR (400 MHz CDCl<sub>3</sub>) δ 6.82 (dd, *J* = 15.6, 10.4 Hz, 1H), 6.05 (d, *J* = 15.6 Hz, 1H), 3.74 (s, 3H), 3.47 (t, *J* = 7.6 Hz, 1H), 1.86 (ddd, *J* = 9.9, 9.9, 7.3 Hz), 1.57-1.66 (m, 2H), 1.24-1.36 (m, 1H) 1.02 (t, *J* = 7.4 Hz, 3H); <sup>13</sup>C NMR (125 MHz, CDCl<sub>3</sub>) δ166.3, 146.2, 123.2, 51.5, 30.9, 26.5, 22.6, 19.8, 13.1; MS (ESI) *m/z* 254.9991 (M +Na)<sup>+</sup> (254.9991 calcd for C<sub>9</sub>H<sub>13</sub>BrNaO<sub>2</sub>).



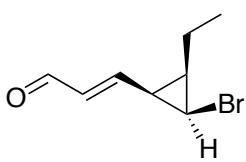
**Allylic alcohol 1.33** To a solution of cyclopropylbromide **1.32** (4.96 g, 17.84 mmol) in dichloromethane (200 mL) at -78 °C was added neat diisobutylaluminum hydride (DIBAL-H) (7.57 mL, 42.46 mmol, 2.0 equiv) dropwise. The resulting solution was maintained at -78 °C for 45 min. The reaction mixture was warmed to rt, quenched with a saturated solution of Rochelle's salt (150 mL) and stirred for 2 h. The aqueous layer was extracted with Et<sub>2</sub>O (3 × 100 mL). The combined organic extracts were dried (MgSO<sub>4</sub>) and concentrated in vacuo. The residue was purified by flash chromatography (4:1 hexane-EtOAc) to afford 3.85 g (95%) of **1.33** as a yellow oil: *R<sub>f</sub>*= 0.30 (hexane-EtOAc, 4:1); IR (neat) 3309, 2964 cm<sup>-1</sup>; <sup>1</sup>H NMR (500 MHz CDCl<sub>3</sub>) δ 5.88 (dt, *J* = 15.35, 6.00 Hz, 1H), 5.51 (dd, *J* = 15.35,

9.30 Hz, 1H), 4.12 (d,  $J = 6.00$  Hz, 2H), 3.34 (t,  $J = 7.45$  Hz, 1H), 1.76-1.70 (m, 1H), 1.51-1.47 (m, 2H), 1.13-1.07 (m, 1H), 0.99 (t,  $J = 7.35$  Hz, 3H);  $^{13}\text{C}$  NMR (125 MHz,  $\text{CDCl}_3$ )  $\delta$  132.7, 128.4, 63.8, 31.1, 23.9, 22.0, 19.7, 13.2; MS (ESI)  $m/z$  187.0088 ( $\text{M} + \text{H} - \text{H}_2\text{O}$ )<sup>+</sup> (187.01 calcd for  $\text{C}_8\text{H}_{12}\text{Br}$ ).



**Phenyl carbamate 1.34** To a solution of alcohol **1.33**

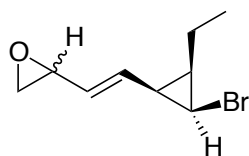
(194 mg, 0.94 mmol) in DCM (18.8 ml) was added phenyl isocyanate (0.206 ml, 1.89 mmol) and triethyl amine (0.263 mL, 1.89 mmol) with stirring. The resulting solution was maintained for 45 minutes, diluted with hexanes (50 mL) and filtered. The resulting solution was concentrated and purified by flash column chromatography (10:1 hexane: $\text{Et}_2\text{O}$ ) to yield **1.34** as a pale yellow oil (202 mg, 0.62 mmol, 66%).  $^1\text{H}$  NMR (400 MHz,  $\text{CDCl}_3$ ):  $\delta$  7.28 (d,  $J = 8.0$  Hz, 2H), 7.31 (dd,  $J = 7.6, 8.4$  Hz, 2H), 7.064 (dd,  $J = 7.2, 7.6$  Hz, 1H), 6.61 (*br s*, 1H), 5.89 (ddd,  $J = 15.2, 6.8, 6.4$  Hz, 1H), 5.66 (dd,  $J = 15.2, 9.2$  Hz, 1H), 4.66 (d,  $J = 6.8$  Hz, 2H), 3.37 (dd,  $J = 7.2, 7.2$  Hz, 1H), 1.77 (ddd,  $J = 9.6, 9.2, 7.6$  Hz, 1H) 1.56-1.49 (m, 2H), 1.18-1.10 (m, 1H), 1.01 (t,  $J = 7.2$  Hz, 3H).



**Enal 1.19** To a solution of allylic alcohol **1.34** (1.0 g, 4.88 mmol)

in dichloromethane (50 mL) was added manganese(IV) oxide (4.24 g, 48.76 mmol). The reaction mixture was stirred for 16 h and filtered through a plug of Celite. The filtrate was concentrated in vacuo. The residue was purified by flash chromatography (8:1 hexane- $\text{Et}_2\text{O}$ ) to afford 0.983 g (99%) of **1.19** as a colorless oil:  $R_f = 0.38$  (4:1 hexane- $\text{EtOAc}$ ); IR (neat) 2965, 2862, 1683  $\text{cm}^{-1}$ ;  $^1\text{H}$  NMR (500 MHz  $\text{CDCl}_3$ )  $\delta$  9.49 (d,  $J = 7.95$  Hz, 1H), 6.67 (dd,  $J = 15.45, 10.15$  Hz, 1H), 6.34 (dd,  $J = 15.50, 7.95$  Hz, 1H), 3.56 (t,  $J = 7.25$  Hz, 1H), 1.98 (dt,  $J = 9.93, 7.15$  Hz, 1H),

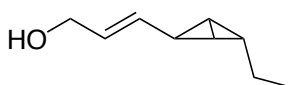
1.65-1.58 (m, 2H), 1.47-1.42 (m, 1H), 1.01 (t,  $J = 7.35$  Hz, 3H);  $^{13}\text{C}$  NMR (125 MHz,  $\text{CDCl}_3$ )  $\delta$  193.0, 155.8, 135.2, 31.6, 27.7, 23.3, 20.0, 13.1; MS (ESI)  $m/z$  224.9879 ( $\text{M} + \text{Na}$ ) $^+$  (224.9885 calcd for  $\text{C}_8\text{H}_{11}\text{BrNaO}$ ).



**Epoxide 1.36** To a solution of aldehyde **1.19** (500 mg, 2.446 mmol) and  $\text{ICH}_2\text{Cl}$  (0.179 mL, 2.46 mmol) in THF (5 mL) at  $-78$  °C was added a solution of *n*-BuLi (1.16 mL, 2.13 M in hexane, 2.46 mmol) dropwise. The resulting solution was maintained for 30 min at  $-78$  °C and quenched with saturated  $\text{NH}_4\text{Cl}$  (10 mL). The reaction mixture was warmed to rt, diluted with water (3 mL) and extracted with  $\text{Et}_2\text{O}$  (3 x 10 mL). Combined ethereal extracts were dried ( $\text{MgSO}_4$ ) and concentrated. Flash column chromatography of the resulting residue (4:1 hexane- $\text{Et}_2\text{O}$  4:1) yielded 318 mg (51%) of a mixture of chlorohydrins **1.37** as a light yellow oil:  $^1\text{H}$  NMR (400 MHz,  $\text{CDCl}_3$ ):  $\delta$  5.77 (dd,  $J = 15.6, 6.4$  Hz, 1H), 5.65 (dd,  $J = 15.2, 8.8$  Hz, 1H), 4.36 (m, 1H), 3.60 (dd,  $J = 11.2, 4.0$  Hz, 1H), 3.52 (dd,  $J = 10.4, 6.8$  Hz, 1H), 3.62 (dd,  $J = 7.6, 7.6$  Hz, 1H), 1.73 (ddd,  $J = 16.8, 9.2, 7.6$  Hz, 1H), 1.53-1.46 (m, 2H), 1.15-1.11 (m, 1H), 0.99 (t,  $J = 7.6$  Hz, 3H).

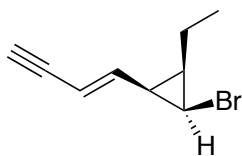
To a solution of chlorohydrins **1.37** (50 mg, 0.20 mmol) in THF (2 mL) was added NaH (9.5 mg, 0.39 mmol). The resulting mixture was stirred for 1 h and quenched with 10%  $\text{NaHCO}_3$  (3 mL) and water (3 mL) and separated. The aqueous was extracted with  $\text{Et}_2\text{O}$  (5 x 5 mL) and the combined organic extracts were dried ( $\text{MgSO}_4$ ) and concentrated. The resulting residue was purified by flash column chromatography (10:1 hexane- $\text{Et}_2\text{O}$ -1%  $\text{Et}_3\text{N}$ ) to yield 36.3 mg (84%) of epoxide **1.36** as a light yellow oil and as a mixture of diastereomers: IR (neat) 2965, 2929, 2873, 1248  $\text{cm}^{-1}$ ;  $^1\text{H}$  NMR (400 MHz,  $\text{C}_6\text{D}_6$ ):  $\delta$  5.75 (ddd,  $J = 15.2, 9.6, 9.2$ ), 5.22 (dd,  $J = 15.2, 8.0$  Hz, 1H), 3.05-3.01 (m, 1H), 2.88 (dd,  $J =$

7.6, 7.6 Hz, 1H), 2.50-2.46 (m, 1H), 2.26 (dd,  $J = 5.6, 2.4$  Hz, 1H), 1.42-1.32 (m, 3H), 1.23-1.17 (m, 1H), 0.87(t,  $J = 7.6$  Hz, 3H).  $^{13}\text{C}$  NMR (150 MHz,  $\text{C}_6\text{D}_6$ ):  $\delta$  132.3, 132.1, 131.9, 131.4, 131.1, 128.5, 128.4, 128.1, 128.0, 52.0, 51.9, 48.5, 48.4, 31.0(4), 31.0(1), 24.3, 24.2, 22.4, 22.3, 19.9, 19.8, 13.1, MS (EI)  $m/z$  216.0167 (M +H)<sup>+</sup> (216.0150 calcd for  $\text{C}_9\text{H}_{14}\text{BrO}$ ).

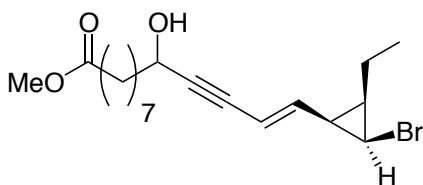


**Bicyclobutane 1.15** To a solution of epoxide **1.36** (50 mg, 0.23 mmol) in THF (2.3 mL) at  $-78^\circ\text{C}$  was added 0.325 mL *n*-BuLi (2.13 M in hexanes, 0.325 mL, 0.69 mmol) slowly. The solution was maintained at  $-78^\circ\text{C}$  for 30 min. In a separate flask CuI (88 mg, 0.46 mmol) and LiCl (39 mg, 0.92 mmol) were weighed and the flask flame dried under vacuum, purged with argon and cooled to rt. The salts were dissolved in THF (1.15 mL) and stirred for 10 min. The resulting yellow solution was cooled to  $-78^\circ\text{C}$ . The prepared solution of cyclopropyllithium was added to the yellow solution of CuI-LiCl dropwise via cannula. The resulting solution was stirred for 2 h, warmed to  $-15^\circ\text{C}$  and quenched with a 9:1 aqueous solution of saturated  $\text{NH}_4\text{Cl}$  and  $\text{NH}_4\text{OH}$  (3 mL). After warming to room temperature, the aqueous layer was extracted with  $\text{Et}_2\text{O}$  (4 x 7 mL). Organic extracts were dried ( $\text{MgSO}_4$ ) and concentrated to yield bicyclobutane **1.15** as a light yellow oil:  $^1\text{H}$  NMR (400 MHz,  $\text{C}_6\text{D}_6$ ):  $\delta$  5.67 (ddd,  $J = 15.2, 5.6, 5.2$  Hz, 1H), 5.27 (dd,  $J = 15.6, 9.2$  Hz, 1H), 3.89 (d,  $J = 3.6$  Hz, 2H), 2.44 (d,  $J = 8.8$  Hz, 1H), 2.04 (m, 1H), 1.45-1.35 (m, 2H), 1.29-1.23 (m, 2H), 0.97 (t,  $J = 7.2$  Hz, 1H).  $^{13}\text{C}$  NMR (100 MHz,  $\text{C}_6\text{D}_6$ ):  $\delta$  129.4 (CH), 129.3 (CH), 63.1( $\text{CH}_2$ ), 45.9 (CH), 44.8 (CH), 17.2 ( $\text{CH}_2$ ), 13.6 ( $\text{CH}_3$ ), 9.18 (CH).



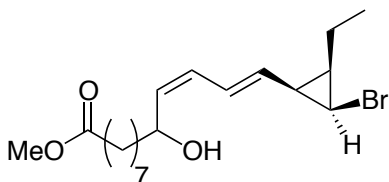


**Alkyne 1.38** To a solution of (bromomethyl)triphenylphosphonium bromide (2.36 g, 5.42 mmol) in THF (25 mL) at  $-78^{\circ}\text{C}$  was added *t*-BuOK (552 mg, 4.92 mmol). Solution was stirred at  $-78^{\circ}\text{C}$  for 20 minutes and became bright yellow. Aldehyde **1.19** (500 mg, 2.46 mmol) was added to the solution dropwise as a solution in THF (1 mL). The reaction mixture was stirred for 2 hours at  $-78^{\circ}\text{C}$ , warmed to room temperature, diluted in EtOAc (30 mL) and washed with  $\text{H}_2\text{O}$  (10 mL). The aqueous layer was extracted with EtOAc (3 x 30 mL). Combined organics were dried ( $\text{MgSO}_4$ ) and concentrated. The resulting residue was diluted in hexane (100 mL) and filtered through a plug of silica and concentrated to yield a pale yellow oil (452 mg). Without further purification, the resulting oil was dissolved in *t*-BuOH (10 mL). *t*-BuOK (544 mg, 4.84 mmol) was added to the solution at room temperature with stirring. The reaction mixture was warmed to  $45^{\circ}\text{C}$  and stirred for 2 hours. After cooling to room temperature, the mixture was washed with  $\text{H}_2\text{O}$  (10 mL). The aqueous layer was extracted with  $\text{Et}_2\text{O}$  (3 x 35 mL). Combined organics were dried ( $\text{MgSO}_4$ ) and concentrated. Flash column chromatography (hexane) of the resulting residue yielded 242.3 mg of alkyne **1.38** (50% over 2 steps) as a pale yellow oil. IR (film)  $\nu_{\text{max}}$  3293, 2965, 2932, 2874, 1249, 951, 641.  $^1\text{H}$  NMR (400 MHz,  $\text{CDCl}_3$ ):  $\delta$  6.09 (dd,  $J = 15.8, 9.7$  Hz, 1 H), 5.68 (dd,  $J = 16.8, 2.2$  Hz, 1H), 3.39 (dd,  $J = 7.4, 7.4$  Hz, 1H), 2.88 (d,  $J = 2.2$  Hz, 1 H), (ddd,  $J = 9.7, 7.4, 7.4$  Hz, 1H), 2.54 (m, 2H), 1.22 (m, 1H), 1.01 (t,  $J = 7.4$  Hz, 3H)  $^{13}\text{C}$  NMR (100 MHz,  $\text{CDCl}_3$ ):  $\delta$  142.4, 111.02, 82.44, 76.88, 30.94, 25.40, 23.06, 19.81, 13.13.



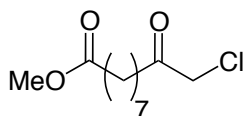
**Propargylic alcohol 1.40** To a solution of **1.38** (283 mg, 1.42 mmol) in THF (14 mL) at  $-78^{\circ}\text{C}$  was added

*n*-BuLi as a 2.35 M solution in hexane (0.67 mL, 1.56 mmol). The resulting mixture was stirred at -78°C for 30 minutes. The resulting golden lithiate solution was added dropwise via canula to a stirred solution of methyl 9-oxononanoate **1.39** (344 mg, 1.85 mmol) as a solution in THF (18 mL). The reaction mixture was stirred for 2.5 hours at -78°C. The cold bath was removed and the reaction mixture was diluted in Et<sub>2</sub>O (30 mL) then washed with H<sub>2</sub>O (10 mL). The aqueous layer was extracted with Et<sub>2</sub>O (3 x 30 mL). Combined organics were dried (MgSO<sub>4</sub>) and concentrated. Flash column chromatography of the residue (3:1 Hexanes:EtOAc) yielded 338 mg of **1.40** (67%) as a light yellow oil. <sup>1</sup>H NMR (400 MHz, CDCl<sub>3</sub>): δ 5.97 (dd, *J* = 16.0, 9.6 Hz, 1H) 5.71 (d, *J* = 16Hz, 1H), 4.47 (dd, *J* = 12.0, 6.4 Hz, 1H), 3.66 (s, 3H), 3.39 (dd, *J*=7.6, 7.6 Hz, 1H), 2.30 (t, *J* = 7.2 Hz, 2H), 1.78 (ddd, *J* = 7.4, 7.4, 9.6 Hz, 1 H), 1.75-1.50 (m, 7H), 1.33 (s(br), 6H), 1.26–1.16 (m, 1H), 1.01 (t *J*= 7.2 Hz, 3H).



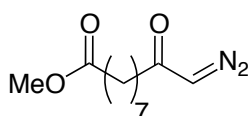
**Dieneol 1.41** To a solution of **1.40** (100 mg, 0.26 mmol) in EtOAc (2.6 mL) at room temperature was added Lindlar's catalyst. Solution was stirred at room

temperature for 4 hours under H<sub>2</sub> (1 atm). The resulting suspension was filtered through a pad of celite with ethyl acetate and concentrated. Flash column chromatography (3:1 hexane-EtOAc) yielded 44.0 mg of **1.41** (44%) as a light yellow oil. <sup>1</sup>H NMR (400 MHz, CDCl<sub>3</sub>): δ 6.57 (dd, *J* = 17.2, 11.2 Hz, 1H), 6.09 (dd, *J* = 11.2, 11.2 Hz, 1H), 5.58 (dd, *J* = 15.2, 9.2 Hz, 1H), 5.31 (dd, *J* = 10.0, 10.0 Hz, 1H), 5.57 (dd, *J* = 14.8, 6.4 Hz, 1H) 3.66 (s, 3H), 3.40 (dd, *J* = 7.2, 7.2 Hz, 1H), 2.30 (t, *J* = 7.2 Hz, 2H), 1.78 (ddd, *J* = 9.2, 8.4, 7.6 Hz, 1H), 1.56-1.44 (m, 9H), 1.37-1.27 (s (br), 6 H), 1.26-1.13 (m, 1H), 1.00 (t, *J* = 7.6 Hz, 3H).



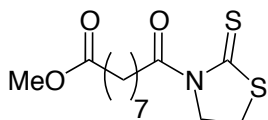
**$\alpha$ -chloro ketone 1.43** To a flask charged with azelaic acid monomethyl ester **1.18** (2.0 g, 9.89 mmol) in EtOAc was added

oxalyl chloride (2.59 mL, 12.93 mmol) dropwise. Mixture was stirred at room temperature for 45 minutes. The remaining oxalyl chloride was removed by evaporation to yield the crude acid chloride. The acid chloride was dissolved in Et<sub>2</sub>O (15 mL) and added to a freshly prepared solution of diazomethane (~19.5 mmol in 70 mL Et<sub>2</sub>O). After 30 minutes, solvent was removed concentrated to yield a yellow residue. Flash column chromatography (4:1 Hexanes:EtOAc) yielded 823.7 mg of  $\alpha$ -chloro ketone **1.43** (37%) as a clear oil. IR (film)  $\nu_{\max}$  2935, 2857, 1738, 1732, 1435, 1175; <sup>1</sup>H NMR (400 MHz, CDCl<sub>3</sub>):  $\delta$  4.02 (s, 2H), 3.59 (s, 3H), 2.51 (t,  $J$  = 7.36, 2H), 2.22 (t,  $J$  = 7.5 Hz, 2H), 1.58-1.48 (m, 4H), 1.24 (s (br), 6H); <sup>13</sup>C NMR (100 MHz, CDCl<sub>3</sub>): 202.5, 174.1, 60.1, 51.3, 48.2, 39.5, 34.2, 33.9, 24.8, 23.4.



This procedure also yielded 1.04 g of  **$\alpha$ -diazo ketone 1.44** (45%) as a pale yellow oil. IR (film)  $\nu_{\max}$  2933, 2857, 2103, 1738, 1651,

1372; <sup>1</sup>H NMR (400 MHz, CDCl<sub>3</sub>):  $\delta$  5.23 (s(br), 1H), 3.66 (s, 3H), 2.29 (t,  $J$  = 7.5 Hz, 4H), 1.66-1.56 (m, 4H), 1.31 (s(br), 6H); <sup>13</sup>C NMR (100 MHz, CDCl<sub>3</sub>):  $\delta$  195.1, 173.9, 51.10, 40.61, 33.7, 33.6, 28.6, 24.8, 24.6, 24.5.

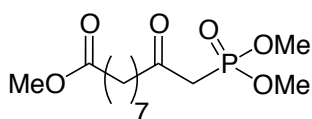


**Amide 1.49** Azelaic acid monomethyl ester **1.18** (404 mg, 2.0

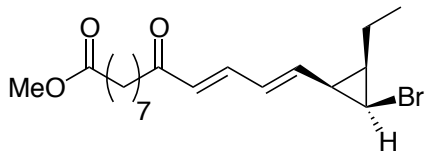
mmol), 2-mercaptopyridine **1.49** (240 mg, 2.0 mmol), N,N-dimethylaminopyridine (48 mg, 0.4 mmol), N,N-dimethylpyridin-

4-aminium chloride (64 mg, 0.4 mmol), and dicyclohexylcarbodiimide were combined in a microwave reaction vessel and dissolved in THF (20 mL). Resulting solution was subjected to microwave irradiation at 85°C for 7.5 minutes. The resulting slurry was

filtered through a plug of silica (3:1 Hexanes:DCM 2% Et<sub>3</sub>N). The resulting solution was concentrated, diluted in EtOAc (150 mL) and washed with 2M HCl (2x 30 mL) and saturated NaHCO<sub>3</sub> (1 x 30 mL). The organic layer was dried (MgSO<sub>4</sub>) and concentrated to a yellow oil. Flash column chromatography (5:1 Hexanes:EtOAc) of the resulting residue yielded 589 mg (94%) of amide **1.49** as a yellow oil that solidified upon storage at 4°C. <sup>1</sup>H NMR (400 MHz, CDCl<sub>3</sub>): δ 4.57 (t, *J* = 7.5 Hz, 2H), 3.66 (s, 3H), 3.28 (t, *J* = 7.5 Hz, 2H), 3.23 (t, *J* = 7.5 Hz, 2H), 2.30 (t, *J* = 7.5 Hz, 2H), 1.71-1.58 (m, 4H), 1.32 (s(br), 6H). Spectral data matched that reported in the literature.<sup>40</sup>

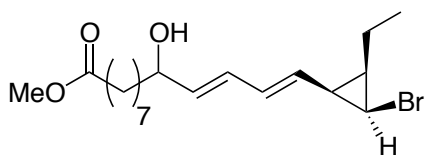


**β-ketophosphonate ester 1.50** To a stirred solution of methyl dimethyl phosphonate (2.09 g, 16.8 mmol) at -65°C (CHCl<sub>3</sub>/dry ice) in THF (100 mL) was added *n*-BuLi as a 2.27 M solution in hexanes (7.4 mL, 16.8 mmol). The resulting mixture was stirred for 30 minutes at -65°C then cooled to -90°C (Hexanes/N<sub>2</sub>(liq)). The lithiate solution was then transferred via canula to a solution of amide **1.49** (2.55 g, 8.4 mmol) in THF (30 mL) at -90°C over ~30 minutes. The resulting solution was maintained at -90°C for an additional 1.5 hours. Oxalic acid (2.27 g, 25.2 mmol) was added to the reaction vessel as a solution in THF (12 mL) at -90°C. After stirring for an additional 30 minutes at that temperature, the vessel was removed from the bath and warmed to room temperature. The resulting slurry was filtered through a pad of celite (EtOAc) and concentrated. Flash column chromatography (EtOAc) of the residue yielded 1.85 g (71%) of β-ketophosphonate ester **1.50** as a clear oil. <sup>1</sup>H NMR (400 MHz, CDCl<sub>3</sub>): δ 3.80 (s, 3H), 3.77 (s, 3H), 3.66 (s, 3H), 3.08, (d, *J* = 22.7 Hz, 2H), 2.60 (t, *J* = 7.3, 2H), 2.30 (t, *J* = 7.5 Hz, 2H), 1.66-1.54 (m, 4H), 1.30 (s(br), 6H). Spectral data matched that reported in the literature.<sup>40</sup>



**Dieneone 1.51** To a solution of  $\beta$ -ketophosphate ester **1.50** (1.32g, 16.8 mmol) in THF at  $-78^{\circ}\text{C}$  was added KHMDS (812 mg, 4.07 mmol). The resulting

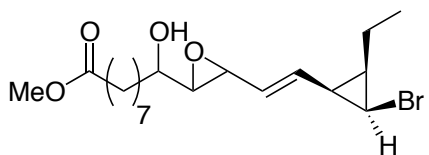
solution was allowed to stir at  $-78^{\circ}\text{C}$  for 30 min then warmed to room temperature. Aldehyde **1.19** (435 mg, 2.14 mmol) was added neat drop-wise and the resulting solution was stirred 16 h. The reaction mixture was quenched with water (10 mL) and extracted with  $\text{Et}_2\text{O}$  (3 x 30 mL). Combined organic extracts were dried ( $\text{MgSO}_4$ ) and concentrated. Flash column chromatography of the residue (8:1 hexane-EtOAc) yielded 762.2 mg (92%) of dieneone **1.51** as a pale yellow oil: IR (neat) 2932, 2858, 1737, 1685, 1660, 1628,  $1595\text{cm}^{-1}$ ;  $^1\text{H}$  NMR (400 MHz,  $\text{CDCl}_3$ ):  $\delta$  7.17 (dd,  $J = 15.5, 10.9$  Hz, 1H), 6.42 (dd,  $J = 15.1, 10.9$ , 1H), 6.09 (d,  $J = 15.5$  Hz, 1H), 6.02 (dd,  $J = 15.1, 9.8$  Hz), 3.66 (s, 3H), 3.45 (dd,  $J = 7.4, 7.4$  Hz, 1H), 2.55 (t,  $J = 7.5$  Hz, 2H), 2.30 (t,  $J = 7.5$  Hz, 2H), 1.85 (ddd,  $J = 9.7, 7.4, 7.4$  Hz, 1H), 1.65-1.50 (m, 6H), 1.32 (br s, 6H), 1.31-1.23 (m, 1H), 1.01 (t,  $J = 7.4$  Hz, 3H);  $^{13}\text{C}$  NMR (125 MHz,  $\text{CDCl}_3$ ):  $\delta$  201.1, 174.3, 142.2, 141.1, 131.6, 128.0, 51.5, 40.4, 34.1, 31.6, 29.2, 29.1, 29.0, 26.1, 25.0, 24.4, 23.4, 19.8, 13.1; MS (ESI)  $m/z$  385.1379 (M + H)<sup>+</sup> (385.1373 calcd for  $\text{C}_{19}\text{H}_{30}\text{BrO}_3$ ).



**Alcohol 1.52** To a stirred solution of dieneone **1.51** (762 mg, 1.98 mmol) in methanol (15 mL) was added  $\text{CeCl}_3 \cdot 7\text{H}_2\text{O}$  (2.2 g, 6.0 mmol). The resulting mixture

was stirred for 30 min and  $\text{NaBH}_4$  (150 mg, 3.95 mmol) was then added in 3 portions. The resulting solution was stirred for 10 min, quenched with water (10 mL), 2 M HCl (10 drops) and extracted with EtOAc (4 x 30 mL). Combined organic extracts were dried ( $\text{MgSO}_4$ ) and concentrated. Flash column chromatography of the residue (4:1 hexane-

EtOAc) yielded 754 mg (98%) of alcohol **1.52** as a colorless oil and as a mixture of diastereomers: IR (neat) 3455 (br), 2931, 2856, 1737  $\text{cm}^{-1}$ ;  $^1\text{H}$  NMR (400 MHz,  $\text{CDCl}_3$ ):  $\delta$  6.33–6.23 (m, 2H), 5.65–5.51 (m, 2H), 3.66 (s, 3H), 3.38 (dd,t,  $J = 7.49, 7.49$  Hz, 1H), 2.29 (t,  $J = 7.5$  Hz, 2H), 1.75 (ddd,  $J = 9.6, 7.5, 7.5$  Hz, 1H), 1.66–1.45 (m, 9H), 1.31 (s (br), 6H), 1.15 (dddd,  $J = 9.66, 7.36, 7.36, 7.28$  Hz, 1H), 1.00 (t,  $J = 7.5$  Hz, 3H)  $^{13}\text{C}$  NMR (125 MHz,  $\text{CDCl}_3$ ):  $\delta$  174.4, 134.4, 134.3, 132.7, 130.5, 130.4, 130.1, 72.7, 72.5, 51.5, 37.3, 37.3, 34.1, 31.5, 29.4, 29.2, 29.1, 25.4, 25.0, 24.5(3), 24.5(1), 22.6, 19.7, 13.1; MS (ESI)  $m/z$  369.1414, (M+H– $\text{H}_2\text{O}$ ) $^+$  (369.1424 calcd for  $\text{C}_{19}\text{H}_{30}\text{BrO}_2$ ).



**Epoxy alcohols 1.47** To a stirred solution of alcohol **5.52** (150 mg, 0.39 mmol) at 0 °C in dichloromethane (15 mL) was added dimethyl dioxirane as a 0.05 M

solution in acetone (7.75 mL, 0.39 mmol). The resulting solution was stirred for 10 min at 0 °C and concentrated to yielded a colorless oil. Flash column chromatography (3:1-1%  $\text{Et}_3\text{N}$  hexane-EtOAc) yielded a mixture of *syn*-**1.47** and *anti*-**1.47** epoxy alcohols. The *syn* isomers ( $R_f = 0.22$ ; *syn*-**1.47**, 99.5 mg, 64%) proved to be the slower eluting mixture and the faster eluting isomers ( $R_f = 0.31$ ; *anti*-**1.47**, 49.0 mg, 31%) *anti*. Diastereomers were separated by HPLC using a Varian Dynamax 8  $\mu\text{m}$  Si column (2.14 x 25 cm) eluted at a flow rate of 10 mL/min with Hexane/*i*-propanol gradient (1%-->3% IPA) with UV light detection at 205 nm using a Varian 230 detector. Diastereomers *syn*-**1.47a/b** and *anti*-**1.47a/b** were not assigned.

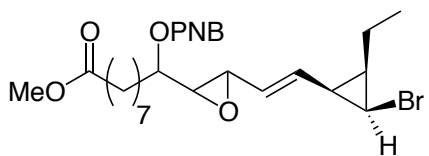
***syn*-1.47a**: 33.2 min;  $^1\text{H}$  NMR (400 MHz,  $\text{CDCl}_3$ ):  $\delta$  5.79 (dd,  $J = 15.5, 9.4$  Hz, 1H), 5.45 (dd,  $J = 15.5, 8.4$  Hz, 1H), 3.84 (m, 1H), 3.66 (s, 3H), 3.49 (dd,  $J = 8.36, 2.28$ , 1H), 3.37 (dd,  $J = 7.4, 7.4$  Hz, 1H), 2.96 (dd,  $J = 2.7, 2.7$  Hz, 1H), 2.30 (t,  $J = 7.5$  Hz, 2H), 1.77

(ddd,  $J = 9.6, 7.6, 7.6$  Hz, 1H), 1.65–1.46 (m, 8H), 1.32 (s(br), 6H), 1.16 (dddd,  $J = 9.8, 9.6, 7.4, 7.4$  Hz, 1H), 1.02 (t,  $J = 7.4$  Hz, 1H);  $^{13}\text{C}$  NMR (150 MHz,  $\text{CDCl}_3$ ): 174.5, 133.0, 130.0, 68.6, 62.8, 55.1, 51.6, 34.2, 33.4, 30.9, 29.9, 29.6, 29.3, 29.2, 25.3, 25.0, 24.4, 22.3, 19.7, 13.2.

***syn-1.47b***: 34.1 min;  $^1\text{H}$  NMR (400 MHz,  $\text{CDCl}_3$ ):  $\delta$  5.78 (dd,  $J = 15.4, 9.4$  Hz, 1H), 5.47 (dd,  $J = 15.4, 8.1$  Hz, 1H), 3.85 (m, 1H), 3.66 (s, 3H), 3.48 (dd,  $J = 8.2, 2.1$  Hz, 1H), 3.37 (dd,  $J = 7.42, 7.42$  Hz, 1H), 2.95 (dd,  $J = 2.64, 2.64$  Hz, 1H), 2.30 (t,  $J = 7.5$  Hz, 2H), 1.77 (ddd,  $J = 9.2, 7.6, 7.6$  Hz, 1H), 1.65–1.45 (m 8H), 1.32 (s(br), 6H), 1.53 (m, 1H), 1.01 (t,  $J = 7.4$  Hz, 3H).  $^{13}\text{C}$  NMR (150 MHz,  $\text{CDCl}_3$ ): 174.5, 132.8, 129.9, 68.5, 62.9, 55.0, 51.6, 34.2, 33.4, 30.9, 29.9, 29.6, 29.3, 29.2, 25.3, 25.0, 24.4, 19.8, 13.1.

***anti-1.47a***: 41.0 min;  $^1\text{H}$  NMR (400 MHz,  $\text{CDCl}_3$ ):  $\delta$  5.77( dd,  $J = 15.4, 9.5$  Hz, 1H), 5.43 (dd,  $J = 15.5, 8.3$  Hz, 1H) 3.66 (s, 3H), 3.52 (m, 1H), 3.39 (dd,  $J = 8.4, 2.2$  Hz, 1H), 3.36 (dd,  $J = 7.5, 7.5$  Hz, 1H), 2.91 (dd,  $J = 4.8, 2.3$  Hz, 1H), 2.30 (t,  $J = 7.5$  Hz, 2H), 1.77 (ddd,  $J = 9.6, 7.4, 7.4$  Hz, 1H), 1.65–1.51 (m, 8H), 1.31 (s(br), 6H), 1.21–1.12 (m, 1H), 1.02 (t,  $J = 7.5$  Hz, 3H);  $^{13}\text{C}$  NMR (125 MHz,  $\text{CDCl}_3$ ): 174.4, 132.9, 129.9, 71.0 63.4 56.9, 51.6, 34.5, 34.2, 30.9, 29.5, 29.3, 29.2, 25.3, 25.0, 24.4, 22.2, 19.7, 13.2.

***anti-1.47b***: 41.9 min;  $^1\text{H}$  NMR (400 MHz,  $\text{CDCl}_3$ ):  $\delta$  5.78 (dd,  $J = 15.5, 9.4$  Hz, 1H), 5.46 (dd,  $J = 15.5, 8.1$  Hz, 1H), 3.66 (s, 3H), 3.53 (m, 1H), 3.39 (dd,  $J = 8.1, 2.3$  Hz, 1H), 3.37 (dd,  $J = 7.4, 7.4$  Hz, 1H), 2.91 (dd,  $J = 4.7, 2.3$  Hz, 1H), 2.30 (t,  $J = 7.5$  Hz, 2H), 1.76 (ddd,  $J = 9.4, 7.4, 7.4$  Hz, 1H), 1.65–1.48 (m, 8H), 1.31 (s(br), 6H), 1.19–1.10 (m, 1H), 1.00 (t,  $J = 7.4$  Hz, 1H).  $^{13}\text{C}$  NMR (125 MHz,  $\text{CDCl}_3$ ): 174.4, 132.8, 129.8, 71.0 63.5 56.8, 51.6, 34.6, 34.2, 30.9, 29.5, 29.3, 29.2, 25.4, 25.0, 24.4, 22.2, 19.7, 13.1.

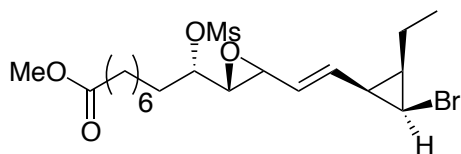


***p*-Nitro benzoate 1.57** To a solution of syn-epoxy alcohols ***syn*-1.47a/b** (182 mg, 0.45 mmol) in THF (4.5 mL) was added PPh<sub>3</sub> (237 mg, 0.90 mmol) and *p*-

nitrobenzoic acid (151 mg, 0.90 mmol). The solution was maintained for 10 min and diisopropylazodicarboxylate (DIAD) was added dropwise. The resulting solution was maintained for 16 h, concentrated in vacuo and the residue purified by flash column chromatography (5:1-1% Et<sub>3</sub>N hexane-EtOAc) to yield 215 mg (86%) of **1.57** as a colorless oil and as a mixture of diastereomers: IR (neat) 2933, 2860, 1729, 1529, 1271 cm<sup>-1</sup>; <sup>1</sup>H NMR (400 MHz CDCl<sub>3</sub>) δ 8.27 (d, *J* = 8.8 Hz, 2H), 8.18 (d, *J* = 8.8 Hz, 2H), 5.71-5.80 (m, 1H), 5.35-5.46 (m, 1H), 5.06-5.13 (m, 1H), 3.63 (s, 3H), 3.42-3.46 (m, 1H), 3.33 (t, *J* = 7.6 Hz, 1H), 3.01-3.05 (m, 1H), 2.26 (t, *J* = 7.6 Hz, 2H), 1.76-1.83 (m, 2H), 1.68-1.75 (m, 1H), 1.57-1.63 (m, 2H), 1.33-1.56 (m, 4H), 1.20-1.30 (m, 6H), 1.04-1.18 (m, 1H), 0.92-1.0 (m, 3H); <sup>13</sup>C NMR (125 MHz, CDCl<sub>3</sub>) δ 193.0, 155.8, 135.2, 31.6, 27.7, 23.3, 20.0, 13.1; MS (ESI) 574.1368 m/z, [(M +Na)<sup>+</sup>, calcd for C<sub>26</sub>H<sub>34</sub>BrNNaO<sub>7</sub>, 574.14].

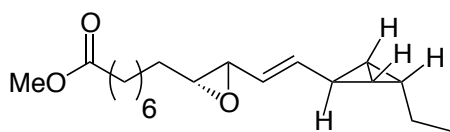
**Methanolysis of 1.57** To a solution of *p*-nitrobenzoate ester **1.57** (44 mg, 0.08 mmol) in MeOH (0.7 mL) was added K<sub>2</sub>CO<sub>3</sub> (11 mg, 0.08 mmol). The resulting solution was stirred for 30 minutes, quenched with saturated ammonium chloride (1 mL) and the aqueous layer extracted with dichloromethane (3 x 5 mL). Combined organic extracts were dried over Na<sub>2</sub>SO<sub>4</sub>, filtered and concentrated in vacuo. Flash column chromatography (4:1-1% Et<sub>3</sub>N hexane:EtOAc) yielded 28 mg (86%) of anti-epoxy alcohol ***anti*-1.47a/b** as a mixture of diastereomers.





**Mesylate 1.53** To a solution of anti-epoxy alcohol *anti*-**1.47a/b** (248 mg, 0.61 mmol) in dichloromethane (20 mL) over activated 4 Å

molecular sieves at 0 °C was added MsCl (0.142 mL, 1.84 mmol). The resulting solution was stirred at that temperature for 5 min and Et<sub>3</sub>N (0.257 mL, 1.84 mmol) was added dropwise. One crystal of 4,4-Dimethylaminopyridine was added and the solution was warmed to room temperature and stirred for 16 h. The resulting solution was diluted with EtOAc (30 mL), washed with 15% NaHCO<sub>3</sub> (15 mL) and extracted EtOAc (3 x 30 mL). Combined organic extracts were dried over Na<sub>2</sub>SO<sub>4</sub>, filtered and concentrated in vacuo. Flash column chromatography (3:1-1% Et<sub>3</sub>N hexane-EtOAc) to yield mesylate **1.53** as a light yellow oil and as a mixture of diastereomers (165.1 mg, 0.34 mmol, 56%): IR (neat) 2934, 1736, 1359, 1175, 925 cm<sup>-1</sup>; <sup>1</sup>H NMR (400 MHz CDCl<sub>3</sub>) δ 5.80 (dd, *J* = 15.2, 9.2 Hz, 1H), 5.40 (dd, *J* = 15.2, 8.4 Hz, 1H), 4.63-4.57 (m, 1H), 3.65 (s, 3H), 3.60-3.45 (m, 1H), 3.38-3.33 (m, 1H), 3.10-3.00 (m, 3H), 2.99-2.96 (m, 1H), 2.28 (t, *J* = 7.6 Hz, 2H), 1.71-1.78 (m, 3H), 1.39-1.63 (m, 6H), 1.21-1.35 (m, 6H), 1.10-1.20 (m, 1H), 0.96-1.03 (m, 3H); <sup>13</sup>C NMR (125 MHz, CDCl<sub>3</sub>) δ 174.3, 133.8, 133.6, 129.0, 128.8, 80.3, 60.0, 59.9, 56.6, 51.6, 38.9, 38.8, 34.1, 32.2, 30.8, 29.1(1), 29.0(5), 24.9, 24.7, 24.5, 24.4, 22.2, 19.7, 13.1; MS (ESI) 521.1176 m/z, [(M+Na+H<sub>2</sub>O)+, calcd for C<sub>20</sub>H<sub>35</sub>BrNaO<sub>7</sub>S, 521.12].



**Bicyclobutane 1.1** To a solution of mesylate **1.53** (53.7 mg, 0.11 mmol) in THF (2.0 mL) and water (2.79 mL) was added LiOH (117 mg, 2.79 mmol) at

room temperature. The resulting solution was warmed to 60 °C, stirred for 2.5 h, cooled to room temperature, diluted with EtOAc (20 mL), and washed with saturated NH<sub>4</sub>Cl (5

mL). The aqueous layer was extracted with EtOAc (4x 20 mL). Combined organic extracts were dried (Na<sub>2</sub>SO<sub>4</sub>) and concentrated in vacuo. Resulting oil was concentrated from benzene (3 x 5 mL) in vacuo, the residue dissolved in THF (14 mL) and the cooled to -78 °C. A solution of *t*-BuLi (1.50 M in pentane, 0.297 mL, 0.45 mmol) was added dropwise to the solution of crude carboxylic acid. The reaction mixture was stirred at -78 °C for 2 h, warmed to -20 °C and stirred an additional 30 min. The mixture was warmed to 0 °C and quenched with saturated NH<sub>4</sub>Cl (0.2 mL). An ethereal solution of diazomethane (7 mL, ~0.25 M) was added and the mixture was stirred an additional 5 min, diluted with H<sub>2</sub>O (10 mL) and extracted with EtOAc (4 x 20 mL). The combined organic extracts were dried over Na<sub>2</sub>SO<sub>4</sub>, filtered and concentrated in vacuo to yield a faint yellow oil (38 mg crude yield). The crude material was purified on RP-HPLC using a Varian microsorb-mv 4.6 x 250 mm column eluting with 85:15 (MeOH:H<sub>2</sub>O) + 20 mM Et<sub>3</sub>N at pH=8 at 0.5 mL/min with a UV detector at 205 nm. Aqueous fractions containing product were extracted with freshly distilled n-pentane (5 x 5 mL) and concentrated to yield 6.87 mg (20.3%) of **1.1** as a colorless oil: Retention time 27 min; <sup>1</sup>H NMR (400 MHz, C<sub>6</sub>D<sub>6</sub>) δ 5.41 (dd, *J* = 8.0, 15.6 Hz, 1H), 5.34 (dd, *J* = 7.2, 15.6 Hz, 1H), 3.37 (s, 3H), 2.93 (dd, *J* = 2.0, 6.8 Hz, 1H), 2.64 (dt, *J* = 2, 5.6 Hz, 1H), 2.34 (d, *J* = 8.0 Hz, 1H), 2.11 (t, *J* = 7.6 Hz, 2H), 1.92 (m, 1H), 1.49-1.58 (m, 2H), 1.23-1.42 (m, 6H), 1.06-1.19 (m, 8H), 0.87 (t, *J* = 7.6 Hz, 3H); <sup>13</sup>C NMR (150 MHz, C<sub>6</sub>D<sub>6</sub>) δ 173.4, 132.8, 128.6, 60.4, 58.0, 51.0, 45.7, 44.6, 34.1, 32.4, 29.5(3), 29.4(8), 26.2, 25.2, 17.1, 13.6, 9.4, 9.3

## References

1. Funk, C. Prostaglandins and leukotrienes: advances in eicosanoid biology. *Science* **2001**, 1871.

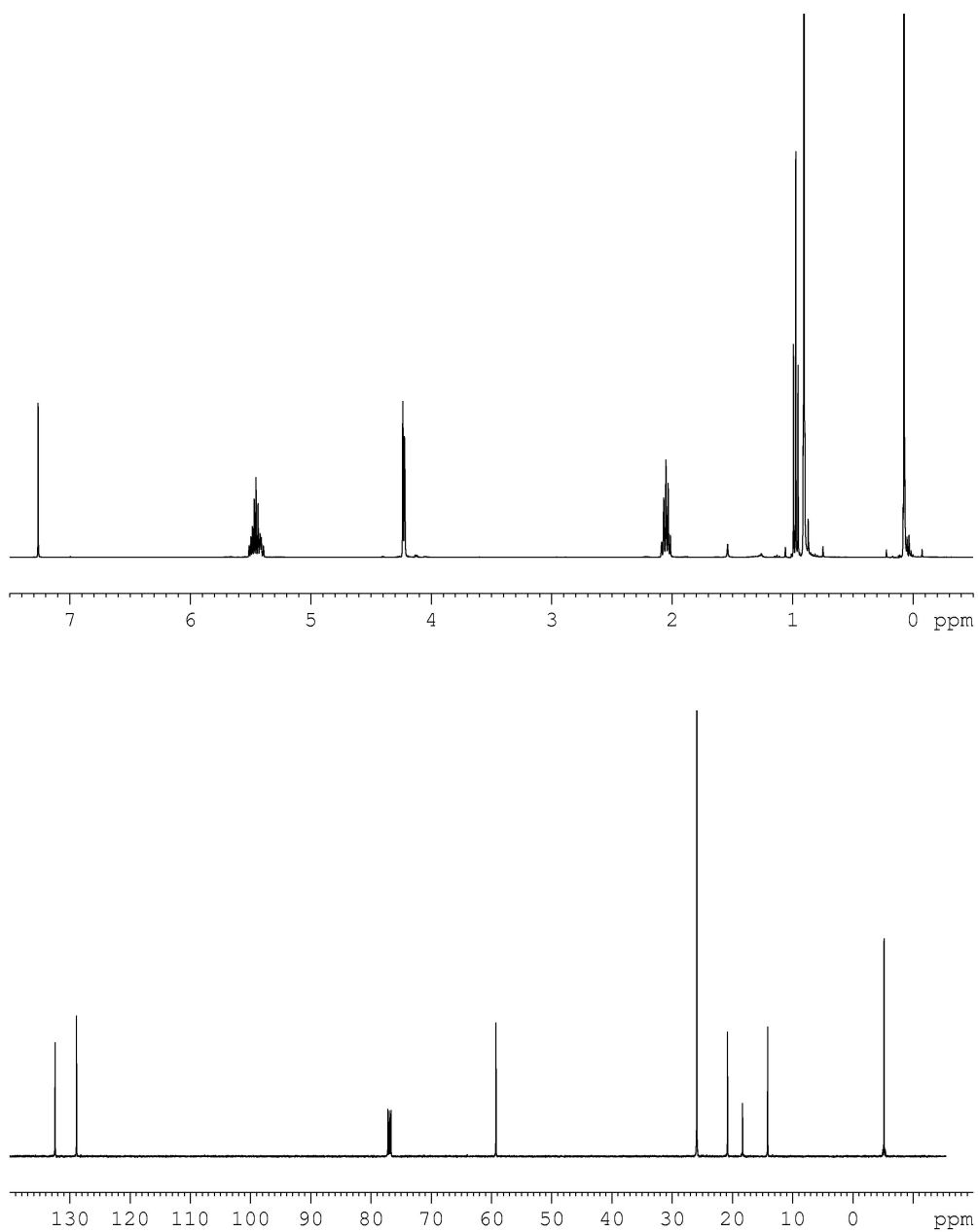
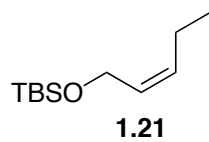
2. Corey, E. J.; Ensley, H. E.; Hamberg, M.; Samuelsson, B. Disparate pathways of prostaglandin biosynthesis in coral and mammalian systems. *J. Chem. Soc., Chem. Commun.* **1975**, 277–278.
3. Koljak, R.; Boutaud, O.; Shieh, B.; Samel, N.; Brash, A. R. Identification of a Naturally Occurring Peroxidase-Lipoxygenase Fusion Protein. *Science* **1997**, *277*, 1994–1996.
4. Järving, R.; Järving, I.; Kurg, R.; Brash, A. R.; Samel, N. On the evolutionary origin of cyclooxygenase (COX) isozymes: characterization of marine invertebrate COX genes points to independent duplication events in vertebrate and invertebrate lineages. *J. Bio. Chem.* **2004**, *279*, 13624–33.
5. Schneider, C.; Niisuke, K.; Boeglin, W. E.; Voehler, M.; Stec, D. F.; Porter, N. a; Brash, A. R. Enzymatic synthesis of a bicyclobutane fatty acid by a hemoprotein lipoxygenase fusion protein from the cyanobacterium *Anabaena* PCC 7120. *Proc. Nat. Acad. Sci. USA*, **2007**, *104*, 18941–5.
6. Mosblech, A.; Feussner, I.; Heilmann, I. Oxylipins: structurally diverse metabolites from fatty acid oxidation. *Plant Physiol. Biochem.* **2009**, *47*, 511–7.
7. Hamberg, M.; Gardner, H. Oxylipin pathway to jasmonates: biochemistry and biological significance. *Biochimica et Biophysica Acta: Lipids and Lipid Metabolism*, **1992**, *5*.
8. Jensen, E. C.; Ogg, C.; Nickerson, K. W. Lipoxygenase inhibitors shift the yeast/mycelium dimorphism in *Ceratocystis ulmi*. *Appl. Environ. Microbiol.*, **1992**, *58*, 2505–8.
9. Horowitz Brown, S.; Zarnowski, R.; Sharpee, W. C.; Keller, N. P. Morphological transitions governed by density dependence and lipoxygenase activity in *Aspergillus flavus*. *Appl. Environ. Microbiol.*, **2008**, *74*, 5674–85.
10. Cantrell, C. L.; Case, B. P.; Mena, E. E.; Kniffin, T. M.; Duke, S. O.; Wedge, D. E. Isolation and identification of antifungal fatty acids from the basidiomycete *Gomphus floccosus*. *J. Agric. Food Chem.* **2008**, *56*, 5062–8.
11. Champe, S. P.; El-Zayat, A. A. Isolation of a sexual sporulation hormone from *Aspergillus nidulans*. *J. Bacteriol.*, **1989**, *171*, 3982–8.
12. Lion, U.; Wiesemeier, T.; Weinberger, F.; Beltrán, J.; Flores, V.; Faugeron, S.; Correa, J.; Pohnert, G. Phospholipases and galactolipases trigger oxylipin-mediated

- wound-activated defence in the red alga *Gracilaria chilensis* against epiphytes. *Chem. Bio. Chem.*, **2006**, *7*, 457–62.
13. Andreou, A.; Brodhun, F.; Feussner, I. Biosynthesis of oxylipins in non-mammals. *Prog. Lipid Res.*, **2009**, *48*, 148–70.
  14. Porta, H.; Rocha-Sosa, M. Lipoxygenase in bacteria: a horizontal transfer event? *Microbiol.*, **2001**, *147*, 3199–200.
  15. Scott, J. J.; Oh, D.; Yuceer, M. C.; Klepzig, K. D.; Clardy, J.; Currie, C. R. Bacterial protection of beetle-fungus mutualism. *Science*, **2008**, *322*, 63.
  16. Wiberg, K. B.; Lampman, G. M.; Ciula, R. P.; Connor, D. S.; Schertler, P.; Lavanish, J. Bicyclo[1.1.0]butane. *Tetrahedron* **1965**, *21*, 2749–2769.
  17. Haller, I.; Srinivasan, R. Vibrational Spectra and Molecular Structure of Bicyclo[1.1.0]butane. *J. Chem. Phys.*, **1964**, *41*, 2745.
  18. Walczak, M. A. A.; Wipf, P. Rhodium(I)-catalyzed cycloisomerizations of bicyclobutanes. *J. Am. Chem. Soc.*, **2008**, *130*, 6924–5.
  19. Schulman, J. M.; Fisanick, G. J. New model for the bonding in bicyclobutanes. *J. Am. Chem. Soc.*, **1970**, *92*, 6653–6654.
  20. Closs, G. L.; Closs, L. E. Carbon Orbital Hybridizations and Acidity of the Bicyclobutane System. *J. Am. Chem. Soc.* **1963**, *85*, 2022–23.
  21. Pomerantz, M.; Abrahamson, E. W. The Electronic Structure and Reactivity of Small Ring Compounds. I. Bicyclobutane. *J. Am. Chem. Soc.* **1966**, *88*, 3970–72.
  22. Masamune, S. Strained systems. III. Bond cleavage reactions of tricyclo[1,1,1,0,4,5]pentane and tricyclo[2,1,1,0,5,6]hexane systems. *Tetrahedron Lett.*, **1965**, *6*, 945–951.
  23. Woodward, R. B.; Dalrymple, D. L. Dimethyl 1,3-diphenylbicyclobutane-2,4-dicarboxylates. *J. Am. Chem. Soc.*, **1969**, *91*, 4612–4613.
  24. Wiberg, K. B.; Ciula, R. P. Ethyl Bicyclo[1.1.0]butane-1-carboxylate. *J. Am. Chem. Soc.*, **1959**, *81*, 5261–5262.
  25. Srinivasa, R. A Simple Synthesis of Bicyclo[1.1.0]butane and its Relation to the Internal Conversion of Electronic Energy in 1,3-Butadiene. *J. Am. Chem. Soc.*, **1963**, *85*, 4045–46.

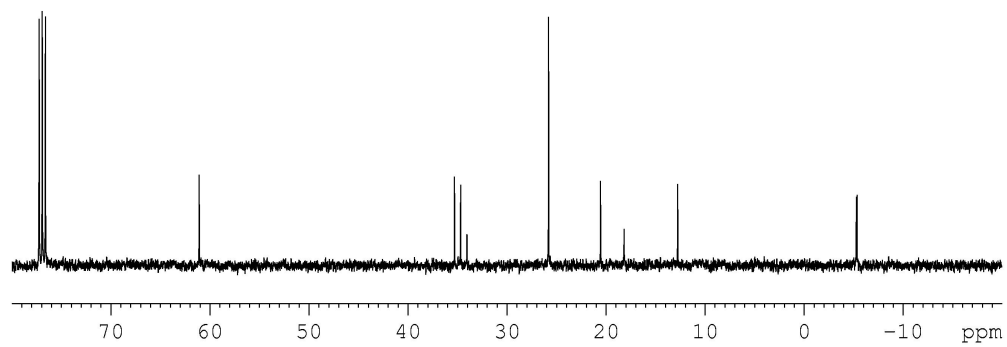
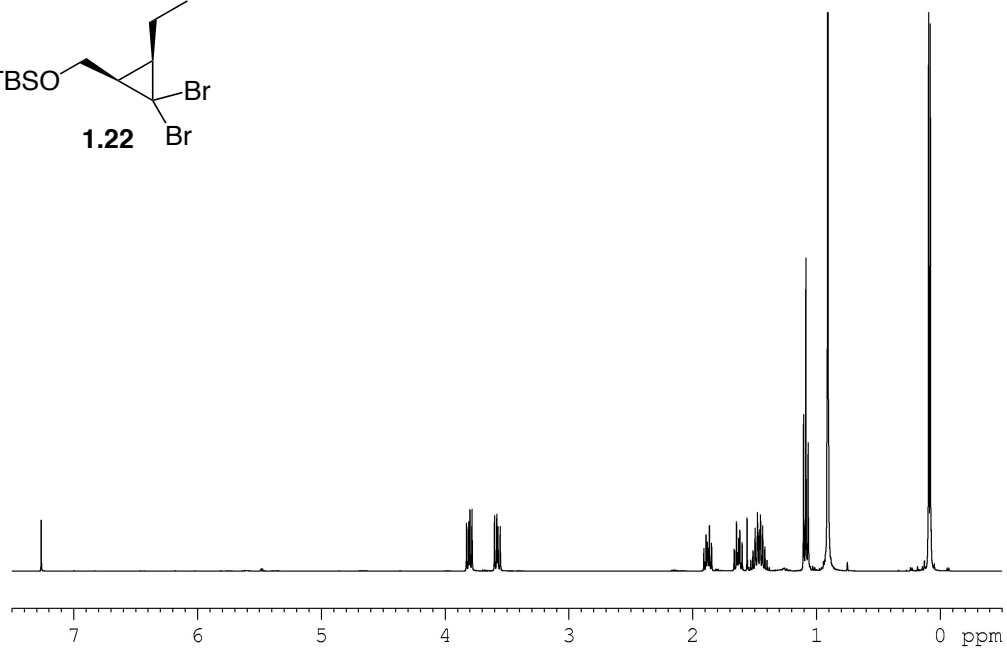
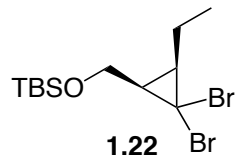
26. Nilsen, N. O.; Skattebøl, L.; Baird, M. S.; Buxton, S. R.; Slowey, P. D. A simple route to 1-bromobicyclo[1.1.0]butanes by intramolecular trapping of 1-bromo-1-lithiocyclopropanes. *Tetrahedron Lett.*, **1984**, *25*, 2887–2890.
27. von E. Doering, W.; Coburn, J. F. 1, 3-dimethylbicyclo[1.1.0]butane. *Tetrahedron Lett.*, **1965**, *6*, 991–995.
28. Wipf, P.; Stephenson, C. R. J.; Okumura, K. Transition-metal-mediated cascade reactions: C,C-dicyclopropylmethylamines by way of double C,C-sigma-bond insertion into bicyclobutanes. *J. Am. Chem. Soc.*, **2003**, *125*, 14694–5.
29. Kelly, C. B.; Colthart, A. M.; Constant, B. D.; Corning, S. R.; Dubois, L. N. E.; Genovese, J. T.; Radziewicz, J. L.; Sletten, E. M.; Whitaker, K. R.; Tilley, L. J. Enabling the synthesis of perfluoroalkyl bicyclobutanes via 1,3  $\gamma$ -silyl elimination. *Org. Lett.*, **2011**, *13*, 1646–9.
30. Bentley, T. W.; Engels, B.; Hupp, T.; Bogdan, E.; Christl, M. Unsubstituted bicyclo[1.1.0]but-2-ylcarbinylium cations. *J. Org. Chem.*, **2006**, *71*, 1018–26.
31. Parikh, J. R.; Doering, W. v. E. Sulfur trioxide in the oxidation of alcohols by dimethyl sulfoxide. *J. Am. Chem. Soc.* **1967**, *89*, 5505–07.
32. Corey, E. J.; Chaykovsky, M. Dimethyloxosulfonium Methylide and Dimethylsulfonium Methylide. Formation and Application to Organic Synthesis. *J. Am. Chem. Soc.* **1965**, *87*, 1343–64.
33. Miura, K.; Ichinose, Y.; Nozaki, K.; Fugami, K.; Oshima, K.; Utimoto, K. Triethylborane-induced hydrodehalogenation of organic halides by tin hydrides. *Bull. Chem. Soc. Jpn.* **1989**, *62*, 143–147.
34. Sadhu, K. M.; Matteson, D. S. (Chloromethyl) lithium in an efficient conversion of carbonyl compounds to chlorohydrins or oxiranes. *Tetrahedron Lett.* **1986**, *27*, 795–798.
35. Schreiber, S. L.; Claus, R. E.; Reagan, J. Ozonolytic cleavage of cycloalkenes to terminally differentiated products. *Tetrahedron Lett.* **1982**, *23*, 3867–3870.
36. Aggarwal, V. K.; Richardson, J. The complexity of catalysis: origins of enantio- and diastereocontrol in sulfur ylide mediated epoxidation reactions. *Chem. Comm.* **2003**, 2644.
37. Illa, O.; Arshad, M.; Ros, A.; McGarrigle, E. M.; Aggarwal, V. K. Practical and highly selective sulfur ylide mediated asymmetric epoxidations and aziridinations

- using an inexpensive, readily available chiral sulfide. Applications to the synthesis of quinine and quinidine. *J. Am. Chem. Soc.* **2010**, *132*, 1828–30.
38. Aggarwal, V. K.; Abdel-Rahman, H.; Jones, R. V. H.; Standen, M. C. H. A novel catalytic cycle for the synthesis-of epoxides using sulfur ylides: Application to base sensitive aldehydes. *Tetrahedron Lett.* **1995**, *36*, 1731–1732.
  39. Newman, M. S.; Magerlein, B. J. *Org. React.*, **1949**, *5*, 413.
  40. Delamarche, I.; Mosset, P. New Syntheses of Some Functionalized and Acetylenic  $\beta$ -Keto Phosphonates. *J. Org. Chem.* **1994**, *59*, 5453–5457.
  41. Nakata, T.; Tanaka, T.; Oishi, T. Highly stereoselective synthesis of  $\alpha$ ,  $\beta$ -epoxy alcohols by the reduction of  $\alpha$ ,  $\beta$ -epoxy ketones with zinc borohydride. *Tetrahedron Lett.* **1981**, *22*, 4723–4726.
  42. Luche, J. L. Lanthanides in organic chemistry. 1. Selective 1,2 reductions of conjugated ketones. *J. Am. Chem. Soc.* **1978**, *100*, 2226–2227.
  43. Adam, W.; Curci, R.; Edwards, J. O. Dioxiranes: a new class of powerful oxidants. *Acc. Chem. Res.* **1989**, *22*, 205–211.
  44. Curci, R.; Dinoi, A.; Rubino, M. F. Dioxirane oxidations: Taming the reactivity-selectivity principle. *Pure & Appl. Chem.* **1995**, *67*, 811.
  45. Hamberg, M.; Herman, R. P.; Jacobsson, U. Stereochemistry of two epoxy alcohols from *saprolegnia parasitica*. *BBA-Lipids Lipid Met.* **1986**, *879*, 410–418.
  46. Mercier, J.; Agoh, B. Comportement d'hydroperoxydes allyliques a longue chaine en presence de complexes de certains metaux de transition. *Chem. Phys. of Lipids* **1974**, *12*, 239–248.
  47. DeGuire, S. M.; Ma, S.; Sulikowski, G. A. Synthesis of a Bicyclobutane Fatty Acid Identified from the Cyanobacterium *Anabaena* PCC 7120. *Angew. Chem. Int. Ed. Engl.* **2011**, *50*, 9940–9942.
  48. Still, W. C.; Kahn, M.; Mitra, A. Rapid chromatographic technique for preparative separations with moderate resolution. *J. Org. Chem.* **1978**, *43*, 2923–2925.

## Spectra Relevant to Chapter 1

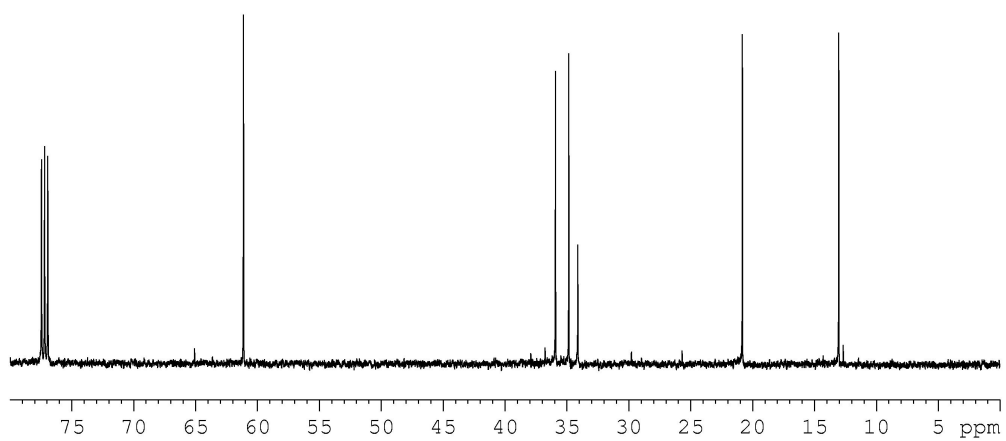
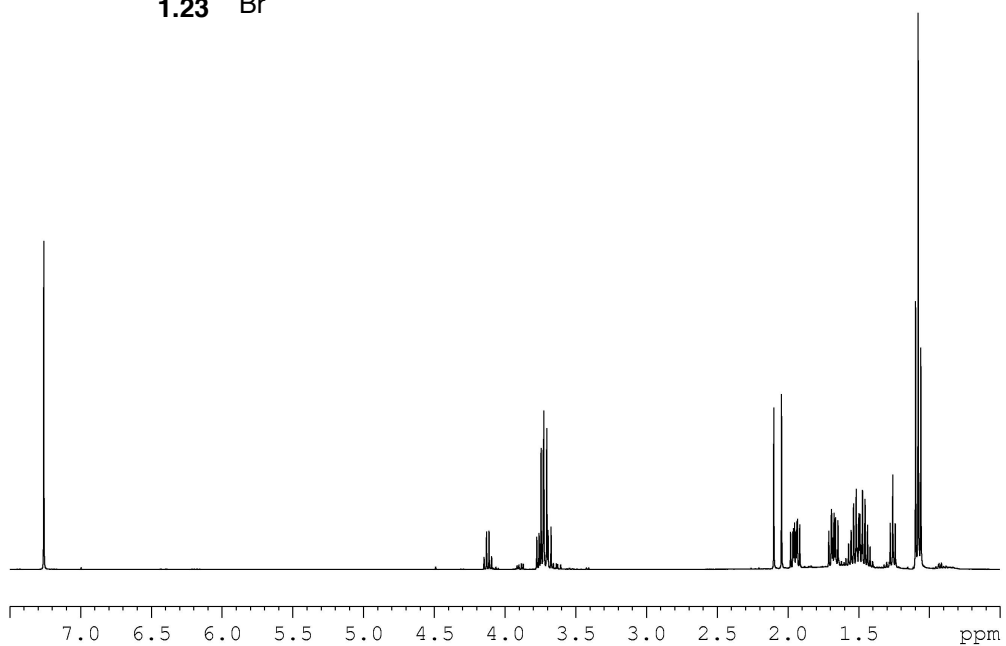
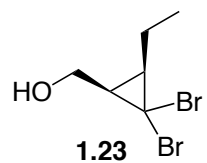


**Spectra I-1:** The 400 MHz  $^1\text{H}$  and 125 MHz  $^{13}\text{C}$  NMR spectra of **1.21** in  $\text{CDCl}_3$ .

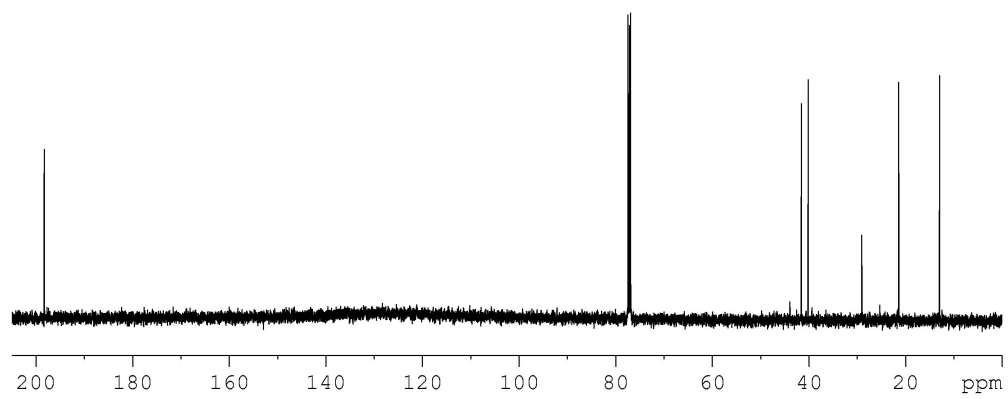
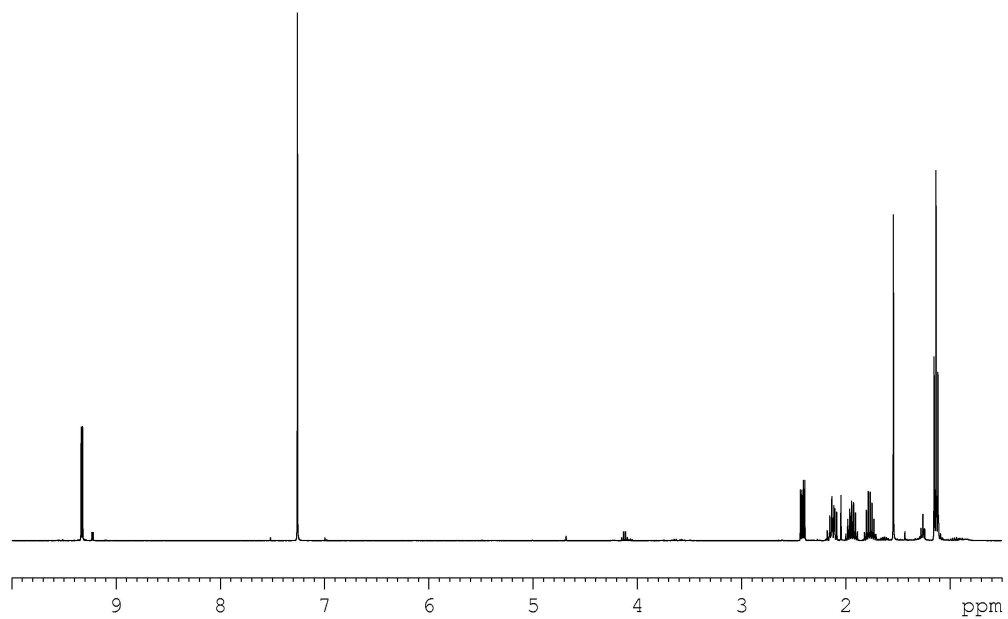
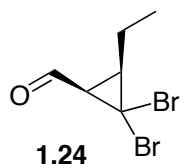


**Spectra I-2:** The 400 MHz  $^1\text{H}$  and 125 MHz  $^{13}\text{C}$  NMR spectra of **1.22** in  $\text{CDCl}_3$ .

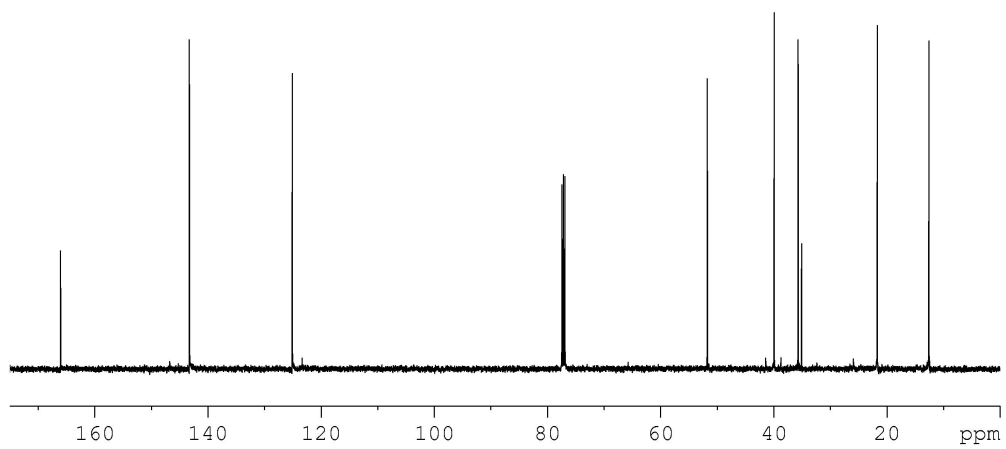
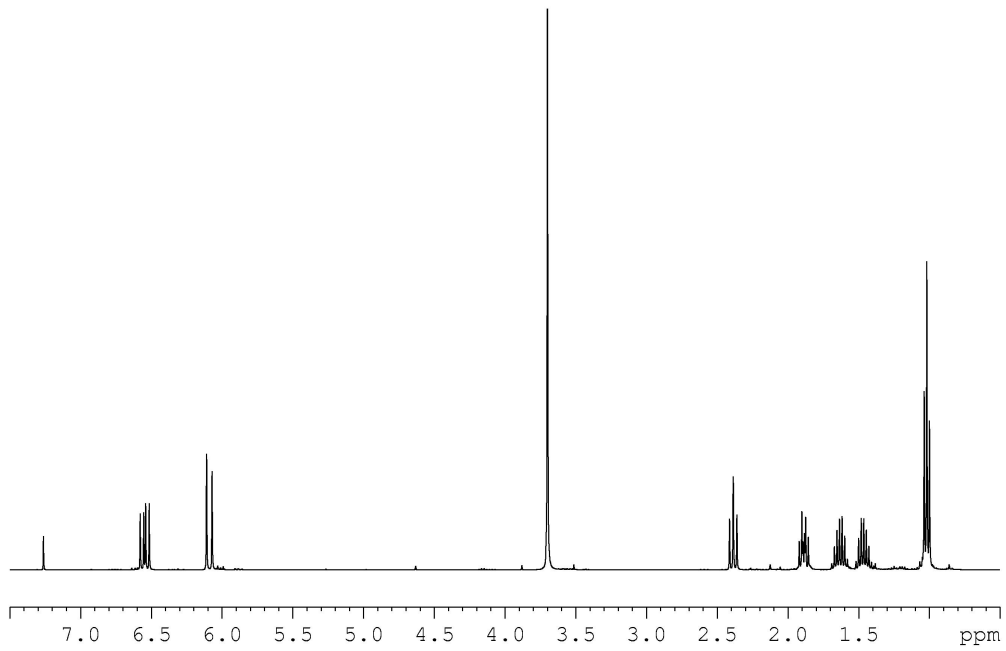
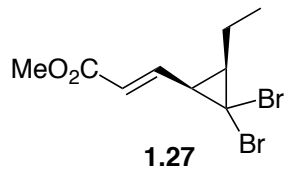




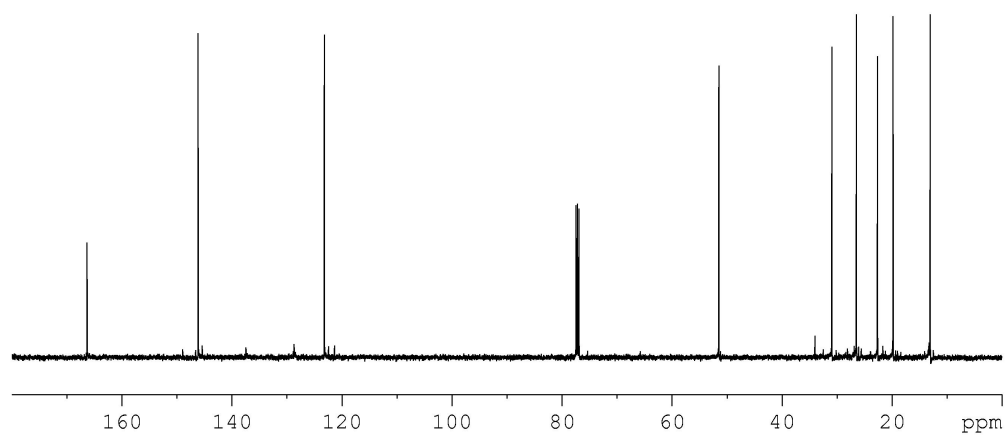
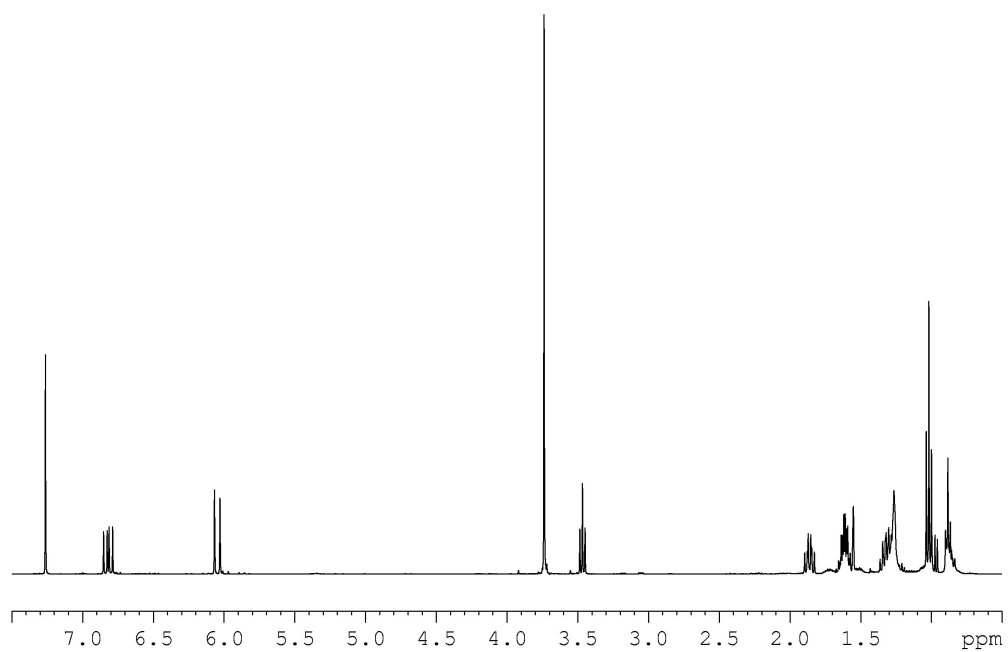
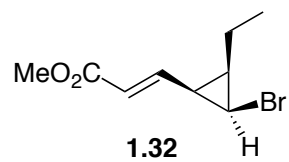
**Spectra I-3:** The 400 MHz  $^1\text{H}$  and 125 MHz  $^{13}\text{C}$  NMR spectra of **1.23** in  $\text{CDCl}_3$ .



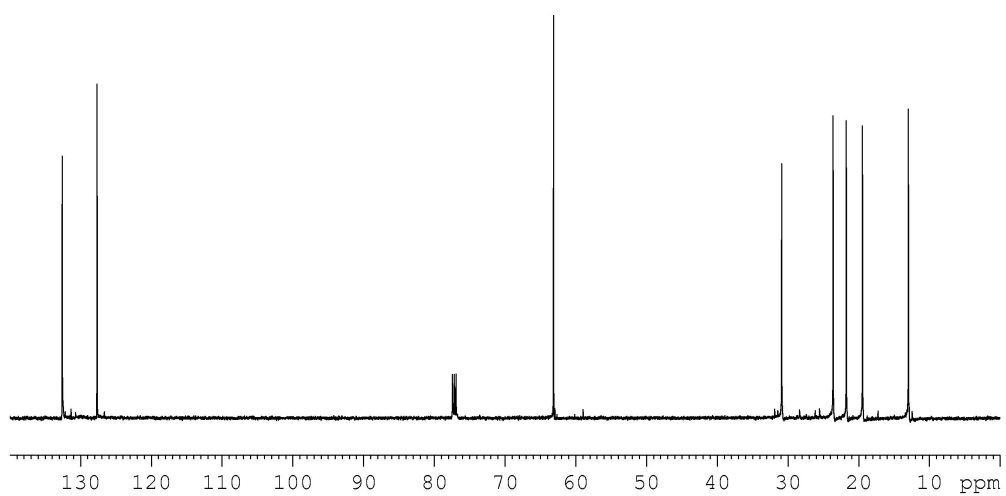
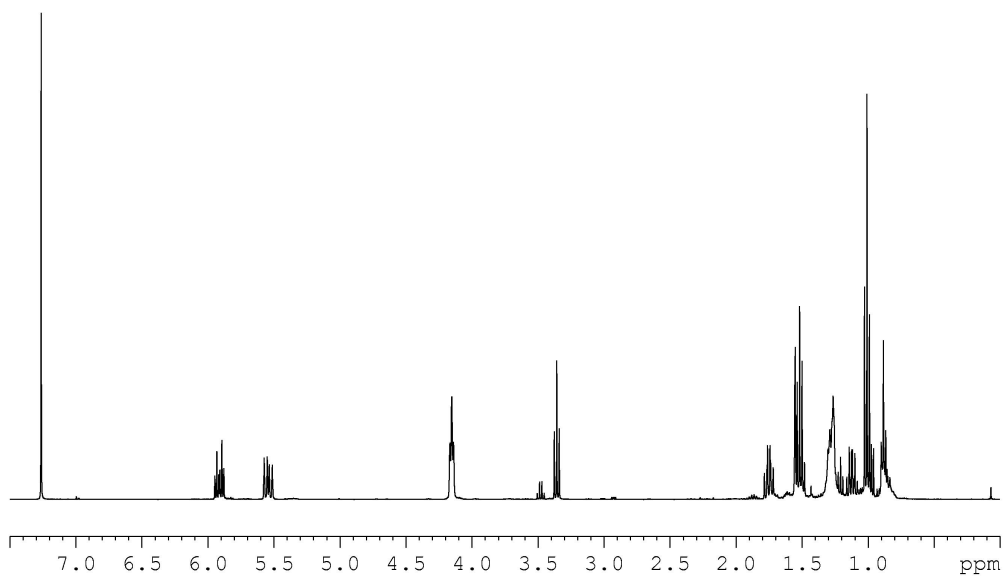
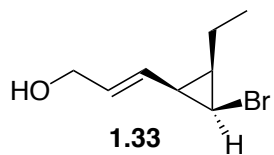
**Spectra I-4:** The 400 MHz  $^1\text{H}$  and 125 MHz  $^{13}\text{C}$  NMR spectra of **1.24** in  $\text{CDCl}_3$ .



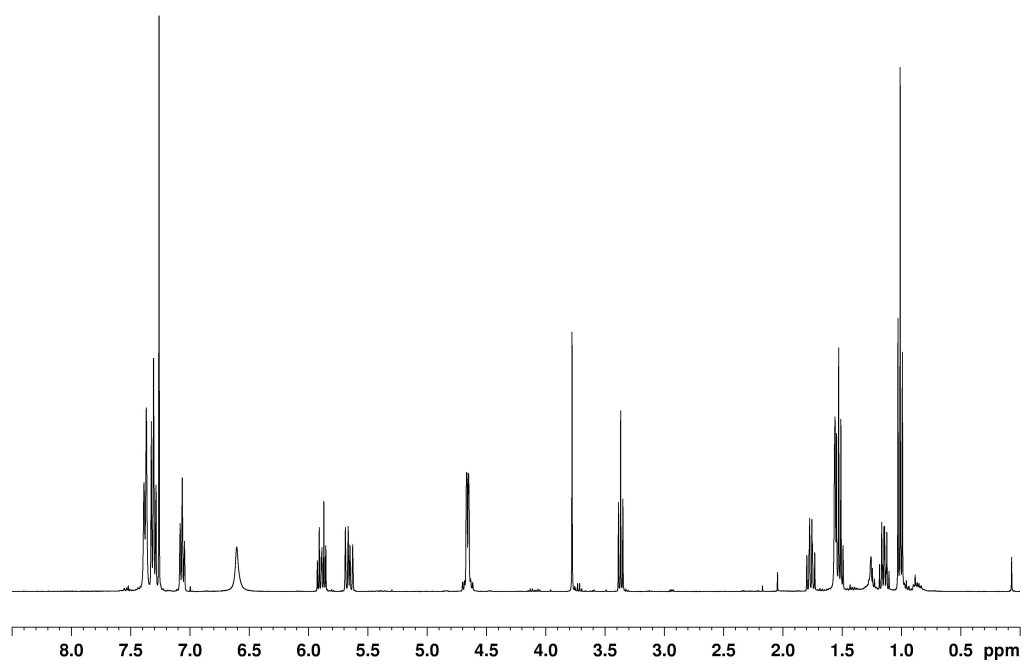
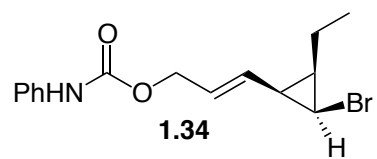
**Spectra I-5:** The 400 MHz  $^1\text{H}$  and 125 MHz  $^{13}\text{C}$  NMR spectra of **1.27** in  $\text{CDCl}_3$ .



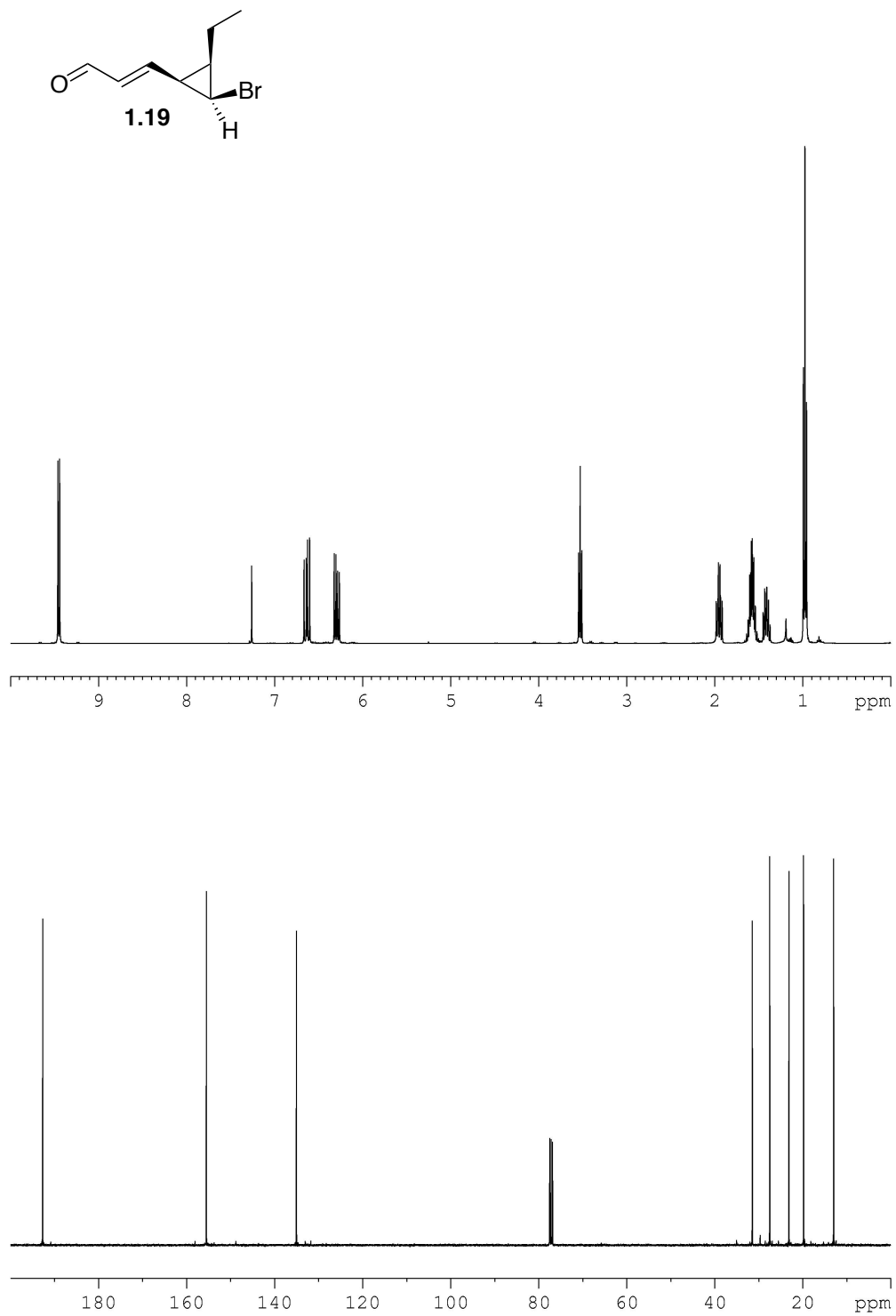
**Spectra I-6:** The 400 MHz  $^1\text{H}$  and 125 MHz  $^{13}\text{C}$  NMR spectra of **1.32** in  $\text{CDCl}_3$ .



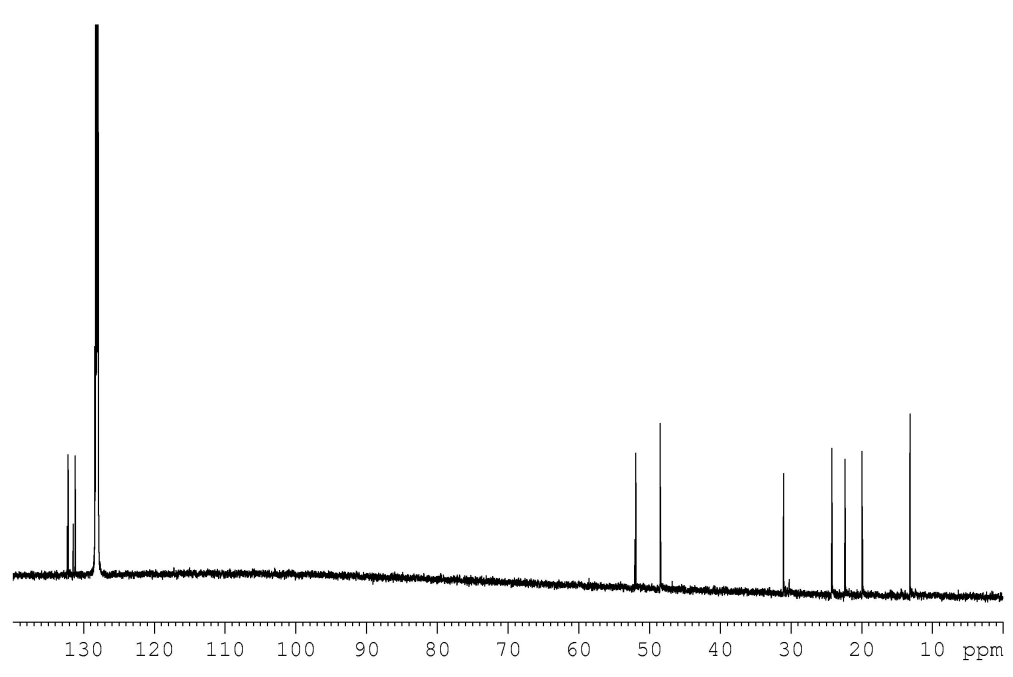
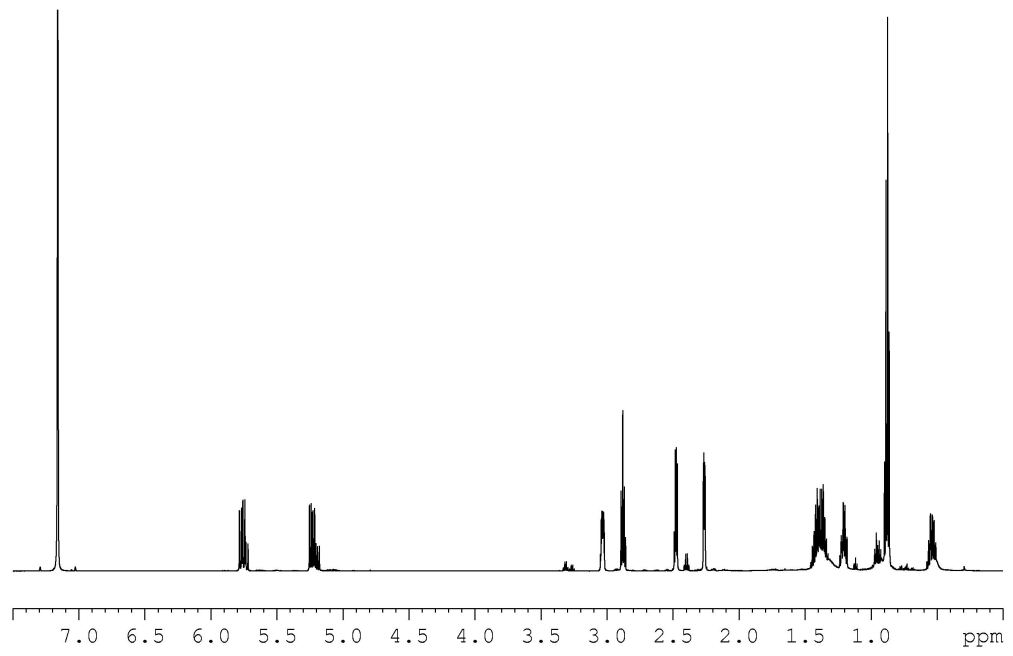
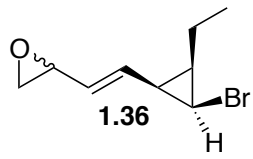
**Spectra I-7:** The 400 MHz  $^1\text{H}$  and 125 MHz  $^{13}\text{C}$  NMR spectra of **1.33** in  $\text{CDCl}_3$ .



**Spectra I-8:** The 400 MHz  $^1\text{H}$  spectra of **1.34** in  $\text{CDCl}_3$ .

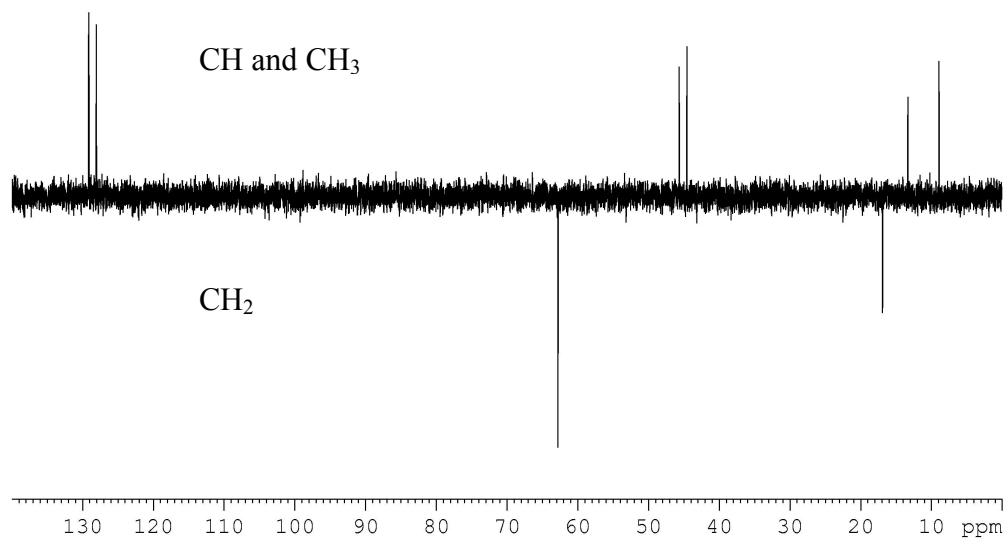
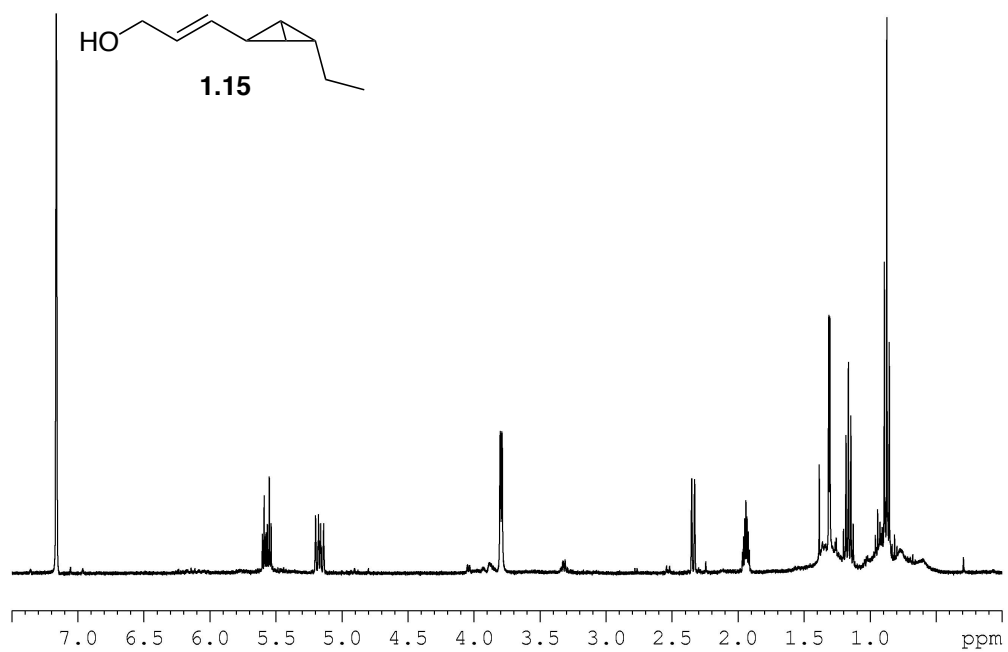


**Spectra I-9:** The 400 MHz  $^1\text{H}$  and 100 MHz  $^{13}\text{C}$  NMR spectra of **1.19** in  $\text{CDCl}_3$ .

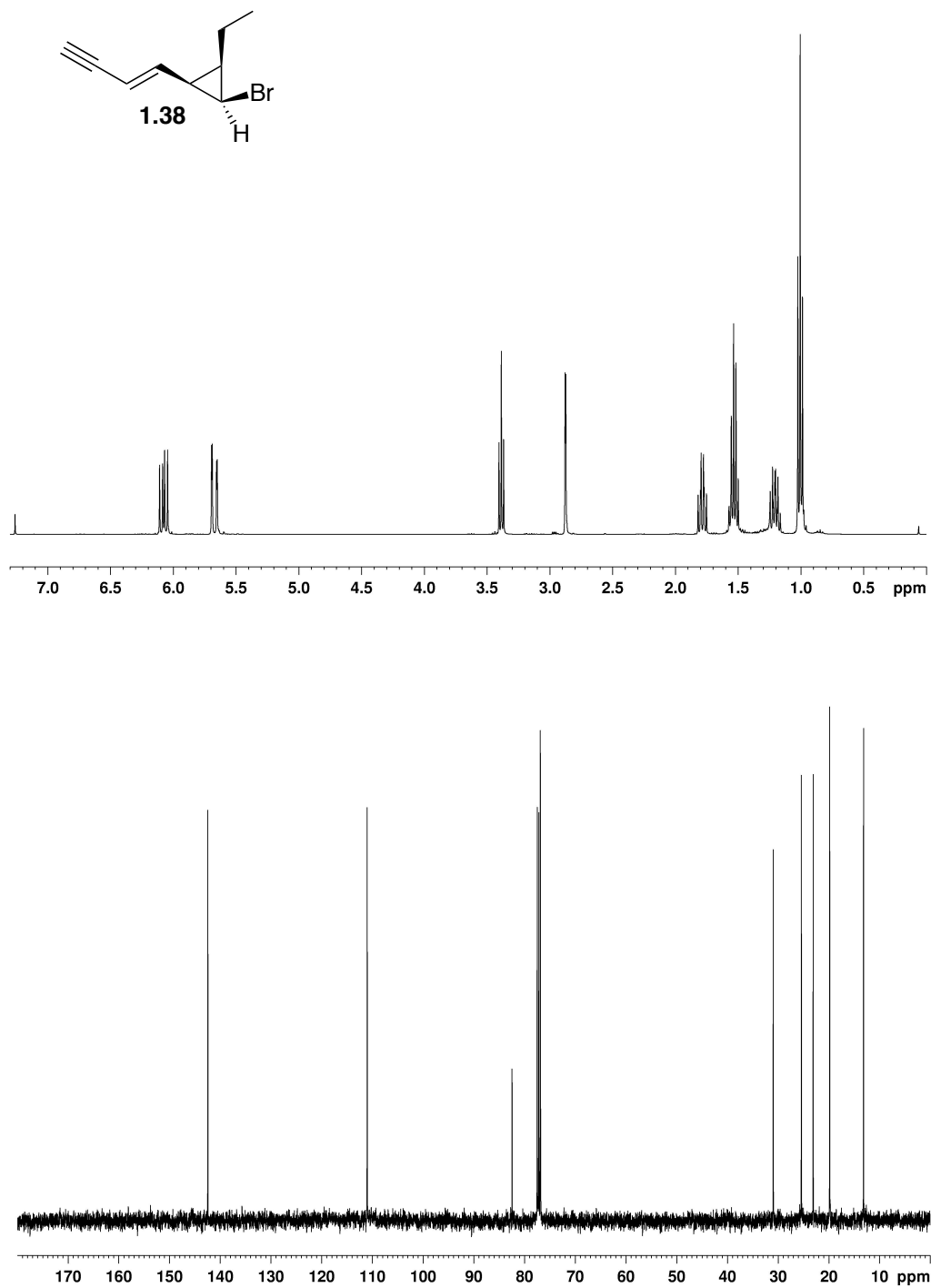


Spectra I-10: The 600 MHz  $^1\text{H}$  and 150 MHz  $^{13}\text{C}$  NMR spectra of **1.36** in  $\text{C}_6\text{D}_6$ .

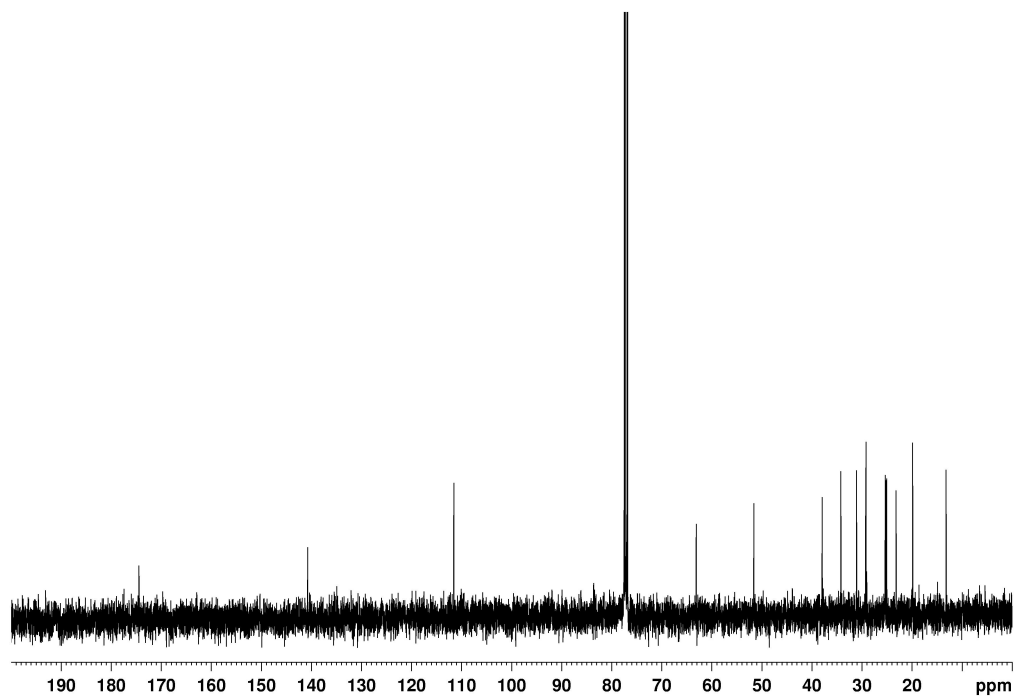
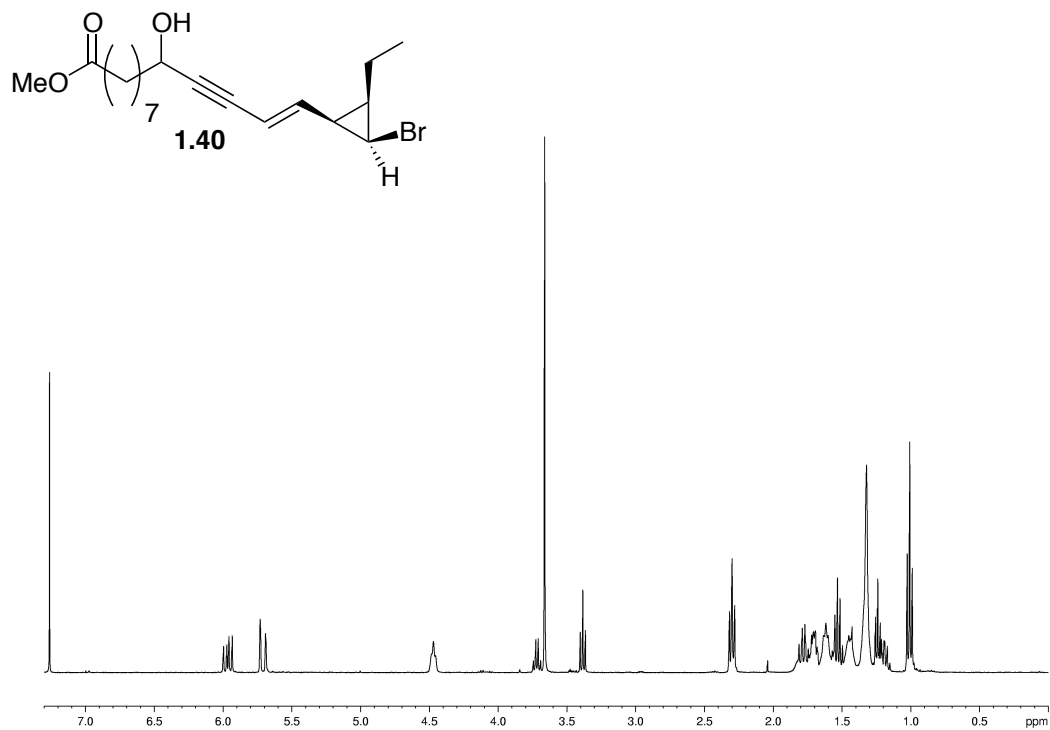




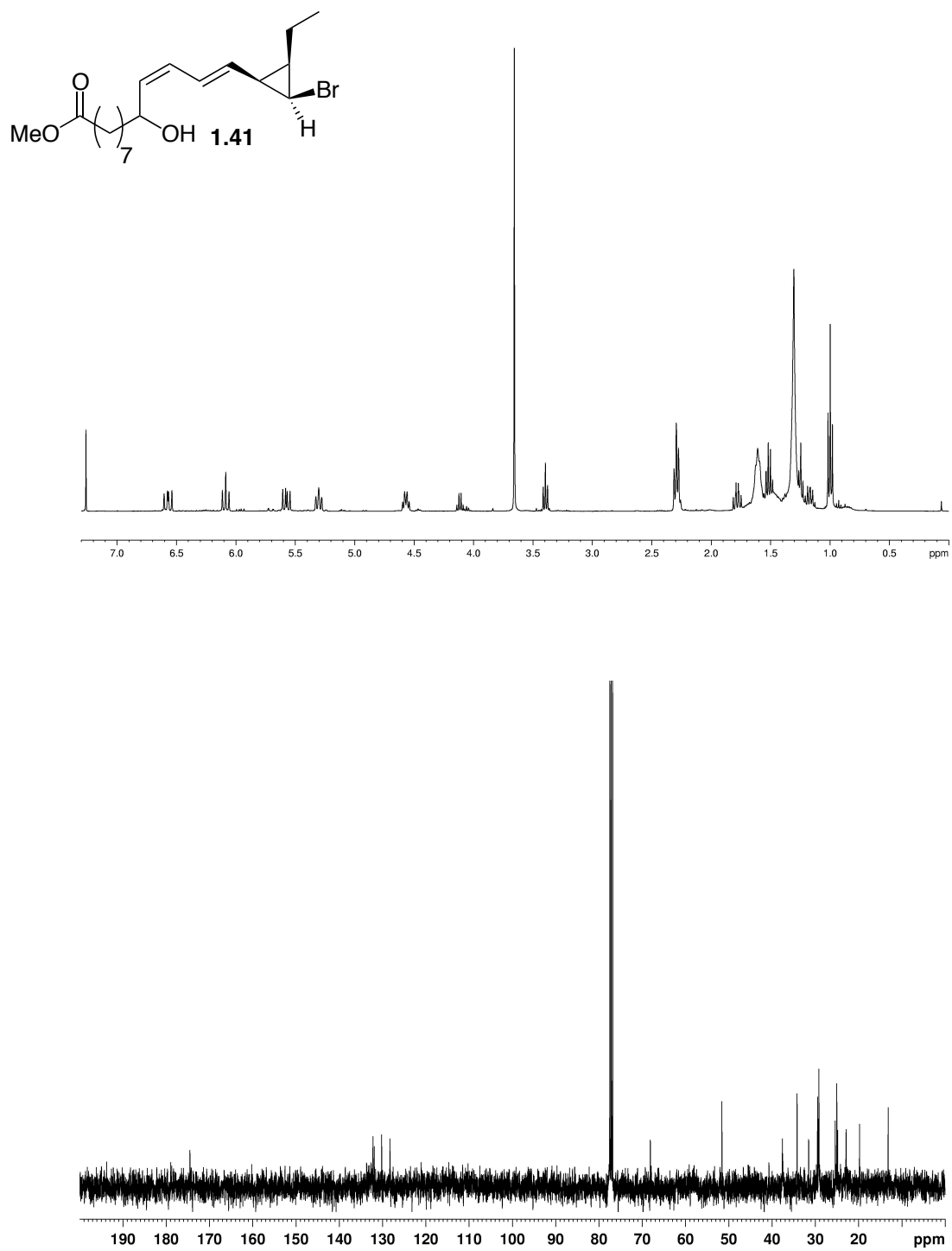
**Spectra I-11:** The 400 MHz  $^1\text{H}$  and 100 MHz  $^{13}\text{C}$  DEPT135 NMR spectra of **1.15** in  $\text{C}_6\text{D}_6$ .



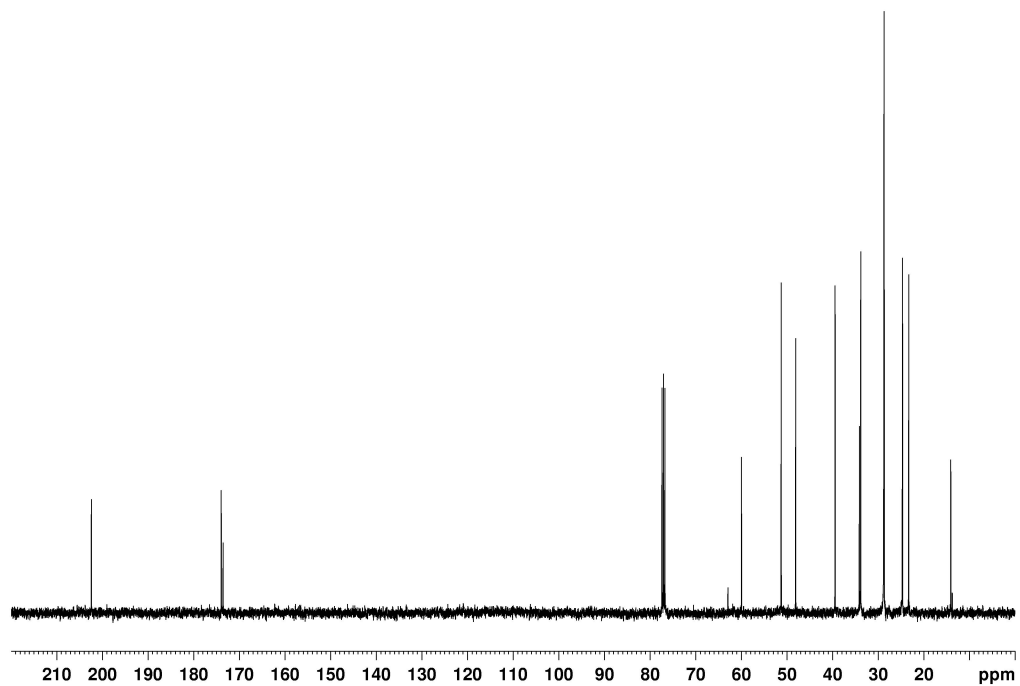
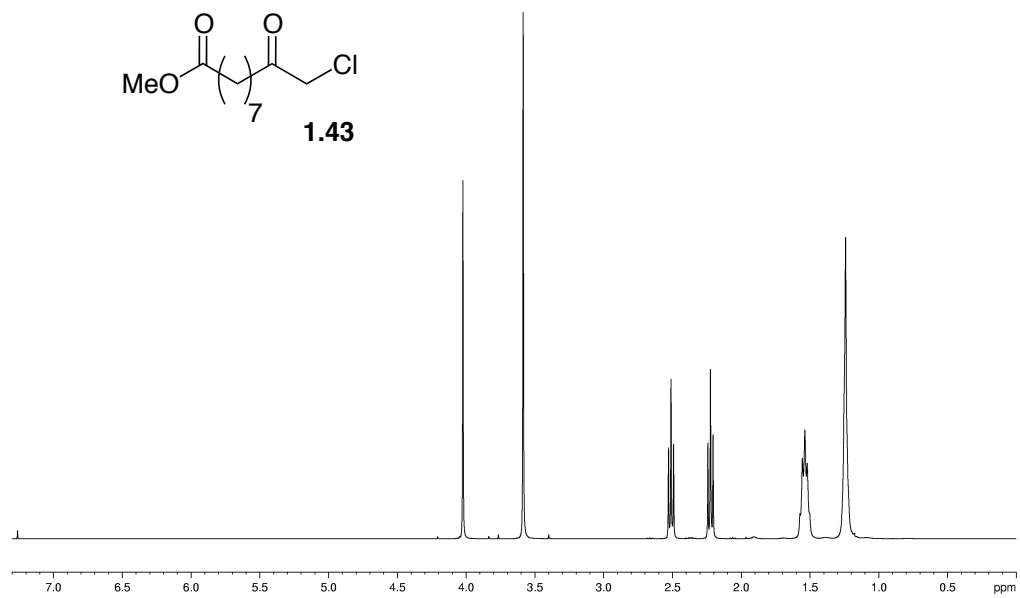
**Spectra I-12:** The 400 MHz  $^1\text{H}$  and 100 MHz  $^{13}\text{C}$  NMR spectra of **1.38** in  $\text{CDCl}_3$ .



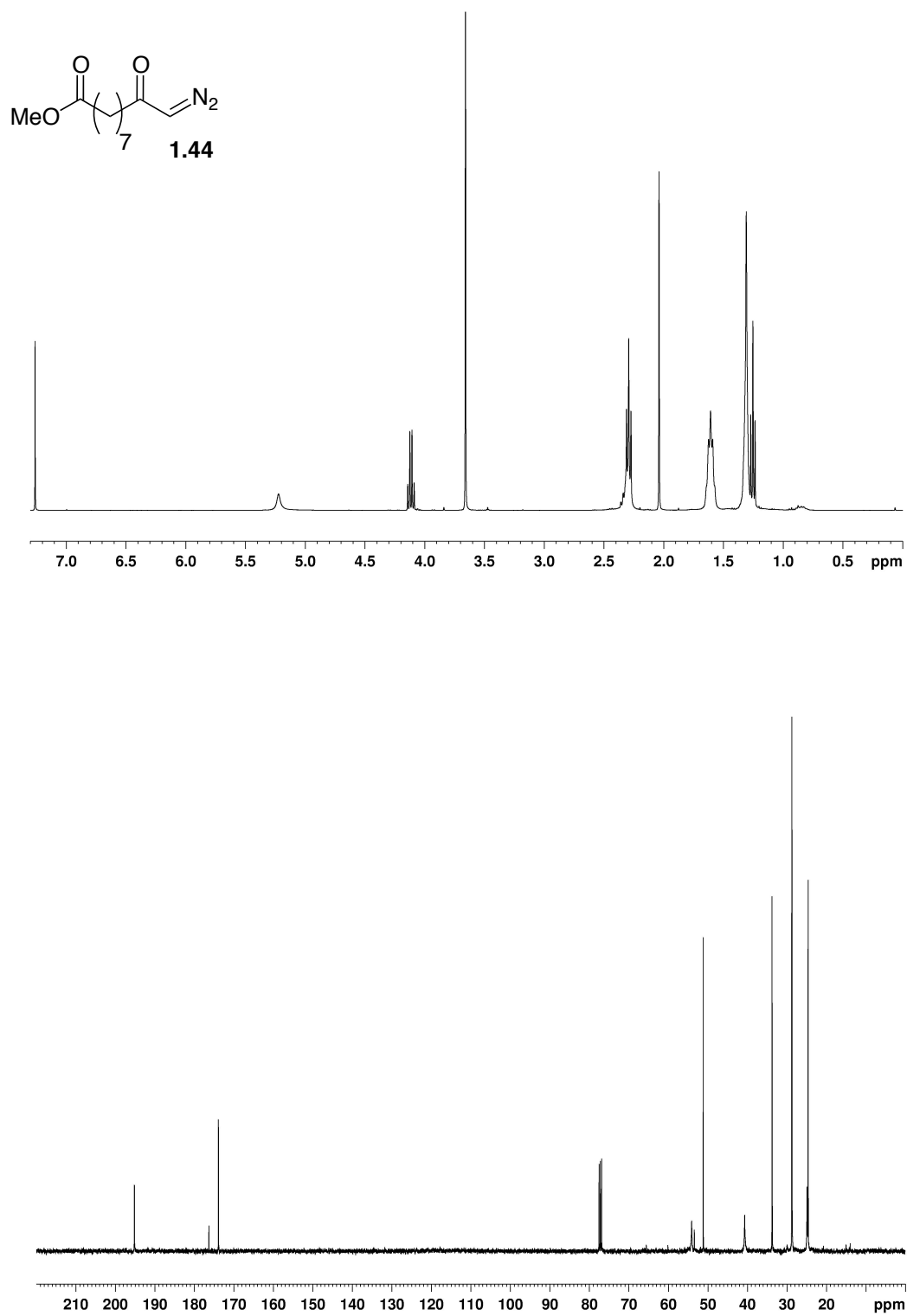
**Spectra I-13:** The 400 MHz  $^1\text{H}$  and 100 MHz  $^{13}\text{C}$  NMR spectra of **1.40** in  $\text{CDCl}_3$ .



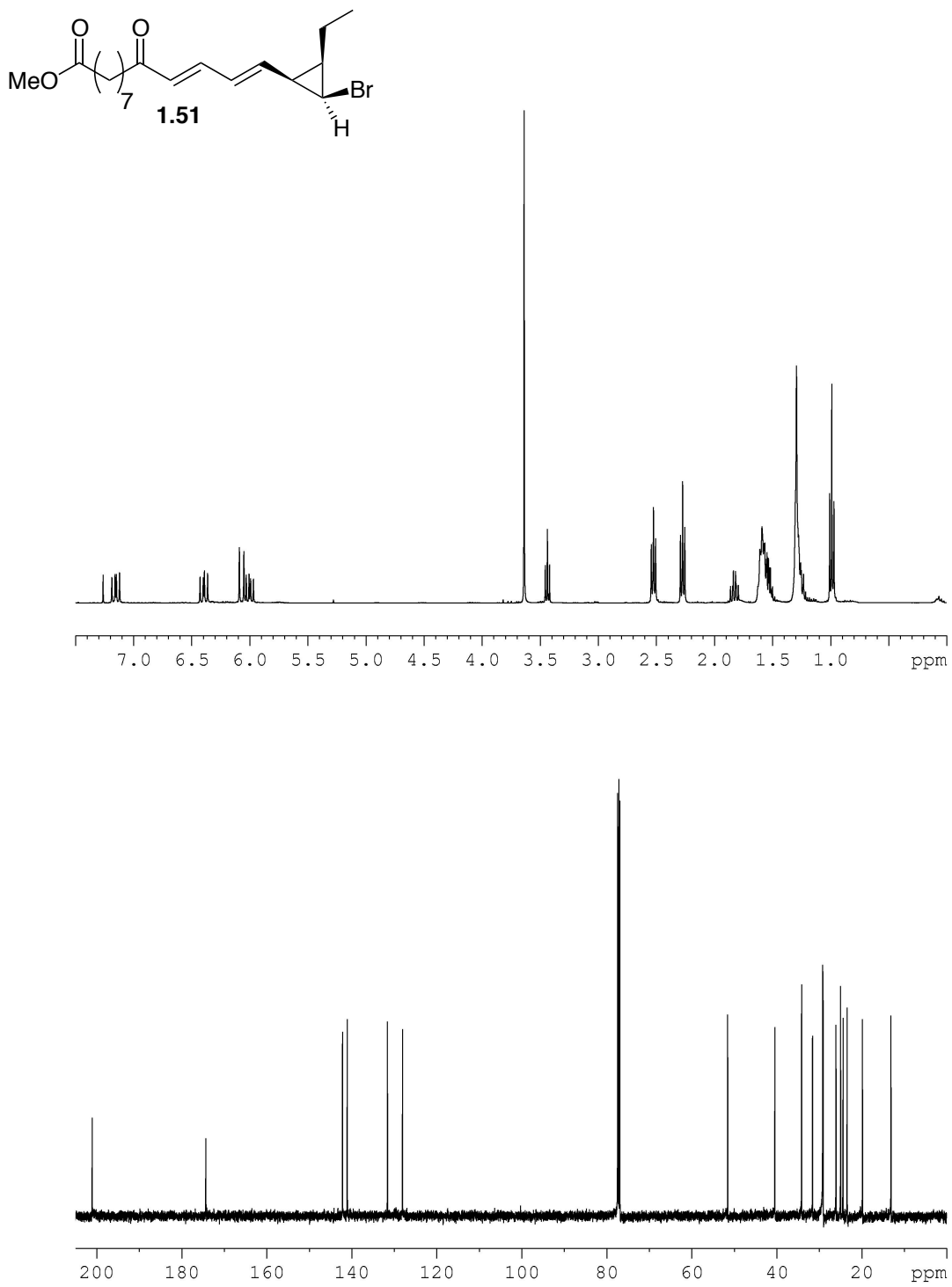
**Spectra I-14:** The 400 MHz  $^1\text{H}$  and 100 MHz  $^{13}\text{C}$  NMR spectra of **1.41** in  $\text{CDCl}_3$ .



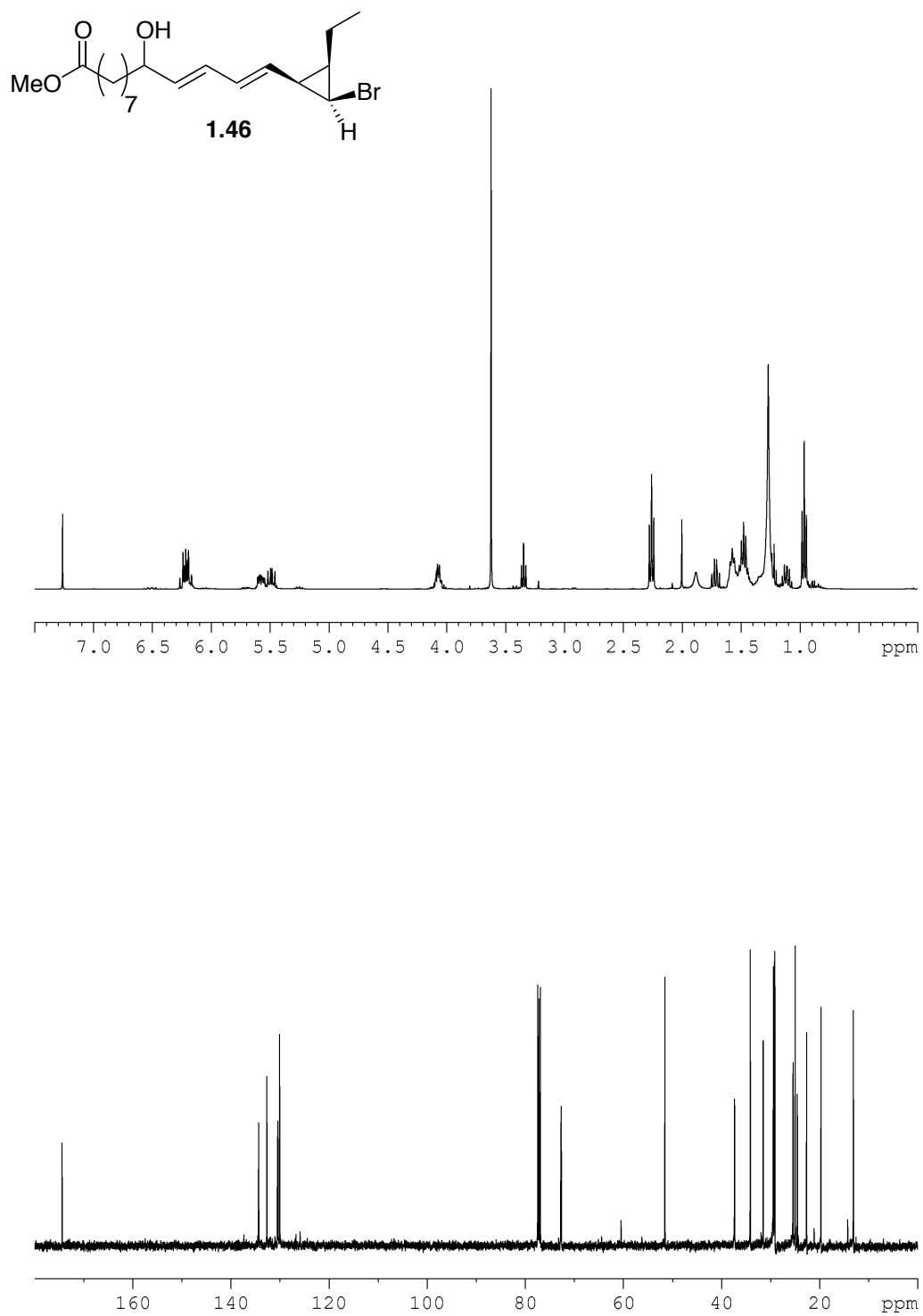
**Spectra I-15:** The 400 MHz  $^1\text{H}$  and 100 MHz  $^{13}\text{C}$  NMR spectra of **1.43** in  $\text{CDCl}_3$ .



**Spectra I-16:** The 400 MHz  $^1\text{H}$  and 100 MHz  $^{13}\text{C}$  NMR spectra of **1.44** in  $\text{CDCl}_3$ .

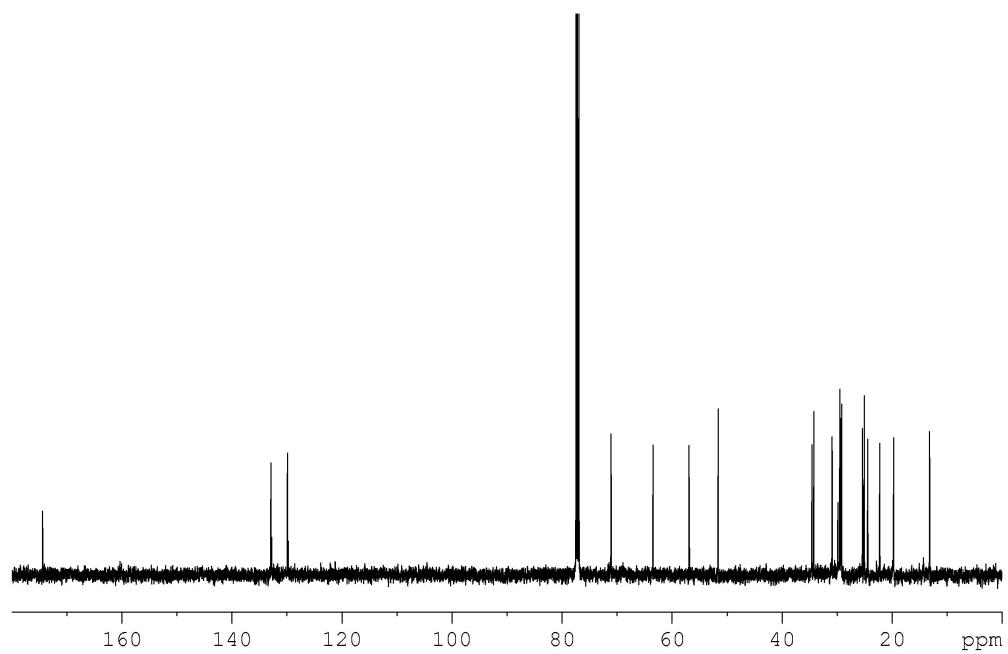
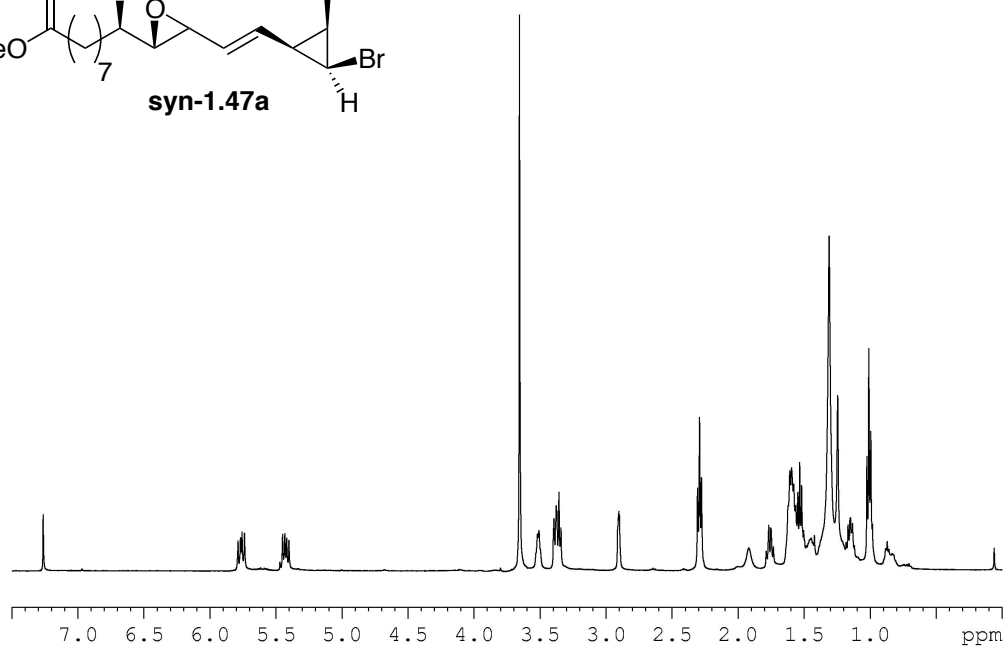
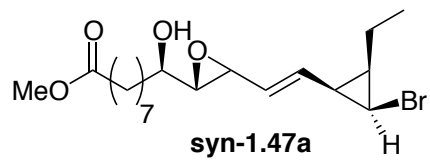


**Spectra I-17:** The 400 MHz  $^1\text{H}$  and 125 MHz  $^{13}\text{C}$  NMR spectra of **1.51** in  $\text{CDCl}_3$ .

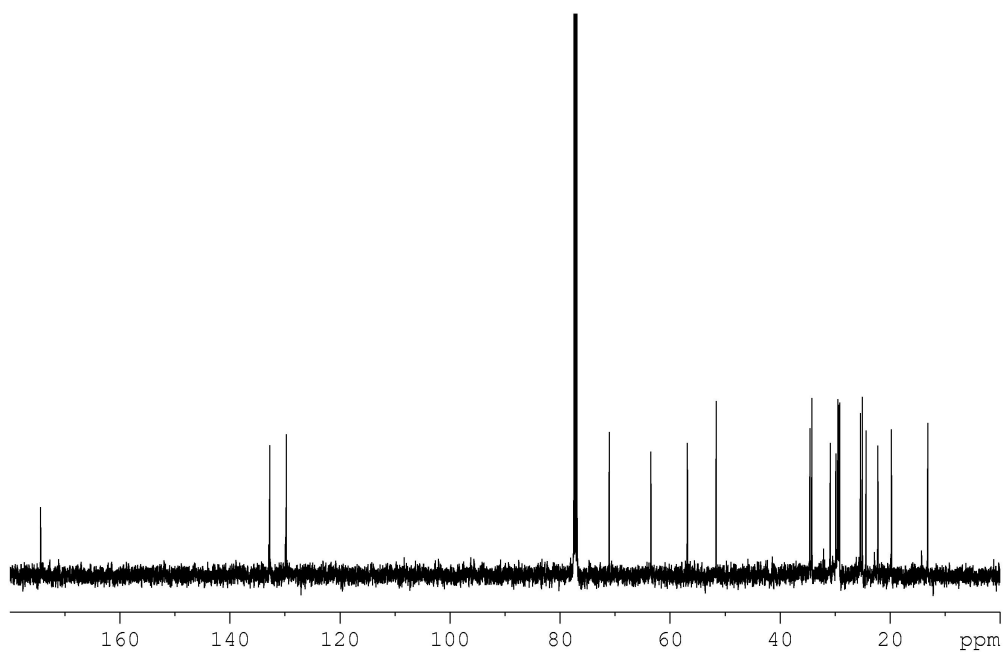
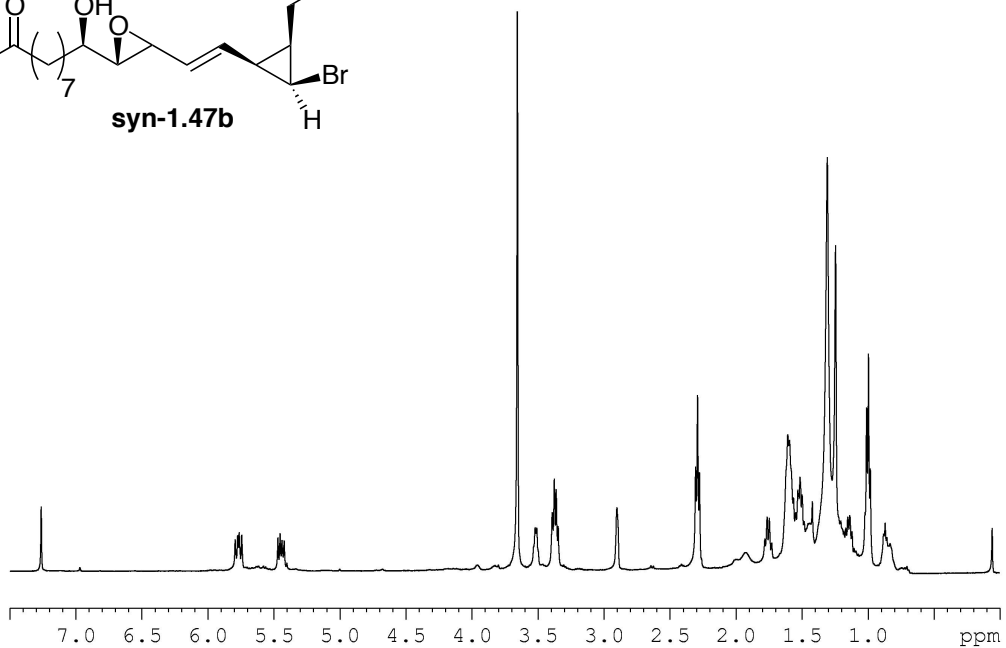
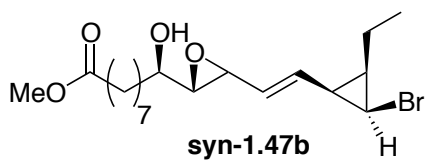


**Spectra I-18:** The 400 MHz  $^1\text{H}$  and 125 MHz  $^{13}\text{C}$  NMR spectra of **1.46** in  $\text{CDCl}_3$ .

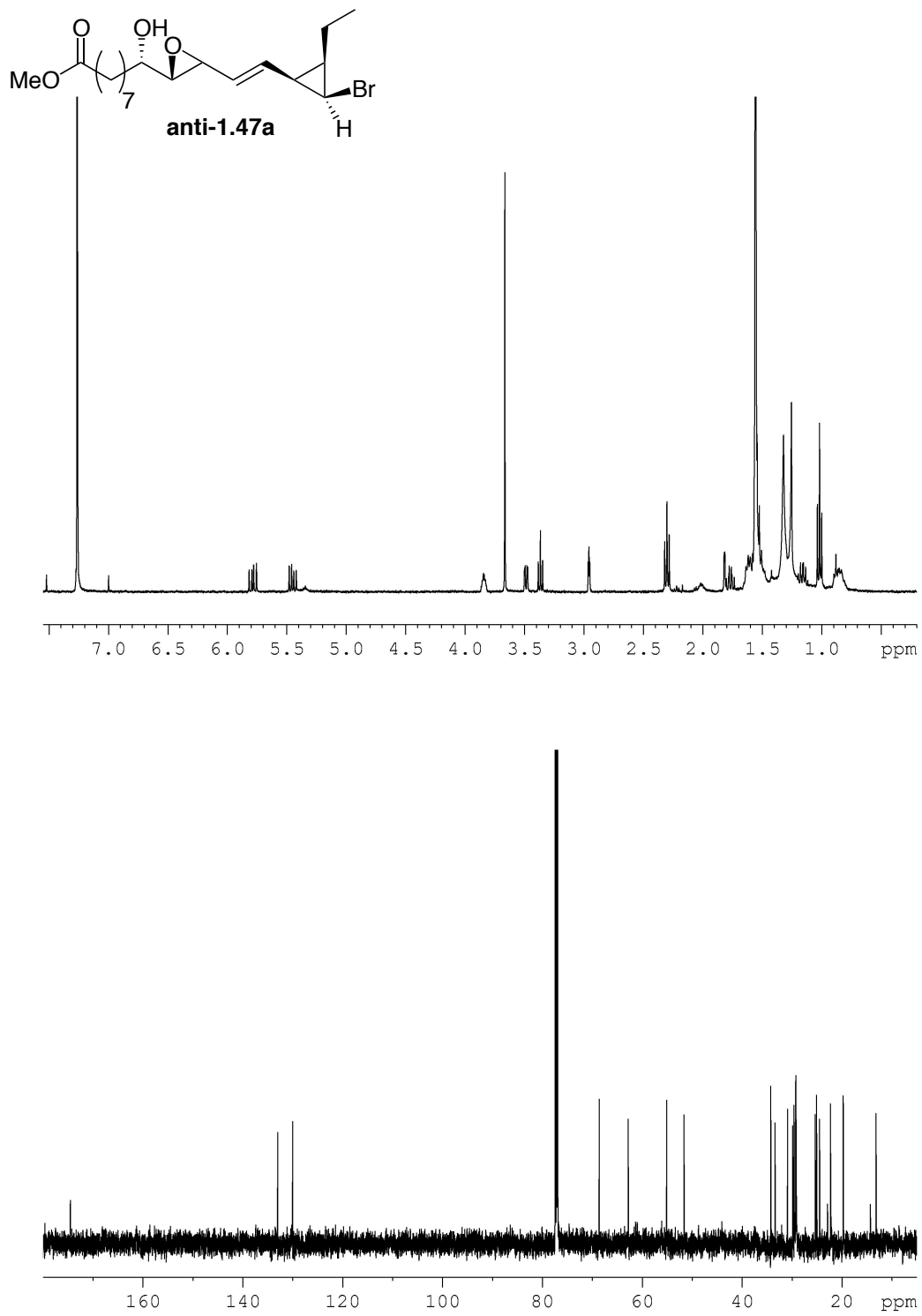




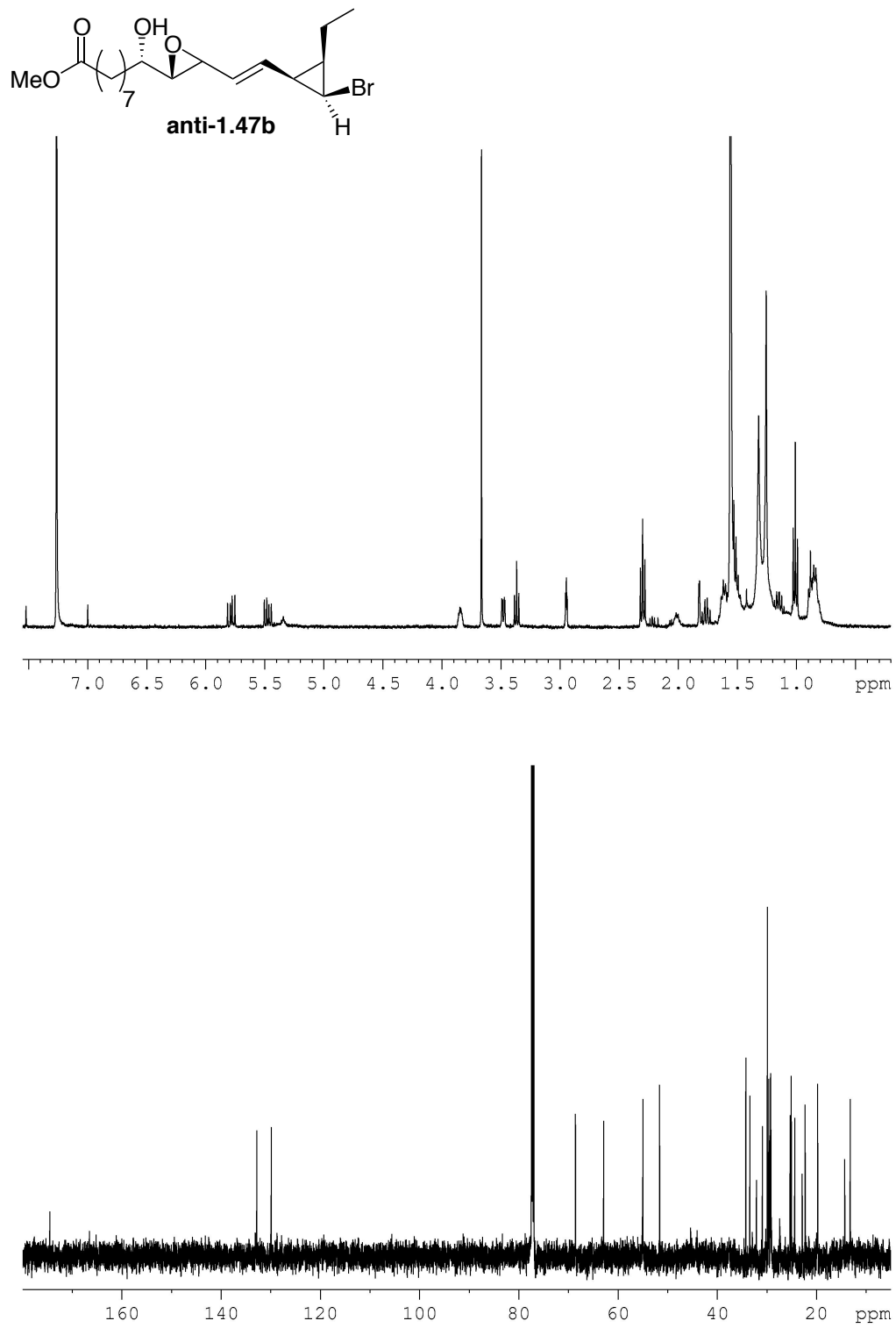
**Spectra I-19:** The 500 MHz  $^1\text{H}$  and 125 MHz  $^{13}\text{C}$  NMR spectra of *syn*-**1.47a** in  $\text{CDCl}_3$ .



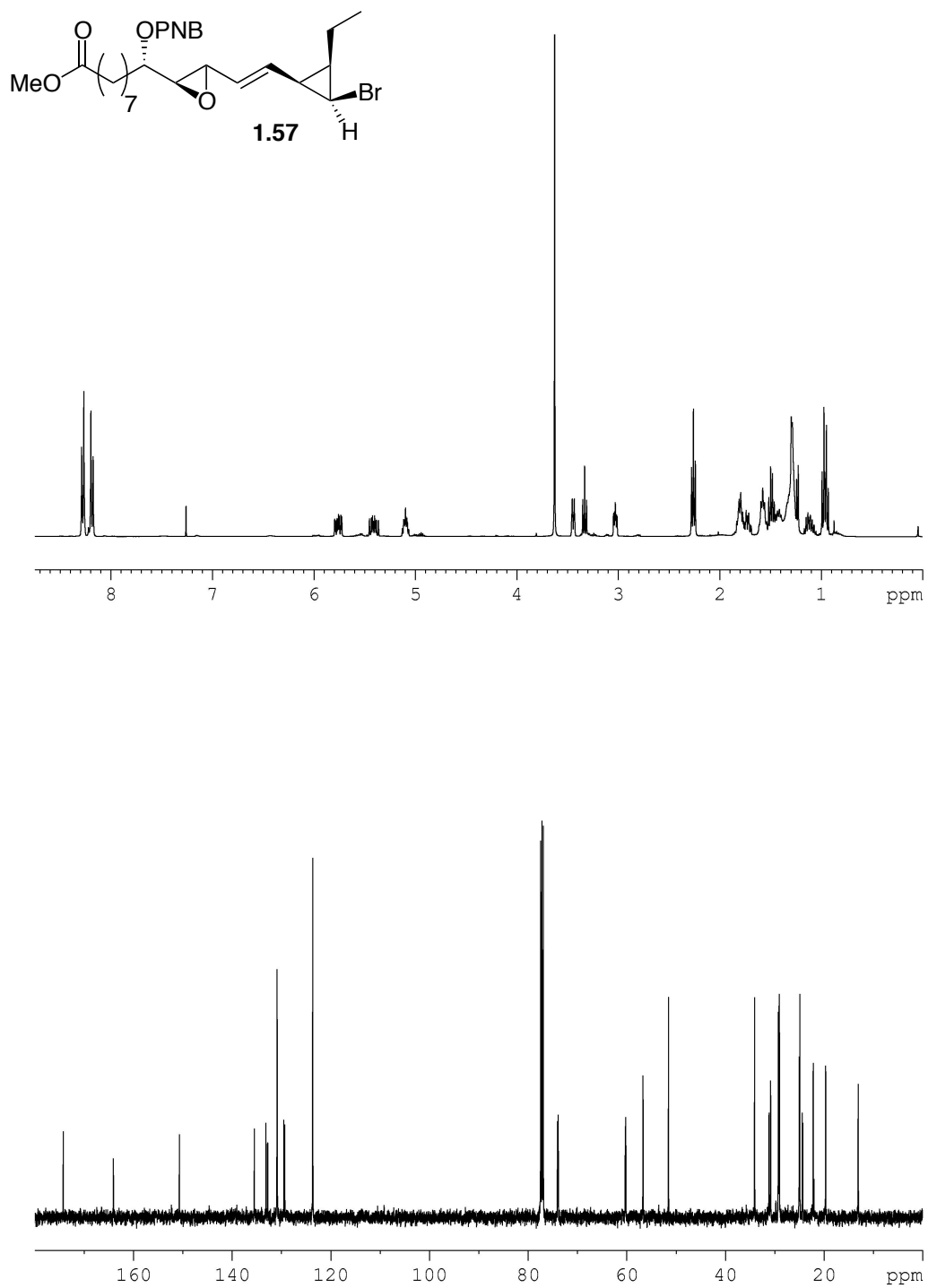
**Spectra I-20:** The 500 MHz  $^1\text{H}$  and 125 MHz  $^{13}\text{C}$  NMR spectra of *syn*-1.47b in  $\text{CDCl}_3$ .



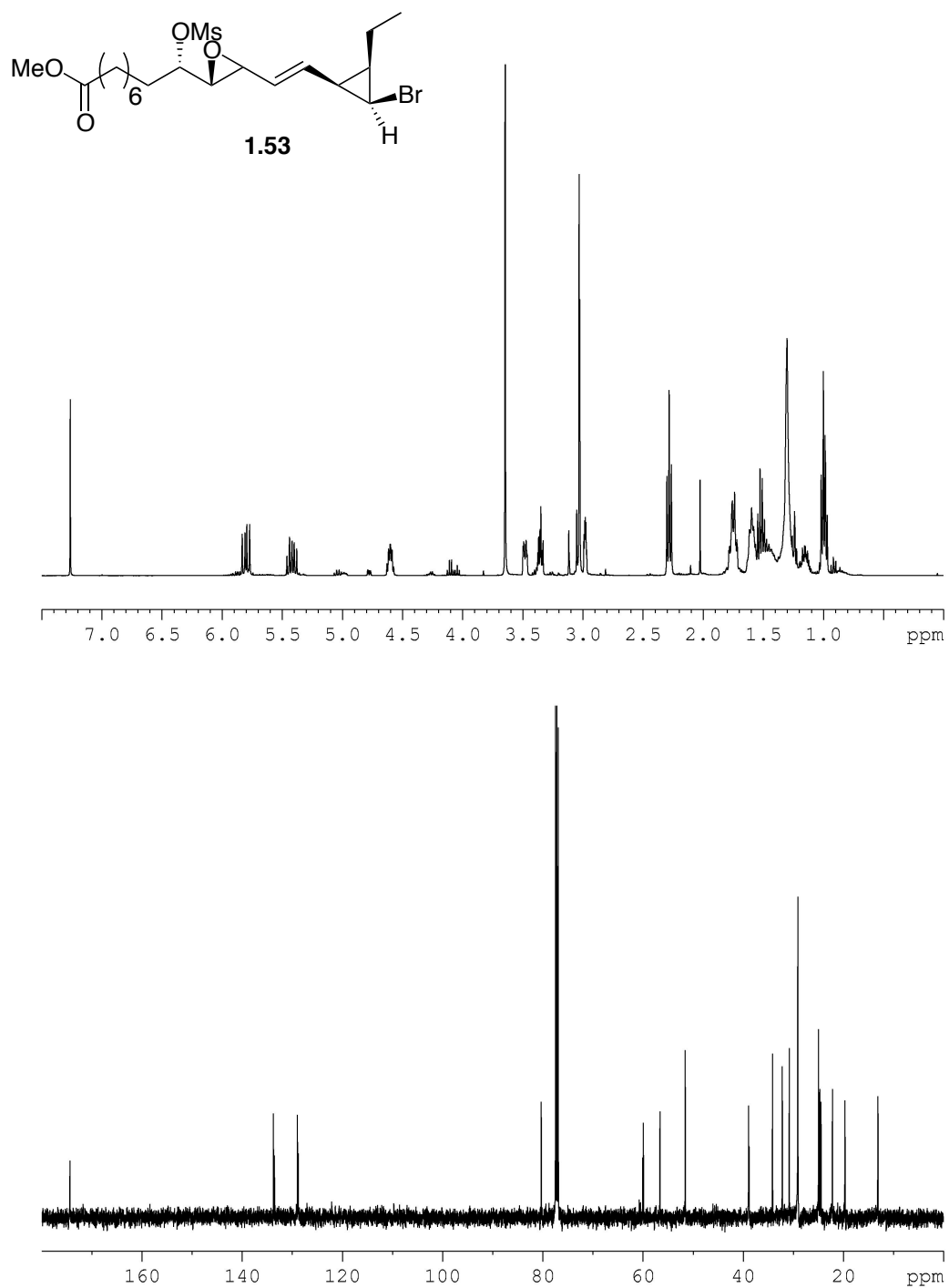
**Spectra I-21:** The 400 MHz <sup>1</sup>H and 150 MHz <sup>13</sup>C NMR spectra of **anti-1.47a** in CDCl<sub>3</sub>.



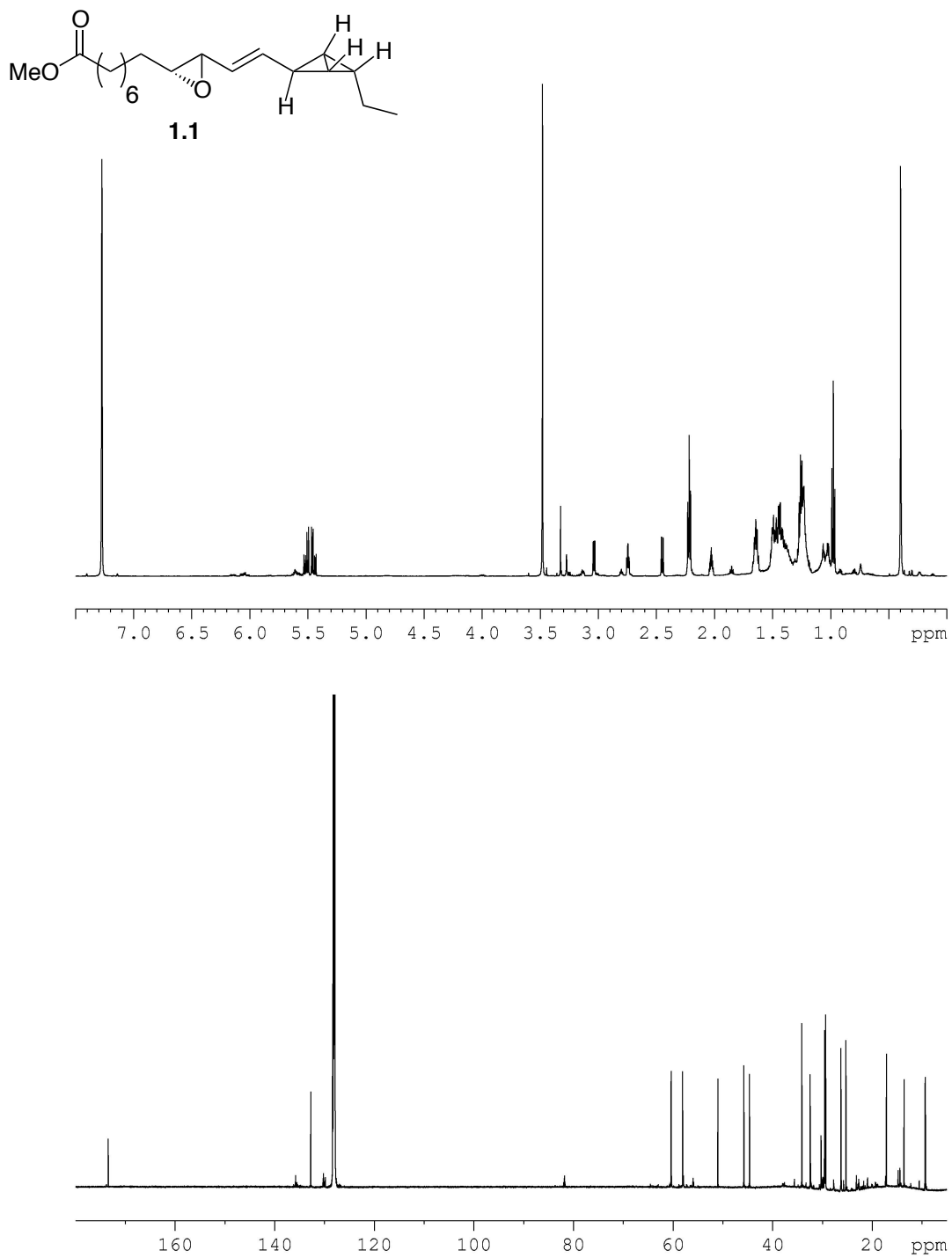
**Spectra I-22:** The 400 MHz  $^1\text{H}$  and 150 MHz  $^{13}\text{C}$  NMR spectra of **anti-1.47b** in  $\text{CDCl}_3$ .



**Spectra I-23:** The 400 MHz <sup>1</sup>H and 125 MHz <sup>13</sup>C NMR spectra of **1.57** in CDCl<sub>3</sub>.



**Spectra I-24:** The 400 MHz <sup>1</sup>H and 125 MHz <sup>13</sup>C NMR spectra of **1.53** in CDCl<sub>3</sub>.



**Spectra I-25:** The 600 MHz  $^1\text{H}$  and 150 MHz  $^{13}\text{C}$  NMR spectra of **1.1** in  $\text{C}_6\text{D}_6$ .

## CHAPTER II

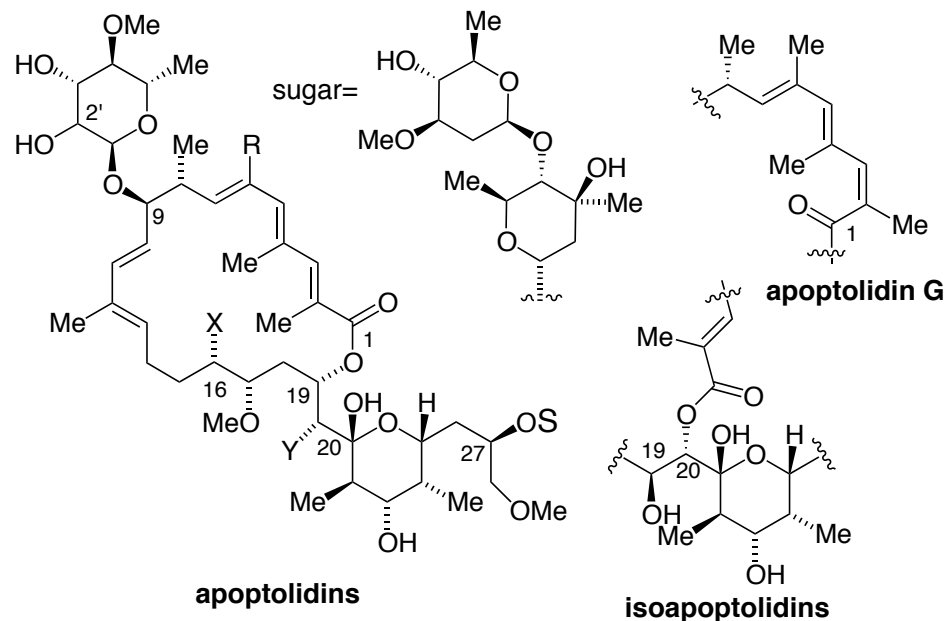
### Structural Diversification of Apoptolidins Through Mutasythesis

#### **Background Information**

##### *Isolation of Apoptolidin*

Apoptolidin **2.1** was isolated from the actinomycete *Nocardioopsis* sp. FU40 while screening bacterial extracts for selective inducers of apoptosis.<sup>1</sup> This novel polyketide natural product was reported to induce apoptosis selectively in *E1A* transformed rat glia cells ( $IC_{50} = 11$  ng/mL) relative to untransformed glia cells ( $IC_{50} > 10$   $\mu$ g/mL). Apoptosis induction in these cells was characterized by the observation of condensed chromatin and fragmented nuclei as visualized by staining with Hoechst Dye 333258 and significant DNA laddering. Subsequent NMR analysis revealed apoptolidin to consist of a 20 membered macrolactone, a highly substituted pyran ring and two sugar residues, located at C9 and C27.<sup>2</sup>





apoptolidin A (**2.1**, R = Me; X = Y = OH; 2' = b-OH; S = sugar)  
 apoptolidin B (**2.2**, R = Me; X = H; Y = OH; 2' = b-OH; S = sugar)  
 apoptolidin C (**2.3**, R = Me; X = Y = H; 2' = b-OH; S = sugar)  
 apoptolidin D (**2.4**, R = H; X = Y = OH; 2' = b-OH; S = sugar)  
 apoptolidin E (**2.5**, R = Me; X = Y = H; 2' = a-OH; S = sugar)  
 apoptolidin F (**2.6**, R = Me; X = Y = H; 2' = a-OH; S = H)  
 apoptolidin G (**2.7**, R = Me; X = Y = OH; 2' = b-OH; S = sugar)  
 isoapoptolidin A (**2.8**, R = Me; X = Y = OH; 2' = b-OH; S = sugar)  
 isoapoptolidin B (**2.9**, R = Me; X = H; Y = OH; 2' = b-OH; S = sugar)  
 isoapoptolidin D (**2.10**, R = H; X = Y = OH; 2' = b-OH; S = sugar)

**Figure II-1:** Structure of natural apoptolidins

Since this initial report, several more apoptolidin natural products have been isolated from *Nocardiosis* sp. FU40 as minor metabolites, now designated apoptolidins B–G (**Figure II-1**). Apoptolidin B **2.2** and C **2.3** are deoxygenated at C16 and both C16 and C18, respectively, but are otherwise identical to the primary metabolite, apoptolidin A **2.1**.<sup>3</sup> Apoptolidins E **2.5** and F **2.6** are also deoxygenated at C16 and C18 but differ in the nature of the deoxy sugar at C9 and C27.<sup>4</sup> Apoptolidin D **2.4** lacks a C6 methyl group relative to other apoptolidins.<sup>5</sup> Also, apoptolidin was first reported to undergo a ring

expansion to give a 21 membered isomeric macrolactone named isoapoptolidin A, **2.8**.<sup>6,7</sup> Similar isomeric forms have subsequently been identified for apoptolidins B and D as well. Finally, Apoptolidin G **2.7** was isolated from a fermentation extract and assigned the C2-C3 configurational isomer of apoptolidin A. We hypothesized that this compound was not being directly synthesized but was the result of a light-induced isomerization of apoptolidin A. To test this, a solution of apoptolidin A **2.1** in acetone was irradiated with a 275 W sunlamp for 16 hours and indeed produced apoptolidin G as a 5:1 mixture with apoptolidin A.<sup>8</sup>

In order to design and access apoptolidin derived chemical probes to support mechanism of action studies, a high yielding source of apoptolidin was required. Fortunately, using a fermentation protocol of *Nocardioopsis* sp. FU40 optimized for the production of apoptolidin A **2.1**, we were able to obtain >100 mg per liter of culture broth. To aid in identification and confirmation of the mechanism of action and more specifically the molecular target of apoptolidin, it is advantageous to also have access to a diverse library of structural analogues of the parent compound. For example, a good indicator that the mechanism and target are correctly identified is the parallel nature of phenotypic (cytotoxicity) and mechanistic (biochemical activity) responses to structural modifications. Furthermore, compound analogues of variable activity can be advantageous in the development of probes that explore the importance of specific structural features in regulating biological activity and identification of a minimum pharmacophore. The minor apoptolidin shunt metabolites (B-G) afford access to only a limited number of structural homologues in trace quantity. Alternatively, novel apoptolidin congeners can be produced either by *de novo* synthesis, synthetic

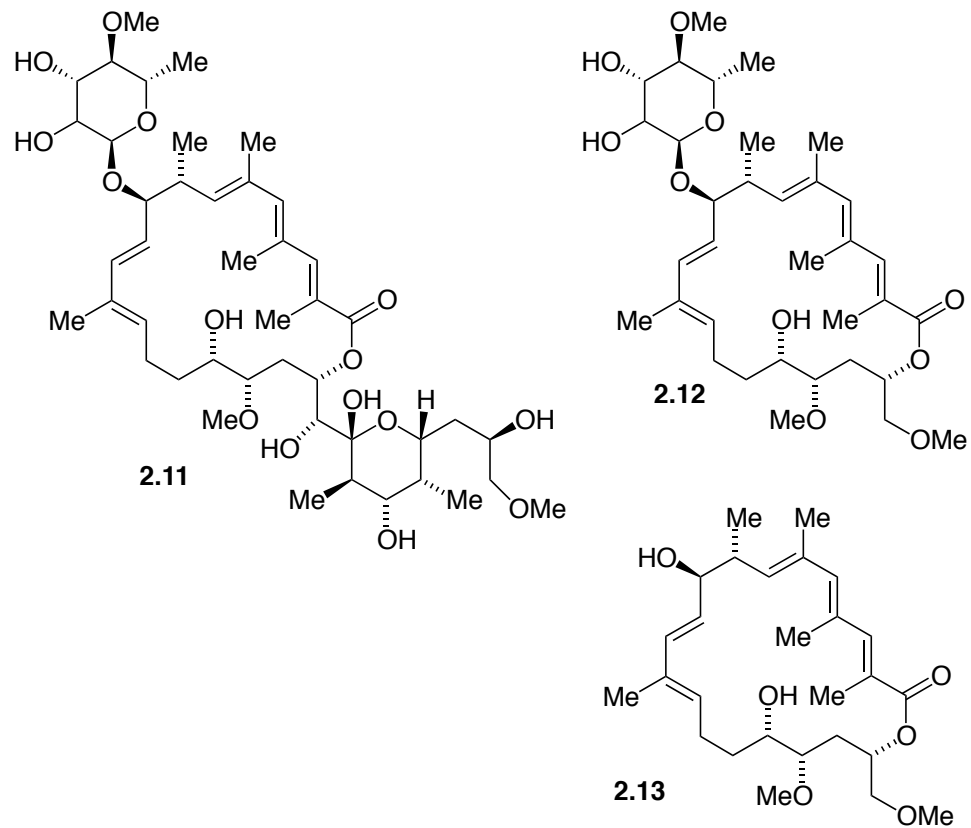
transformation of natural apoptolidin isolated from bacterial fermentation or by modification of the producing organism's biosynthetic machinery to provide access to large quantities of apoptolidin congeners.

### *Synthesis of Apoptolidins*

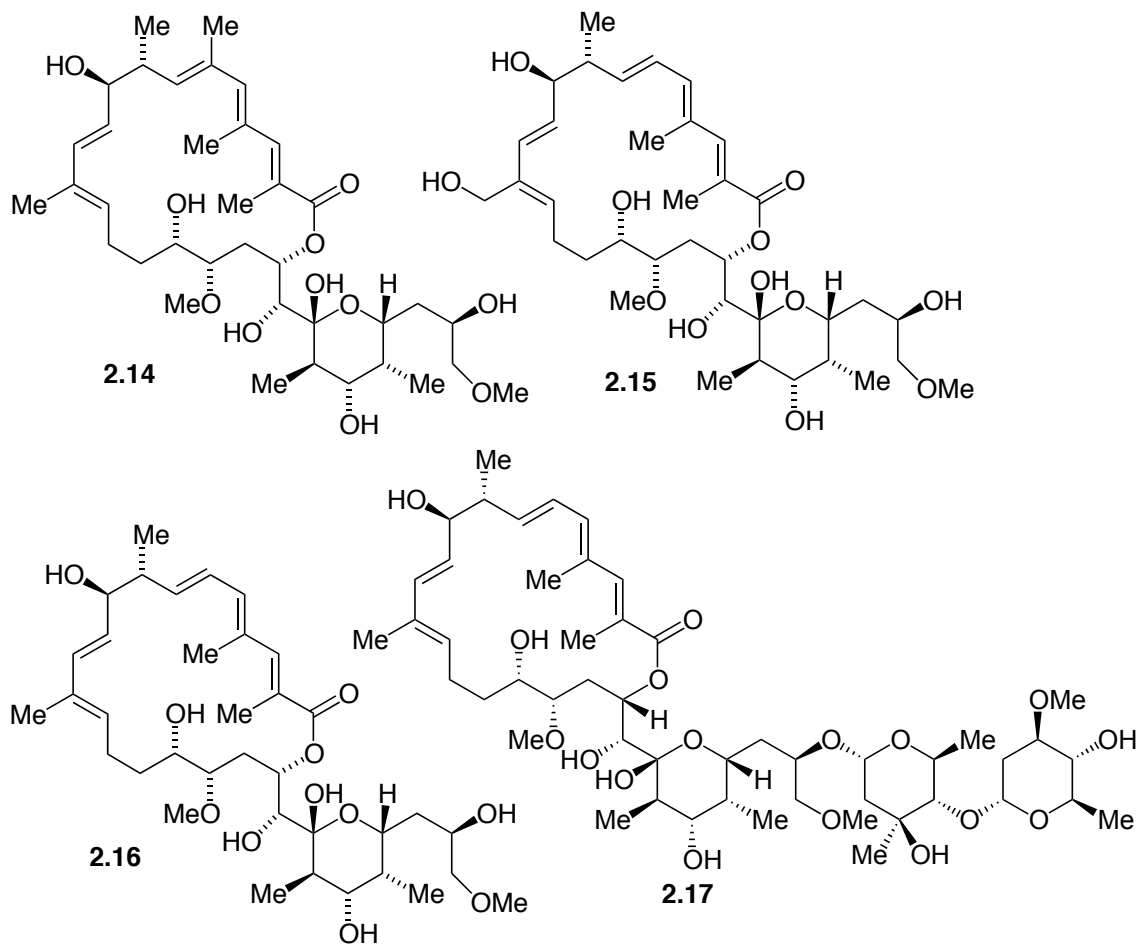
The reported potent, selective cytotoxicity of apoptolidin as well as its complex structural features have prompted multiple research groups to pursue its total synthesis.<sup>9</sup> More significantly, various routes aimed at total syntheses have also produced novel apoptolidin analogues. The first total synthesis of apoptolidin A was reported by Nicolaou and co-workers in 2003.<sup>10</sup> Utilizing late stage glycosylations and macrolactonization in their strategy, they were also able to prepare three novel apoptolidin analogues (**Figure II-2**) including C27-hydroxy apoptolidin A **2.11** and two macrolactones missing the pyran fragment (**2.12** and **2.13**). Previous work in the Sulikowski laboratory planned to implement a bioglycosylation of synthetic apoptolidin agylcones (apoptolidinones) for the synthesis of apoptolidin A and D and potentially novel apoptolidin congeners. To this end, our group developed routes to three apoptolidin agylcones (**Figure II-3**).<sup>11,12</sup> Successful whole cell glycosylation of apoptolidinone D was realized at C27 only, providing access to the apoptolidin D disaccharide **2.17**.<sup>13</sup> While the low yield of apoptolidin compounds from time and labor intensive total synthesis makes it an inefficient method to access the natural compounds, relative to fermentation, studies towards this end have provided access to novel apoptolidins for early biological testing (*vida infra*).

To further investigate SAR of apoptolidin natural products, several groups have successfully modified apoptolidin isolated from bacterial fermentation culture (**Figure**

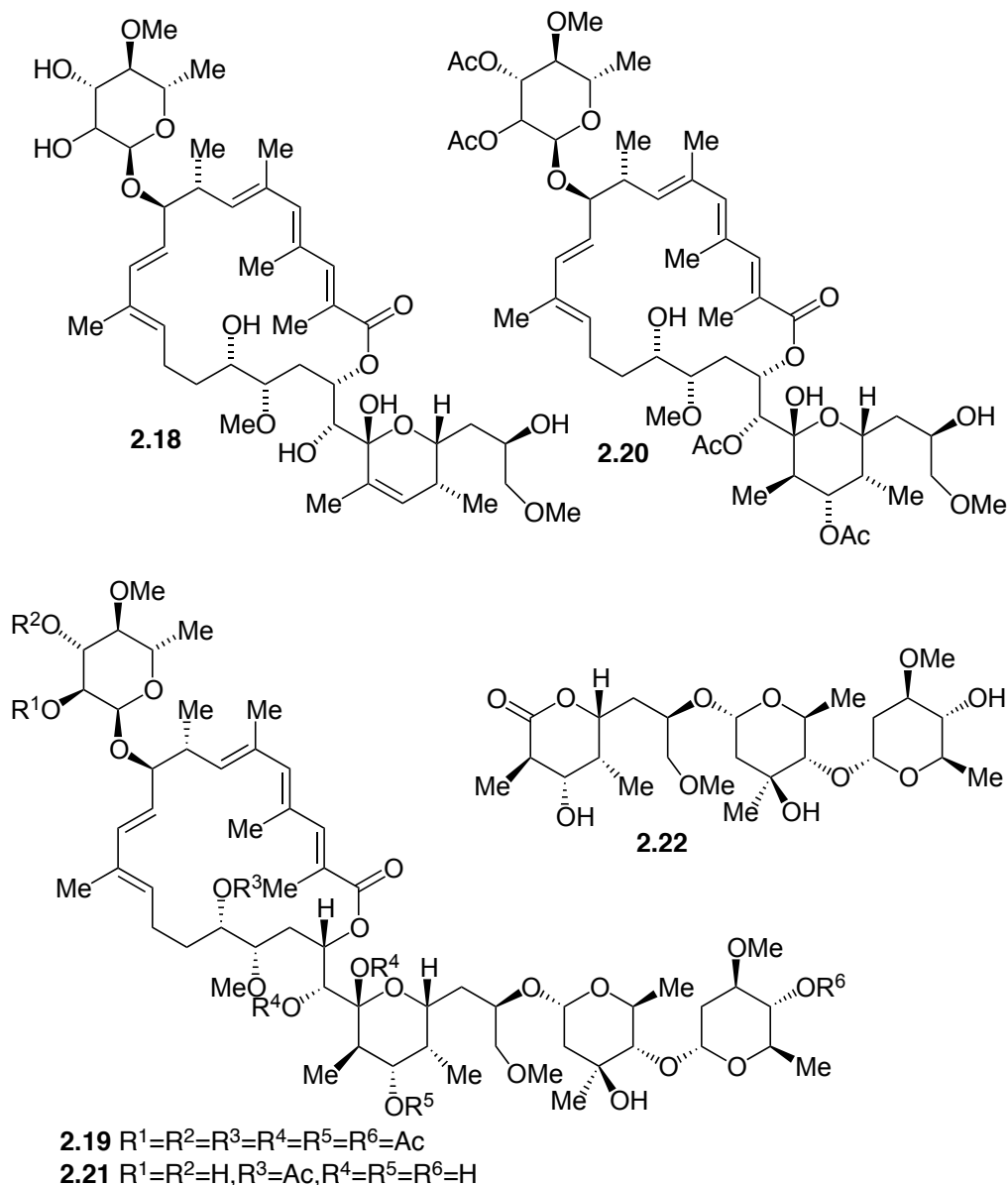
**II-4).** Salomon and coworkers generated a truncated apoptolidin **2.18** by acid hydrolysis of the C27 disaccharide accompanied by elimination of water in the pyran moiety.<sup>14</sup> In the Sulikowski laboratory, nonselective acetylation of apoptolidin A provided hexaacetylated apoptolidin A **2.19**, which allowed for deglycosylation at C27 by treatment with methanolic hydrochloric acid to provide acylated apoptolidin monosaccharide **2.20**.<sup>7</sup> Wender and coworkers were able to generate a variety of apoptolidin analogues by functionalizing the various hydroxyl groups of apoptolidin using careful protecting group manipulation<sup>15</sup> or peptide catalysis, a single example (**2.21**) is shown.<sup>16</sup> Wender and coworkers also prepared a few analogues of macrocycle **2.12** and  $\delta$ -lactone apoptolidin fragment **2.22** by way of oxidative cleavage of apoptolidin A **2.1**.<sup>17</sup>



**Figure II-2:** Nicolaou's apoptolidin analogues



**Figure II-3:** Sulikowski's apoptolidin analogues



**Figure II-4:** Semisynthetic apoptolidin analogues

Together, total synthesis and semisynthesis have afforded a small group of structural analogues of apoptolidin that aid investigations of the mechanism of its observed selective cytotoxicity. However, the preparation of apoptolidins by total synthesis is limited by high costs in terms of both time and reagents and typically very

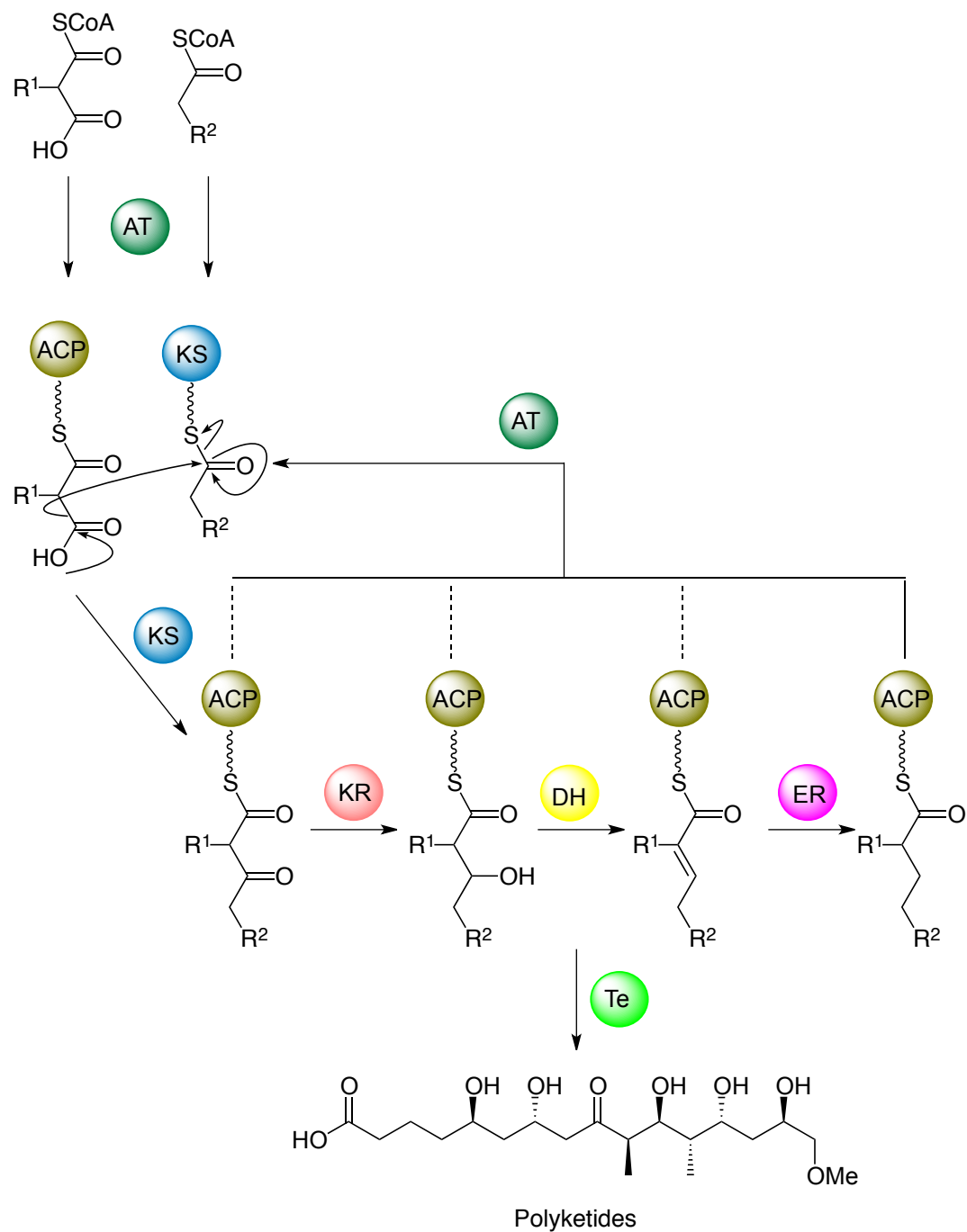
low yields. For example, our group's optimized, high yielding synthesis of apoptolidinone **2.14** resulted in the isolation of only 2-5 mg of material over 14 linear steps in a total of 2.6% yield.<sup>11</sup> Furthermore, minor structural changes to target analogues on complex polyketides such as apoptolidin frequently require a significant change in synthetic strategy, limiting rapid diversification. Preparation of new apoptolidin congeners through semisynthesis is limited by the relatively poorly selective reactivity of apoptolidin with reagents and its tendency to undergo decomposition under either acidic or basic reaction conditions. To avoid these limitations and create low cost, high yielding sources of apoptolidin congeners for use in studying apoptolidin cytotoxicity, we sought to instead employ a strategy taking full advantage of the high yielding apoptolidin fermentation protocol. Specifically, we aimed to efficiently produce analogues of apoptolidin by genetic manipulation of the apoptolidin producing machinery followed by fermentation of the transformed microbe.

#### *Biosynthesis of Apoptolidin: Type I PKS*

To identify parts of the biosynthesis of apoptolidin that might be modified to produce interesting apoptolidin congeners from fermentation of mutant producers, it is important to first understand the biogenesis of apoptolidin. Apoptolidin is the product of a type I polyketide synthase (PKS). Type 1 PKS's are multi-domain megasynthases that construct the core of many polyketide natural products. Chain elongation is achieved through a non-iterative series of decarboxylative Claisen condensations and  $\beta$ -reductions. Briefly, acyltransferase (AT) domains transfer the elongation units (various C2 substituted malonate derivatives) from a molecule of coenzyme A (CoA) to a phosphopantathienylated acyl carrier protein domain (ACP) for activation. Ketosynthase



(KS) domains then transfer this activated malonate unit to a cysteine residue and catalyzes the decarboxylative Claisen condensation onto the downstream malonyl ACP (**Scheme II-1**). The  $\beta$ -ketoacyl moiety is then variably transformed to the appropriate oxidation state by the action of ketoreductase (KR), dehydratase (DH) and enoylreductase (ER) domains. When chain elongation is complete, a thioesterase (TE) domain then catalyzes the cleavage and/or macrolactonization to the polyketide product.<sup>18</sup>



**Scheme II-1:** Biosynthesis of polyketides

In type 1 PKS, the ordering of genes encoding the catalytic domains in each module typically corresponds to the order of reactions in the biosynthesis, making it

possible to predict the structure of the polyketide chain from the genetic sequence of the PKS. Given this mechanism and the structure of apoptolidin, we expect the PKS to be encoded by a 14-module domain sequence. Several more transformations must occur in the biosynthesis of apoptolidin after completion of the polyketide core (post-PKS modifications). The variable oxidation at C16 and C20 of apoptolidins B and C suggest that these positions are oxidized by one or more P450 oxidases. Glycosylation at C9 and C27 will also require up to three glycosyltransferases as well as enzymes involved in biosynthesis of the unusual deoxysugars L-olivomycose and D-oleandrose. While the order of events in the post-PKS modification are unknown, the failure of apoptolidinones **2.14** and **2.16** to be bioglycosylated at C9 in studies in our lab<sup>12</sup> suggest that apoptolidin is glycosylated at C9 at an earlier stage of biosynthesis, perhaps even during chain elongation process.

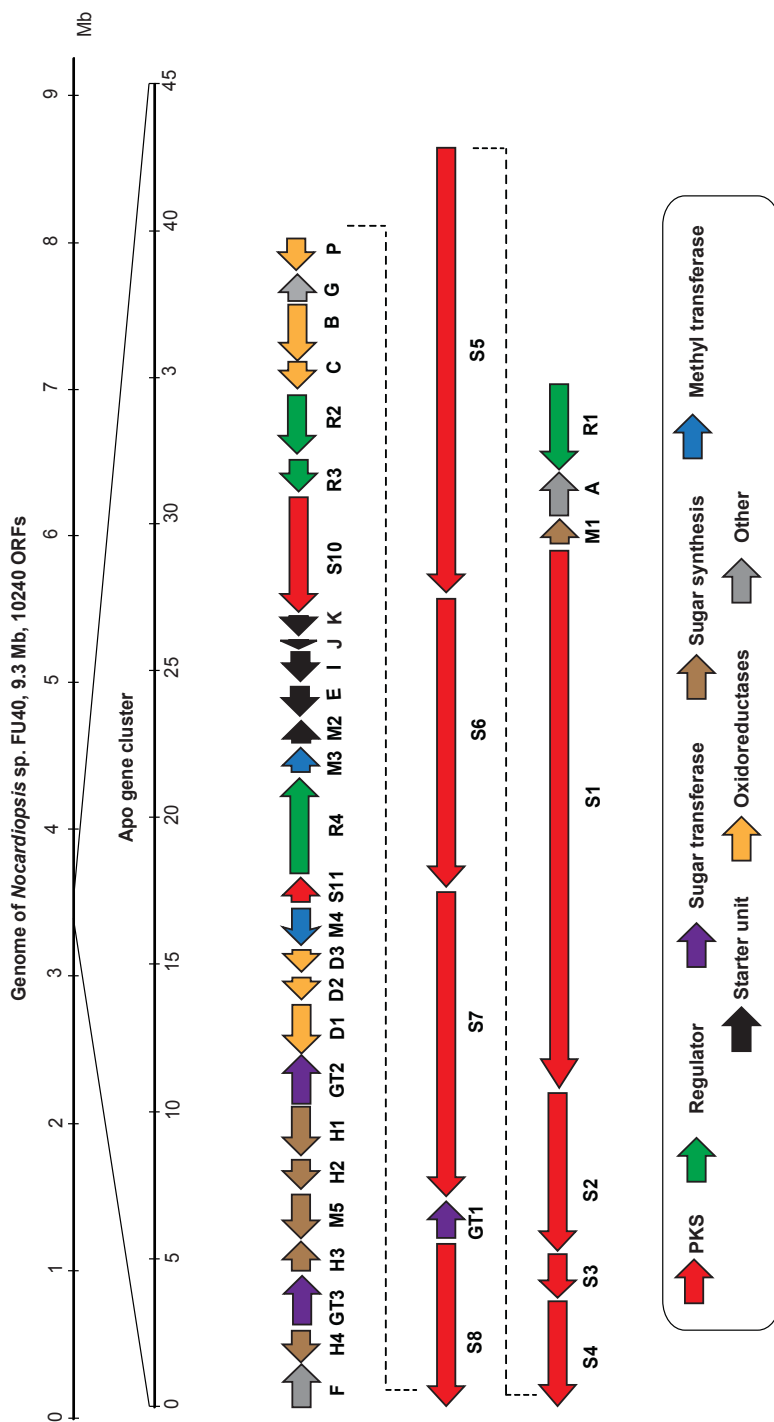
## **Genetic Manipulation of Apoptolidin Biosynthesis**

### *Identifying the Apoptolidin Biosynthetic Gene Cluster*

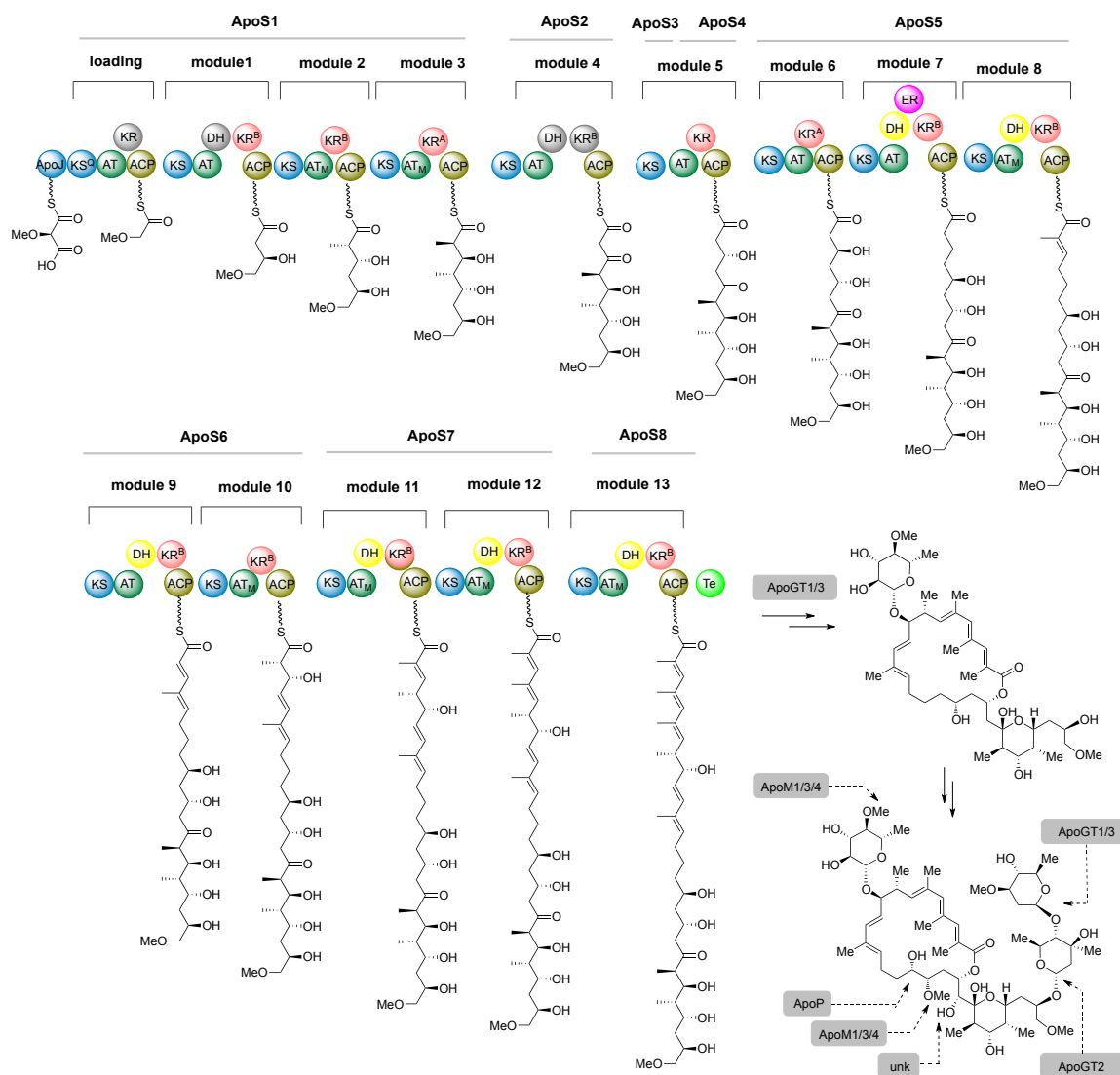
In order to increase the understanding of apoptolidin biosynthesis as well as to identify genes to target for disruption to afford access to structural analogues, our collaborators in the Bachmann lab sequenced the genome of *Nocardiosis* sp. FU40 with a goal of identifying the biosynthetic gene cluster.<sup>20</sup> The organism's genomic DNA was isolated, sequenced and assembled yielding an estimated 9,433,896 bp genome, in agreement with actinomycete genomes previously sequenced. BLAST-based algorithms<sup>19</sup> were used to identify two gene clusters within the genome that putatively encoded type 1

PKS.<sup>20</sup> While one of these only possessed eight intact PKS modules, the second ~ 116 kb region contained, as expected, 14 PKS modules and appeared to also contain genes necessary for all post-PKS elaboration to apoptolidin.

The identified gene cluster *apo* is 115.74 kb and contains 39 individual open reading frames (ORFs). By sequence homology, these genes were identified as shown in **Figure II-5** and include nine type 1 PKS genes, six oxidoreductase genes, four methyltransferase genes, three glycosyltransferases and other genes responsible for sugar and starter unit biosynthesis. The PKS genes *ApoS1–S8* encode the synthases responsible for the biosynthesis of the polyketide backbone of apoptolidin. The protein product of *ApoS1* contains the KS<sup>Q</sup> domain that is responsible for initiating the polyketide synthesis. From this point, domains are organized as predicted based upon the structure of apoptolidin in *ApoS1–S7* and terminate with a thioesterase domain in *ApoS8* required for release from the megasynthase. Of the two remaining PKS genes *ApoS9* and *ApoS10*, *ApoS10* is proposed to be responsible for macrocyclization and *ApoS9* appears to be an incomplete module sequence with no obvious function. Upon cyclization, it is expected that the compound is further modified by glycosylation, oxidation and O-methylation but the exact order of these events and the specific genes responsible for each of these reactions cannot be predicted from the genetic sequence alone (**Figure II-6**).



**Figure II-5:** Genetic organisation of the apoptolidin gene cluster in *Nocardioopsis* sp. FU40



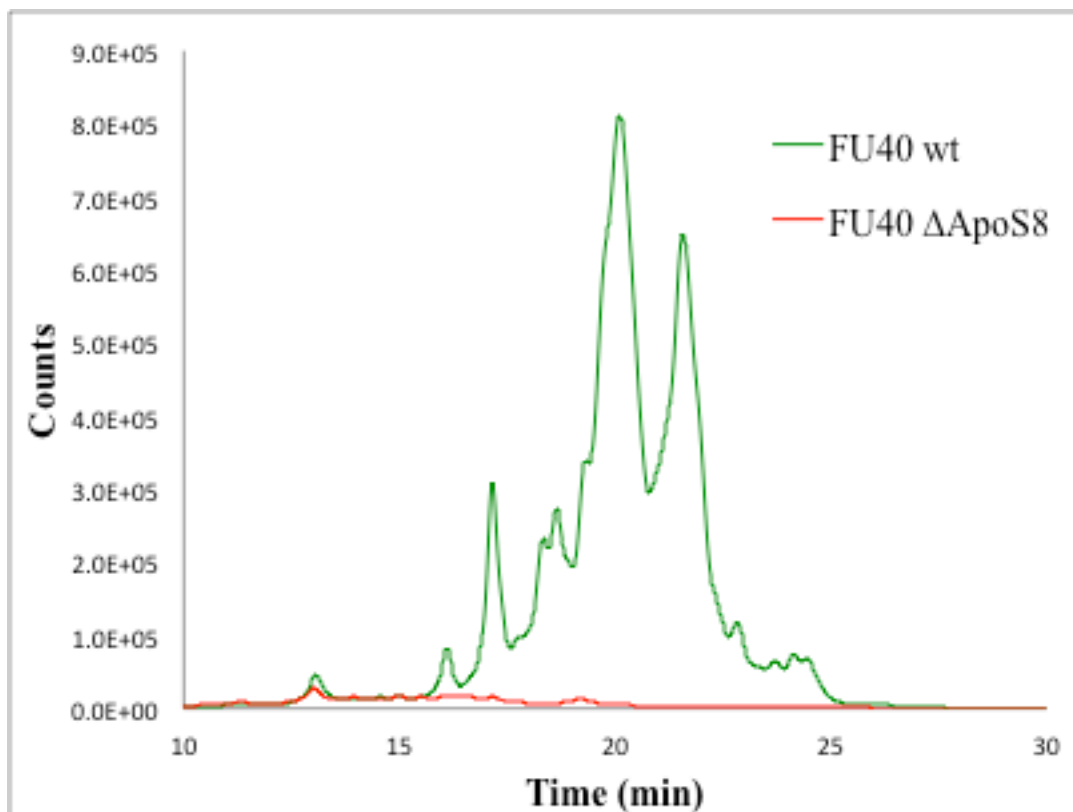
**Figure II-6:** Overview of the proposed biosynthetic pathway for apoptolidin

### Genetic Knockouts

In order to both confirm the identification of the apoptolidin gene cluster, as well as to create mutant producers, a method for selective gene knockout of the apoptolidin gene cluster was developed by Du *et al.*<sup>20</sup> Briefly, a cosmid library was created in *E. coli* from the genomic DNA of *Nocardioopsis* sp. FU40. Oligonucleotides of *ApoM2*, *ApoGT1*

and *ApoM1* were generated and used as hybridization probes to screen the library to identify 3 cosmids containing the gene cluster *apo*. Sequencing of these cosmids confirmed that they covered the *apo* gene cluster of interest in its entirety. Genetic knockouts were then introduced by replacing targeted genes with apramycin resistance gene makers by double homologous recombination in *E. coli*. The resulting cosmids were introduced into nocardiosis using either interspecies conjugation or electroporation.<sup>20</sup>

To validate the identification of *apo* as the biosynthetic gene cluster responsible for the apoptolidin biogenesis, a gene was targeted for disruption that would ideally eliminate the ability of *Nocardiosis* sp. FU40 to produce apoptolidin. To this effect, *ApoS8* was disrupted. Fermentation and subsequent extraction of this mutant producer (FU40 $\Delta$ ApoS8) with ethyl acetate resulted in the production of no apoptolidin compounds as indicated by HPLC/MS analysis (**Figure II-8**: Mass selective (858.5 m/z) LCMS trace of FU40 $\Delta$ ApoGT2**Figure II-7**). Furthermore, pulse feeding of FU40 $\Delta$ ApoS8 with apoptolidin monosaccharide **2.11** restored production of apoptolidin A. These results confirmed the disruption of the apoptolidin polyketide synthase without disruption of other genes involved in biosyntheses.



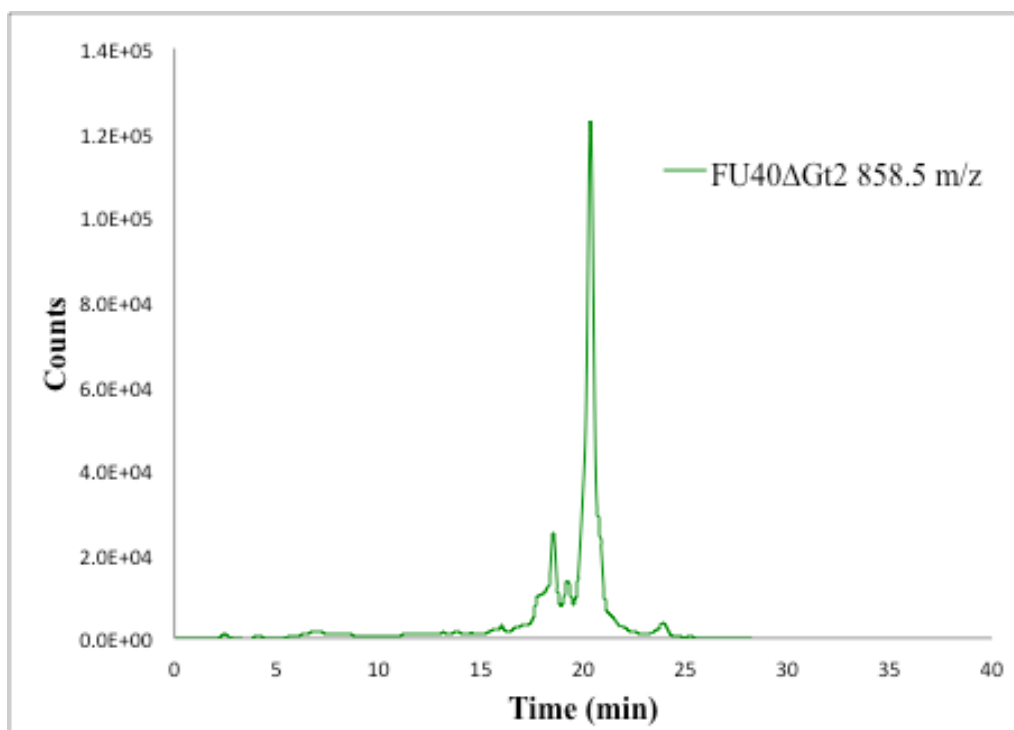
**Figure II-7:** Mass selective (1146.5 m/z) LCMS trace of FU40 wt and FU40 $\Delta$ ApoS8

Equipped with a method for selective gene disruption in *Nocardioopsis* sp. FU40, disruption of genes that would produce novel apoptolidins was next pursued. Since the disruption of *ApoS8*, our collaborators in the Bachmann laboratory have been able to successfully produce several knockout strains. Genes successfully targeted for disruption include the oxygenase genes *ApoP* and *ApoD2*, the methyl transferase *ApoM2*, genes responsible for the synthesis of the initiating methoxymalonyl ACP starting subunit *ApoJ/K*, as well as glycosyl transferase knockouts *ApoGT1/2*. These mutant producers are beginning to shed light on the specifics of the post-PKS modifications of apoptolidin by various tailoring enzymes. For use in our studies of the biological activity of apoptolidin,



we have selected to pursue structure activity relationships of variable apoptolidin glycosylation. A few mutant *Nocardiopsis* were generated that produced novel apoptolidin compounds with reduced glycosylation of the polyketide core.

First, a selective knockout of *ApoGT2* was produced. The resulting mutant *Nocardiopsis* was cultured and extracted. Analysis of the crude extracts revealed that production of apoptolidins A-G had been eliminated. Instead, the organism produced two compounds with the signature UV absorbance of apoptolidin ( $\lambda_{\text{max}} = 232, 333$ ), with a product ion mass of 858.5 m/z. This ion corresponds to the ammonium adduct of the apoptolidin polyketide core, glycosylated at C9 only, confirming the role of *ApoGT2* in the installation of the disaccharide moiety at the C27 hydroxyl group. One compound was tentatively assigned the name apoptolidin H and the second compound was suspected to be the ring expanded isomer, isoapoptolidin H.

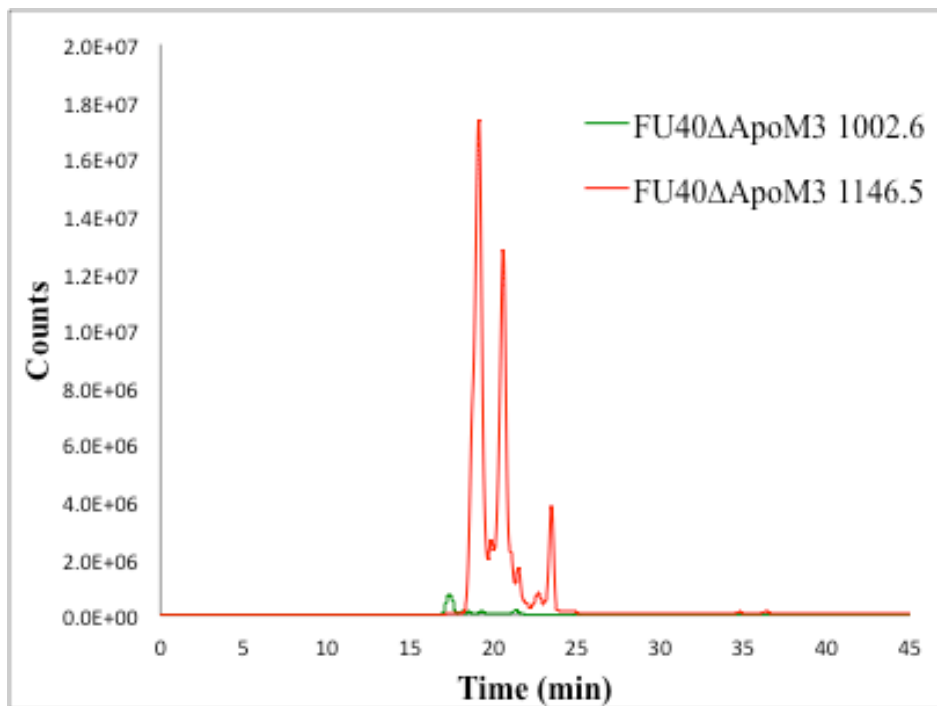


**Figure II-8:** Mass selective (858.5 m/z) LCMS trace of FU40 $\Delta$ ApoGT2

To confirm the structure of these products, FU40 $\Delta$ GT2 was cultured on large scale. Extraction and purification conditions were optimized leading to the isolation of >60 mg of apoptolidin H and 45 mg of isoapoptolidin H per liter of media. Subsequent NMR characterization verified the identity of apoptolidin H as 27-hydroxyapoptolidin A **2.11** as previously synthesized by Nicolaou *et al.*<sup>10</sup> Furthermore, the structure of isoapoptolidin H **2.23** was solved through extensive NMR experiments. <sup>1</sup>H and <sup>13</sup>C shifts of the two compounds are shown in **Table II-1**.

While knockout strains of *ApoGT1* have not resulted in new congener isolation and knockouts of *ApoGT3* have yet to be realized, an additional apoptolidin congener was identified from a knockout of *ApoM3* with apparent reduced glycosylation. Although analysis of the extracts of this mutant producer still revealed a high level of apoptolidin A

production, a minor metabolite was identified with the characteristic UV signature of apoptolidin natural products and a product ion of 1002.6 m/z. This mass corresponds to an apoptolidin ammonium adduct of apoptolidin that is missing the D-oleandrose sugar of the disaccharide at C27. Scale-up fermentation of this mutant followed by extraction and careful chromatographic purification resulted in the isolation of a very small amount of this compound ( $\gg 1$  mg) as confirmed by MALDI-MS. The low yield and challenge of purification of this minor metabolite in the presence of large amounts of apoptolidin A have prohibited NMR characterization and limit the utility of this strain in probe development.



**Figure II-9:** Mass selective (1002.6 and 1146.5 m/z) LCMS trace FU40ΔApoM3

While new mutant producers are currently being pursued in the Bachmann lab, our lab has been investigating the biological activity of apoptolidin using the parent compound apoptolidin A produced from wild type *Nocardioopsis* sp. FU40 and apoptolidin H from the mutant producer FU40 $\Delta$ ApoGT1. These efforts have involved experiments aimed at characterizing and quantifying the reported selective cytotoxicity and the semisynthesis of molecular probes for understanding apoptolidin SAR and identifying any molecular targets.

$\delta_C$		$\delta_C$		$\delta_C$		$\delta_C$					
C#	2.11	2.23	C#	2.11	2.23	C#	2.11	2.23	C#	2.11	2.23
<b>1</b>	172.5	170.3	<b>12</b>	134.8	134.2	<b>23</b>	73.7	73.3	<b>22-Me</b>	12.2	12.0
<b>2</b>	123.9	124.9	<b>13</b>	133.3	133.6	<b>24</b>	40.7	40.7	<b>24-Me</b>	5.3	5.3
<b>3</b>	149.0	147.1	<b>14</b>	24.6	25.4	<b>25</b>	69.1	69.0	<b>17-OMe</b>	61.4	60.0
<b>4</b>	133.4	132.7	<b>15</b>	36.5	33.7	<b>26</b>	38.4	38.0	<b>28-OMe</b>	59.4	59.4
<b>5</b>	147.1	143.5	<b>16</b>	74.5	68.1	<b>27</b>	68.1	74.1	<b>1'</b>	96.0	96.2
<b>6</b>	133.2	132.8	<b>17</b>	83.8	82.2	<b>28</b>	78.6	78.4	<b>2'</b>	73.9	73.7
<b>7</b>	142.9	136.9	<b>18</b>	38.5	36.0	<b>2-Me</b>	14.0	13.4	<b>3'</b>	74.9	74.9
<b>8</b>	38.9	39.4	<b>19</b>	72.3	67.8	<b>4-Me</b>	17.8	17.9	<b>4'</b>	87.5	87.5
<b>9</b>	84.1	84.0	<b>20</b>	75.4	75.3	<b>6-Me</b>	16.5	17.6	<b>5'</b>	68.2	68.2
<b>10</b>	126.4	125.8	<b>21</b>	101.2	102.9	<b>8-Me</b>	18.2	18.4	<b>6'</b>	18.3	18.3
<b>11</b>	141.2	141.0	<b>22</b>	36.3	36.6	<b>12-Me</b>	12.0	12.1	<b>4'-OMe</b>	61.0	61.0

$\delta_H$		$\delta_H$		$\delta_H$		$\delta_H$					
C#	2.11	2.23	C#	2.11	2.23	C#	2.11	2.23	C#	2.11	2.23
<b>1</b>	--	--	<b>12</b>	--	--	<b>23</b>	2.04	3.76	<b>22-Me</b>	1.03	1.05
<b>2</b>	--	--	<b>13</b>	5.68	5.47	<b>24</b>	1.76	1.78	<b>24-Me</b>	0.88	0.86
<b>3</b>	7.36	7.34	<b>14</b>	2.47,2.05	2.49,1.94	<b>25</b>	4.09	4.28	<b>17-OMe</b>	3.36	3.50
<b>4</b>	--	--	<b>15</b>	1.53,1.41	1.39	<b>26</b>	1.58,1.29	1.78,1.41	<b>28-OMe</b>	3.29	3.38
<b>5</b>	6.19	5.97	<b>16</b>	3.44	3.86	<b>27</b>	3.55	3.47	<b>1'</b>	4.82	4.80
<b>6</b>	--	--	<b>17</b>	2.72	3.36	<b>28</b>	3.21,3.17	3.38	<b>2'</b>	3.39	3.39
<b>7</b>	5.23	5.08	<b>18</b>	2.15,1.72	1.68,1.39	<b>2-Me</b>	2.11	2.06	<b>3'</b>	3.72	3.73
<b>8</b>	2.75	2.75	<b>19</b>	5.31	4.45	<b>4-Me</b>	2.19	2.09	<b>4'</b>	2.71	2.72
<b>9</b>	3.83	3.78	<b>20</b>	3.54	4.94	<b>6-Me</b>	1.93	1.73	<b>5'</b>	3.74	3.75
<b>10</b>	5.22	5.26	<b>21</b>	--	--	<b>8-Me</b>	1.26	1.16	<b>6'</b>	1.36	1.25
<b>11</b>	6.18	6.05	<b>22</b>	2.04	1.78	<b>12-Me</b>	1.68	1.71	<b>4'-OMe</b>	3.58	3.58

**Table II-1:**  $^{13}\text{C}$  (150 MHz) and  $^1\text{H}$  (600 MHz) NMR shifts for apoptolidin H **2.11** and isoapoptolidin H **2.23**

## Experimental Methods

**Light-induced isomerization of apoptolidin A:** To a 6 mg (0.005mmol) sample of apoptolidin A in a borosilicate glass NMR tube was added deuterated acetone (0.6 mL). Additionally. The solution was exposed to a 275 watt sunlamp. The solution was removed from irradiation and monitored by  $^1\text{H}$  NMR for the appearance of the new isomer. After 16 hours, the solution was concentrated and the resulting photoisomerized product was purified from the mixture using flash chromatography (silica gel, 2.5% methanol in dichloromethane then 10-15% methanol in dichloromethane) to give 2.3 mg (0.002 mmol) of apoptolidin G isomer as a white solid.  $^1\text{H}$  NMR (600 MHz,  $\text{CD}_3\text{OD}$ ):  $\delta$  6.21 (d,  $J = 15.7$  Hz, 1H), 6.09 (s, 1H), 5.88 (s, 1H), 5.69 (dd,  $J = 7.8, 7.8$  Hz, 1H), 5.34 (dd,  $J = 9.0, 15.7$  Hz, 1H), 5.21 (dd,  $J = 5.0, 11.7$  Hz, 1H), 5.03 (d,  $J = 4.2$  Hz, 1H), 4.94 (d,  $J = 10.0$  Hz, 1H), 4.83 (dd,  $J = 1.7, 9.8$  Hz, 1H), 4.80 (d,  $J = 3.84$  Hz, 1H), 4.07 (d,  $J = 9.8$  Hz, 1H), 3.91 (m, 1H), 3.68–3.82 (m, 5H), 3.57 (s, 3H), 3.54 (s, 3H), 3.43 (s, 3H), 3.38 (m, 1H), 3.37 (m, 1H), 3.33 (s, 3H), 3.33–3.30 (m, 2H), 3.22 (dd,  $J = 7.2, 14.5$  Hz, 1H), 3.22–3.15 (m, 2H), 2.97 (dd,  $J = 9.0, 9.0$  Hz, 1H), 2.81 (m, 1H), 2.71 (dd,  $J = 9.3, 9.3$  Hz, 1H), 2.36–2.46 (m, 3H), 2.18 (m, 1H), 2.11 (m, 1H), 2.01 (s, 3H), 1.98 (d,  $J = 13.4$ , 1H), 1.79 (m, 2H), 1.73 (s, 3H), 1.71 (s, 3H), 1.73–1.69 (m, 4H), 1.60 (s, 3H), 1.40–1.48 (m, 2H), 1.34 (s, 3H), 1.2–1.3 (m, 9H), 1.09 (d,  $J = 6.5$  Hz, 3H), 1.5 (d,  $J = 6.7$  Hz, 3H), 0.89 (d,  $J = 6.9$  Hz, 3H);  $^{13}\text{C}$  NMR (150 MHz,  $\text{CD}_3\text{OD}$ ):  $\delta$  172.1, 141.4, 139.2, 138.4, 135.1, 133.6, 133.5, 133.0, 132.9, 128.7, 126.4, 101.9, 101.4, 99.5, 95.5, 87.6, 86.0, 86.0, 82.7, 82.0, 77.3, 77.3, 77.0, 76.2, 75.8, 75.8, 75.0, 73.9, 73.2, 73.1, 73.0, 68.6, 68.2, 67.5, 61.0, 61.0, 59.5, 57.3, 45.2, 40.7, 39.6, 37.8, 37.8, 37.3, 36.8, 36.8, 24.1, 23.0, 22.7,

18.4, 18.4, 18.3, 18.0, 17.8, 16.1, 12.4, 12.0, 5.4; HRMS (ESI-TOF MS)  $m/z$  1151.6336 (M+Na)<sup>+</sup> calculated for C<sub>58</sub>H<sub>96</sub>NaO<sub>21</sub>, measured 1151.6372.

### **Apoptolidin A fermentation procedure**

**Plate Culture:** 20 microliters of glycerol stock of *Nocardioopsis* sp. FU40 was plated onto a Petri dish containing Bennett's medium and incubated upside down at 30 °C for 3 days. Dishes with spores can then be sealed with parafilm and stored at room temperature for up to 1 month for future use. The composition of Bennett's medium was as follows: yeast extract 1.0 g, beef extract 1.0 g, NZ amine A (casein digest) 2.0 g, glucose 10.0 g, agar 20.0 g per liter of deionized water. The pH of the medium was adjusted to 7.0 with 1 M HCl and 1 M NaOH. After autoclaving, the solution was cooled to room temperature and poured into sterile Petri dishes (30 mL/dish).

**Seed Culture:** The production fermentation was initiated by aseptically inoculating one full loop of mycelia grown on Bennett's agar plate into a sterile 50 mL Falcon tube containing 5 mL seed medium. The seed cultures were incubated for 4 days in a rotary shaker (170 rpm) at 30 °C. The composition of seed medium was as follows: soluble starch 10.0 g, molasses 10.0 g, peptone 10.0 g, beef extract 10.0 g per liter of deionized water. The pH of the medium was adjusted to 7.2 with 1 M HCl and 1 M NaOH. After autoclaving, the solution was cooled to room temperature and distributed into sterile 50 mL Falcon tubes (5 mL/tube). Typically, for compound production, 20 tubes of seed culture were used.

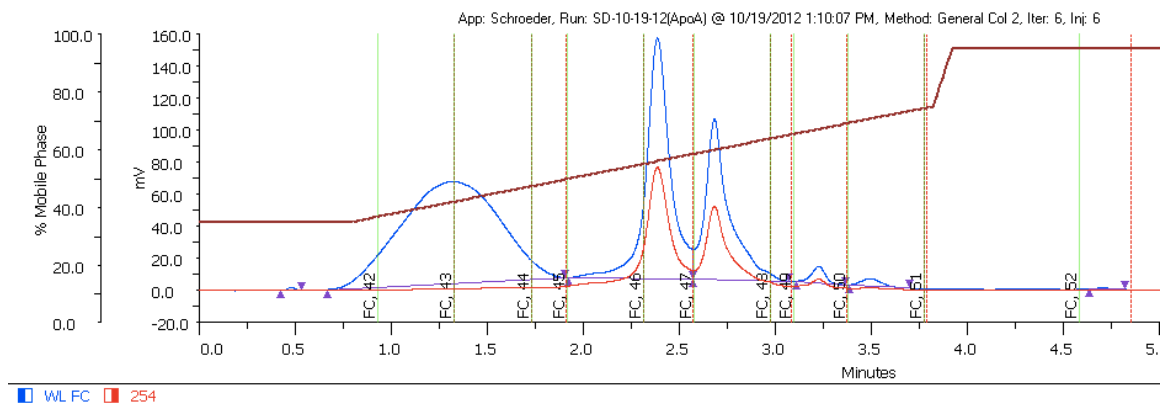
**Production Culture and Extraction:** Each 5 mL seed culture was poured into a 250 mL Erlenmeyer flask containing 50 mL production medium. In a typical production, 20 flasks

were used to create a total of 1 L of production culture. The flasks were incubated for 6 days in a rotary shaker (170 rpm) at 30 °C. The composition of production medium was as follows: glycerol 20.0 g, molasses 10.0 g, casamino acids 5.0 g, peptone 1.0 g, calcium carbonate (CaCO<sub>3</sub>) 4.0 g per liter of deionized water. Specifically, 200 mg of calcium carbonate was first distributed into each 250 mL Erlenmeyer flask. The remaining media components were dissolved in an appropriate volume of water and 50 mL of this solution was distributed into each Erlenmeyer flask. The pH of each flask was individually adjusted to 7.2 with 1 M HCl and 1 M NaOH. The resulting suspensions were autoclaved to produce the production media flasks. After 6 days' incubation, the cell bodies were scraped from each flask and transferred into 50 mL Falcon tubes. The resulting suspensions were centrifuged at 3750 rpm for 30 minutes. The supernatants were decanted and combined into a separatory funnel and extracted with ethyl acetate (3x 750 mL for 20 flasks). The combined ethyl acetate extracts were dried (Na<sub>2</sub>SO<sub>4</sub>) and concentrated under reduced pressure at 29 °C.

**Apoptolidin A/isoapoptolidin A Purification:** The resulting residue from concentration of ethyl acetate extracts were dissolved in 3 mL of DMSO/1L culture and filtered through a 0.2 µm filter. The resulting DMSO solution was purified with preparative reverse phase HPLC (Gilson) with multiple 300 µL injections using a 4 minute gradient of 35-70% acetonitrile in water at a flowrate of 30 mL/min with UV detection at 220 nm and a Phenomenex Luna column (100 Å, 50 x 21.20 mm, 5 µm C18). Apoptolidin A r.t.= 2.69 min/ isoapoptolidin A r.t.=2.69 min. Fractions containing each product were combined into a round bottomed flask and concentrated (T < 31°) to remove acetonitrile. Resulting



aqueous solution was frozen at  $-80\text{ }^{\circ}\text{C}$  and water was removed by lyophilization to yield white solids. NMR spectral data matched the literature.<sup>2,6,7</sup>



**Figure II-10:** HPLC trace of apoptolidin A/isoapoptolidin A purification

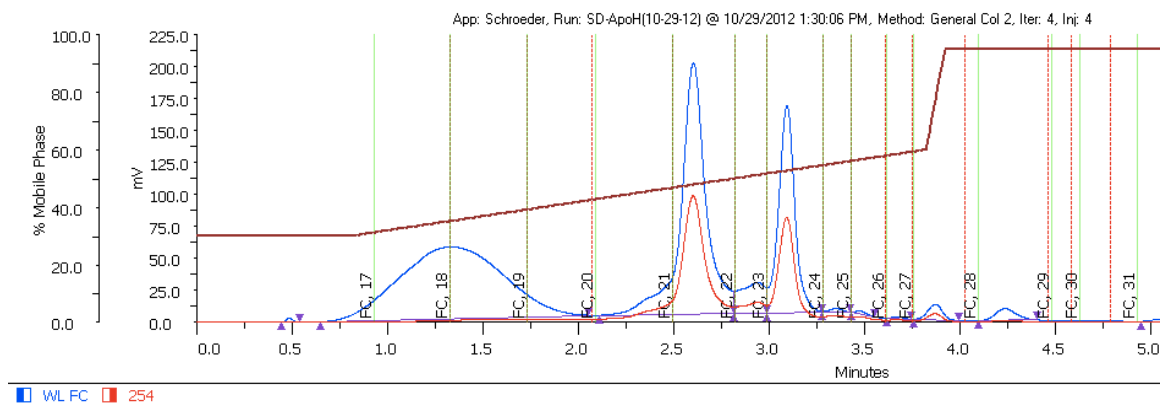
### Apoptolidin H fermentation procedure

**Plate Culture:** 20 microliters of glycerol stock of *Nocardioopsis* sp. FU40 $\Delta$ ApoGT2 (also labeled as FU40 $\Delta$ 412) was plated onto a Petri dish containing apramycin dosed Bennett's medium and incubated upside down at  $30\text{ }^{\circ}\text{C}$  for 3 days. Dishes with spores can then be sealed with parafilm and stored at room temperature for up to 1 month for future use. The composition of apramycin dosed Bennett's medium was as follows: yeast extract 1.0 g, beef extract 1.0 g, NZ amine A (casein digest) 2.0 g, glucose 10.0 g, agar 20.0 g per liter of deionized water. The pH of the medium was adjusted to 7.0 with 1 M HCl and 1 M NaOH. After autoclaving, the solution was cooled to near room temperature, 80 mg apramycin was added per liter and the resulting solution was poured into sterile Petri dishes (30 mL/dish).

**Seed Culture:** The production fermentation was initiated by aseptically inoculating one full loop of mycelia grown on Bennett's agar plate into a sterile 50 mL Falcon tube containing 5 mL seed medium. The seed cultures were incubated for 4 days in a rotary shaker (170 rpm) at 30 °C. The composition of seed medium was as follows: soluble starch 10.0 g, molasses 10.0 g, peptone 10.0 g, beef extract 10.0 g per liter of deionized water. The pH of the medium was adjusted to 7.2 with 1 M HCl and 1 M NaOH. After autoclaving, the solution was cooled to room temperature, 80 mg apramycin was added per liter and the resulting solution was distributed into sterile 50 mL Falcon tubes (5 mL/tube). Typically, for compound production, 20 tubes of seed culture were used.

**Production Culture and Extraction:** Production culture and extraction procedure was identical to that used for apoptolidin A. No apramycin is added to the production media.

**Apoptolidin H/isoapoptolidin H Purification:** The resulting residue from concentration of ethyl acetate extracts were dissolved in 3 mL of DMSO/1L culture and filtered through a 0.2 µm filter. The resulting DMSO solution was purified with preparative reverse phase HPLC (Gilson) with multiple 300 µL injections using a 4 minute gradient of 30-60% acetonitrile in water at a flow-rate of 30 mL/min with UV detection at 220 nm and a Phenomenex Luna column (100 Å, 50 x 21.20 mm, 5 µm C18). Apoptolidin A r.t.= 2.63 min/ isoapoptolidin A r.t.=3.13 min. Fractions containing each product were combined into a round bottomed flask and concentrated ( $T < 31^{\circ}$ ) to remove acetonitrile. Resulting aqueous solution was frozen at -80 °C and water was removed by lyophilization to yield white solids.



**Figure II-11:** HPLC trace for apoptolidin H/isoapoptolidin H purification

**Apoptolidin H:**  $^1\text{H}$  NMR (600 MHz,  $\text{CD}_3\text{OD}$ ):  $\delta$  7.36 (s, 1H), 6.19 (s, 1H), 6.18 (d,  $J = 15.7$  Hz, 1H), 5.69 (dd,  $J = 2.2, 9.1$  Hz, 1H), 5.30 (d,  $J = 11.4$  Hz, 1H), 5.23 (dd,  $J = 9.1, 9.1$ , 1H), 5.21 (d,  $J = 9.0$  Hz, 1H), 4.82 (d,  $J = 3.8$  Hz, 1H), 4.09 (ddd,  $J = 2.1, 3.1, 7.9$  Hz, 1H), 3.83 (dd,  $J = 9.2, 9.2$  Hz, 1H), 3.75 (ddd,  $J = 4.8, 6.3, 11.1$  Hz, 2H), 3.72 (dd,  $J = 9.2, 9.2$  Hz, 1H), 3.58 (s, 3H), 3.54 (m, 2H), 3.44 (m, 1H), 3.40 (dd,  $J = 3.8, 9.8$  Hz, 1H), 3.37 (dd,  $J = 7.0, 7.0$  Hz, 1H), 3.36 (s, 3H), 3.31 (ddd,  $J = 1.6, 1.6, 3.2$ , 1H), 3.29 (s, 3H), 3.21 (dd,  $J = 4.7, 9.4$  Hz, 1H), 3.17 (dd,  $J = 6.3, 9.4$  Hz, 1H), 2.70-2.80 (m, 2H), 2.72 (dd,  $J = 29.1, 9.1$ , 1H), 2.46 (m, 1H), 2.18 (s, 3H), 2.16 (m, 1H), 2.12 (s, 3H), 2.05 (m, 1H), 2.04 (m, 1H), 1.93 (s, 3H), 1.76 (m, 1H), 1.74 (m, 1H), 1.71 (m, 1H), 1.68 (s, 3H), 1.58 (ddd,  $J = 2.6, 2.7, 5.4, 8.9$  Hz, 1H), 1.48-1.55 (m, 1H), 1.37-1.45 (m, 1H), 1.29 (m, 1H), 1.26 (d,  $J = 6.3, 3\text{H}$ ), 1.03 (d,  $J = 6.7$  Hz, 3H), 0.88 (d,  $J = 6.9$  Hz, 3H);  $^{13}\text{C}$  NMR (150 MHz,  $\text{CD}_3\text{OD}$ ):  $\delta$  172.6, 149.0, 147.1, 142.9, 141.2, 134.8, 133.4, 133.3, 133.2, 126.4, 123.9, 101.2, 96.0, 87.5, 84.1, 83.8, 78.6, 75.4, 74.9, 74.5, 73.7, 73.6, 72.3, 69.1, 68.2, 68.1, 61.4, 61.0, 59.4, 40.7, 38.9, 38.5, 38.4, 36.5, 36.3, 24.6, 18.3(2), 18.2(6), 17.8, 16.5, 14.0, 12.2, 12.0, 5.3; HRMS (ESI-TOF MS)  $m/z$  863.4769 ( $\text{M}+\text{Na}$ ) $^+$  calculated for  $\text{C}_{44}\text{H}_{72}\text{NaO}_{15}$ , measured 863.4766.

**Isoapoptolidin H:**  $^1\text{H}$  NMR (600 MHz,  $\text{CD}_3\text{OD}$ ):  $\delta$  7.34 (s, 1H), 6.04 (d,  $J = 15.8$ , 1H), 5.97 (s, 1H), 5.47 (dd,  $J = 6.5, 8.8$  Hz, 1H), 5.26 (dd,  $J = 8.8, 15.8$  Hz, 1H), 5.07 (d,  $J = 10.4$  Hz, 1H), 4.94 (d,  $J = 2.4$  Hz, 1H), 4.80 (d,  $J = 3.8$  Hz, 1H) 4.45 (ddd,  $J = 2.0, 2.0, 11.3$  Hz, 1H), 3.86 (m, 1H), 3.78 (m, 1H), 3.76 (m, 1H), 3.75 (m, 1H), 3.73 (m, 1H), 3.58 (s, 3H), 3.49 (s, 3H), 3.47 (m, 1H), 3.40 (m, 1H), 3.38 (s, 3H), 3.37 (m, 1H), 3.35 (m, 1H), 2.75 (m, 1H), 2.72 (dd,  $J = 9.2, 9.2$  Hz, 1H), 2.48 (m, 1H), 2.09 (s, 3H), 2.06 (s, 3H), 1.94 (m, 1H), 1.6-1.8 (m, 4H), 1.73 (s, 3H), 1.71 (s, 3H), 1.42 (m, 1H), 1.39 (m, 3H), 1.25 (d,  $J = 6.2$  Hz, 3H), 1.17 (d,  $J = 6.5$  Hz, 3H), 1.05 (d,  $J = 6.6$  Hz, 3H), 0.86 (d,  $J = 6.9$  Hz, 3H);  $^{13}\text{C}$  NMR (150 MHz,  $\text{CD}_3\text{OD}$ ):  $\delta$  170.3, 147.1, 143.5, 141.0, 136.9, 134.2, 133.6, 132.8, 132.7(9), 125.8, 124.9, 102.9, 96.2, 87.5, 84.0, 82.2, 78.4, 75.3, 74.9, 74.1, 73.7, 73.3, 69.0, 68.1(6), 68.0(9), 67.8, 61.0, 60.0, 59.4, 40.7, 39.4, 38.0, 36.6, 36.0, 33.7, 25.4, 18.4, 18.3, 17.9, 17.6, 13.4, 12.1, 12.0, 5.3; HRMS (ESI-TOF MS)  $m/z$  863.4769 ( $\text{M}+\text{Na}$ ) $^+$  calculated for  $\text{C}_{44}\text{H}_{72}\text{NaO}_{15}$ , measured 863.4764.

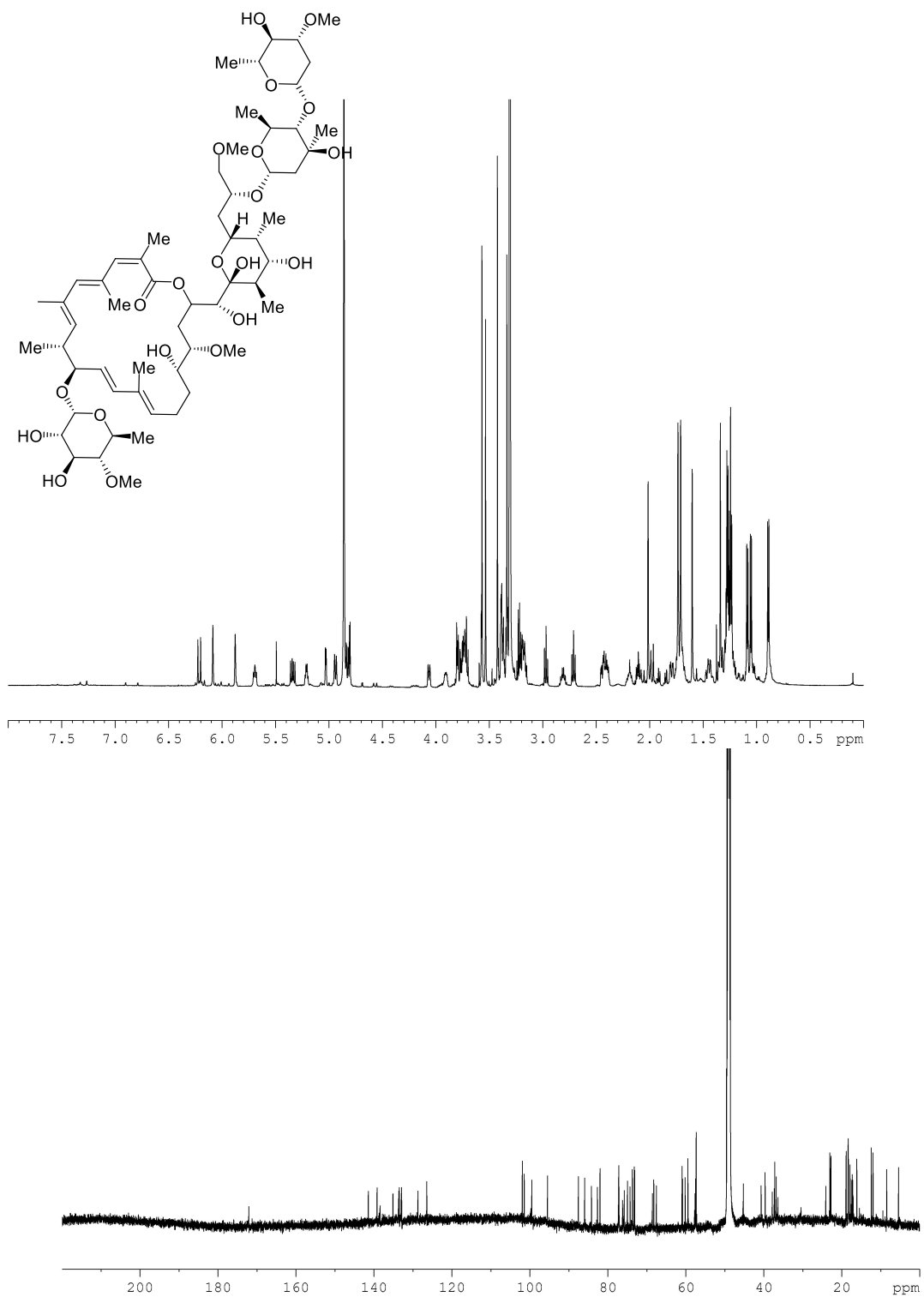
## References

1. Kim, J.; Adachi, H.; Shin-Ya, K. Apoptolidin, a New Apoptosis Inducer in Transformed Cells from *Nocardiosis* sp. *J. Antibiot.* **1997**, *50*, 628–630.
2. Hayakawa, Y.; Kim, J. W.; Adachi, H.; Shin-ya, K.; Fujita, K.; Seto, H. Structure of Apoptolidin, a Specific Apoptosis Inducer in Transformed Cells. *J. Am. Chem. Soc.* **1998**, *120*, 3524–3525.
3. Wender, P. A.; Sukopp, M.; Longcore, K. Apoptolidins B and C: isolation, structure determination, and biological activity. *Org. Lett.* **2005**, *7*, 3025–8.
4. Wender, P. A.; Longcore, K. E. Apoptolidins E and F, new glycosylated macrolactones isolated from *Nocardiosis* sp. *Org. Lett.* **2009**, *11*, 5474–7.

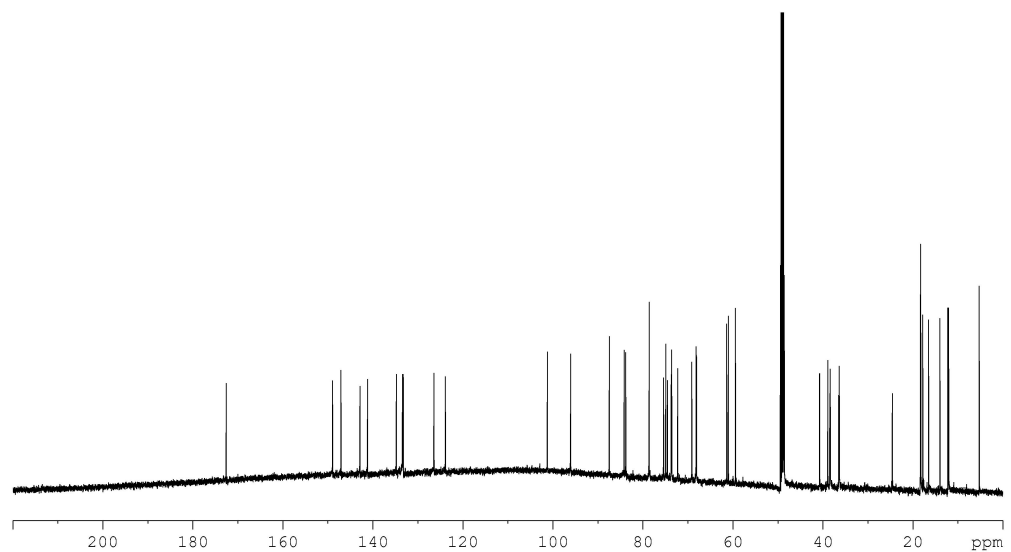
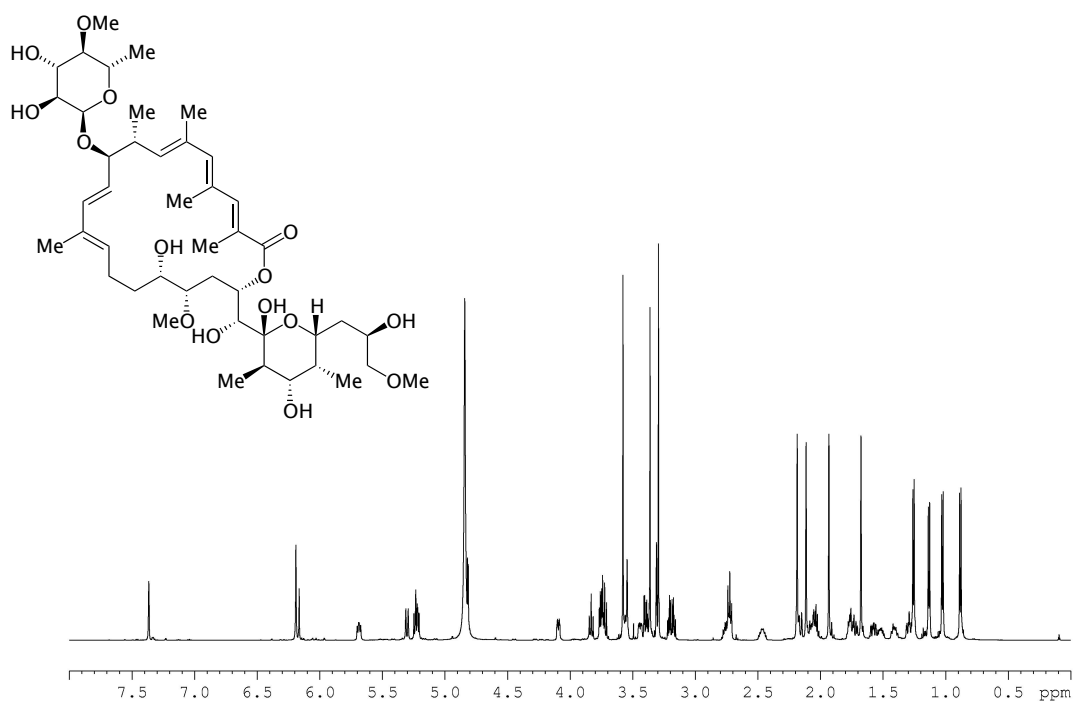
5. Wender, P. A.; Longcore, K. E. Isolation, structure determination, and anti-cancer activity of apoptolidin D. *Org. Lett.* **2007**, *9*, 691–4.
6. Wender, P. A.; Gullledge, A. V.; Jankowski, O. D.; Seto, H. Isoapoptolidin: structure and activity of the ring-expanded isomer of apoptolidin. *Org. Lett.* **2002**, *4*, 3819–22.
7. Pennington, J. D.; Williams, H. J.; Salomon, A. R.; Sulikowski, G. A. Toward a stable apoptolidin derivative: identification of isoapoptolidin and selective deglycosylation of apoptolidin. *Org. Lett.* **2002**, *4*, 3823–5.
8. Bachmann, B. O.; McNeese, R.; Melancon, B. J.; Ghidu, V. P.; Clark, R.; Crews, B. C.; DeGuire, S. M.; Marnett, L. J.; Sulikowski, G. A. Light-induced isomerization of apoptolidin leads to inversion of C2-C3 double bond geometry. *Org. Lett.* **2010**, *12*, 2944–7.
9. Daniel, P. T.; Koert, U.; Schuppan, J. Apoptolidin: induction of apoptosis by a natural product. *Angew. Chem. Int. Ed. Engl.* **2006**, *45*, 872–93.
10. Nicolaou, K. C.; Li, Y.; Sugita, K.; Monenschein, H.; Guntupalli, P.; Mitchell, H. J.; Fylaktakidou, K. C.; Vourloumis, D.; Giannakakou, P.; O’Brate, A. Total synthesis of apoptolidin: Completion of the synthesis and analogue synthesis and evaluation. *J. Am. Chem. Soc.* **2003**, *125*, 15443–15454.
11. Wu, B.; Liu, Q.; Sulikowski, G. A. Total synthesis of apoptolidinone. *Angew. Chem. Int. Ed. Engl.* **2004**, *43*, 6673–5.
12. Wang, J. Ph.D. Thesis, Vanderbilt University, Nashville, TN, 2009.
13. Ghidu, V. P.; Ntai, I.; Wang, J.; Jacobs, A. T.; Marnett, L. J.; Bachmann, B. O.; Sulikowski, G. a Combined chemical and biosynthetic route to access a new apoptolidin congener. *Org. Lett.* **2009**, *11*, 3032–4.
14. Salomon, a R.; Zhang, Y.; Seto, H.; Khosla, C. Structure-activity relationships within a family of selectively cytotoxic macrolide natural products. *Org. Lett.* **2001**, *3*, 57–9.
15. Wender, P. a; Jankowski, O. D.; Tabet, E. a; Seto, H. Toward a structure-activity relationship for apoptolidin: selective functionalization of the hydroxyl group array. *Org. Lett.* **2003**, *5*, 487–90.
16. Lewis, C. a; Longcore, K. E.; Miller, S. J.; Wender, P. a An approach to the site-selective diversification of apoptolidin A with peptide-based catalysts. *J. Nat. Prod.* **2009**, *72*, 1864–9.

17. Wender, P. a; Jankowski, O. D.; Tabet, E. a; Seto, H. Facile synthetic access to and biological evaluation of the macrocyclic core of apoptolidin. *Org. Lett.* **2003**, *5*, 2299–302.
18. Smith, S.; Tsai, S.-C. The type I fatty acid and polyketide synthases: a tale of two megasynthases. *Nat. Prod Rep.* **2007**, *24*, 1041–72.
19. Bachmann, B. O.; Ravel, J. Chapter 8. Methods for in silico prediction of microbial polyketide and nonribosomal peptide biosynthetic pathways from DNA sequence data. *Methods Enzymol.* **2009**, *459*, 143–163.
20. Du, Y.; Derewacz, D. K.; DeGuire, S. M.; Teske, J.; Ravel, J.; Sulikowski, G. A.; Bachmann, B. O. Biosynthesis of the Apoptolidins in *Nocardioopsis* sp. FU 40. *Tetrahedron* **2011**, *67*, 6568–6575.

## Spectra Relevant to Chapter 2

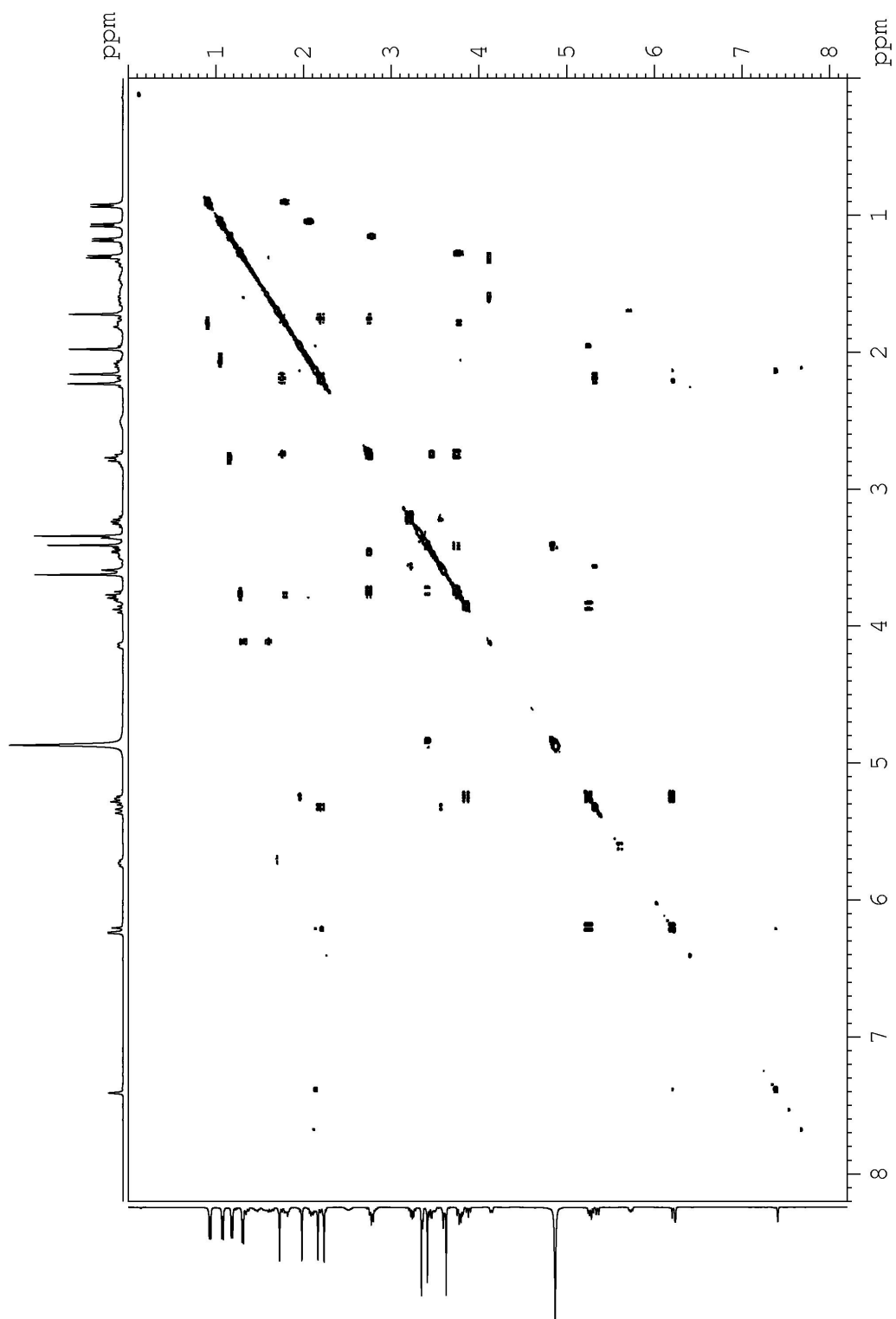


**Spectra II-1:** The 600 MHz  $^1\text{H}$  and 150 MHz  $^{13}\text{C}$  NMR spectra of **2.7** in  $\text{CD}_3\text{OD}$

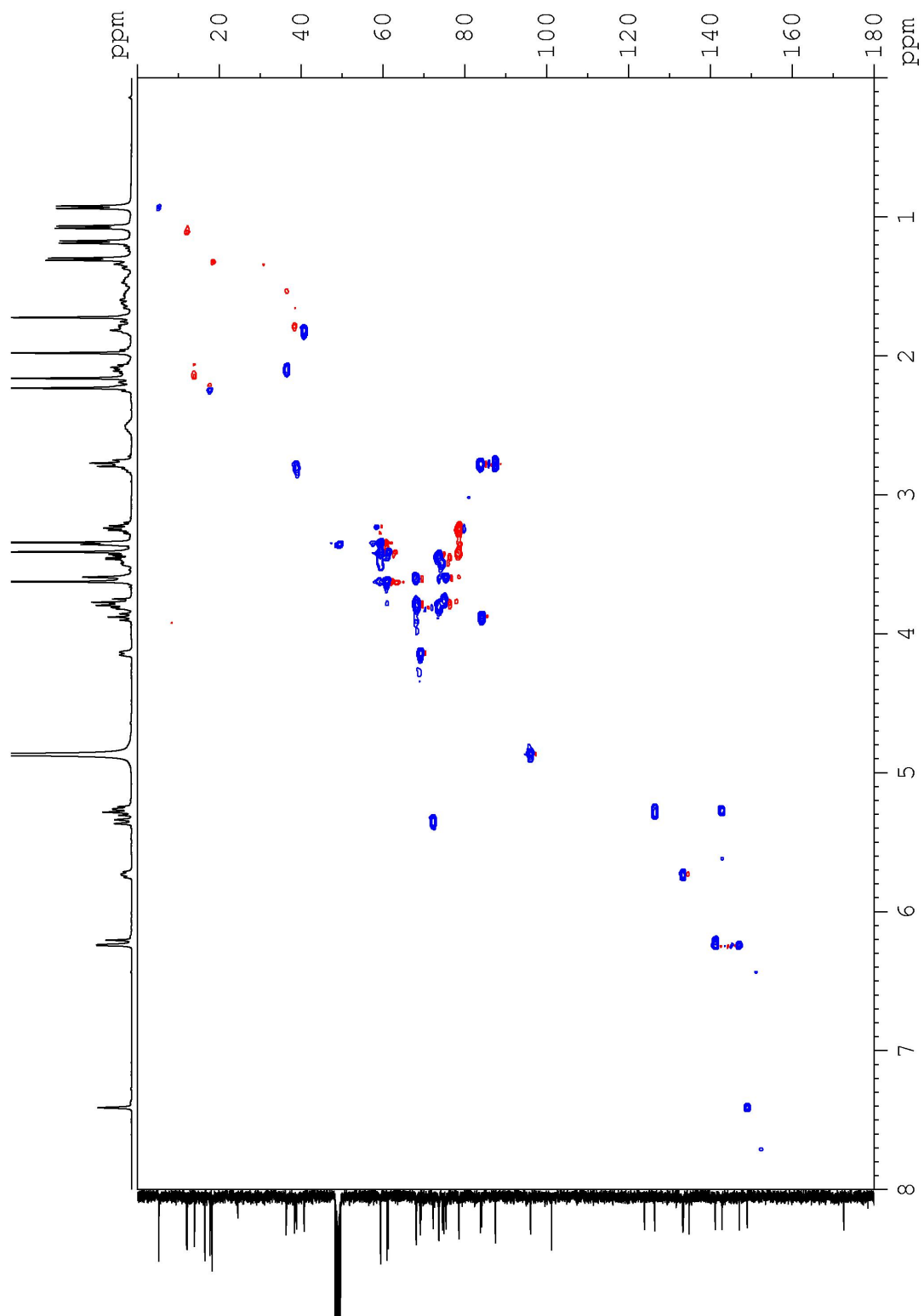


**Spectra II-2:** The 600 MHz  $^1\text{H}$  and 150 MHz  $^{13}\text{C}$  NMR spectra of **2.11** in  $\text{CD}_3\text{OD}$ .

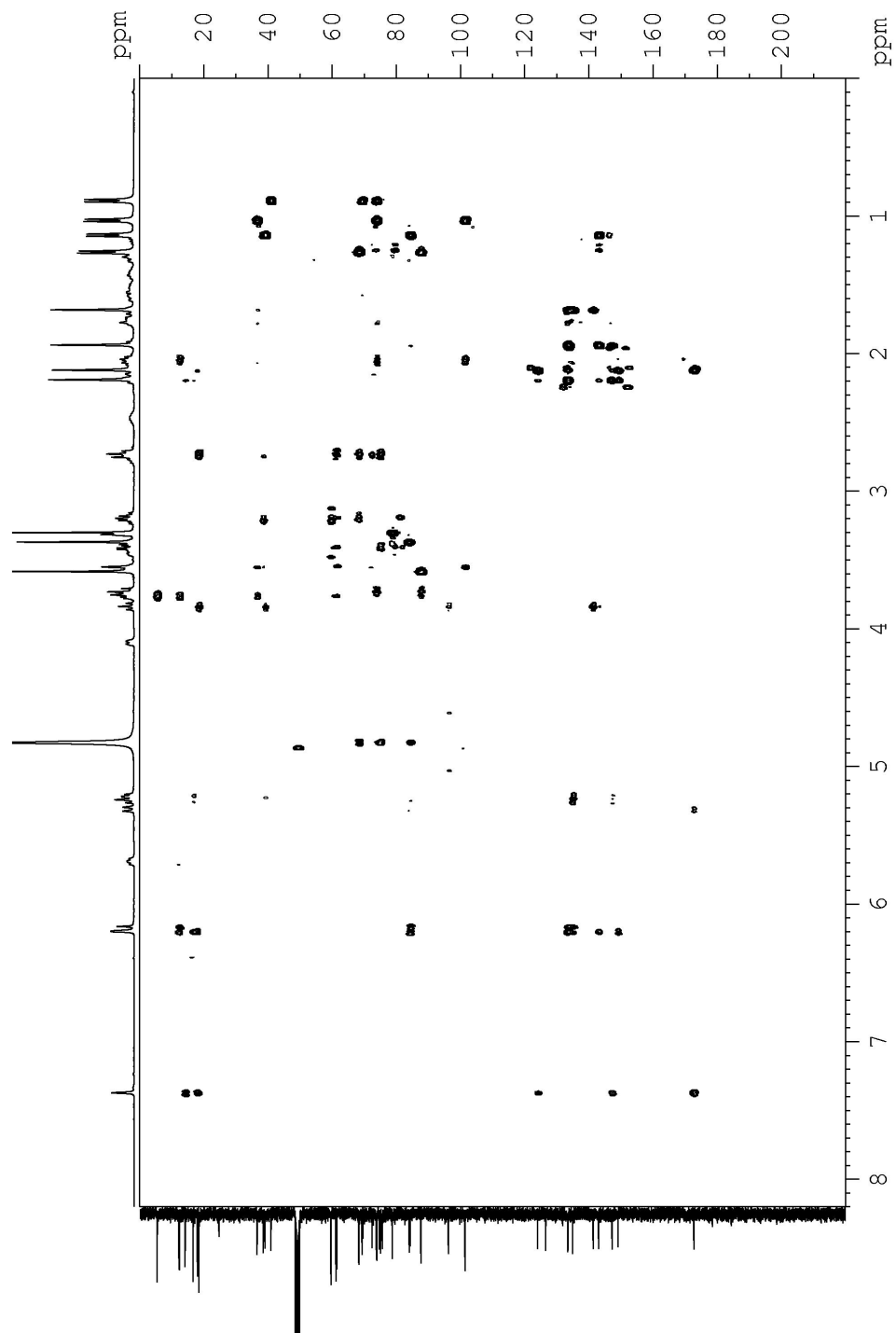




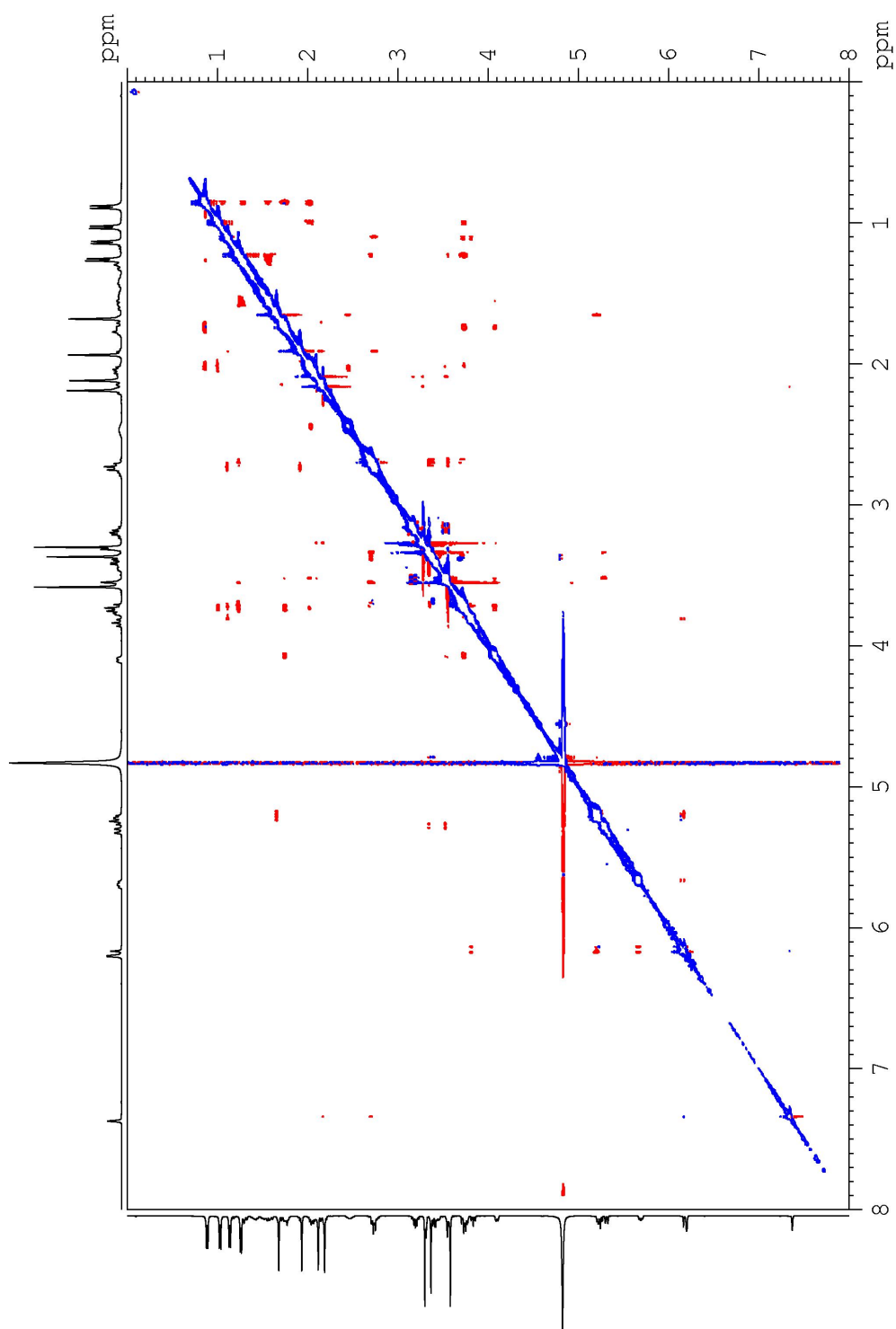
**Spectra II-3:** The 400 MHz COSY NMR of **2.11** in CD<sub>3</sub>OD



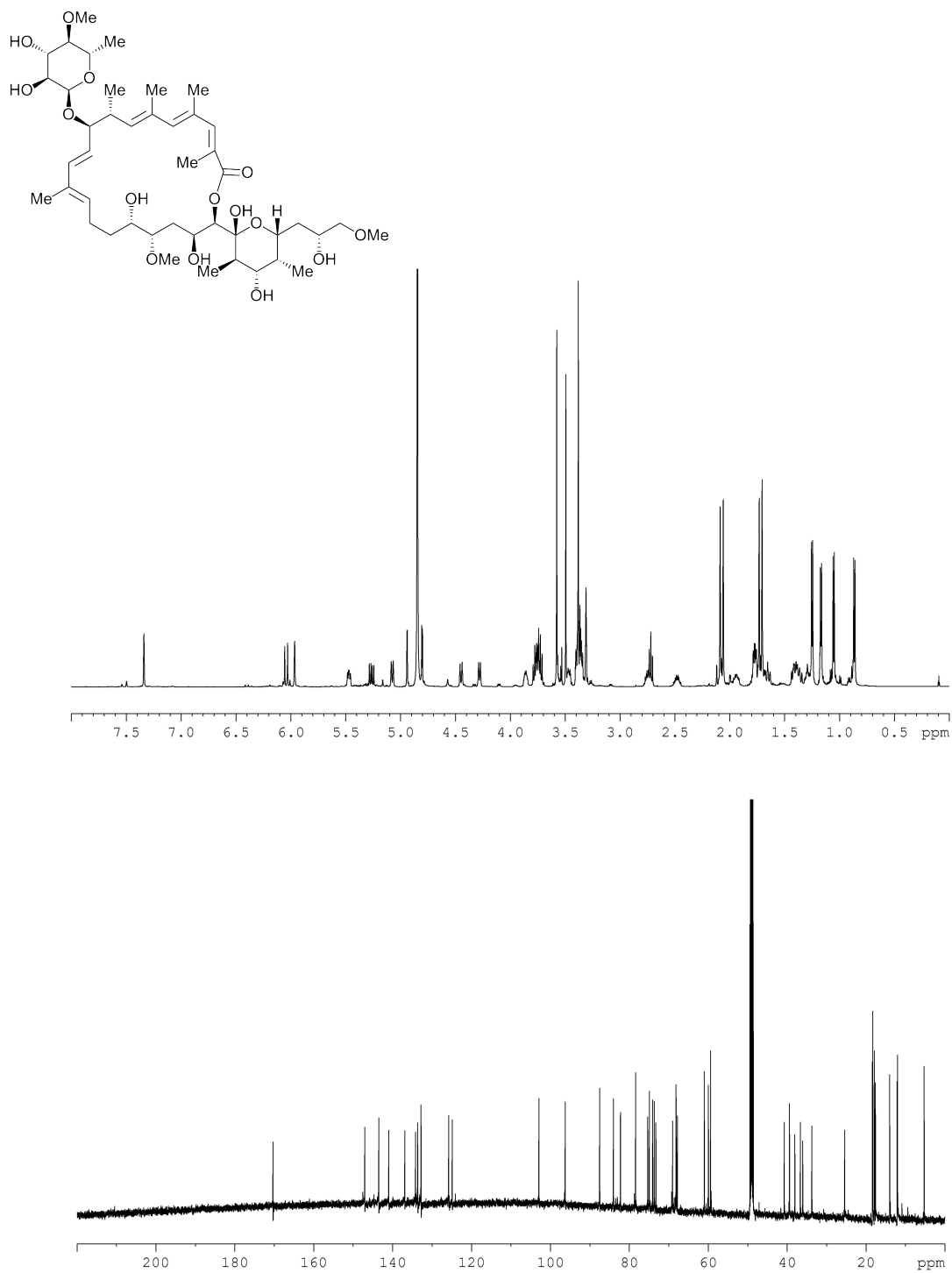
**Spectra II-4:** The 400 MHz HSQC NMR spectrum of **2.11**  $\text{CD}_3\text{OD}$



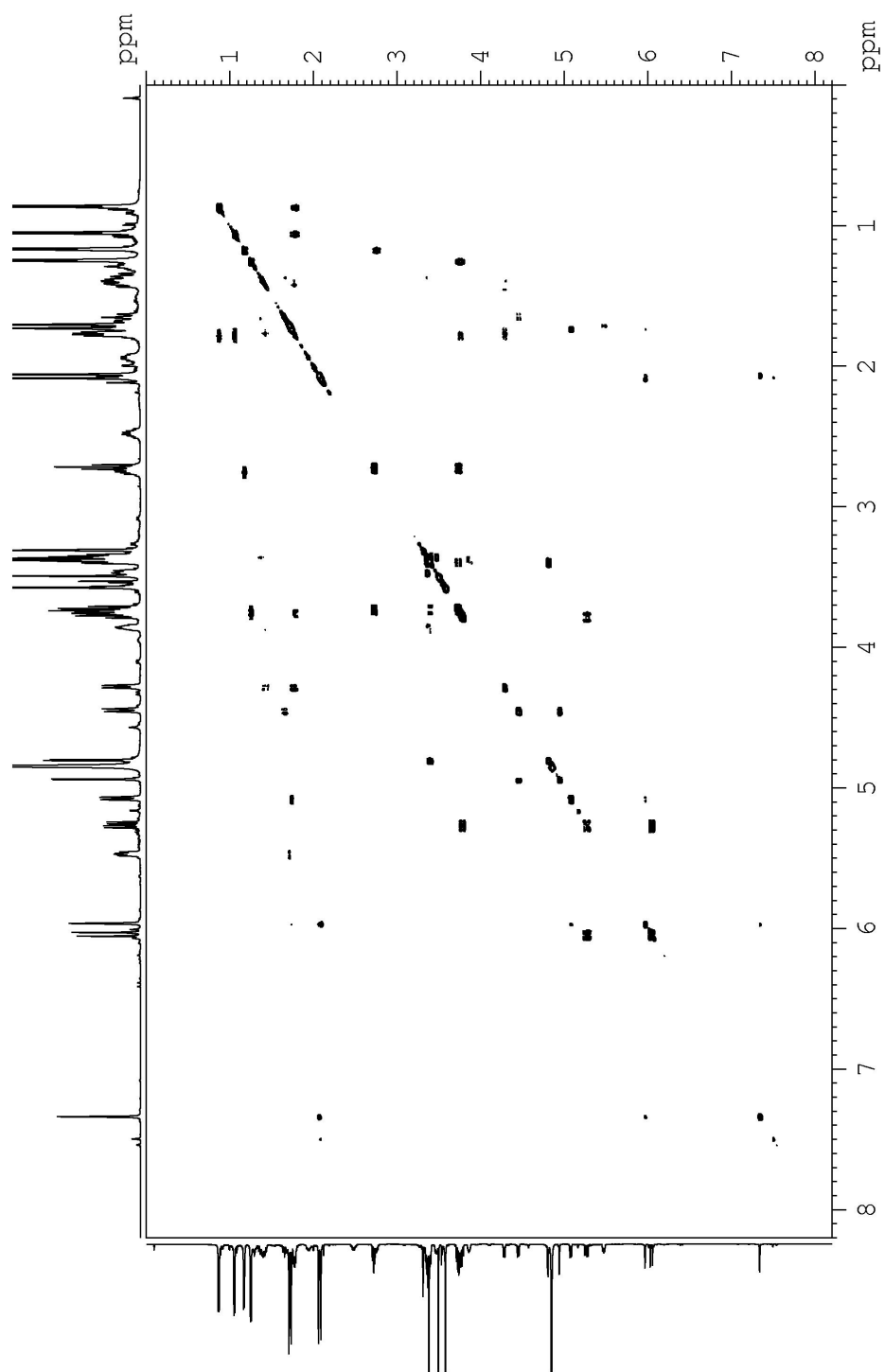
Spectra II-5: The 400 MHz HMBC NMR spectrum of **2.11** in  $\text{CD}_3\text{OD}$ .



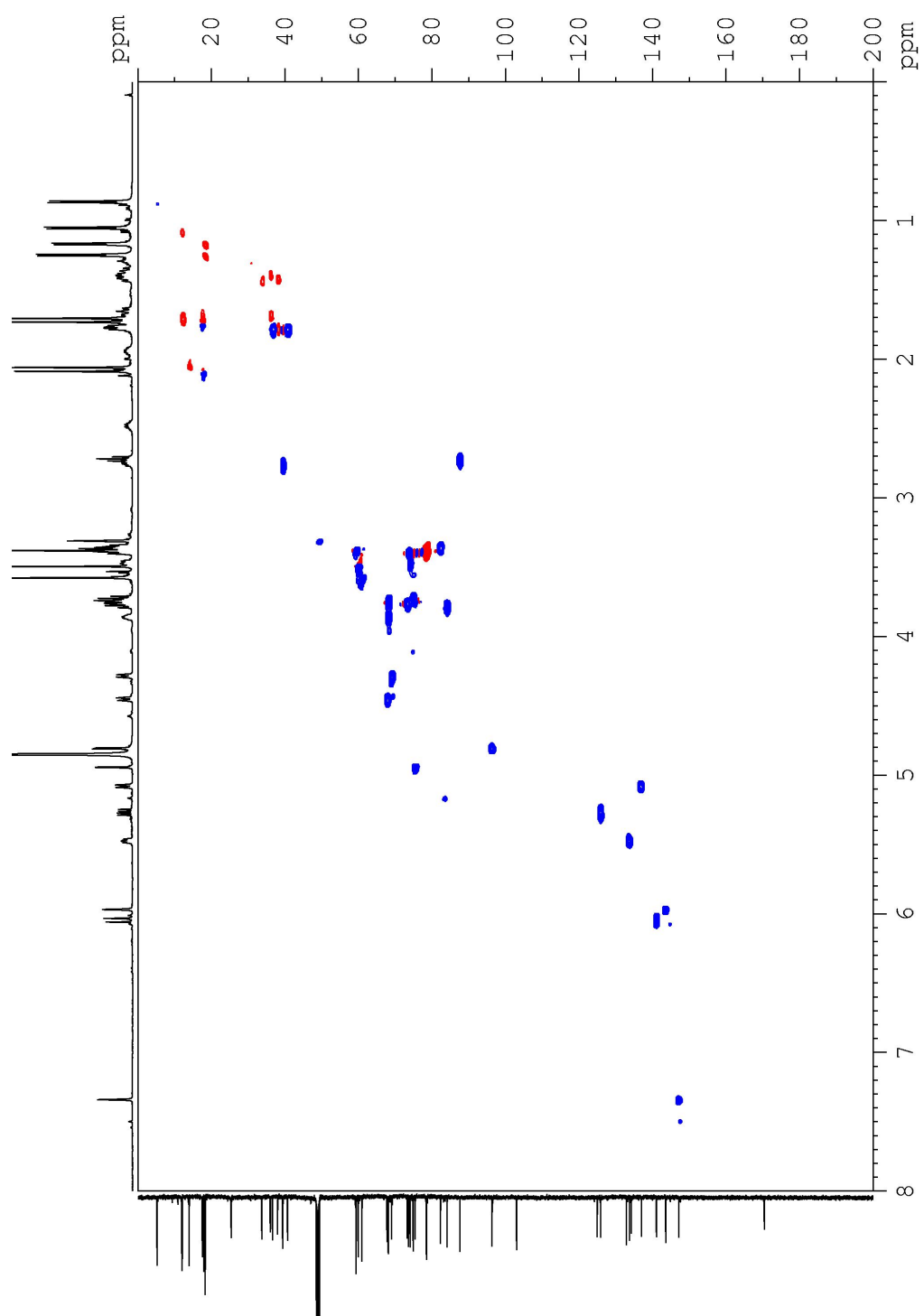
**Spectra II-6:** The 400 MHz NOESY NMR spectrum of **2.11** in CD<sub>3</sub>OD.



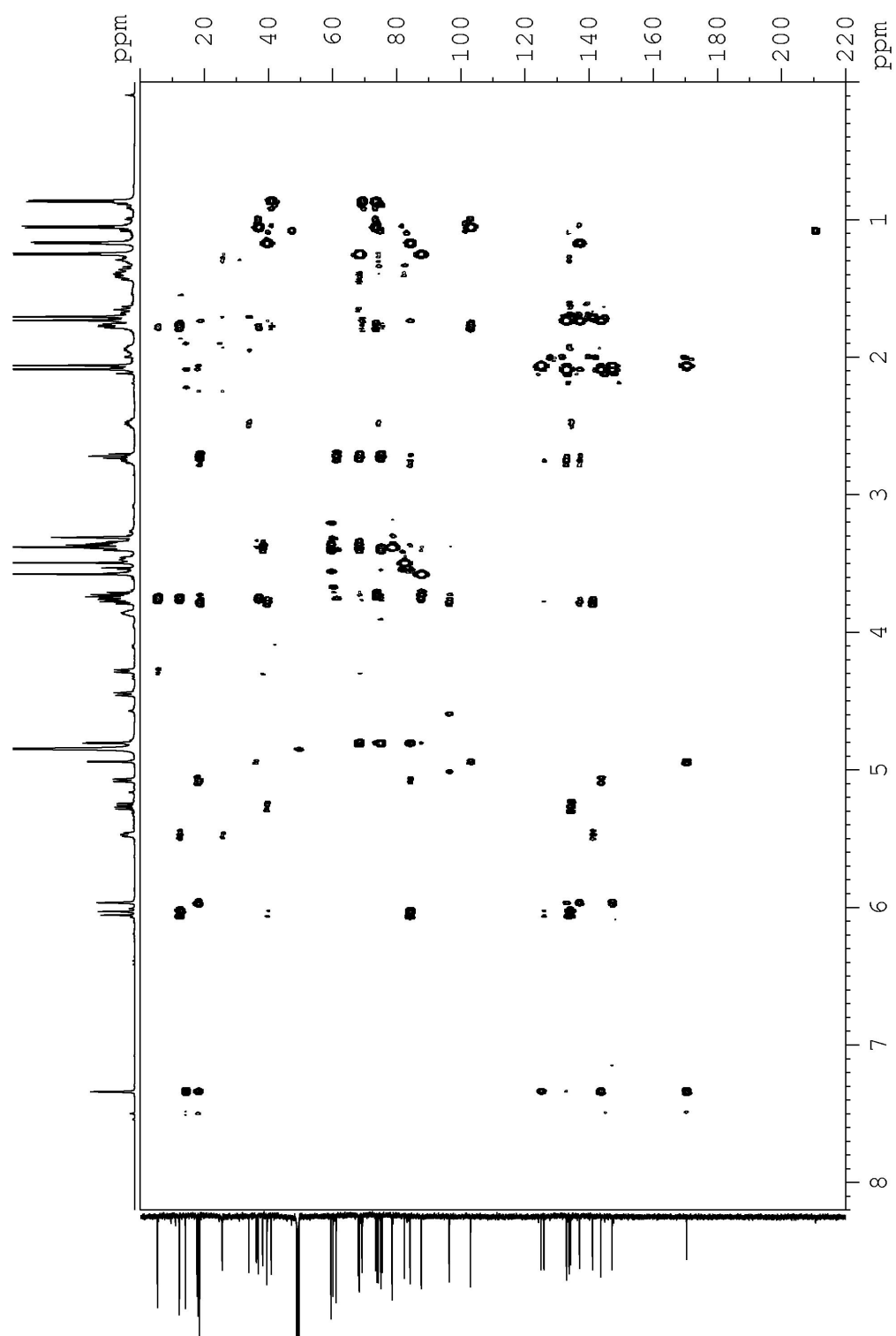
**Spectra II-7:** The 600 MHz  $^1\text{H}$  and 150 MHz  $^{13}\text{C}$  NMR of **2.23** in  $\text{CD}_3\text{OD}$ .



**Spectra II-8:** The 400 MHz COSY NMR spectrum of **2.23** in CD<sub>3</sub>OD.

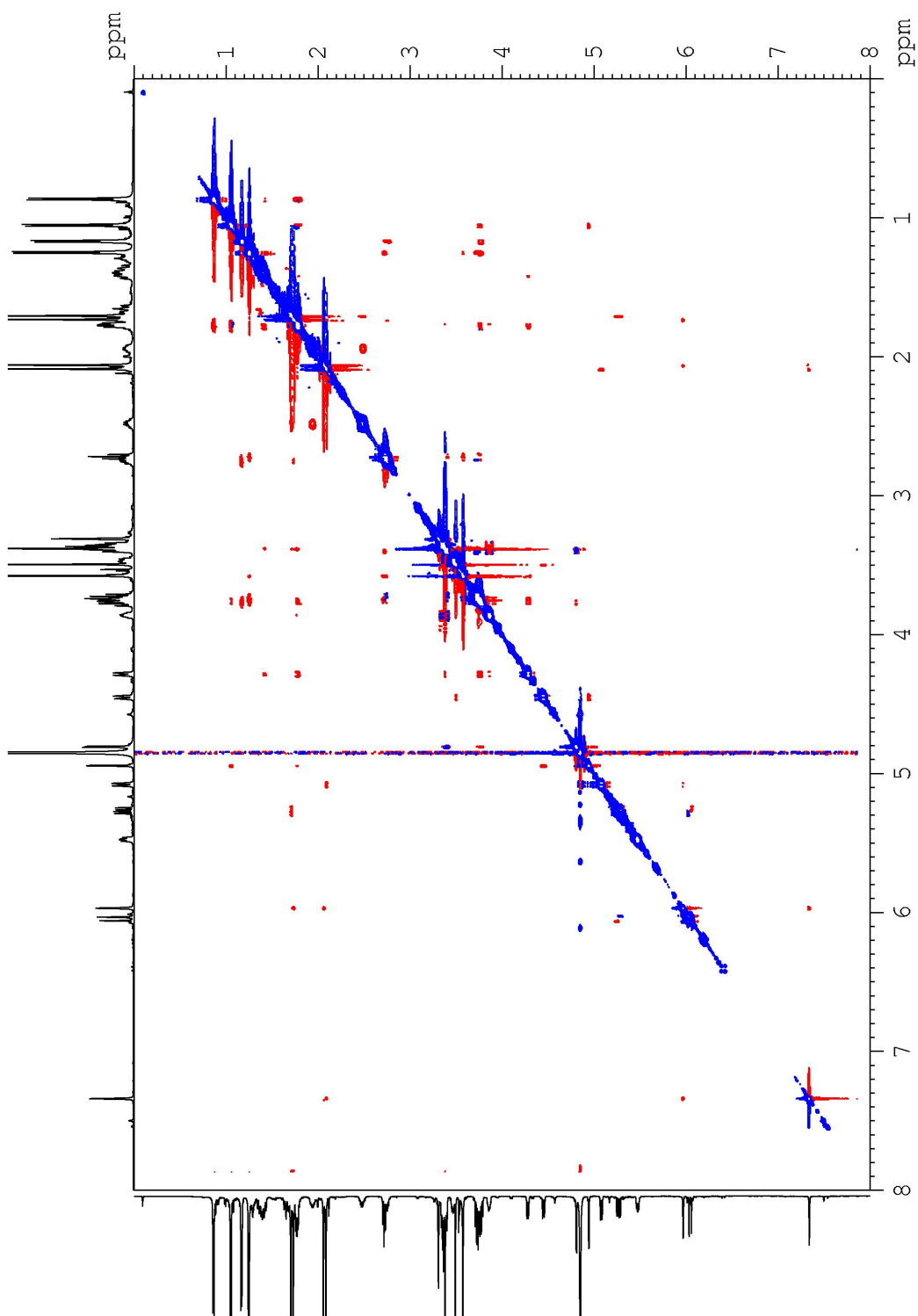


**Spectra II-9:** The 400 MHz HSQC NMR spectrum of **2.23** in CD<sub>3</sub>OD.



**Spectra II-10:** The 400 MHz HMBC NMR spectrum of **2.23** in CD<sub>3</sub>OD.





**Spectra II-11:** The 400 MHz NOESY NMR spectrum of **2.23** in CD<sub>3</sub>OD.

## CHAPTER III

### Apoptolidin Biological Activity Studies

#### **Background: Previous Reports on Biological Activity**

##### *A Cell Selective Cytotoxic Polyketide Natural Product*

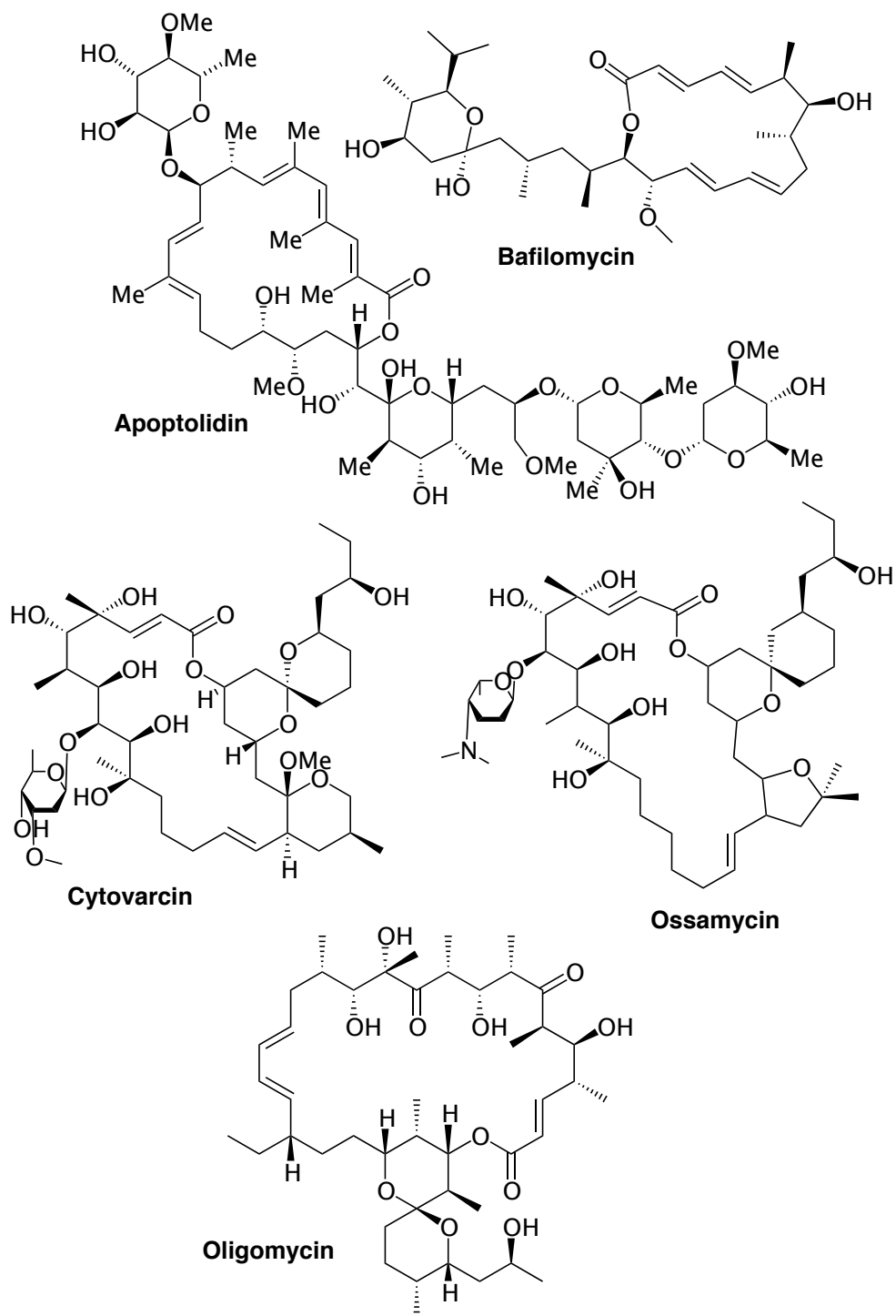
Apoptolidin's reported selective and potent cytotoxicity in *E1A* transformed primary rat glia cells, compared to untransformed cells, has prompted significant study in several laboratories.<sup>1</sup> Transformation with the *E1A* adenovirus oncogene is used to create a simplified model of cancer. E1A is a transcription regulator that increases expression of genes that promote rapid proliferation and inhibit protective apoptotic responses, effectively mimicking cancerous phenotypes<sup>2,3</sup> Using this model, apoptolidin was reported to induce apoptosis as indicated by chromatin condensation and DNA laddering.

Apoptolidin was later submitted for testing against the National Cancer Institute's 60-cell line panel (NCI-60) to determine if the observed potency and selectivity in rat models would track into human models of cancer.<sup>4</sup> The resulting data showed a high level of cell line selective activity in this assay (**Figure III-1**). Indeed, apoptolidin was cited by Salomon *et al* to be "ranked in the top 0.1% most selective agents of the 37,000 compounds screened up to that time" based on these data.<sup>5</sup> To properly appreciate these results, it is important to understand the basics of the assay employed by the NCI in the 60-cell line cancer panel.<sup>6,7</sup> The NCI 60-cell line assay was developed to rapidly screen

compounds under a defined set of cell culture conditions to provide the most information possible, recognizing that this single set of conditions might lead to false positives and false negatives given the many possible mechanisms of cytotoxicity. This assay simultaneously assays for both cytotoxicity (a reduction in cell population after treatment compared to a  $t=0$  measurement) and growth rate inhibition (a reduction in cell population due to treatment compared to a vehicle control) from a two day treatment at a single cell density per cell line. Under the conditions employed by the NCI, apoptolidin showed potent growth rate inhibition in select cell lines, but no cytotoxicity was observed at concentrations up to 10  $\mu\text{M}$  in any of the lines tested.<sup>4</sup>

The Stanford research group indicated the pattern of activity of apoptolidin correlates with a family of highly cell line selective cytotoxic macrocyclic natural products (**Figure III-2**). These complex polyketides were isolated from diverse bacterial species, have different selectivity profiles in the NCI-60 and significantly different structures but all exert potent cytotoxicity in cancer cells under specific conditions. Some of these compounds have known targets that include both  $F_0F_1\text{ATPase}$  (oligomycin) and vacuolar  $\text{ATPase}$  (bafilomycin) but knowledge of the exact mechanisms of their selectivity and toxicity is poor. The identification of novel biological targets for the selective induction of cell death in cancer is highly desired in designing new therapeutics.<sup>8</sup> While apoptolidin is expected to induce cell death through an apoptotic mechanism, mounting evidence suggests the possibility of alternative death pathways. Cell death is currently classified into three primary categories based upon biochemical and morphological hallmarks: necrosis, apoptosis, and autophagic cell death.<sup>9</sup>





**Figure III-2:** Cytotoxic macrocycles

Apoptosis was initially described by Kerr *et al* in 1972 as a morphologically distinct form of cell death.<sup>10</sup> This death is programmed and highly regulated in all eukaryotes. Apoptosis is an evolutionarily conserved pathway that is responsible for complex morphological changes ranging from the metamorphosis of insects and amphibians to human embryonic development. Apoptosis also occurs normally in mature organisms to both maintain cell populations in tissues and as a defense mechanism in immune response through the elimination of damaged cells resulting from disease, toxic agents or environmental stress. The highly regulated nature of this cytotoxicity and its dysregulation in diseases of neurodegeneration and cancer has prompted significant study to understand its mechanism.<sup>11</sup>

Apoptosis signaling results from the activation of various executioner caspases (3, 6, and 7) by way of the activation of initiator caspases (2, 8, 9, and 10). Caspases are proteolytic enzymes that are constitutively expressed in the inactive procaspase form. The ability of each caspase to proteolytically activate other caspases quickly commits the cell to apoptosis upon receipt of a death signal. Upon activation, executioner caspases, most significantly caspase 3, begin to activate endonucleases that fragment chromosomal DNA and cause chromatin condensation.<sup>11</sup> Depolarization of the plasma membrane is also observed, resulting in the external presentation of phosphatidylserine on the cell surface marking the cell for phagocytosis. Morphological features accompanying apoptosis include reduction in cell volume (pyknosis) and plasma membrane blebbing.<sup>9</sup>

A second, morphologically distinct form of cell death is necrosis. Classically, necrosis was described as accidental (as opposed to programmed) cell death. Growing evidence, however, suggests that necrotic cell death may involve regulated biochemical

reactions of its own, leading to the increased popularity of the term ‘necroptosis’ to indicate programmed necrosis.<sup>12,13</sup> The biochemical reactions involved in necrosis are still poorly understood, making it difficult to positively confirm necrosis through a biochemical assay. Because of this, necrosis can only be implicated by the absence of data to suggest an alternative cell death (e.g. apoptosis or autophagy). While the most common causes of necrosis appear to be interference with cellular energy supply or direct damage to the plasma membrane, diverse stimuli can also induce necrosis including many of the stimuli associated with apoptosis induction. Morphologically, necrosis is characterized by cytoplasmic swelling, plasma membrane rupture, swelling of cytoplasmic organelles as well as moderate chromatin condensation.<sup>9</sup>

Finally, cell death has also been implicated to be the result of macroautophagy called autophagic cell death.<sup>14</sup> Autophagy is a catabolic cellular process whereby specialized vesicles are formed, called autophagosomes, which engulf organelles and macromolecules to be broken down by lysosomes to regenerate cellular building blocks. Not surprisingly, autophagy is known to have a protective role when stimulated by nutrient deprivation.<sup>15</sup> Autophagic cell death is defined as cell death that is accompanied by massive autophagic vacuolization but occurs without chromatin condensation.<sup>9</sup>

The observed cytotoxicity of apoptolidin was initially attributed to apoptosis due to observed DNA laddering and chromatin condensation in *E1A* transformed rat glia cells.<sup>1</sup> While experiments with human cancer cell lines have shown potent cytotoxicity under specific conditions with select cell lines (*vida infra*) and indicate the central importance of mitochondria in this toxicity, little evidence exists to indicate that the toxicity is the result of apoptosis. A careful analysis of what is currently known about the

mechanisms of apoptosis, the best characterized of the three principle forms of cell death, and specifically those initiated by the mitochondria helps to appreciate the details of these results.

### *Known Mechanisms of Apoptosis Induction*

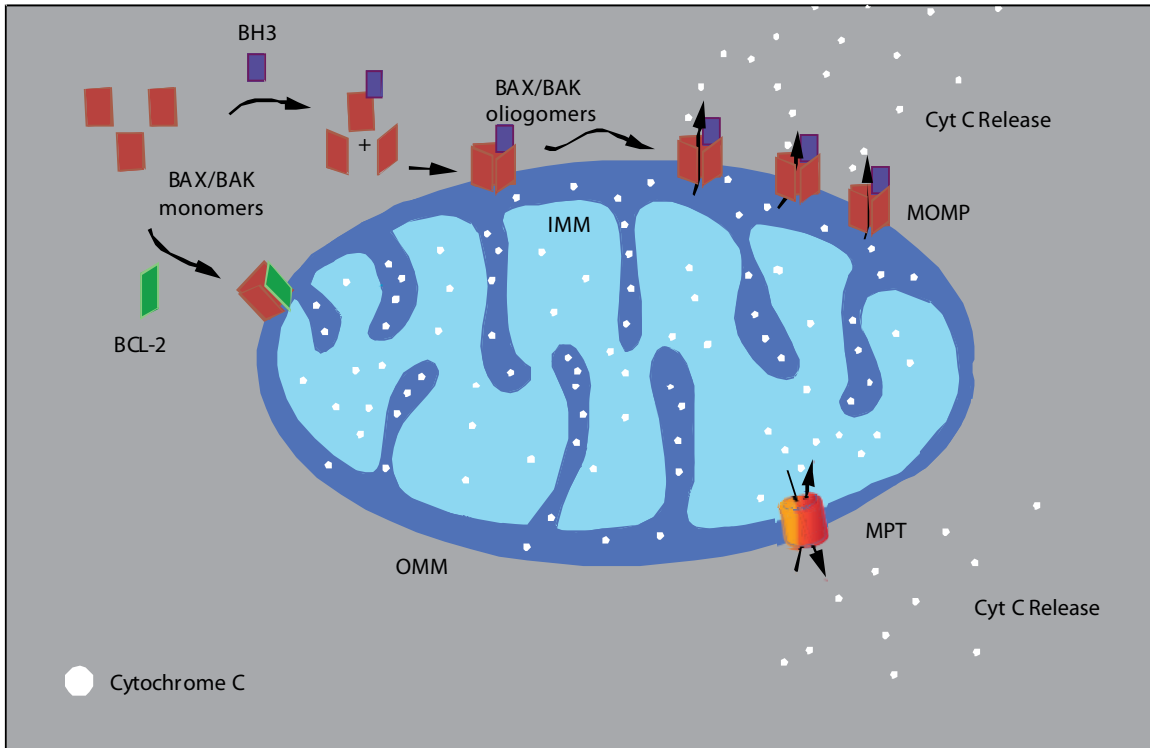
Two pathways for apoptosis initiation have been identified, namely the extrinsic (death receptor) and the intrinsic (mitochondrial) pathways. The extrinsic pathway is initiated in response to the binding of an extracellular death ligand to one of several death receptors (typically members of the tumor necrosis factor TNF family) at the cell surface. This binding results in the recruitment and activation of the initiator procaspase 8.<sup>11</sup> Alternatively, the intrinsic pathway is initiated by the release of various proapoptotic factors from within the mitochondria, most notably cytochrome C (cyt c). The release of cytochrome C and other mitochondrial apoptosis initiator proteins occurs in response to many stimuli including but not limited to reactive oxygen species (ROS), DNA damage, radiation and viral infections.<sup>11</sup> Release of cytochrome c from the mitochondria results in the activation of the initiator procaspase 9, beginning the proteolytic cascade that results in apoptosis. Initial results of experiments on the activity of apoptoludin by Salomon *et al* confirm that apoptoludin acts upon a mitochondrial target (*vida infra*).<sup>4,16</sup>

In addition to their ability to initiate programmed cell death through apoptosis, the mitochondria are responsible for many vital processes in cell survival and proliferation.<sup>17</sup> One of the primary roles of the mitochondria is energy production through the synthesis of ATP by oxidative phosphorylation. The mitochondria also house key enzymes involved in the biosynthesis of heme, steroids, fatty acids and Fe/S clusters. Mitochondria are involved in the metabolism of some amino acids, contain all enzymes of the Krebs



cycle and are responsible for calcium homeostasis in the cell.<sup>18</sup> Dysregulation of many of these processes or of cytosolic protein concentrations can result in mitochondrial membrane permeabilization (MMP) and subsequent apoptosis signaling. MMP results in the dissipation of the mitochondrial membrane potential ( $\Delta\psi_m$ ) thereby halting ATP synthesis, which leads to the release of mitochondrial proteins that trigger apoptosis. There are two known mechanisms for MMP<sup>19</sup> that result in the induction of apoptosis from the mitochondria (**Figure III-3**).

A well-characterized pathway for mitochondrial apoptosis regulation is mediated by the Bcl-2 family of proteins. Bcl-2 proteins are divided into three subcategories: Bax-like (pro-apoptotic), Bcl-2-like (anti-apoptotic) and BH3-only (BH=bcl-2 homology domain).<sup>20</sup> The Bax-like proteins consist of membrane permeable moieties and with the assistance of certain BH3-only proteins can oligomerize and insert into the outer mitochondrial membrane (OMM) to form pores (**Figure III-3**, top).<sup>21</sup> These pores allow for the release of cyt c from within the mitochondria and thereby initiate the apoptotic cascade. The Bcl-2-like proteins can bind to the Bax-like proteins and prevent their oligomerization. Therefore, a careful balance in the concentration of these proteins in favor of the anti-apoptotic proteins must be maintained in the cytosol in order for cells to survive but still be responsive to apoptotic signals that increase pro-apoptotic factors. In many cancer cells, the ratio of anti-apoptotic/pro-apoptotic Bcl-2 proteins is disproportionately high, making them resistant to apoptosis.<sup>22</sup>



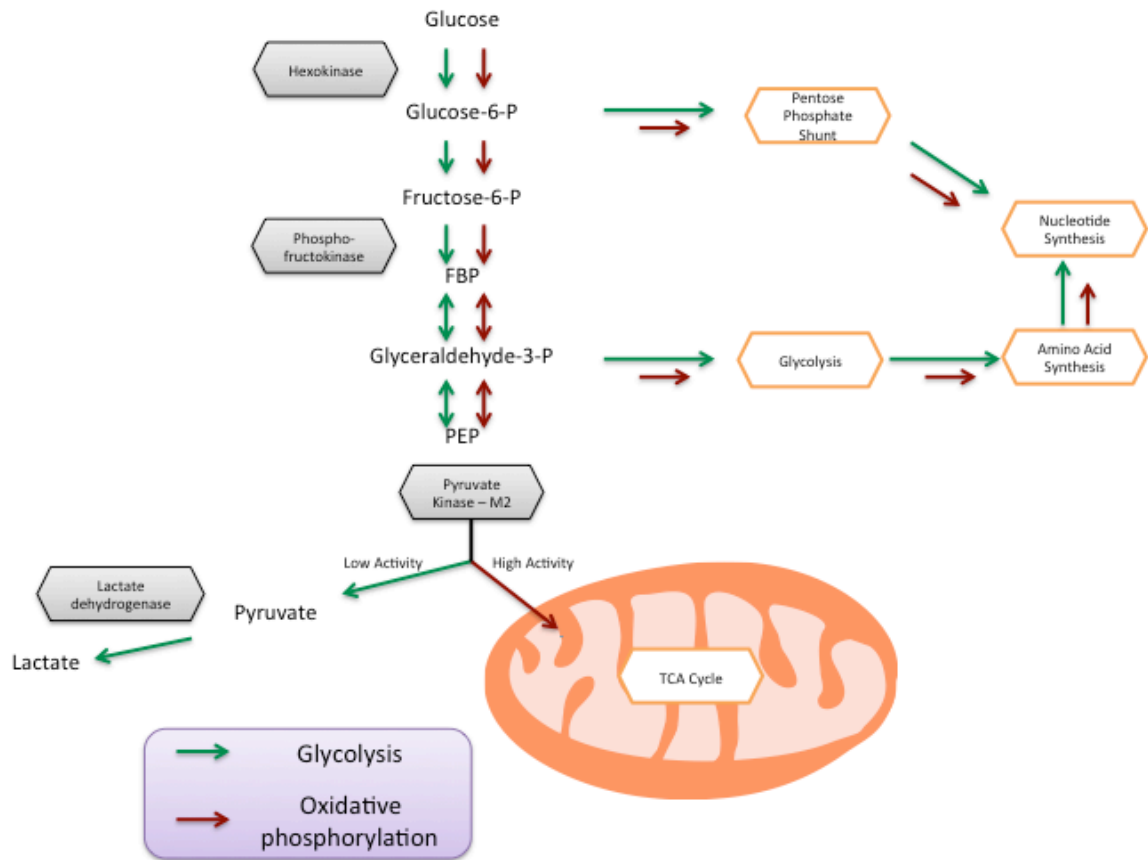
**Figure III-3:** Known mechanisms for mitochondrial apoptosis initiation

The second pathway by which the mitochondrial membrane can be permeabilized centers around the voltage-dependent anion channel (VDAC).<sup>23</sup> VDAC is the primary gateway through the OMM by which metabolites (ATP and ADP) enter and leave the mitochondria. Closure of VDAC is thought to lead to the formation of the mitochondrial permeability transition (MPT) complex (**Figure III-3**).<sup>24</sup> MPT is a nonspecific pore from the cytosol through both the OMM and the inner mitochondrial membrane (IMM). The formation of MPT is understood to be  $\text{Ca}^{2+}$  dependent and can be facilitated by multiple stimuli including ATP depletion and the presence of reactive oxygen species (ROS).<sup>25</sup> Interestingly, Bcl-2-like proteins are also known to stabilize the open conformation of VDAC giving these proteins anti-apoptotic effects by this mechanism as well.

Apart from apoptosis initiation, a primary role of the mitochondria is glucose metabolism and ATP generation through oxidative phosphorylation. Apoptolidin is proposed to initiate cell death in select cancer cell lines by acting upon a mitochondrial target. Among the most significant differences between cancerous and healthy cells is a common reprogramming of glucose metabolism known as the Warburg effect. To understand the cell line selectivity of apoptolidin's potent cytotoxicity, one must consider the metabolic changes commonly associated with cancerous cells.

### *Metabolic Reprogramming*

Among the most common traits of cancer cells is an observed preference for aerobic glycolysis commonly referred to as the Warburg effect.<sup>26</sup> Typically, per the Pasteur hypothesis, mammalian cells prefer to produce ATP primarily through the energetically more efficient mitochondrial (oxidative phosphorylation) pathway. Under hypoxic (anaerobic) conditions, glycolysis by the less efficient Embden-Meyerhof pathway is preferred (**Figure III-4**). Cancer cells, however, prefer glycolytic fermentation of glucose to lactate despite the much greater efficiency of oxidative phosphorylation with respect to glucose consumption.<sup>27</sup> Aerobic glycolysis yields only ~4 molecules of ATP per molecule of glucose, whereas oxidative phosphorylation gives ~36 molecules of ATP per glucose molecule.<sup>28</sup> Warburg initially hypothesized that this preference was due to mutations that caused a defect in mitochondrial respiration,<sup>29</sup> however it has been shown that most cancer cells do not have impaired mitochondrial function.<sup>30</sup>



**Figure III-4: Glucose Metabolism Pathways**

The primary reason for this preference for aerobic glycolysis is made apparent by the observation that non-cancerous proliferating tissues also display a preference for aerobic glycolysis.<sup>17</sup> Cells driven to rapid proliferation are understood to generate ATP through glycolysis because it allows for more efficient use of glucose in the anabolism of other building blocks (amino acids, lipids, etc) required for cellular replication (**Figure III-4**). Regardless of the mode of metabolism, neither ATP generation nor glucose availability is typically a limiting factor to drive selection for rapidly proliferating mammalian cells. However, due to the constant presence of growth promoting stimuli in cancer cells, factors that contribute to rapid proliferation do drive selection. Moreover, a

balance of the ratio of ATP/ADP must be maintained within the cell for production of NADH and acetyl-CoA (vital for macromolecular biosynthesis). Reliance on oxidative phosphorylation for ATP generation would tip this balance to greatly favor ATP in order to anabolize a comparable amount of these building blocks and effectively slow proliferation. Studies have also shown that lactate waste excreted by cancer cells can be reabsorbed and further catabolized in some cases.<sup>31</sup> Furthermore, cancerous cells frequently proliferate at a rate that exceeds the rate of angiogenesis, thus decreasing the availability of oxygen.

There are other factors that make the Warburg effect desirable for cancer cells, particularly in protection from the damaging effects of reactive oxygen species (ROS). Oxidative phosphorylation is the primary cellular source of ROS. Indeed, it is estimated that 2% of molecular oxygen used in respiration is converted into superoxide ( $O_2^{\bullet-}$ ).<sup>32</sup> ROS production can trigger the detachment of cyt c (typically membrane bound by way of cardiolipin) from the IMM. Furthermore, ROS can affect the activation of Bax and allow for MMP and subsequently apoptosis initiation. The formation of ROS in the mitochondria also hazardous to mitochondrial DNA (mtDNA).<sup>33</sup> This DNA contains the genes of many vital mitochondrial proteins and is, as a result of the highly oxidized environment of the mitochondria, easily damaged. Damage to mtDNA can in turn cause mitochondrial protein dysfunction and result in further ROS production. Increased ROS production can also reduce cell proliferation rates.<sup>34</sup> ROS production is known to be exacerbated under hypoxic conditions. The drastic reduction in the activity of oxidative phosphorylation helps to contribute to the stability of the cell with respect to apoptosis as well as protecting the cell from self-damaging ROS production.

In order to study these metabolic pathways, a few key enzymes have been identified as “switches” between aerobic glycolysis (**Figure 2.5**) and mitochondrial respiration including lactate dehydrogenase (LDH) and pyruvate kinase (PK). PK catalyzes the conversion of phosphoenolpyruvate (PEP) and ADP into pyruvate and ATP. Pyruvate kinase is known to exist in two distinct isoforms designated M1 and M2.<sup>35</sup> The M2 form is expressed in many forms of embryonic cells, but PK-M1 is the isoform most commonly expressed in differentiated tissues. All cancer cells express PK-M2, and PK-M2 expression has long been a biomarker for malignancy.<sup>36</sup> Active PK exists as a homotetramer and has a known allosteric modulation site with a natural modulator, fructose-1,6-bis-phosphate (FBP). However, in cancer cells, PK-M2 exists as a dimer that shows greatly reduced activity. This reduced activity is thought to cause a preference for glycolysis and a backup in previous steps of glucose metabolism, allowing redirection of intermediates into anabolic pathways like the pentose phosphate shunt (**Figure III-4**).

Another indication of the Warburg effect is up-regulation of hypoxia-inducible factor 1 subunit alpha (HIF-1 $\alpha$ ) despite the presence of oxygen (common among many cancers).<sup>37</sup> HIF-1 $\beta$  is constitutionally expressed in cells, and the  $\alpha$  subunit is expressed in response to hypoxic conditions. When both subunits are present, they complex to form active HIF-1.<sup>38</sup> HIF-1 activation causes many cellular signals including the induction of genes controlling angiogenesis, glucose metabolism, and cell proliferation and the activation of proteins involved in glycolysis.

The mitochondria of cancer cells have key differences relative to mitochondria of normal differentiated cells, both in metabolic activity and apoptosis regulation. While many of the known differences help to contribute to stability and proliferation rates, the

existence of such differences may allow for the identification of novel therapeutic targets for the treatment of cancer. Apoptolidin A has been stated to induce cell death in multiple cancer cell lines. Some preliminary studies have been undertaken to determine the mechanism of this activity, but more work remains to be done in order to detail the mechanism of cell death and identification of a apoptolidin's cellular target.

#### *F<sub>0</sub>F<sub>1</sub>ATPase: A Target of Apoptolidin?*

Initial studies on the mechanism of action of apoptolidin's selective cytotoxicity was undertaken by Salomon *et al* (Stanford University). These studies ultimately concluded that apoptolidin's activity was associated with its inhibition of F<sub>0</sub>F<sub>1</sub>-ATPase. Furthermore, the observed cell line selectivity was attributed to metabolic differences among cancer cell lines.<sup>4,16</sup> A few inconsistencies among data reported for apoptolidin suggests a more significant molecular target may exist.

The Stanford group's investigations began with pharmacological experiments to determine the mechanism of cell death induction by identifying the dependency of the toxicity on specific proteins.<sup>16</sup> The first such experiment was on the dependence of cell death on p53, a protein responsible for inducing the pro-apoptotic gene *bax*. To determine the dependence on p53 status, HCT116 wild type and *p53* null cells were each treated with apoptolidin A. Similar growth inhibition was observed for both cell lines, indicating that this activity was independent of p53 status. The key role of Bcl-2 proteins in mitochondrial apoptosis signaling pathways prompted experiments to determine the significance of these proteins in apoptolidin induced toxicity. To this effect, LYas cells (wild type do not have *bcl-2*) were transfected with *bcl-2* and the resulting cells were compared to wild type for apoptolidin sensitivity. Bcl-2 overexpression was found to

make cells completely resistant to apoptolidin induced toxicity, as measured by Annexin V. Furthermore, cells were found to become completely resistant to apoptolidin by co-treatment with a caspase-9 inhibitor, suggesting a mitochondrial apoptosis initiation pathway. These experiments show that apoptolidin cytotoxicity is independent of *p53* expression, inhibited by the expression of anti-apoptotic Bcl-2 proteins and caspase-9 dependent.

The Stanford group further suggested structural similarities between apoptolidin, oligomycin, and bafilomycin (**Figure III-2**). Oligomycin is a known inhibitor of  $F_1F_0$ -ATPase and bafilomycin is a selective inhibitor of vacuolar ATPase; both have known cytotoxicity. Furthermore, they noted some overlap in the cytotoxicity profiles from the NCI-60 assay of oligomycin with other macrolactones such as cytovaricin and ossamycin, proposed inhibitors of  $F_1F_0$ -ATPase. Based on this comparison, apoptolidin was tested in mitochondrial preparations from yeast and determined to be an inhibitor of  $F_0F_1$ -ATPase with a  $K_i$  of 5  $\mu\text{M}$ .<sup>16</sup>

To investigate the means by which inhibition of  $F_0F_1$ -ATPase might lead to selective cytotoxicity, they further noted similarities in gene expression profiles for known  $F_0F_1$ -ATPase inhibitor cytovaricin within the NCI-60.<sup>13</sup> Specifically within leukemia cell lines in the NCI-60, cytovaricin was found to be most active in lines that had increased expression levels of PK and aspartate aminotransferase (AAT) and decreased expression of HIF-1 $\alpha$ . These expression profiles indicate a preference for mitochondrial ATP production, rather than aerobic glycolysis. Based on this fact, he hypothesized that inhibitors of  $F_1F_0$ -ATPase might be inducing apoptosis in cells that rely heavily on the mitochondria for glucose metabolism.



To further evaluate this hypothesis, cells were co-treated with apoptolidin and glycolysis inhibitors 2-deoxyglucose or oxamate. 2-deoxyglucose is known to inhibit glucose transport while oxamate is a known inhibitor of lactate dehydrogenase (LDH) preventing lactate formation that results in a shift in preference towards mitochondrial respiration. Co-treatment of Jurkat cells with either compound (50 mM) and apoptolidin (1  $\mu$ M) showed a strong increase in sensitivity to apoptolidin induced cell death. Furthermore, assays were performed that showed similar sensitization of nine different cell lines to apoptolidin induced apoptosis, including lines that were otherwise resistant. While these studies do not confirm the exact mechanism of action of apoptolidin, they do provide good evidence that cell death is induced in the mitochondria and show a requirement for reliance on mitochondrial respiration over glycolysis in order to observe apoptolidin cell sensitivity.

#### *Structure Activity Relationships of Apoptolidins*

Many of the apoptolidin analogues that have been either isolated from fermentation (apoptolidins A-G) or produced by total synthesis and semisynthesis have been evaluated for cytotoxicity. The various research groups involved in these studies have produced data from different assays, cell lines, and conditions but have lead to some basic definitions of apoptolidin SAR (**Table III-1**).

Apoptolidin A has been tested in cell viability assays against multiple cell lines and typically has an EC<sub>50</sub> in the low nanomolar range (~10-20 nM). While the Stanford group's initial report on apoptolidin A measured an IC<sub>50</sub> of 5  $\mu$ M for F<sub>1</sub>F<sub>0</sub>ATPase inhibition, subsequent analysis has resulted in reports as low as 0.7  $\pm$  0.5  $\mu$ M. In cell viability assays on H292 human lung cancer cells, apoptolidins B and C show

comparable activity to the parent compound.<sup>39</sup> Apoptolidin D,<sup>40</sup> E<sup>41</sup> and the photoisomerized apoptolidin G<sup>42</sup> all show only moderately reduced activity in cell viability assays. Apoptolidin F, which is missing the C27 disaccharide moiety, is notably less potent than apoptolidin A.<sup>41</sup> The ring expanded isoapoptolidin A showed potent activity in cell viability assays on Ad12-3Y1 cells but minimal activity in ATPase inhibition.<sup>43</sup> This difference in potency can be attributed to the equilibration of isoapoptolidin to apoptolidin during the lengthy cell viability assays (2-4 days) but minimal conversion during the short time course (~30 min) of the ATPase inhibition assay.

Evaluation of synthetic and semisynthetic apoptolidin congeners has added significantly to knowledge of the structure-activity relationships (**Table III-1**). Selective modification of the hydroxyl group array at multiple positions by Wender showed a minimal effect on activity in both cell based and ATPase assays.<sup>43</sup> Conversely, peracetylation of apoptolidin A hydroxyl groups resulted in a complete loss in ATPase inhibition.<sup>44</sup> Evaluation of the C27 deglycosylated apoptolidin A **2.11**, prepared by Nicolaou and coworkers, in cell viability assays with 1A9 human ovarian carcinoma cells showed a significant loss (~48 X) in activity compared to apoptolidin A (IC<sub>50</sub> 240 μM in this cell line).<sup>45</sup> While C9 deglycosylated apoptolidin D **2.17** showed minor reduction in potency in cell viability assays.<sup>46</sup> Synthetic aglycones (apoptolidinones) showed complete loss of cytotoxic activity.<sup>47</sup> Analysis of macrolide fragments such as **2.13** all showed a significant (~215 X) loss in activity from cell based assays accompanied by a relatively small loss (~23 X) in ATPase inhibition. Finally, the lactone fragment **2.22** produced by oxidative cleavage of apoptolidin A was found to be completely inactive in both assays.<sup>43</sup>

Compound	EC <sub>50</sub> (nM)	K <sub>i</sub> (μM)
Apoptolidin A (2.1)	13 <sup>*</sup>	0.7
Apoptolidin B (2.2)	7 <sup>*</sup>	n/a
Apoptolidin C (2.3)	24 <sup>*</sup>	n/a
Apoptolidin D (2.4)	110 <sup>*</sup>	n/a
Apoptolidin E (2.5)	< 100 <sup>*</sup>	n/a
Apoptolidin F (2.6)	> 10x Apo A <sup>*</sup>	n/a
Apoptolidin G (2.7)	150 <sup>*</sup>	n/a
Isoapoptolidin A (2.8)	9 <sup>‡</sup>	17
Selectively Acylated (2.21)	56 <sup>‡</sup>	0.8
Peracetylated (2.19)	n/a	>100
C27 Hydroxyapoptolidin A (2.11)	11,500 <sup>†</sup>	n/a
Apoptolidin D disaccharide (2.17)	200 <sup>*</sup>	n/a
Apoptolidinone A (2.14)	>10,000 <sup>*</sup>	
Macrolide Fragment (2.13)	1,400 <sup>‡</sup>	16
Lactone Fragment (2.22)	>12,000 <sup>‡</sup>	190

**Table III-1:** Apoptolidin structure activity relationships (<sup>\*</sup>H292 Human Lung Carcinoma, <sup>†</sup>1A9 Human Ovarian Carcinoma, <sup>‡</sup>AD12-3Y1)

These data, taken together, shed some light on the importance of specific structural features in biological activity. First, minor modifications to the macrocyclic core are tolerated (shunt metabolites and selective hydroxyl group acylation) while more

significant modifications are not (peracetylation). Second, the C9 sugar can be either modified or removed to retain significant biological activity while the C27 disaccharide appears to be requisite for cellular activity. The relatively minor loss in ATPase activity of fragments such as **2.13** compared to the loss of toxicity indicates that the C27 disaccharide moiety might be important for cellular transport and not for target binding.<sup>47</sup> Alternatively, such discrepancies in activity might indicate that the most significant biological target may not actually be the F<sub>1</sub>F<sub>0</sub>ATPase. Structure activity relationships are somewhat challenging to analyze due to the multiple cell lines and assays used in these experiments.

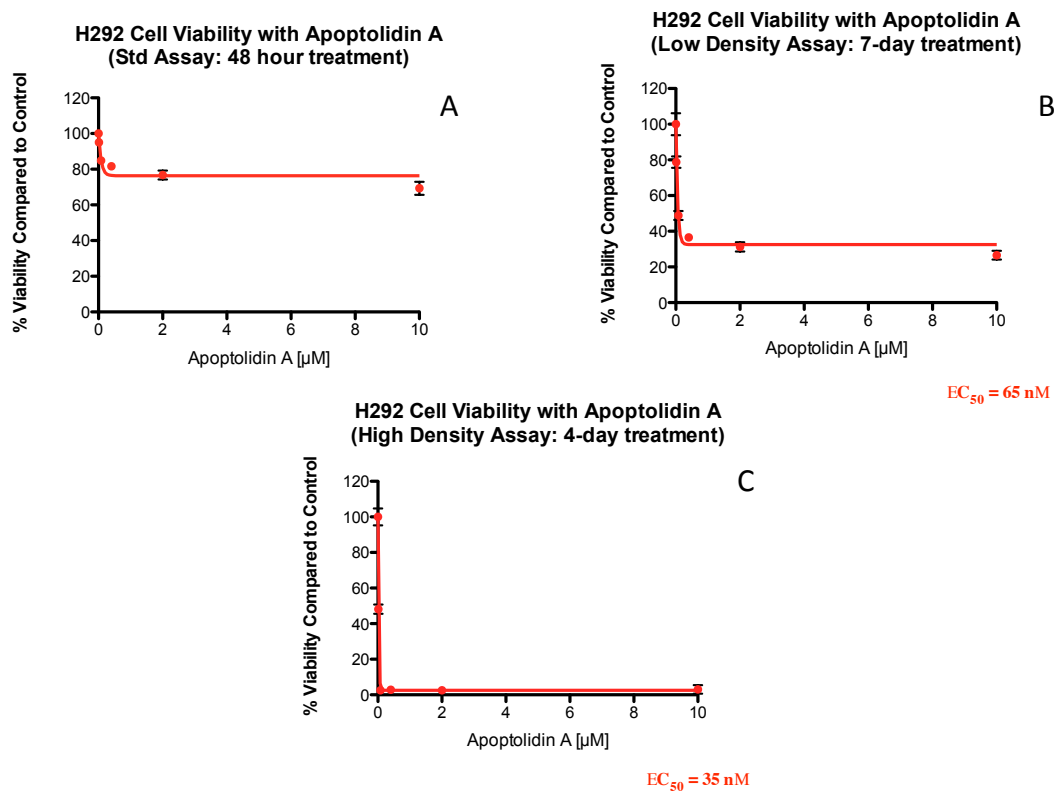
The large difference in the EC<sub>50</sub> for cytotoxicity in cell based assays (10-20 nM) and the K<sub>i</sub> for enzyme inhibition (~1-4 μM) further call to question the validity of the F<sub>1</sub>F<sub>0</sub>ATPase as the most significant biological target of apoptolidin. Furthermore, the cytotoxicity of apoptolidin is expected to occur by the same mechanism as oligomycin. However, unlike apoptolidin, oligomycin's activity is not prevented by caspase 9 inhibitors.<sup>48</sup> This target fails to account for the selectivity of apoptolidin towards cancer models over untransformed cells (typically preferring oxidative phosphorylation) as originally reported by Seto and Hiyawaka.<sup>1</sup> Finally, none of the data to date from human models of cancer definitively confirm that apoptotic signaling is responsible for the cytotoxicity. Caspase inhibition and Bcl-2 overexpression experiments were performed on LYas (mouse) cells. While Salomon *et al* performed multiple assays using an Annexin V readout, any Annexin V staining was always either accompanied by propidium iodide staining (indicating necrosis) or data from propidium iodide staining was not reported. Such inconsistencies and unanswered questions have prompted our investigations into

apoptolidin biological activity to quantify apoptolidin cytotoxicity, understand the requirements for this cytotoxicity and identify the mechanism of cell death.

## **Results: Investigations in the Sulikowski Lab**

### *Cytotoxicity of Apoptolidins*

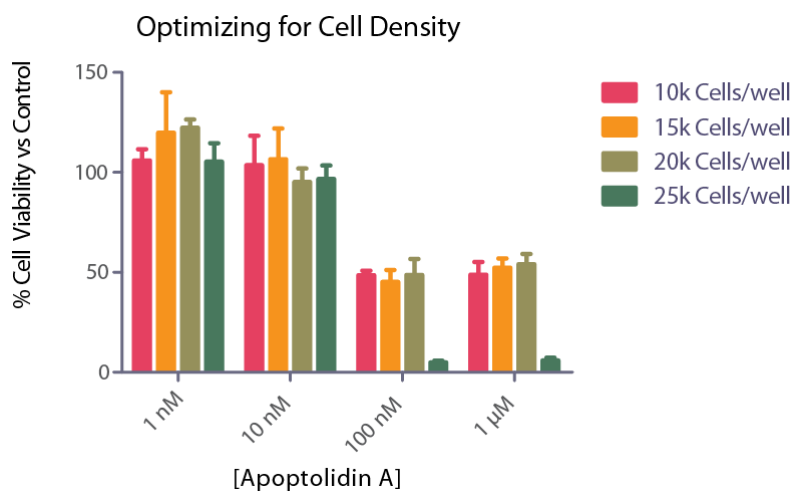
We began our investigations of apoptolidin biological activity with experiments aimed to replicate the reported potent cytotoxicity in cancer cell lines. Initially, these experiments were carried out by our collaborators in the Marnett lab. Using their standard cell viability assay conditions, only growth inhibition was observed in H292 cells (**Figure III-5, A**). In these experiments, cells were treated with various apoptolidin concentrations at ~20% confluence for 48 hours then assayed for cell viability compared to a vehicle control employing a tetrazole based (MTT or WST) colorimetric assay.<sup>49</sup> A similar growth inhibition result was observed when cells were treated at very low confluence for seven days (**Figure III-5, B**). In both of these conditions a cytostatic effect was observed but there was no apparent cytotoxicity. However, when cells were grown to near confluence before treatment with apoptolidin, a cytotoxic effect was observed at concentrations similar to those previously reported (**Figure III-5, C**).<sup>39</sup>



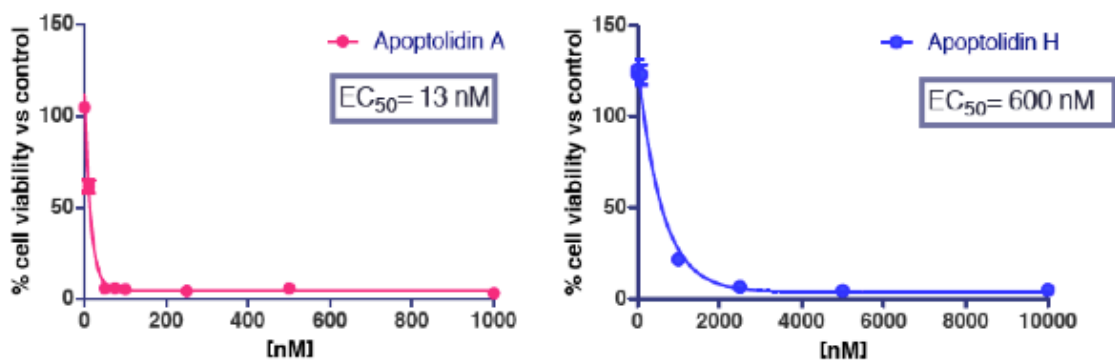
**Figure III-5:** Preliminary data from apoptolidin testing

When we started to perform these experiments in our lab, challenges with reproducibility were initially encountered. We identified the problem as difficulty in objectively measuring cell confluence at the time of treatment. To eliminate variability in this measurement, a standard protocol was developed based upon plated cell number. Cells were plated in 96-well plates at 10, 15, 20 and 25 thousand cells per well, allowed to attach for 16 hours, then treated with apoptolidin A. After four days, cells from each condition were assayed for cell viability compared to a vehicle control using the MTT (3-(4,5-Dimethylthiazol-2-yl)-2,5-diphenyltetrazolium bromide) colorimetric assay. These data indicated that 25,000 cells/well was the optimal plating conditions for reproducibly

observing apoptolidin induced cytotoxicity in H292 cells. When cells were treated with apoptolidin at a lower cell number, a uniform reduction in cell growth rate was observed. With these optimized conditions, we were able to quantify the cytotoxicity of apoptolidin and any derivatives. Apoptolidin A was found to have an EC<sub>50</sub> of 13 nM in this assay (**Figure III-7**). Apoptolidin H isolated from mutant *Nocardiosis* sp. FU40ΔG2 had an EC<sub>50</sub> in this assay of 600 nM, ~46 times less potent.



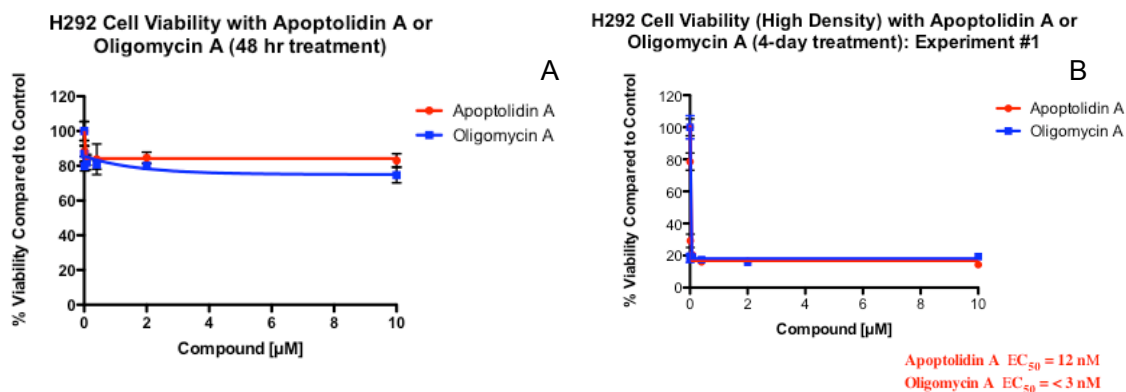
**Figure III-6:** Apoptolidin cell density assay



**Figure III-7:** Apoptolidin A and H H292 cell viability assay

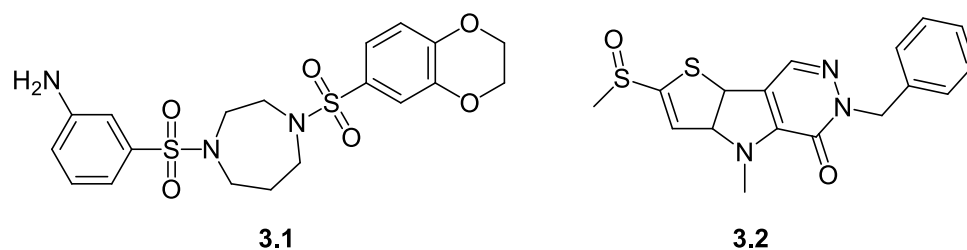
We were intrigued by the unusual dependency of cytotoxicity on cell density. H292 cells are not among the cells in the NCI's 60 cell line panel assay nor were they among those co-treated by the Stanford group with glycolytic inhibitors to induce apoptolidin sensitivity. This cell line was chosen due to its prevalent use in the Wender laboratory for testing of apoptolidin shunt metabolites (Apoptolidin B-F) and in SAR studies. Interestingly, the same effect of cell density was observed in this cell line for oligomycin A (**Figure III-8**) giving credence to reports that the two compounds share a common target and mechanism.





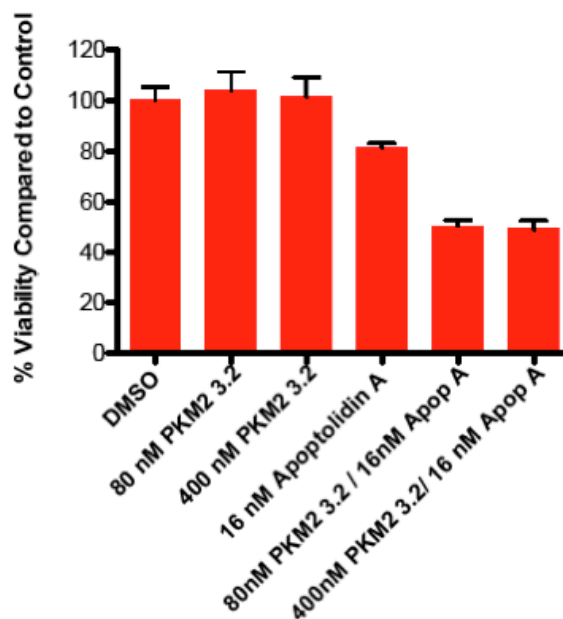
**Figure III-8:** Oligomycin cell density requirement

Based upon the previous reports for the dependency of apoptolidin cytotoxicity on metabolic preference for oxidative phosphorylation, we hypothesized that these cells were undergoing a metabolic shift as they neared confluence. We thought that within the experimental constraints of a 96-well plate, the cells could sense that they were unable to continue to rapidly proliferate when grown to confluence (proliferation contact inhibition) and respond by shifting glucose metabolism from aerobic glycolysis to oxidative phosphorylation, enhancing sensitivity to apoptolidin.<sup>50</sup> We wondered if we could induce the potent cytotoxicity by creating this sort of metabolic shift at low cell density, in a similar way to that employed by Salomon *et al.* Instead of using inhibitors of glycolysis, we instead investigated the use of recently reported PK-M2 activators. A highly activated PK-M2 should, in theory, mimic the activity of the more active isoform PK-M1 and thereby increase metabolic flux into the mitochondria. Recent reports have identified potent allosteric activators of PK-M2 (**Figure III-9**).<sup>51</sup>



**Figure III-9:** PK-M2 allosteric activators

To test our hypothesis, cells were treated with each activator as well as with apoptolidin under the seven day, low cell density assay conditions. First, neither activator was shown to influence growth significantly in the absence of apoptolidin (up to 10  $\mu$ M, data not shown). Second, a significant difference was observed in the growth inhibition activity of apoptolidin at 16 nM in the presence of 80 nM PK-M2 activator (**Figure III-10**). Indeed, at 16 nM, apoptolidin alone only inhibited 18.6% cell growth, but when co-dosed with PK-M2 activator **3.2** at 80 nM, 48.9% growth inhibition was observed. While increased sensitivity to apoptolidin was observed in these experiments resulting in increased growth inhibition, we did not observe the potent cytotoxic effects observed in the high cell density experiments. It is possible that PK-M2 activation by these compounds is not sufficient to facilitate a complete switch to mitochondrial respiration required for cytotoxicity.



**Figure III-10:** PKM2 activator co treatment results

We have developed assay conditions to quantify the activity of apoptolidin natural products as well as unnatural apoptolidin congeners prepared by semisynthesis or mutasynthesis in H292 human lung carcinoma cells. In doing so, we observed a dependency of cytotoxicity on high cell density conditions. A similar result was observed for oligomycin, a known inhibitor of the  $F_1F_0$ ATPase. Metabolic profiling studies on HepG2 cells indicate that at low cell density, glucose consumption is strongly correlated with lactate production but this relationship was lost at cell densities nearing confluence.<sup>52</sup> These results appear to indicate a shift from aerobic glycolysis to mitochondrial respiration for ATP production as cell density reaches a maximum for some cell lines. Such cell density based contact inhibition effects are stronger and more common among primary tissue cultures than in cell lines, likely contributing to the cell line selectivity of apoptolidin and other inhibitors of mitochondrial ATP synthesis. Future

work in this area will involve testing in additional cell lines reported to be sensitive or resistant to apoptolidin by the NCI at high and low cell densities. For example, testing in similar pairs such as the adenocarcinomas MCF-7 (sensitive) and MDA-MB-231 (insensitive) would reveal if high cell density enhances sensitivity in these cell lines as well.

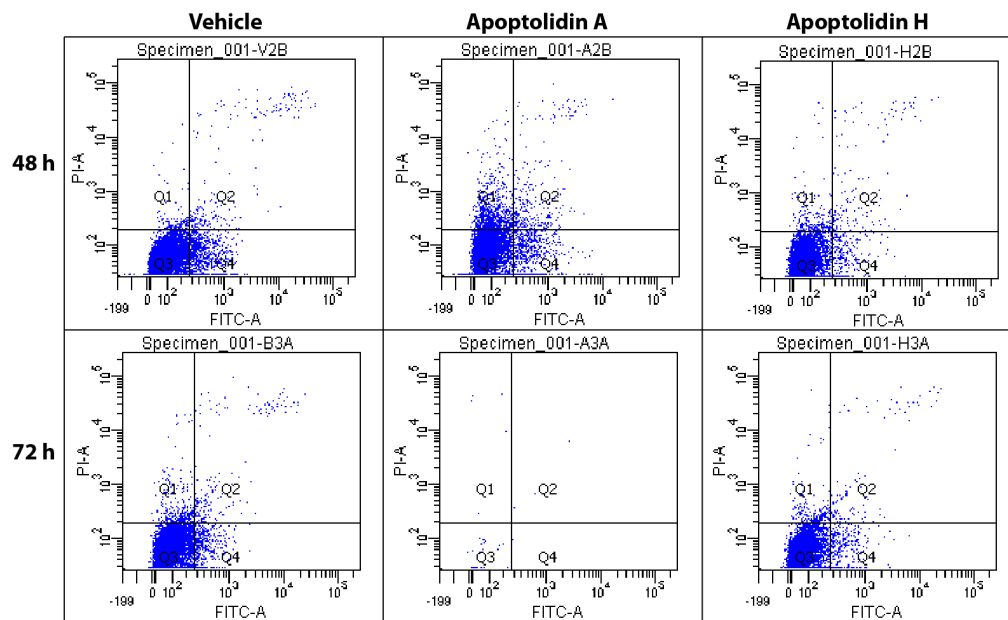
The Stanford group demonstrated that many cell lines gain sensitivity to apoptolidin by co-treatment with inhibitors of glycolysis. Allosteric activation of PKM2 with small molecules was insufficient to induce cell death at low cell densities in H292 cells. Inhibition of both glycolytic and mitochondrial ATP production would result in cellular energy crisis leading to the reported cell death. Activation of PKM2 may allow for sufficient ATP synthesis for survival via aerobic glycolysis when mitochondrial respiration is inhibited by apoptolidin but leads to the observed reduction in growth rate. A massive reduction in cellular ATP is implicated as a cause of both necrosis and apoptosis. This knowledge coupled with the lack of definitive data confirming apoptosis induction by apoptolidin in human cancer cell lines prompts further investigation to determine the mechanism of apoptolidin induced cytotoxicity.

#### *Toxicity Through Apoptosis or Necrosis*

To assay for apoptosis signaling in H292 cell lines as a response to treatment with apoptolidin, we employed a standard Annexin V and propidium iodide (PI) staining assay for use in fluorescence assisted cell sorting (FACS) experiments. Annexin V selectively binds to lipoproteins, and is covalently bound to a fluorophore (FITC) for use in FACS. As Annexin V is not cell permeable, positive signal from this fluorophore can be attributed to external presentation of phosphatidyl serine, an early hallmark of apoptosis.

Propidium iodide is used as a complimentary probe to detect cell death through other mechanisms. PI can intercalate into DNA but only when the plasma membrane is sufficiently compromised. In these experiments, cells undergoing apoptosis are positive for Annexin V staining but negative for PI, as disruption of the plasma membrane can allow Annexin V to stain internal phosphatidyl serine.

H292 cells were plated at high cell density in 6-well plates and treated with apoptolidin A and H at concentrations from 1 nM to 1  $\mu$ M for one to four days. The cells were then detached from the plates using by proteolytic digestion with trypsin and resuspended in media. After washing with phosphate buffered saline (PBS), cells were suspended in binding buffer and treated with PI and Annexin V-FITC then analyzed by FACS. No statistically significant difference was observed between one or two day treatments with either compound at any concentration and vehicle control. However, three and four day treatments showed no surviving cells when treated with apoptolidin A at 100 nM or more. Indeed, in these experiments almost no intact cells were observed (**Figure III-11**).



**Figure III-11:** Annexin V-FITC (X-axis) and propidium iodide (Y-axis) FACS results from 100 nM treatment with apoptolidin A and H for two and three days

As cells have been reported to undergo apoptosis rapidly (as quickly as two hours) we next assayed at more time points. First, a 60 hour treatment gave similar results to a two day treatment, suggesting that apoptosis was occurring between 60 and 72 hours. Experiments with treatments at two hour increments between 60 and 72 h failed to show any significant Annexin V-FITC staining. Again treated cells were either identical to control or only debris was collected. We observed that in conditions where treatment resulted in the collection of debris alone, the cells required a significantly longer treatment with trypsin to detach. Attempts at manual cell lifting, however, gave PI and Annexin V-FITC positive cells in vehicle controls.

The lack of data supporting apoptosis as a cell death pathway is insufficient to confirm that the cells are undergoing necrosis. Future studies should include Western blot experiments for caspase activation and additional cell sorting assays to sufficiently confirm or refute apoptosis. Additionally, these experiments should be performed on other cell lines known to be sensitive to apoptolidin. Both apoptolidin A and H have been submitted for testing by a collaborating group to determine if they are able to induce autophagy.

### **Experimental Methods**

**MTT Cell Viability Assay for Cell Density Requirement:** Low passage (P#<25) H292 human lung carcinoma cells (obtained from the American Type Culture Collection, ATCC) were plated at 5, 10, 15, 20 or 25 thousand cells per well in 96-well plates in 100  $\mu$ L of RPMI 1640 medium containing 10% fetal bovine serum and 100 IU penicillin and 100 mg/mL streptomycin and incubated for 16 hours to attach. Apoptolidin A was dissolved in DMSO at 1  $\mu$ M, 10  $\mu$ M, 100  $\mu$ M and 1 mM. The resulting DMSO stock solutions were diluted in complete RPMI medium 1000:1 to yield medium solutions containing 1 nM, 10 nM, 100 nM, and 1  $\mu$ M apoptolidin A or DMSO to give a final DMSO concentration of 0.1%. Media was removed from each well by aspiration and replaced with media containing DMSO vehicle or apoptolidin A for a total of n=4 wells per cell density and concentration. Cells were incubated for four days (96 hours). The media from each well was then aspirated and replaced with 100  $\mu$ L of complete RPMI medium containing 3-(4,5-Dimethylthiazol-2-yl)-2,5-diphenyltetrazolium bromide (MTT) at 0.5 mg/mL and returned to the incubator at 37 °C for two hours. Media from

each well was aspirated and replaced with 100  $\mu$ L DMSO. Absorbance was measured at 560 nM using a GloMax Multiplate reader (Promega, Madison, WI, USA). Blank absorbance from the average of 8 wells treated with MTT in cell-free medium was subtracted from each value. The percent cell viability of each well was calculated as the fraction of the average absorbance of DMSO control treated cells at each condition and data was plotted in **Figure III-6**.

**Standard MTT Cell Viability Assay:** Low passage (P#<25) H292 human lung carcinoma cells were plated at 25,000 cells per well in 96-well plates in 100  $\mu$ L of RPMI 1640 medium containing 10% fetal bovine serum and 100 IU penicillin and 100 mg/mL streptomycin and incubated for 16 hours to attach. Compounds used for testing were dissolved in DMSO at various concentrations from 1  $\mu$ M to 10 mM. The resulting DMSO stock solutions were diluted in complete RPMI medium 1000:1 to yield medium solutions containing 1 nM to 10  $\mu$ M of the respective compound to be assayed and a uniform DMSO concentration of 0.1%. Media was removed from each well by aspiration and replaced with media containing DMSO vehicle or compound for a total of n=8 wells per concentration. Cells were incubated for four days (96 hours). The media from each well was then aspirated and replaced with 100  $\mu$ L of complete RPMI medium containing MTT at 0.5 mg/mL and returned to the incubator at 37  $^{\circ}$ C for two hours. Media from each well was aspirated and replaced with 100  $\mu$ L DMSO. Absorbance was measured at 560 nM using a GloMax Multiplate reader (Promega, Madison, WI, USA). Blank absorbance from the average of 8 wells treated with MTT in cell-free medium was subtracted from each value. The percent cell viability of each well was calculated as the fraction of the average absorbance of DMSO control treated cells. Data was plotted



GraphPad Prism 5 and fitted with a non-linear regression curve. Effective concentration 50 (EC<sub>50</sub>) was estimated graphically as the concentration at which 50 % of control formazan product absorbance was detected.

**Standard WST Cell Viability Assay:** Low passage (P#<25) H292 human lung carcinoma cells were plated at 25,000 cells per well in 96-well plates in 100  $\mu$ L of RPMI 1640 medium containing 10% fetal bovine serum and 100 IU penicillin and 100 mg/mL streptomycin and incubated for 16 hours to attach. Compounds used for testing were dissolved in DMSO at various concentrations from 1  $\mu$ M to 10 mM. The resulting DMSO stock solutions were diluted in complete RPMI medium 1000:1 to yield medium solutions containing 1 nM to 10  $\mu$ M of the respective compound to be assayed and a uniform DMSO concentration of 0.1%. 90  $\mu$ L of media was removed from each well by multichannel micropipeter and replaced with 100  $\mu$ L of media containing DMSO vehicle or compound for a total of n=8 wells per concentration. Cells were incubated for four days (96 hours). Viability was measured by adding 10  $\mu$ L Cell Proliferation Reagent WST-1 to each well then incubating for 1 hour at 37 °C. Absorbance was measured at 450 nm less reference absorbance at 690 nm using a VERSAMax (Molecular Devices) 96-well plate reader. Blank absorbance from the average of 8 wells treated with WST-1 in cell-free medium was subtracted from each value. The percent cell viability of each well was calculated as the fraction of the average absorbance of DMSO control treated cells. Data was plotted GraphPad Prism 5 and fitted with a non-linear regression curve. Effective concentration 50 (EC<sub>50</sub>) was estimated graphically as the concentration at which 50 % of control formazan product absorbance was detected.

**Annexin V/ Propidium Iodide FACS Assay:** Low passage (P#>25) H292 human lung carcinoma cells were plated at either 700,000 cells per well (Low density) or 1,200,000 cells per well (high density) in 6-well plates in 2.0 mL of RMPI 1640 medium containing 10% fetal bovine serum and 100 IU penicillin and 100 mg/mL streptomycin and incubated for 16 hours to attach. Media was removed and replaced with complete media containing 1 nM, 10 nM, 100 nM, or 1  $\mu$ M of apoptolidin A or H or DMSO vehicle control give a uniform DMSO concentration of 0.1%. Treatment with compounds was continued for 2, 3, or 4 days by staggering plating and treatment times such that all treatment conditions could be assayed at once. Subsequent experiments also investigated 2.5 day (60 hour) treatments as well as treatment every 2 hours between 60 and 72 hours. After the desired treatment time, media was removed from each well by aspiration. Cells were treated with 0.05% trypsin-EDTA and returned to the incubator for 3-15 minutes or until detached. Detached cells from each well were suspended in 5 mL phosphate buffered saline (PBS) and centrifuged at 1500 RPM for 5 minutes to pellet cells in 15 mL Falcon tubes. Media was aspirated and cells were resuspended in 2 mL PBS and pelleted again (this PBS was repeated 2x to remove EDTA from trypsin digestion). Cells were resuspended in 1 mL of PBS and transferred to 1.5 mL Eppendorf tubes and repelleted. Media was aspirated again and cells were resuspended in 100  $\mu$ L 1 x binding buffer (BD Biosciences Annexin V:FITC Apoptosis Detection Kit). Vehicle treated well was suspended in 400  $\mu$ L of binding buffer instead and split between 4 tubes. 5  $\mu$ L of PI and Annexin V:FITC solutions were added to each cell suspension with the exception of 3 of the suspensions of the vehicle treated cells. One of these was left unstained, and one was treated with only PI and one only Annexin V: FITC. After 15 minutes incubation at room

temperature, each suspension was diluted to 500  $\mu$ L with 1x binding buffer and cells were sorted using a BD LRSIFortessa cell analyzer (BD Biosciences).

### References

1. Kim, J.; Adachi, H.; Shin-Ya, K. Apoptolidin, a New Apoptosis Inducer in Transformed Cells from *Nocardiosis* sp. *J. Antibiot.* **1997**, *50*, 628–630.
2. Dyson, N. The regulation of E2F by pRB-family proteins. *Genes Dev.* **1998**, *12*, 2245–2262.
3. Nahle, Z.; Polakoff, J.; Davuluri, R. V.; McCurrach, M. E.; Jacobson, M. D.; Narita, M.; Zhang, M. Q.; Lazebnik, Y.; Bar-Sagi, D.; Lowe, S. W. Direct coupling of the cell cycle and cell death machinery by E2F. *Nat. Cell Biol.* **2002**, *4*, 859–64.
4. Salomon, a R.; Voehringer, D. W.; Herzenberg, L. a; Khosla, C. Understanding and exploiting the mechanistic basis for selectivity of polyketide inhibitors of F(0)F(1)-ATPase. *Proc. Natl. Acad. Sci. USA* **2000**, *97*, 14766–71.
5. Wender, P. a; Sukopp, M.; Longcore, K. Apoptolidins B and C: isolation, structure determination, and biological activity. *Org. Lett.* **2005**, *7*, 3025–8.
6. Shoemaker, R. H. The NCI60 human tumour cell line anticancer drug screen. *Nature Rev. Cancer* **2006**, *6*, 813–23.
7. Boyd, M. The NCI In Vitro anticancer drug discovery screen. *Anticancer drug development guide; preclinical Screening, Clinical Trials, and Approval* **1997**, 23–42.
8. Kerr, J. F.; Winterford, C. M.; Harmon, B. V. Apoptosis. Its significance in cancer and cancer therapy. *Cancer* **1994**, *73*, 2013–26.
9. Kroemer, G.; Galluzzi, L.; Vandenabeele, P.; Abrams, J.; Alnemri, E. S.; Baehrecke, E. H.; Blagosklonny, M. V.; El-Deiry, W. S.; Golstein, P.; Green, D. R.; Hengartner, M.; Knight, R. a; Kumar, S.; Lipton, S. a; Malorni, W.; Nuñez, G.; Peter, M. E.; Tschopp, J.; Yuan, J.; Piacentini, M.; Zhivotovsky, B.; Melino, G. Classification of cell death: recommendations of the Nomenclature Committee on Cell Death 2009. *Cell Death Diff.* **2009**, *16*, 3–11.
10. Kerr, J. F. R.; Wyllie, A. H.; Currie, A. R. Apoptosis: A Basic Biological Phenomenon with Wideranging Implications in Tissue Kinetics. *Br J Cancer* **1972**, *26*, 239–257.

11. Elmore, S. Apoptosis: a review of programmed cell death. *Toxicol. Pathol.* **2007**, *35*, 495–516.
12. Golstein, P.; Kroemer, G. Cell death by necrosis: towards a molecular definition. *Trends Biochem. Sci.* **2007**, *32*, 37–43.
13. Festjens, N.; Vanden Berghe, T.; Vandenabeele, P. Necrosis, a well-orchestrated form of cell demise: signalling cascades, important mediators and concomitant immune response. *Biochim. Biophys. Acta* **2006**, *1757*, 1371–87.
14. Tsujimoto, Y.; Shimizu, S. Another way to die: autophagic programmed cell death. *Cell Death Diff.* **2005**, *12*, 1528–34.
15. Gump, J. M.; Thorburn, A. Autophagy and apoptosis: what is the connection? *Trends Cell Biol.* **2011**, *21*, 387–92.
16. Salomon, a R.; Voehringer, D. W.; Herzenberg, L. a; Khosla, C. Apoptolidin, a selective cytotoxic agent, is an inhibitor of F0F1-ATPase. *Chem. Biol.* **2001**, *8*, 71–80.
17. Galluzzi, L.; Morselli, E.; Kepp, O.; Vitale, I.; Rigoni, A.; Vacchelli, E.; Michaud, M.; Zischka, H.; Castedo, M.; Kroemer, G. Mitochondrial gateways to cancer. *Mol. Aspects Med.* **2010**, *31*, 1–20.
18. Reichert, A. S.; Neupert, W. Mitochondriomics or what makes us breathe. *TIG* **2004**, *20*, 555–62.
19. Kroemer, G.; Galluzzi, L.; Brenner, C. Mitochondrial membrane permeabilization in cell death. *Physiol. Rev.* **2007**, *87*, 99–163.
20. Festjens, N.; van Gurp, M.; van Loo, G.; Saelens, X.; Vandenabeele, P. Bcl-2 family members as sentinels of cellular integrity and role of mitochondrial intermembrane space proteins in apoptotic cell death. *Acta Haematol.* **2004**, *111*, 7–27.
21. Antonsson, B.; Montessuit, S.; Lauper, S.; Eskes, R.; Martinou, J. C. Bax oligomerization is required for channel-forming activity in liposomes and to trigger cytochrome c release from mitochondria. *Biochem. J.* **2000**, *345*, 271–8.
22. Abel, F.; Sjöberg, R.-M.; Nilsson, S.; Kogner, P.; Martinsson, T. Imbalance of the mitochondrial pro- and anti-apoptotic mediators in neuroblastoma tumours with unfavourable biology. *Eur. J. Cancer* **2005**, *41*, 635–46.
23. Vander Heiden, M. G.; Li, X. X.; Gottlieb, E.; Hill, R. B.; Thompson, C. B.; Colombini, M. Bcl-xL promotes the open configuration of the voltage-dependent

- anion channel and metabolite passage through the outer mitochondrial membrane. *J. Biol. Chem.* **2001**, *276*, 19414–9.
24. Haworth, R. A.; Hunter, D. R. The Ca<sup>2+</sup>-induced membrane transition in mitochondria. II. Nature of the Ca<sup>2+</sup> trigger site. *Arch. Biochem. Biophys.* **1979**, *195*, 460–7.
  25. Tan, W.; Colombini, M. VDAC closure increases calcium ion flux. *Biochim. Biophys. Acta* **2007**, *1768*, 2510–5.
  26. Warburg, O. Über den Stoffwechsel der Tumore. **1926**. Translated: The Metabolism of Tumors, London: Arnold Constable, **1930**.
  27. Vander Heiden, M. G.; Cantley, L. C.; Thompson, C. B. Understanding the Warburg effect: the metabolic requirements of cell proliferation. *Science* **2009**, *324*, 1029–33.
  28. Lehninger, D. L., Nelson, M. M.; *Principles of Biochemistry*, **1993**, 2.
  29. Warburg, O. On the Origin of Cancer Cells. *Science* **1956**, *123*, 309–314.
  30. Moreno-Sánchez, R.; Rodríguez-Enríquez, S.; Marín-Hernández, A.; Saavedra, E. Energy metabolism in tumor cells. *FEBS J.* **2007**, *274*, 1393–418.
  31. Sonveaux, P.; Végran, F.; Schroeder, T.; Wergin, M. C.; Verrax, J.; Rabbani, Z. N.; De Saedeleer, C. J.; Kennedy, K. M.; Diepart, C.; Jordan, B. F.; Kelley, M. J.; Gallez, B.; Wahl, M. L.; Feron, O.; Dewhirst, M. W. Targeting lactate-fueled respiration selectively kills hypoxic tumor cells in mice. *J. Clin. Investig.* **2008**, *118*, 3930–42.
  32. Gogvadze, V.; Zhivotovsky, B.; Orrenius, S. The Warburg effect and mitochondrial stability in cancer cells. *Mol. Aspects Med.* **2010**, *31*, 60–74.
  33. Anderson, S.; Bankier, A. T.; Barrell, B. G.; de Bruijn, M. H. L.; Coulson, A. R.; Drouin, J.; Eperon, I. C.; Nierlich, D. P.; Roe, B. A.; Sanger, F.; Schreier, P. H.; Smith, A. J. H.; Staden, R.; Young, I. G. Sequence and organization of the human mitochondrial genome. *Nature* **1981**, *290*, 457–465.
  34. Aulwurm, U. R.; Brand, K. a Increased formation of reactive oxygen species due to glucose depletion in primary cultures of rat thymocytes inhibits proliferation. *Eur. J. Biochem.* **2000**, *267*, 5693–8.
  35. Mazurek, S.; Boschek, C. B.; Hugo, F.; Eigenbrodt, E. Pyruvate kinase type M2 and its role in tumor growth and spreading. *Seminars in cancer biology* **2005**, *15*, 300–8.

36. Eigenbrodt, E.; Basenau, D.; Holthusen, S.; Mazurek, S.; Fischer, G. Quantification of tumor type M2 pyruvate kinase (Tu M2-PK) in human carcinomas. *Anticancer Res.* **17**, 3153–6.
37. Wang, G. L.; Semenza, G. L. General involvement of hypoxia-inducible factor 1 in transcriptional response to hypoxia. *Proc. Natl. Acad. Sci. USA* **1993**, *90*, 4304–8.
38. Semenza, G. L. Hydroxylation of HIF-1: oxygen sensing at the molecular level. *Physiol.* **2004**, *19*, 176–82.
39. Wender, P. a; Sukopp, M.; Longcore, K. Apoptolidins B and C: isolation, structure determination, and biological activity. *Org. Lett.* **2005**, *7*, 3025–8.
40. Wender, P. a; Longcore, K. E. Isolation, structure determination, and anti-cancer activity of apoptolidin D. *Org. Lett.* **2007**, *9*, 691–4.
41. Wender, P. a; Longcore, K. E. Apoptolidins E and F, new glycosylated macrolactones isolated from *Nocardiosis* sp. *Org. Lett.* **2009**, *11*, 5474–7.
42. Bachmann, B. O.; McNeese, R.; Melancon, B. J.; Ghidu, V. P.; Clark, R.; Crews, B. C.; Deguire, S. M.; Marnett, L. J.; Sulikowski, G. A. Light-induced isomerization of apoptolidin a leads to inversion of C2-C3 double bond geometry. *Org. Lett.* **2010**, *12*, 2944–7.
43. Wender, P. a; Jankowski, O. D.; Longcore, K.; Tabet, E. a; Seto, H.; Tomikawa, T. Correlation of F0F1-ATPase inhibition and antiproliferative activity of apoptolidin analogues. *Org. Lett.* **2006**, *8*, 589–92.
44. Pennington, J. D.; Williams, H. J.; Salomon, A. R.; Sulikowski, G. a Toward a stable apoptolidin derivative: identification of isoapoptolidin and selective deglycosylation of apoptolidin. *Org. Lett.* **2002**, *4*, 3823–5.
45. Nicolaou, K. C.; Li, Y.; Sugita, K.; Monenschein, H.; Guntupalli, P.; Mitchell, H. J.; Fylaktakidou, K. C.; Vourloumis, D.; Giannakakou, P.; O’Brate, A. Total synthesis of apoptolidin: Completion of the synthesis and analogue synthesis and evaluation. *J. Am. Chem. Soc.* **2003**, *125*, 15443–15454.
46. Ghidu, V. P.; Ntai, I.; Wang, J.; Jacobs, A. T.; Marnett, L. J.; Bachmann, B. O.; Sulikowski, G. a Combined chemical and biosynthetic route to access a new apoptolidin congener. *Org. Lett.* **2009**, *11*, 3032–4.
47. Daniel, P. T.; Koert, U.; Schuppan, J. Apoptolidin: induction of apoptosis by a natural product. *Angew. Chem. Int. Ed. Engl.* **2006**, *45*, 872–93.

48. Nakamura, N.; Wada, Y. Properties of DNA fragmentation activity generated by ATP depletion. *Cell Death Diff.* **2000**, *7*, 477–84.
49. Mosmann, T. Rapid colorimetric assay for cellular growth and survival: application to proliferation and cytotoxicity assays. *J Immunol. Methods* **1983**, *65*, 55–63.
50. Bereiter-Hahn, J.; Münnich, a; Woiteneck, P. Dependence of energy metabolism on the density of cells in culture. *Cell Struct. Funct.* **1998**, *23*, 85–93.
51. Boxer, M. B.; Jiang, J.; Vander Heiden, M. G.; Shen, M.; Skoumbourdis, A. P.; Southall, N.; Veith, H.; Leister, W.; Austin, C. P.; Park, H. W.; Inglese, J.; Cantley, L. C.; Auld, D. S.; Thomas, C. J. Evaluation of substituted N,N'-diarylsulfonamides as activators of the tumor cell specific M2 isoform of pyruvate kinase. *J. Med. Chem.* **2010**, *53*, 1048–55.
52. Miccheli, A. T.; Miccheli, A.; Di Clemente, R.; Valerio, M.; Coluccia, P.; Bizzarri, M.; Conti, F. NMR-based metabolic profiling of human hepatoma cells in relation to cell growth by culture media analysis. *Biochim. Biophys. Acta* **2006**, *1760*, 1723–31.

## CHAPTER IV

### Probing the Role of Apoptolidin Deoxy Sugars

#### **Fluorescent Apoptolidin Probe Syntheses**

Many bioactive natural products contain sugar moieties that are critical for activity, however the specific reason(s) for this is often unstudied. It is typically expected that such essential sugars are either involved in critical interactions with a cellular target or associated with transport of the natural product into the cell or into specific subcellular compartments to allow for target binding. For apoptolidin A, the C9 and C27 deoxy sugars have different effects on biological activity. The sugar at C9 can be removed or modified with minimal effect on activity but removal of the C27 disaccharide moiety greatly reduces cytotoxicity (46 fold less potent). While the  $F_1F_0$ ATPase inhibition SAR data is incomplete, the data available suggest that the resulting loss in enzyme activity is much less significant (**Table III-1**). We therefore hypothesize that removal of the C27 disaccharide moiety does not significantly affect the binding to its biological target, assuming  $F_1F_0$ ATPase,<sup>1</sup> but instead inhibits the transport of the compound to its target within the mitochondria. To test this, we have developed a strategy for the site selective modification of both apoptolidin A and apoptolidin H with fluorescent tags and designed experiments using the derived fluorescent probes to compare both subcellular localization and any significant differences in compound uptake rates.



### *Mitochondrial Co-localization and Transport Experiment Plan*

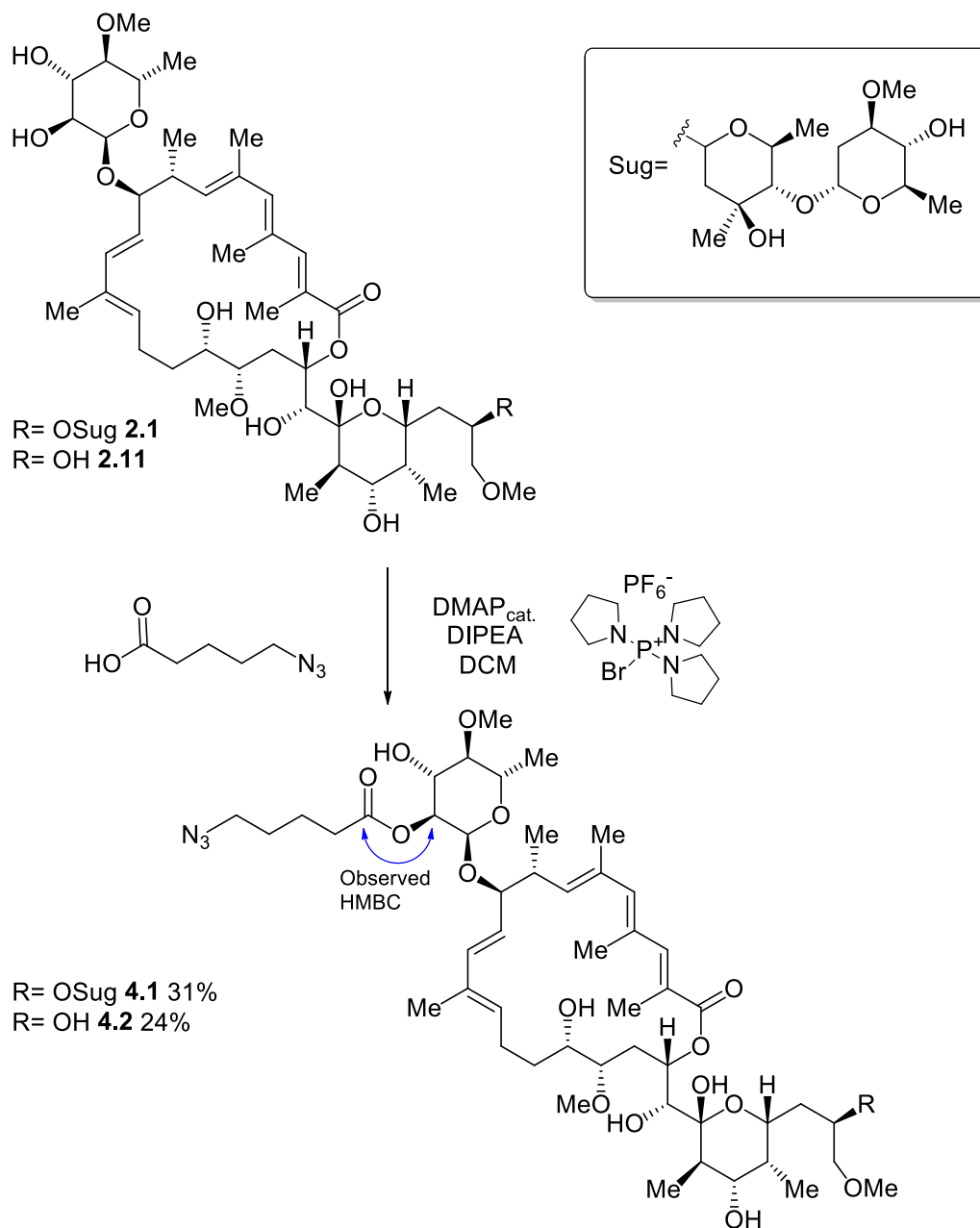
We planned to implement several confocal microscopy experiments to test our hypothesis. First, we needed to identify a method for the site selective modification of both apoptolidin A and H with a fluorescent moiety in a position that would have a minimal effect on activity in our H292 cell viability assay. Second, we would employ fluorescence confocal microscopy to image H292 cells that were treated with fluorescent apoptolidin A and organelle specific dyes to determine if localized in the mitochondria.<sup>1,2</sup> Next, we could perform identical experiments with a fluorescent probe of apoptolidin H. We expect that if apoptolidin H transport to the mitochondria is significantly slower than that of apoptolidin A, the target staining with this compound would be greatly reduced in a short treatment time. Finally, we could measure the rate of mitochondrial staining in real time after treatment to attempt to quantify any differences in transport.

To realize our first goal, we desired a method to couple apoptolidin to diverse fluorophores in a site selective manner. Recognizing the large number of reactive functional groups, the tendency towards isomerization and instability of apoptolidin, we chose to pursue a synthetic strategy implementing the Huisgen [3+2] cycloaddition or “click” reaction.<sup>3</sup> In this reaction, two bioorthogonal functional groups, an alkyne and an azide, react selectively under mild reaction conditions (copper(I) catalyzed or strain promoted) to produce a coupled triazole. For this strategy, we sought to prepare azido-modified analogues of apoptolidin A and H and alkyne-modified fluorophores. The fluorophore would be tethered to the alkyne by a linker to minimize steric interactions between the fluorescent moiety and the biological target. This convergent strategy limits the number of synthetic transformations to be carried out on apoptolidin and allows for

simple optimization of both the fluorophore moiety and the linker to maintain biological activity.

### *Synthesis and Biological Evaluation of Azido Apoptolidin A and H*

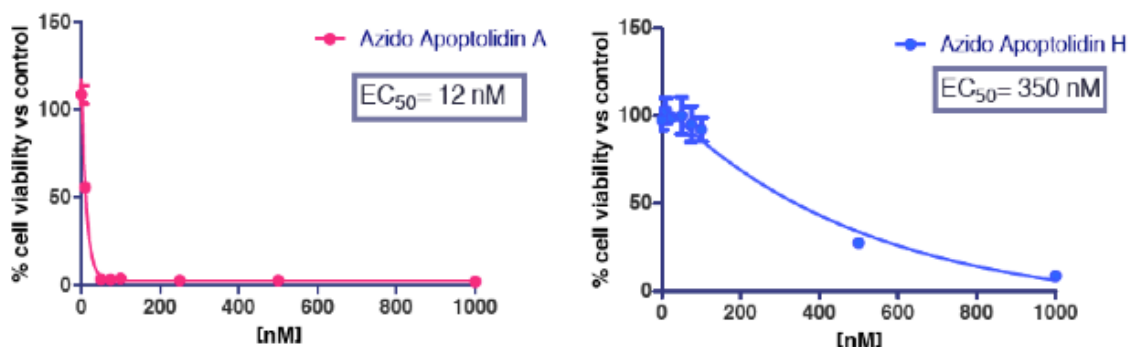
To maintain structural similarity of apoptolidins A and H probes we required the azido group to be introduced at the same position. Previous studies by Wender *et al* revealed some selectivity for the acylation of apoptolidin A at the C2' hydroxyl group of the C9 sugar which resulted in a negligible change in activity in both cell viability assays and F<sub>1</sub>F<sub>0</sub>ATPase inhibition assays.<sup>4</sup> Optimal regioselectivity was reported with the use of either a peptide catalyst<sup>5</sup> or by treatment of a preformed C2'-C3' apoptolidin stanylidine acetal with an acyl chloride.<sup>6</sup> The stanylidine acetal conditions were applied for the acylation of apoptolidin A and H with  $\delta$ -azidopentanoyl chloride to produce azido apoptolidin A **4.1** and azido apoptolidin H **4.2**. However, preparative RP-HPLC purification of the resultant mixture revealed a lower isolated yield than reported for the benzylation by Wender *et al*, likely due to an observed second, isomeric product not separated by flash chromatography. Ultimately, investigations with various coupling reagents identified the use of PyBrop produced superior yields under mild conditions (**Scheme IV-1**). The desired regioselectivity in the acylation was confirmed by <sup>1</sup>H-<sup>13</sup>C couplings from CIGAR-HMBC experiments. Similar results for both apoptolidin A and H were observed for both sets of reaction conditions.



**Scheme IV-1:** Synthesis of azido apoptolidin A **4.1** and H **4.2**

Next, azido apoptolidin A and H were tested in our H292 cell viability assay (**Figure IV-1**). Both compounds retained cytotoxicity with  $EC_{50}$ 's comparable to the parent compounds apoptolidin A and H ( $EC_{50}$  = 12 and 600 nM respectively). With these

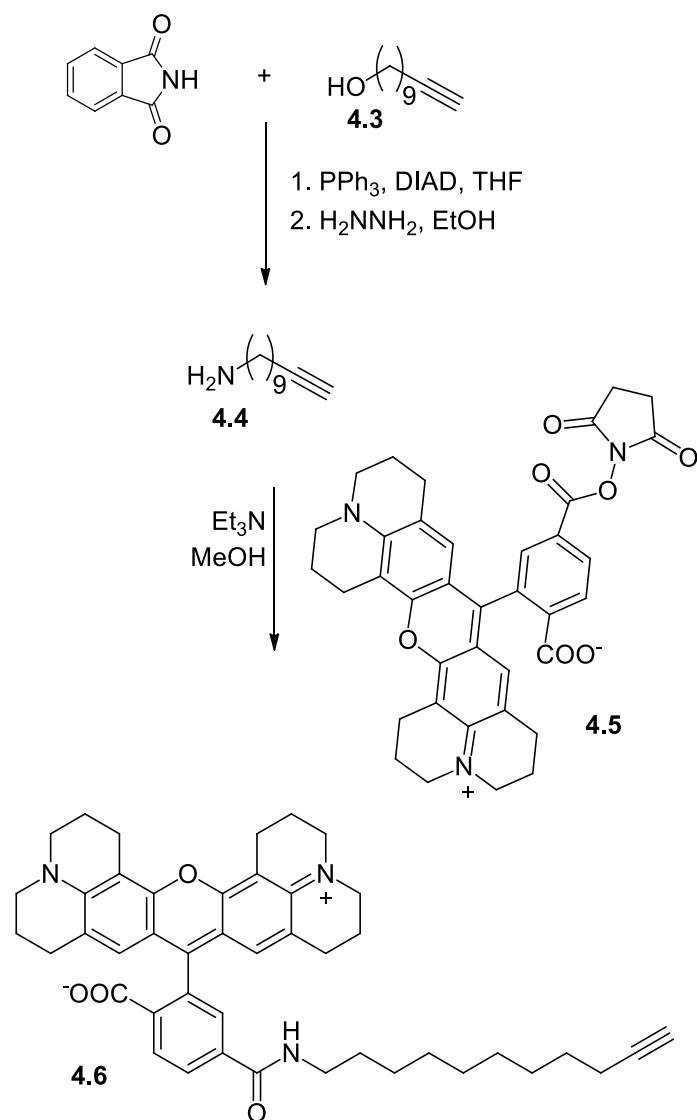
compounds in hand we began to investigate the synthesis of an optimal alkyne fluorophore conjugate for preparation of the desired fluorescent probes.



**Figure IV-1:** Azido apoptolidin A and H H292 cell viability assay

#### *First Generation “Click” Fluorophore: Terminal Alkyne*

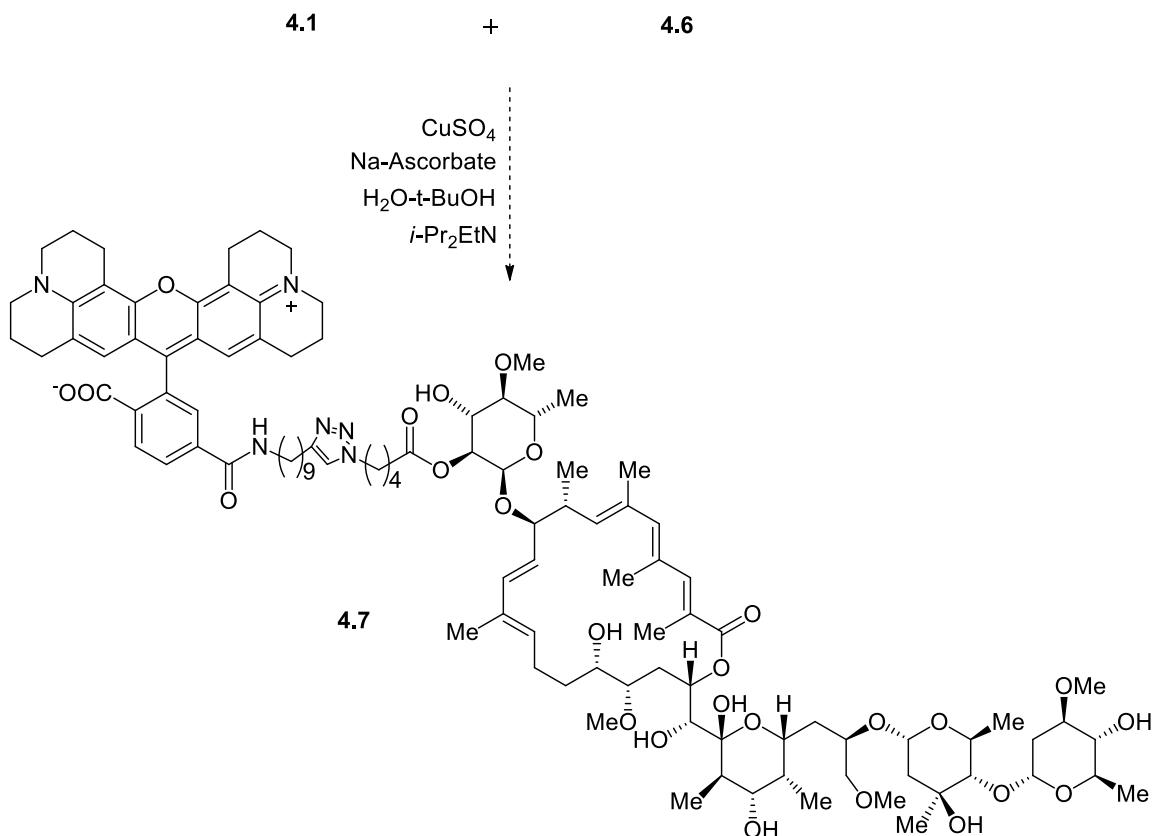
Our initial investigations into the preparation of fluorescent alkyne conjugates focused on the use of the standard copper(I) catalyzed Huisgen [3+2] cycloaddition reaction. For this “click” reaction a terminal alkyne is required. Because of its ready availability from collaborators<sup>7</sup> and good spectral properties for use in confocal microscopy, Rhodamine X (RhoX) was chosen as a fluorophore to begin investigation. A (9 methylene) alkyl chain was used as a linker between the alkyne and RhoX for this first generation probe. Specifically, undecynol **4.3** was converted to amine **4.4** by a Gabriel synthesis sequence. This amine was treated with the N-Hydroxy succinimidyl ester of RhoX **4.5** to produce RhoX alkyne conjugate **4.6**.



**Scheme IV-2:** Synthesis of RhoX-alkyne **4.6**

In an initial experiment, treatment of azido apoptolidin A **4.1** with RhoX alkyne conjugate **4.6** in the presence of copper(I) produced a brightly fluorescent product, by TLC (**Scheme IV-1**). While attempts at purification of this product by flash column chromatography failed to produce spectral data confidently indicating the structure of the desired product, the compound was assumed to be the triazole **4.7**. Furthermore, in the

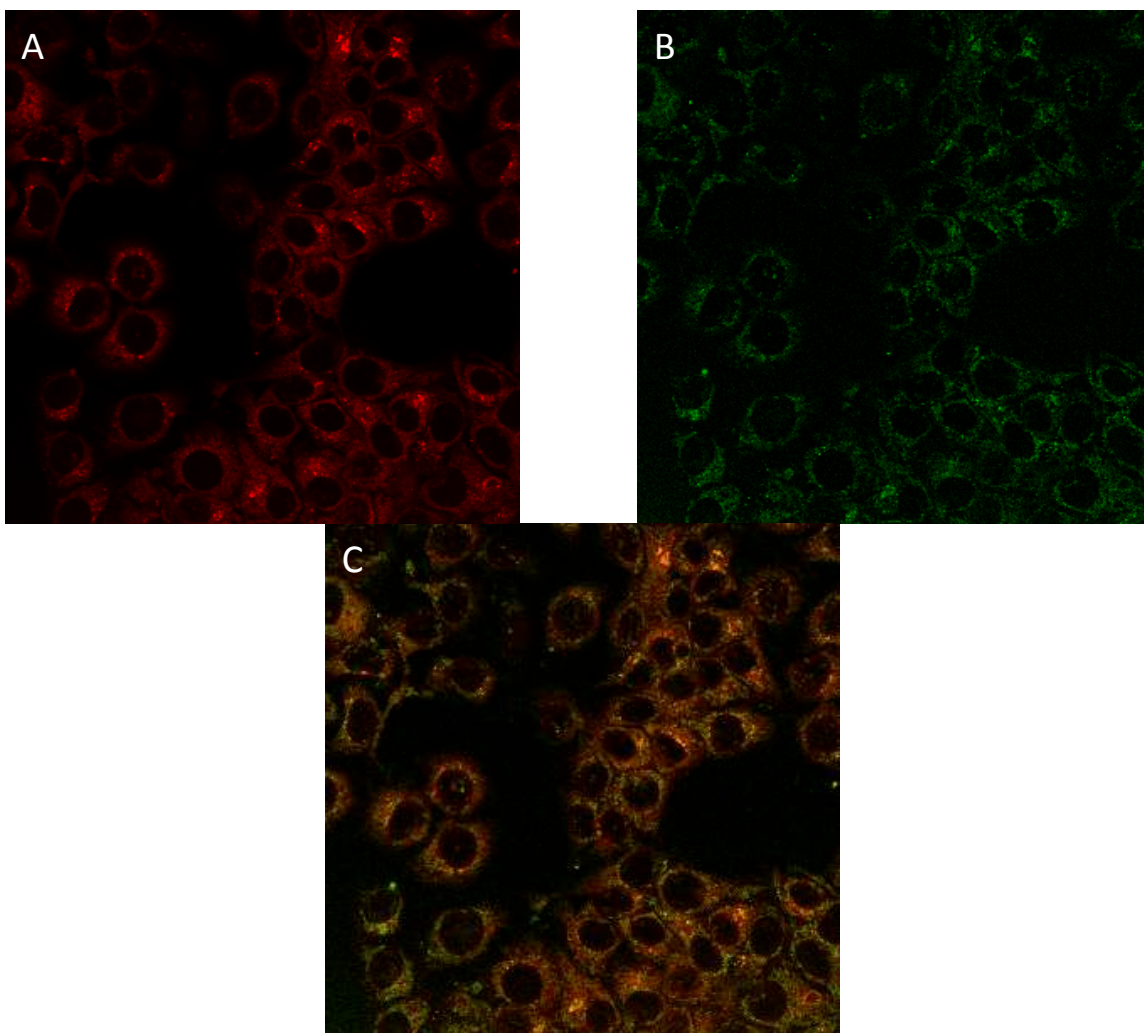
standard H292 cell viability assays, this material gave an estimated EC<sub>50</sub> of 18 nM, further suggesting the success of the cycloaddition reaction in coupling the fluorophore to azido apoptolidin A **4.1**.



**Scheme IV-3:** First generation fluorescent apoptolidin synthesis

While we were less than confident of the structure of the compound and dissatisfied with the low level of purity, we performed initial assays to attempt to measure any co-localization of the new probe with the mitochondria specific dye Mitotracker Green FM. H292 cells were treated with conjugate **4.7** for 45 minutes, then

with mitotracker for 30 minutes followed by a washout period to eliminate non-specifically bound fluorophore. The cells were then imaged by confocal fluorescence microscopy and an example of the resulting images is shown (**Figure IV-1**). Fluorescence from conjugate **4.7** shown in panel A in red, mitotracker in B in green and the images are overlaid in panel C revealing areas of significant co-localization in yellow. Co-localization analysis of these images using the Costes method<sup>8</sup> gave a Pearson's coefficient of  $P_c = 0.7$  indicating a significant amount of overlap between the two signals. A control treatment with RhoX acid showed no staining (data not shown).



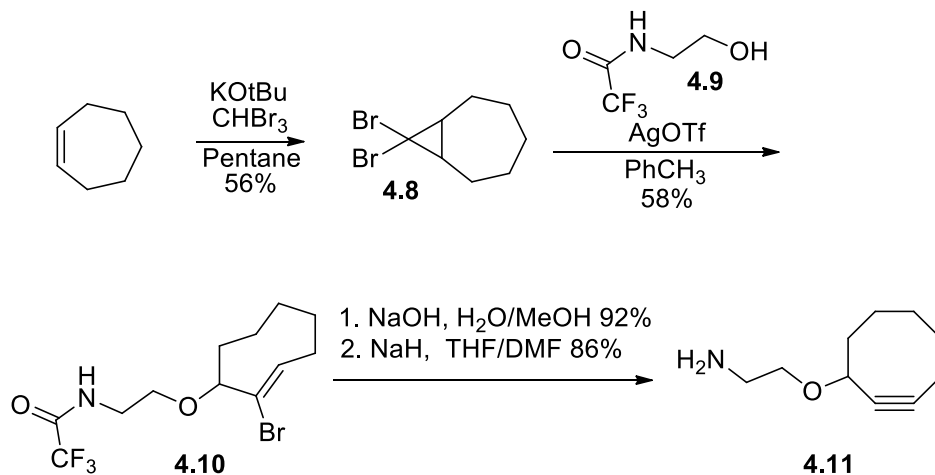
**Figure IV-2:** Initial confocal microscopy results with compound 4.7

While these initial results were somewhat promising, neither NMR nor MS analysis confirmed the structural assignment. Furthermore, the compound mixture had particularly weak fluorescence, requiring high loading concentration (2  $\mu\text{M}$ ) to give good signal in confocal microscopy experiments. Finally, multiple attempts at repeating the reaction gave rise only to products containing the Rhox chromophore that were separable from any peaks containing the apoptolidin chromophore by RP-HPLC. We suspected that



the copper catalyzed “click” reaction was somehow incompatible with our coupling partners and instead turned our attention to copper-free click reactions.

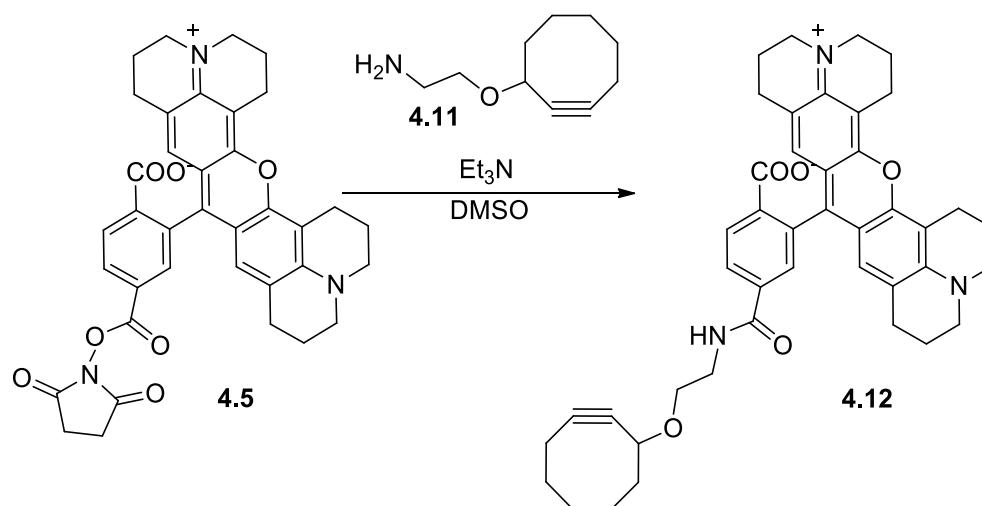
*Second Generation “Click” Fluorophore: Cyclooctyne*



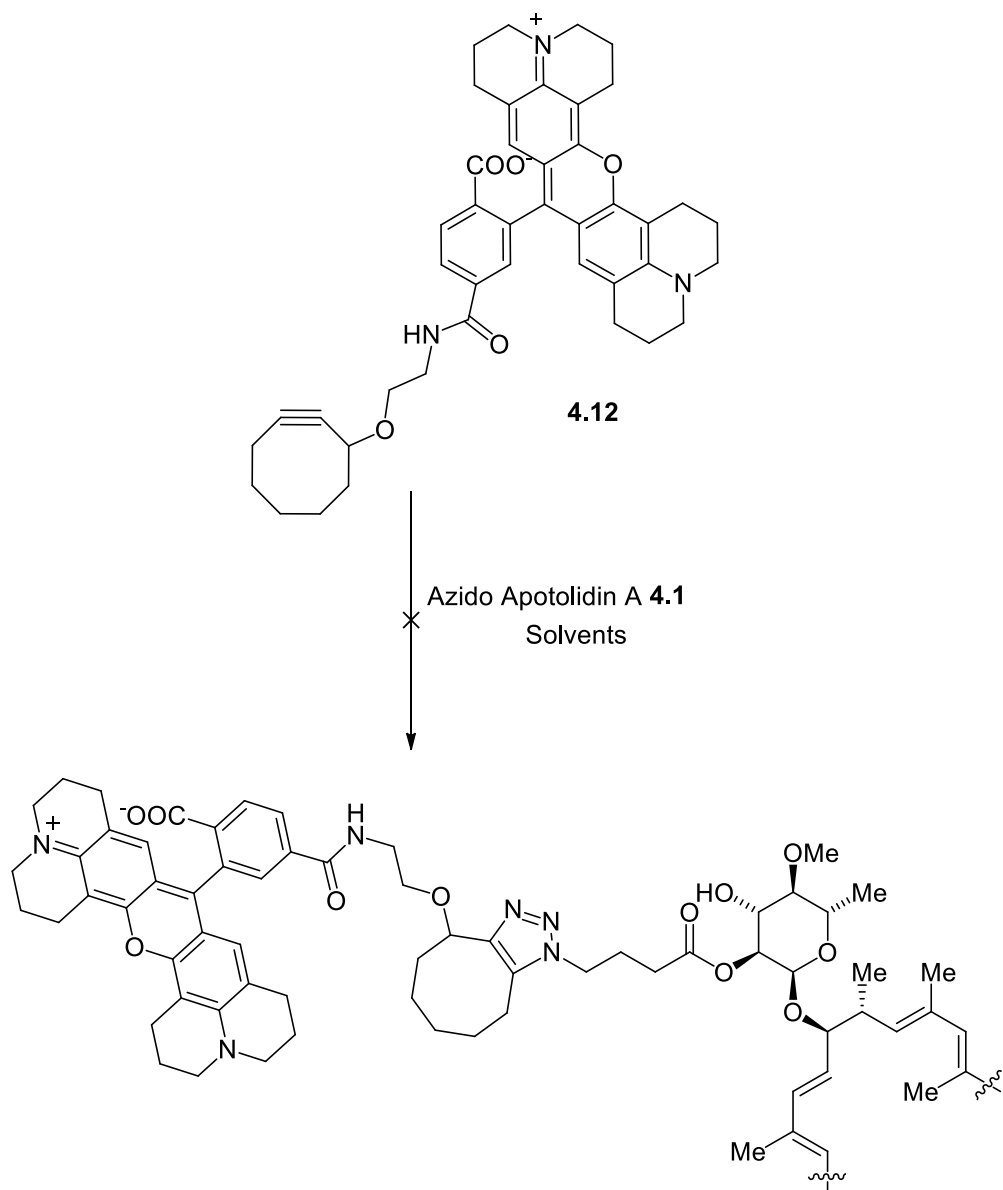
**Scheme IV-4:** Synthesis of cyclooctyne amine **4.11**

Bertozzi *et al* developed a copper free variant of the Huisgen cycloaddition that utilizes ring strain to activate the alkyne for cyclization rather than copper catalysis.<sup>9</sup> To investigate this method, we prepared a cyclooctyne amine as reported in the literature (**Scheme IV-4**).<sup>10</sup> Briefly, carbene addition to cycloheptene provided dibromobicyclo[5.1.0]octane **4.8**. Treatment of **4.8** with silver triflate in the presence of trifluoroacetate protected ethanolamine **4.9** yielded vinyl bromide **4.10**. Hydrolysis to the amine followed by dehydrobromination yields cyclooctyne **4.11**. This amine was then coupled to the N-hydroxysuccinimide ester of Rhox to give cyclooctyne fluorophore **4.12** (**Scheme IV-5**).<sup>11</sup> Treatment of azidoapoptolidin A with this compound, however,

resulted only in the recovery of starting material (**Scheme IV-6**). The strain promoted azide alkyne cycloaddition reaction with simple cyclooctynes such as **4.12** often requires significant heating to temperatures likely to decompose apoptolidin in order to observe fast reaction rates.



**Scheme IV-5:** Cyclooctyne RhoX conjugate **4.12**

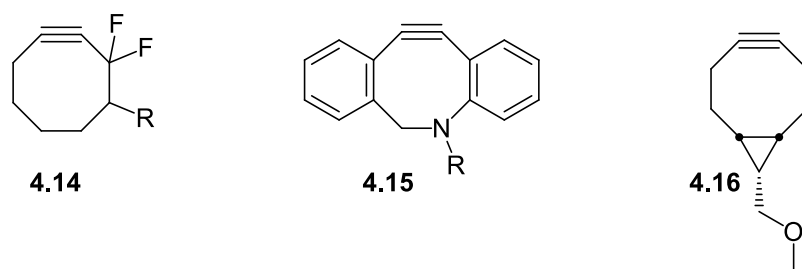


**Scheme IV-6:** Unsuccessful cyclooctyne “click” reaction

*Third Generation “Click” Fluorophore: Bicyclononyne*

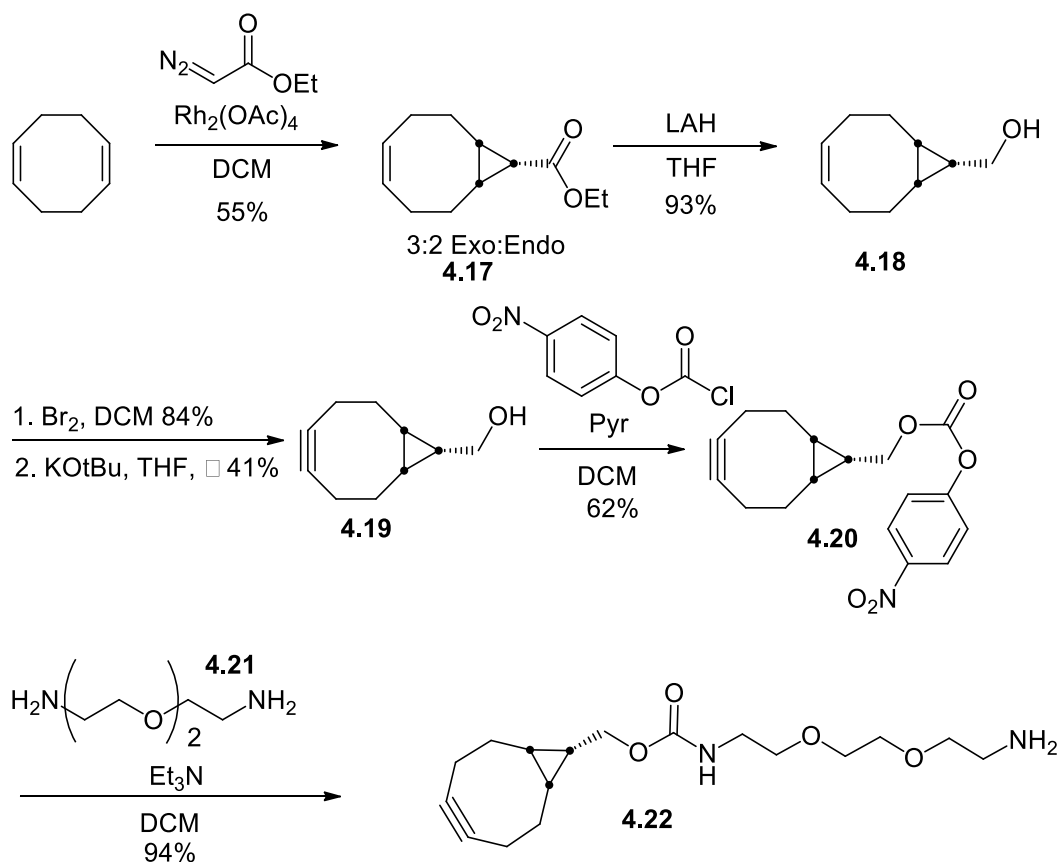
Since the initial use of the copper-free click reaction was reported by Bertozzi utilizing cyclooctyne, several more reactive cyclic alkynes have been developed that take advantage of altered electronics and increased ring strain to greatly increase [3+2]

cycloaddition rates.<sup>12</sup> In order to ensure rapid and selective reactivity with the azido apoptolidin conjugates, we selected from among the most reactive of these compounds as candidates for our probe synthesis (**Figure IV-3**). A significant improvement in cyclooctyne reactivity is observed by placing electron withdrawing groups (e.g. difluoromethylene) adjacent to the alkyne as in **4.14**. Increasing strain energy by fusing the cyclooctyne to two aryl groups also significantly enhances reaction rates as reported for compounds such as **4.15**. A similar rate enhancement is also observed for bicyclononyne derivatives **4.16** by the fusion of the octyne to a cyclopropane. While reaction rates for each of these cyclooctynes are comparable, the synthesis of **4.14** and **4.15** require eight and nine steps respectively and are relatively poor yielding. In **4.15**, the addition of the biaryl groups significantly increases lipophilicity, enhancing nonspecific protein binding in biological systems. Finally, due to the asymmetry of **4.14** and **4.15**, “click” reactions with azides will produce regioisomeric mixtures. Bicyclononyne (**4.16**, BCN) was chosen to investigate next as it can be assembled in good yield over four simple steps from cyclooctadiene, requires a minimal addition of hydrophobic groups and is symmetric.<sup>13</sup>



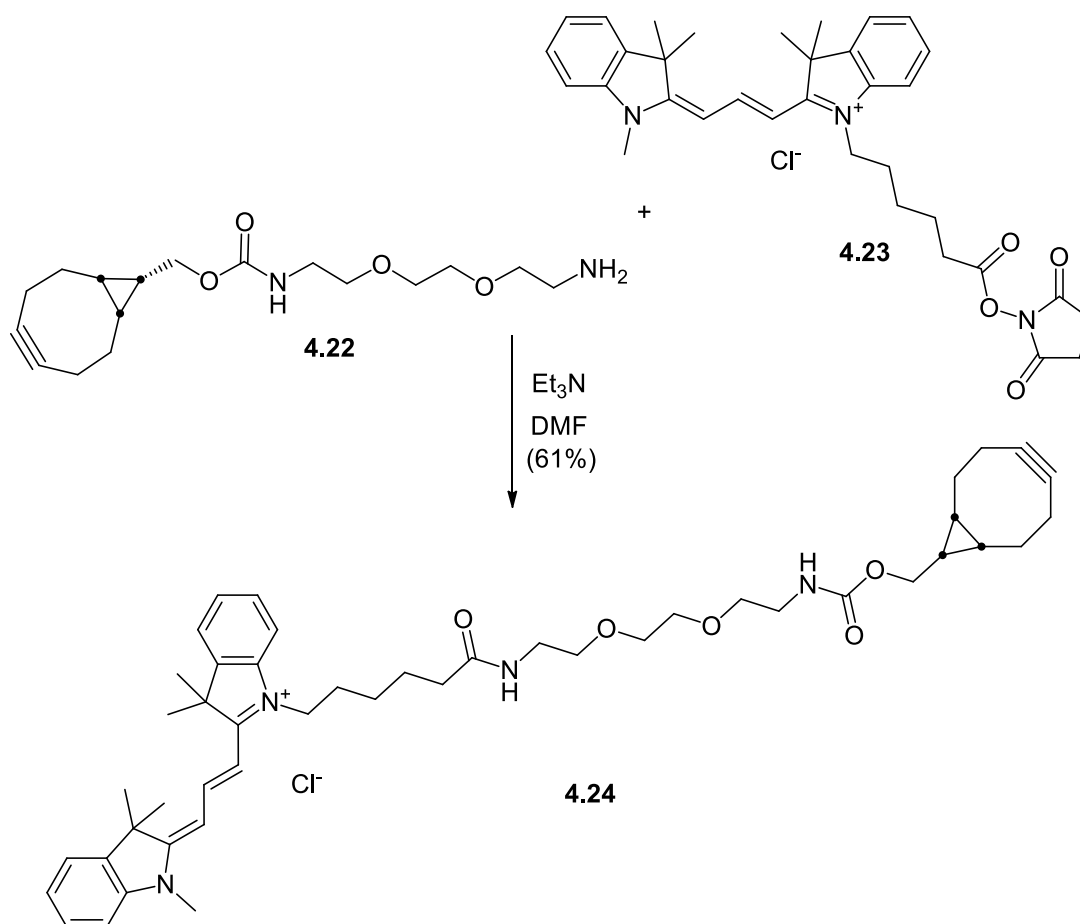
**Figure IV-3:** Highly reactive cyclooctynes for “click” chemistry

A bicyclononyne amine was prepared as previously described from cyclooctadiene (**Scheme IV-7**).<sup>13</sup> Cyclopropanation of cyclooctadiene with ethyl diazoacetate in the presence of catalytic rhodium acetate afforded bicyclononene **4.17** as a separable mixture of diastereomers. The minor, but more strained endo product was taken forward to provide the most reactive bicyclononyne. Reduction of ester **4.17** with lithium aluminum hydride provided alcohol **4.18**. Bromination of the alkene followed by double dehydrobromination produced the desired bicyclononyne **4.19**. At this stage, a short PEG linker was introduced to balance lipophilicity and hydrophilicity while providing distance between the fluorophore and apoptolidin moieties. To that end, alcohol **4.19** was coupled to *p*-nitrochloroformate to give carbonate **4.20**. Treatment of **4.20** with diamine **4.21** provided amino bicyclononyne **4.22** in good yield.



**Scheme IV-7:** Synthesis of bicyclononyne amine **4.22**

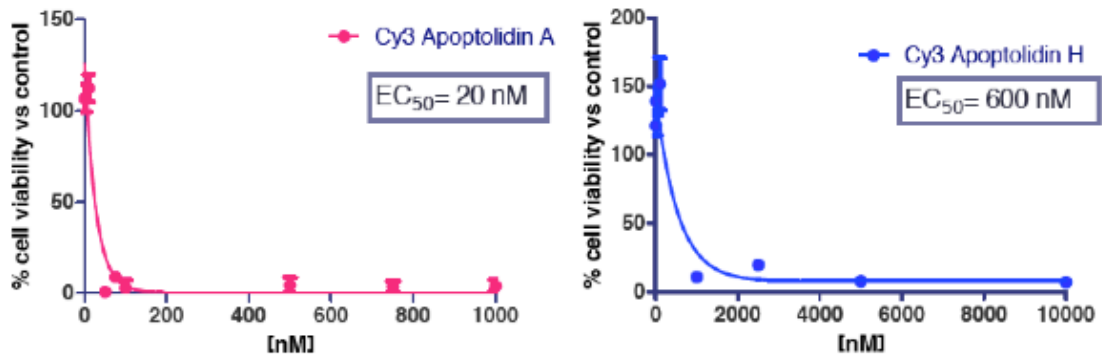
Having had poor success with Rhox based probes in our previous “click” reactions; we decided to investigate alternative fluorophores. The cyanine dye Cy3, was selected first due to its optical properties (excitation/emission spectra), photostability, relatively low molecular weight and commercial availability.<sup>14</sup> Treatment of the N-hydroxysuccinimide ester of Cy3 **4.23** with amino bicyclononyne **4.22** afforded the Cy3 bicyclononyne (**4.24**, Cy3-BCN).



**Scheme IV-8:** Preparation of Cy3 bicyclononyne conjugate **4.24**

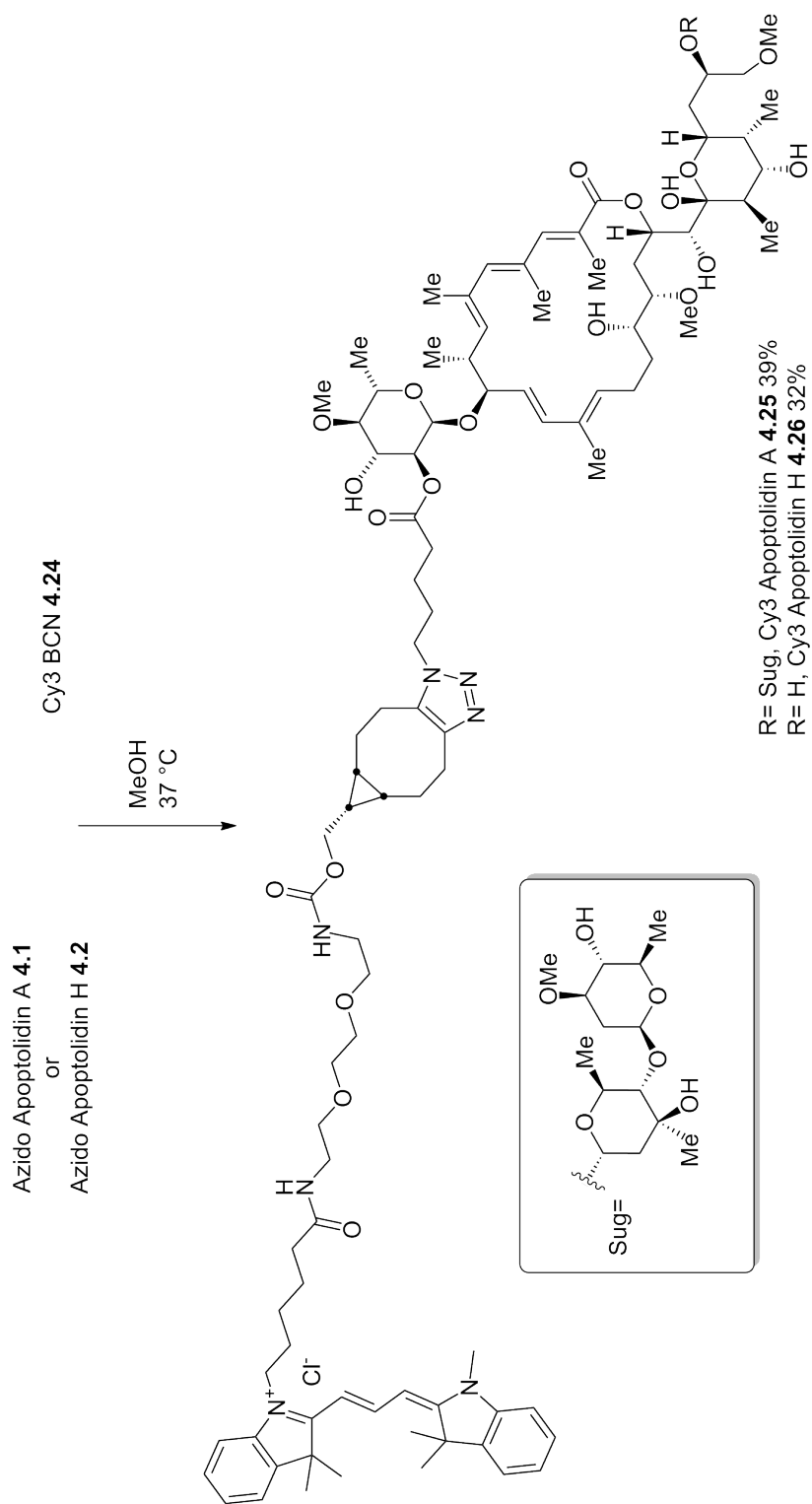
Treatment of azido apoptolidin A **4.1** with Cy3–BCN **4.24** in methanol at 37°C for 4 h resulted in complete consumption of **4.1** and the formation of a new product with the signature chromophore of both apoptolidin and Cy3 as indicated by HPLC. Isolation and spectral characterization of this product indicated that it was the desired Cy3 apoptolidin A conjugate **4.25**. Analogous results were obtained from the reaction of Cy3–BCN **4.24** with azido apoptolidin H **4.2** to produce the Cy3 apoptolidin H conjugate **4.26** (Scheme IV-9). Finally, Cy3 conjugates **4.25** and **4.26** were tested for activity in the H292 cell viability assay. Gratifyingly both compounds showed comparable activity to

apoptolidin A and H, respectively (**Figure IV-4**). Having prepared these fluorescent probes of both apoptolidin A and H and confirmed the retention of their biological activity in H292 cells, we next began to investigate their subcellular localization using confocal microscopy.



**Figure IV-4:** Cy3 apoptolidin A and H H292 cell viability assay



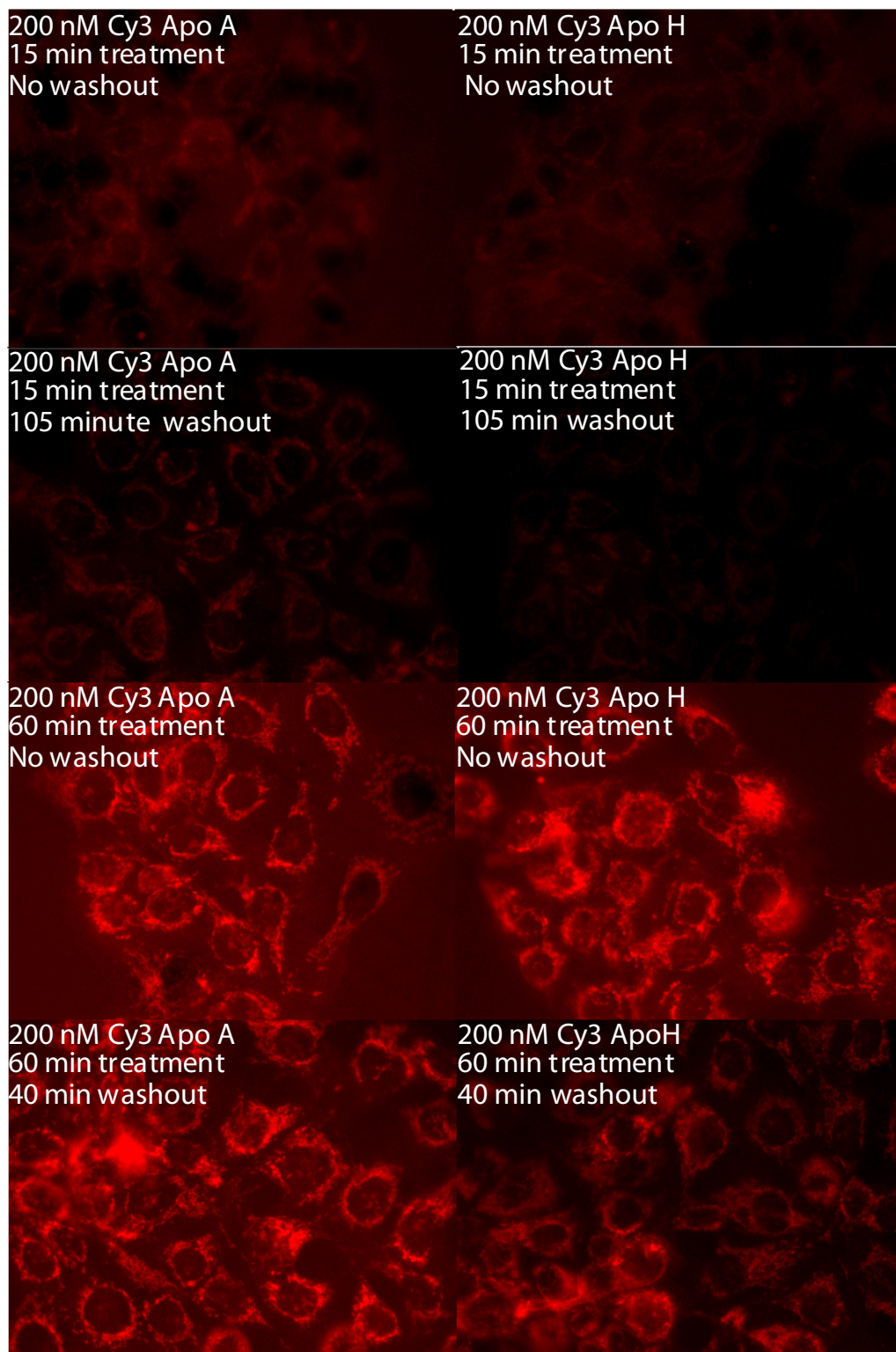


**Scheme IV-9:** Preparation of Cy3 Apoptolidin A and H Conjugates

## Cyanine Apoptolidin Conjugate Microscopy Studies

### *Cy3 Conjugate Treatment Conditions*

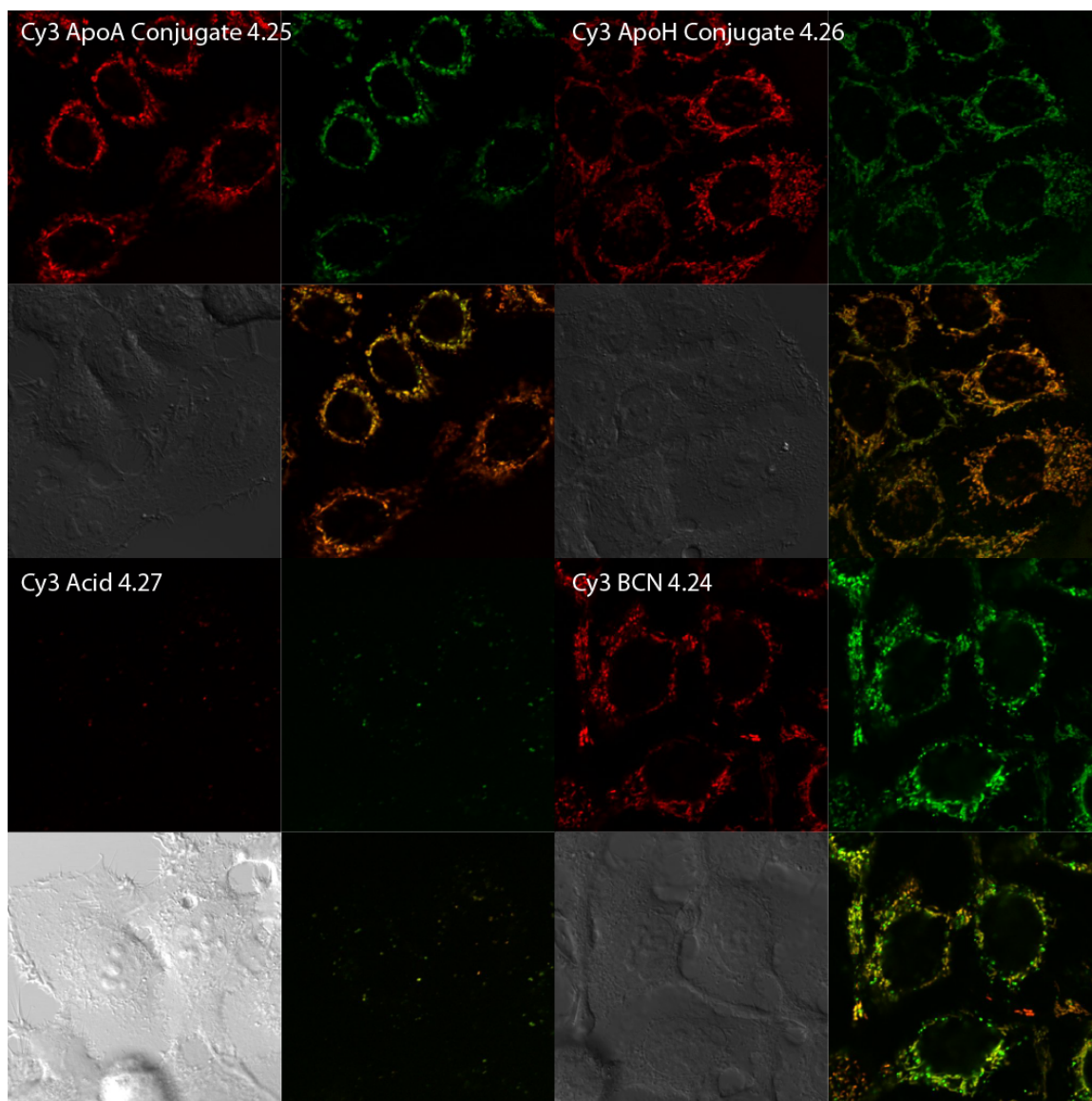
To determine the necessary treatment conditions to observe an ideal level of cellular staining in H292 cells with Cy3 apoptolidin conjugates **4.25** and **4.6**, optimization experiments were performed using a standard fluorescence microscope. H292 cells were treated with 200 nM of each compound for 15–90 minutes. The culture media was then replaced with new media to allow for any nonspecific staining to diffuse for either 40 or 105 minutes. After only 15 minutes, a significant amount of staining was observed for both compounds (**Figure IV-5**). After washout, most diffuse staining, apparently in the cytosol and intercellular space, was eliminated. Increased treatment time significantly increased the brightness of the staining but also increased diffuse, nonspecific signal. Based upon these results, we chose to use a 15 minute treatment at 200 nM of each Cy3 conjugate, followed by a 60 minute washout to remove nonspecific binding for use in our confocal microscopy experiments. These results showed lower fluorescence signal for staining with Cy3 apoptolidin H conjugate **4.26** at treatment times up to 60 minutes. However, 90 minute treatments with either compound were similarly saturated. While this indicated a minor reduction in cell permeability of apoptolidin H compared to apoptolidin A, this difference would be inconsequential in the course of a four day treatment in cell viability testing.



**Figure IV-5:** Treatment of H292 cells for 15 or 60 minutes with 200 nM Cy3 Apoptolidin A or H with or without washout as indicated.

### *Cy3 Confocal Microscopy: Subcellular Localization*

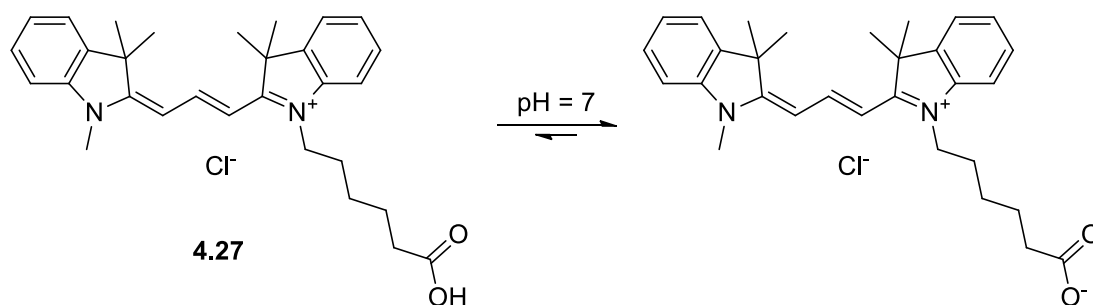
Our first confocal microscopy experiments with these probes examined co-localization of either Cy3 carboxylic acid **4.27**, Cy3 apoptolin A **4.25** or Cy3 apoptolidin H **4.26** with Mitotracker Green FM to determine if the compounds bound to a target in the mitochondria. Mitotracker Green FM was added into the washout media of the Cy3 treatment conditions for the final 30 minutes. For each compound, 3 dishes of cells were treated and 10 random fields were captured for each dish (**Figure IV-6**). Treatment with Cy3 carboxylic acid **4.27** showed no Cy3 specific staining. Both of the cy3 apoptolidin conjugates, however, showed a high degree of staining that appeared to significantly overlap with staining from Mitotracker Green FM. Indeed, Costes's analysis of this data revealed excellent overlap for both compounds providing Pearson's coefficients ( $P_c$ ) of 0.89 and 0.88 for Cy3 apoptolidin A and H conjugates, respectively. However, it seemed arguable that the Cy3 carboxylic acid might not be a sufficient negative control in these experiments for localization contribution of the fluorophore and linker portion of the molecule. H292 cells were treated with Cy3-BCN **4.24**. A high amount of mitochondrial specific staining was observed for this compound as well. While the overlap of Cy3-BCN **4.24** ( $P_c=0.80$ ) was less than that of the Cy3 apoptolidin conjugates, it was still significant enough to cause us to question the validity of these results.



**Figure IV-6:** H292 cells stained with **4.25** (top left), **4.26** (top right), **4.27** (bottom left) and **4.24** (bottom right) and with Mitotracker Green FM. Cy3 fluorescence is shown in red, Mitotracker in green.

The mitochondrial staining of the Cy3–BCN **4.24**, while unanticipated, should not be surprising. One explanation is that the hydrophobicity of the linker and the bicyclononyne moiety cause the probe to be nonspecifically bound to lipid bilayers in the plasma membrane as well as the membrane of organelles, including mitochondria.

However, the high Pearson's coefficient with the mitochondria and the lack of obvious staining of the plasma membrane in these experiments suggest that this is likely an insufficient explanation. Given the previous reports of the bioorthogonal nature of the alkyne moiety and the lack of other reactive functional groups within **4.24**, it is not expected that the compound is specifically reacting with any biomolecules to cause the staining. A survey of the literature on uses of cyanine dyes found examples of where certain aliphatic cyanine esters had been used as a means of measuring the mitochondrial membrane potential.<sup>15</sup> The use of cationic fluorophores, for example Rhodamine 123, for the quantification of the mitochondrial membrane potential is well precedented.<sup>16,17</sup> The equilibrium of fluorophore concentration between the mitochondria and the cytosol is highly predictable by the positive charge of the fluorophore and  $\Delta\Psi_m$  by the Nernst equation. Under biological conditions, the carboxylic acid of Cy3 would be deprotonated, resulting in a net neutral charge for the molecule and thus no staining of the mitochondria was observed with this compound (**Scheme IV-10**). However, when coupled to non-acidic moieties, as in **4.24**, **4.25** and **4.26**, the net charge is positive at physiological pH, resulting in a high degree of mitochondrial staining as observed in our experiments.



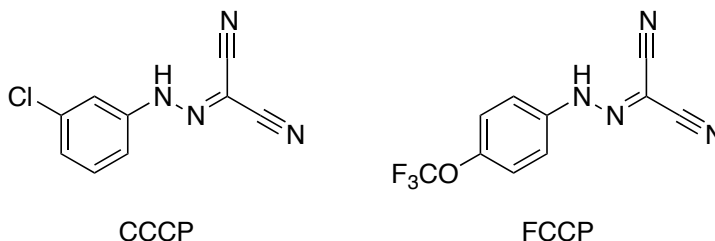
**Scheme IV-10:** Cy3 acid **4.27** at physiological pH

While this control calls to question the significance of the co-localization results, there are still positive indications from these studies. First, any increase in localization at the mitochondria due to the incorporation of the fluorophore moiety neither significantly disrupts nor enhances the cytotoxicity of either apoptolidin A or H, suggesting that the important biological target of these compounds may indeed lie in the mitochondria. Furthermore, no significant differences were observed between Cy3 apoptolidin A and H conjugates with respect to cellular and mitochondrial uptake rates. While the rapid transport to the mitochondria could easily be attributed to the cationic cyanine moiety, if differential transport rates were responsible for the reduced potency of Cy3 apoptolidin H conjugate **4.26** this compound would likely have activity more comparable to apoptolidin A. This data, therefore, suggests that the disaccharide moiety is likely important for target affinity and not cellular or subcellular transport, as previously hypothesized.

#### **Current Studies: Depolarization and Non-cationic Fluorophores**

With possible reasons attributed for the unacceptable staining by Cy3–BCN **4.24** in our experiments, we have identified two strategies to circumvent the problem. First, the conditions of our treatment protocol could be modified in a way that eliminates Cy3 specific staining of the mitochondria with control compound **4.24**. Second, additional, noncationic fluorescent conjugates of apoptolidins could be prepared for these studies. We are currently pursuing both of these strategies.

## Mitochondrial Decoupling Strategy



**Figure IV-7:** Protonophore mitochondrial decouplers

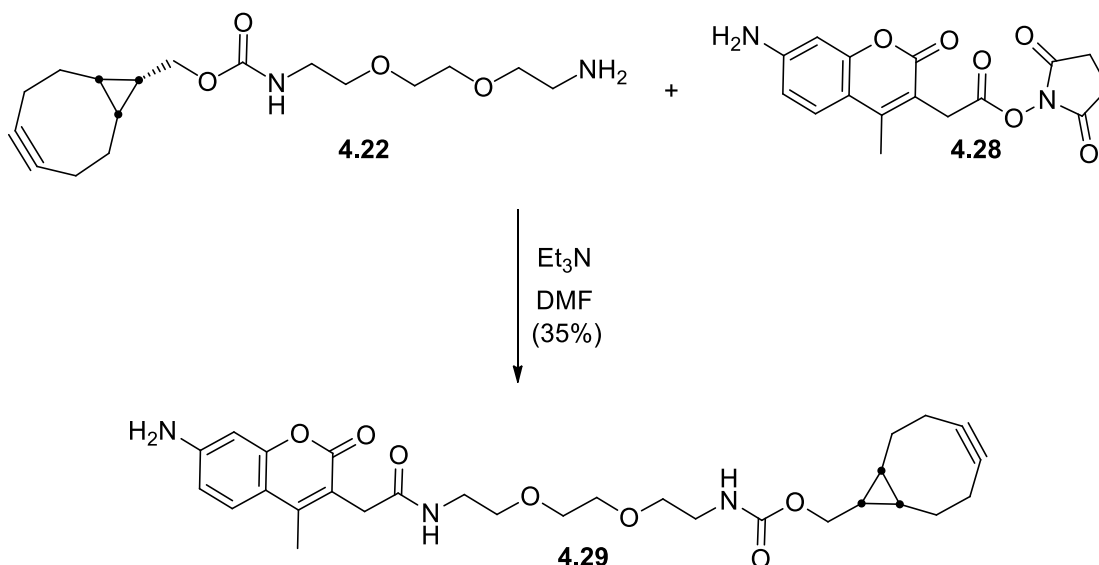
Assuming that Cy3-BCN **4.24** staining is caused by the cationic nature of the fluorophore and the mitochondrial membrane potential, dissipation of the membrane potential should result in the elimination of the undesired staining.<sup>18</sup> Several compounds are known to cause changes in  $\Delta\Psi_m$  either by inhibition of the mitochondrial respiratory chain or by transferring protons into the mitochondria from the cytosol. Protonophores such as FCCP and CCCP can be used to rapidly dissipate  $\Delta\Psi_m$ . These compounds are easily protonated in the cytosol, causing them to rapidly diffuse into the mitochondria and be deprotonated. The resultant rapid catalytic influx of protons into the mitochondria eliminates  $\Delta\Psi_m$ . If conditions can be found to eliminate mitochondrial staining by Cy3-BCN **4.24** by dissipation of  $\Delta\Psi_m$ , these conditions could be applied to assays with Cy3 conjugates **4.25** and **4.26** to measure apoptolysin specific staining only. Preliminary confocal microscopy experiments with treatment of H292 cells with 200 nM **4.24**, followed by treatment with 5  $\mu$ M CCCP and immediate imaging showed only a small decrease in mitochondrial staining (results not shown). Further experimentation is



underway to determine the optimal order and duration of treatment with each compound to effectively eliminate  $\Delta\Psi_m$ .

*Fourth Generation “Click” Fluorophores: Non-cationic Fluorophores*

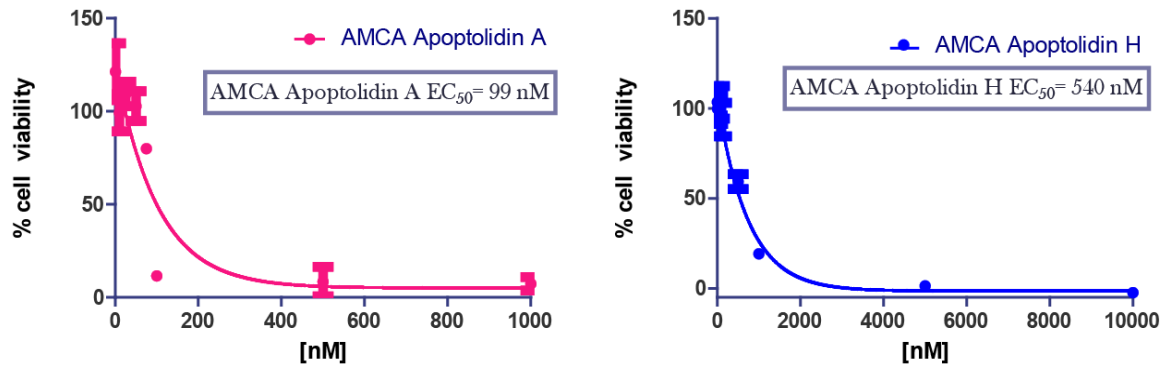
The synthesis of our Cy3 fluorescent probes was designed in a way that would allow for facile alteration of the fluorophore moiety. Amine **4.22** can be easily coupled to the commercially available N-hydroxysuccinimide ester of many fluorophores to provide clickable intermediates. Two new fluorophores were selected for investigation that would not be cationic under physiological conditions. Aminomethylcoumarin acetate (AMCA) was selected for its relatively small molecular weight, neutral charge and affordability but suffers from poor optical characteristics (namely a short excitation wavelength). Alternatively, Alexafluor 568 (Af568) was selected due to superior optical qualities despite its larger molecular weight, high cost and the fact that it is sold as a mixture of isomers, significantly complicating spectral characterization of probes incorporating this fluorophore.



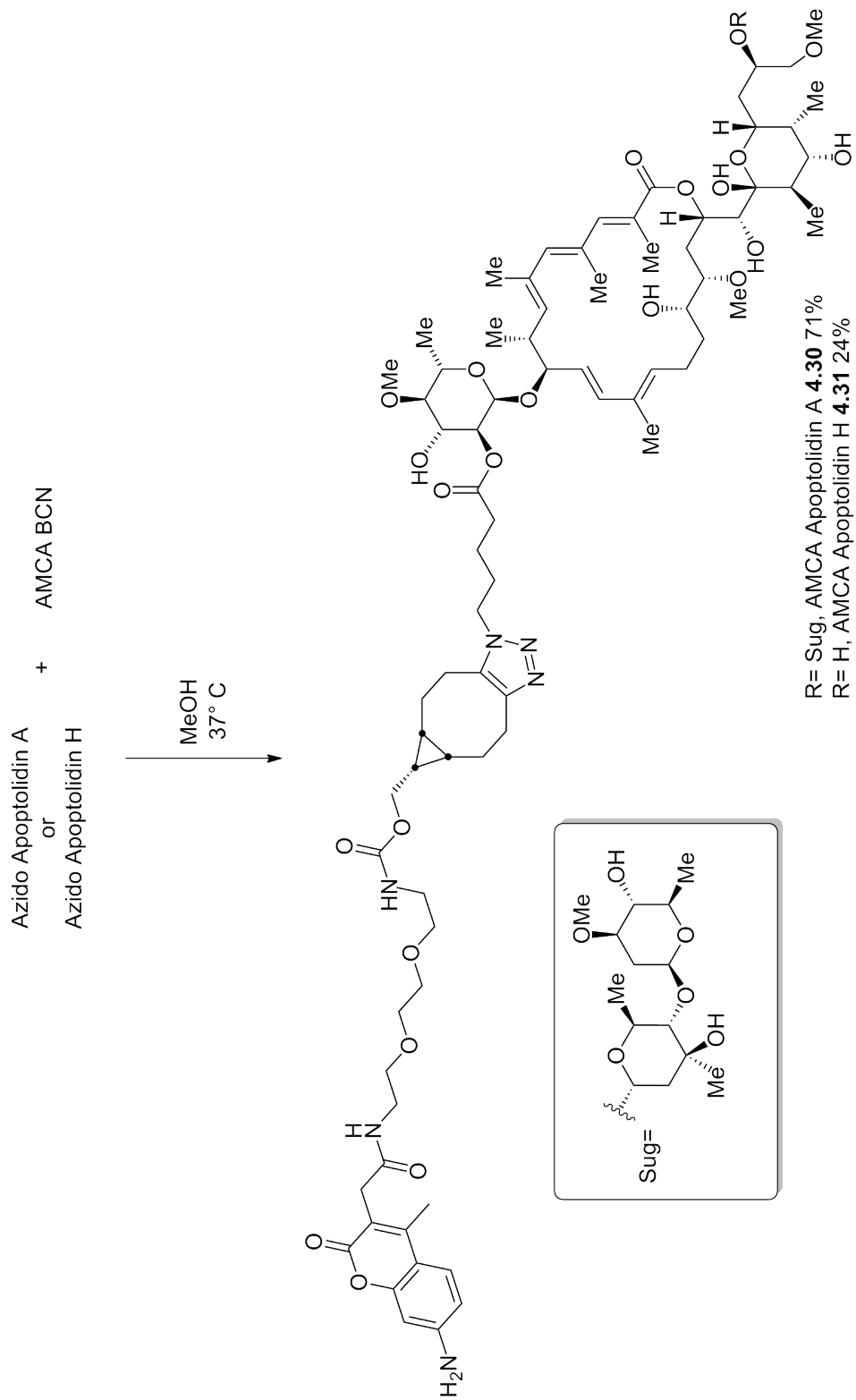
**Scheme IV-11:** Preparation of AMCA bicyclononyne conjugate **4.29**

The synthesis of AMCA apoptolidin A and H conjugates proceeded without significant complications using conditions previously developed for Cy3 conjugate synthesis (**Scheme IV-11**, **Scheme IV-12**). Evaluation of these compounds in cell viability assays gave  $\text{EC}_{50}$ 's of 99 (**4.30**) and 540 (**4.31**) nM, showing a retention of activity to apoptolidin A and H. Initial treatment of H292 cells with 200 nM AMCA BCN conjugate **4.29** resulted in no staining compared to untreated cells. The short excitation wavelength of the ACMA derivatives requires the use of two photon excitation methods by a long wavelength IR laser in confocal microscopy experiments. Unfortunately, the excitation of NADH autofluorescence overlaps significantly with that of AMCA, causing signal to be observed in the absence of AMCA treatment. However, the level of NADH can be significantly knocked down by glucose deprivation immediately prior to treatment. Studies utilizing this technique and the AMCA fluorescent conjugates **4.30** and **4.31** are

currently in progress to determine apoptolidin subcellular localization and evaluate the effect of the C27 disaccharide on cellular transport rates.

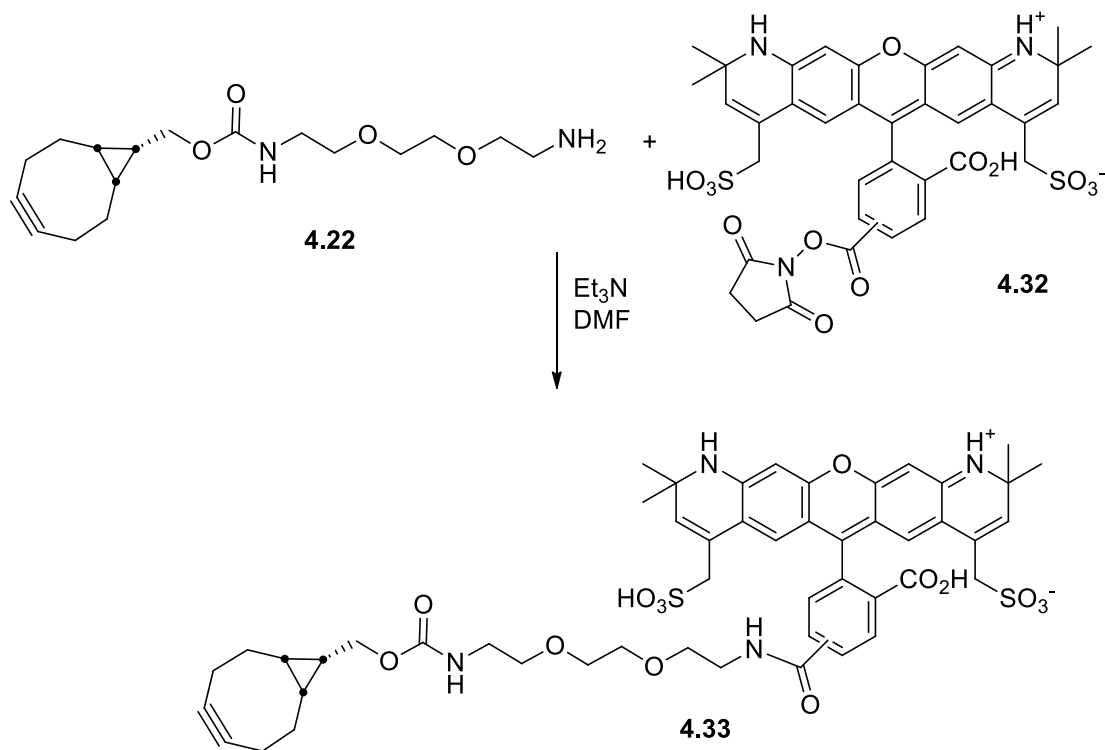


**Figure IV-8:** AMCA apoptolidin A and H H292 cell viability assay



**Scheme IV-12:** Preparation of AMCA apoptolidin A and H conjugates **4.30** and **4.31**.

Due to the exceptional cost of Alexafluor 568 NHS, only the Alexafluor 568 BCN derivative (**Scheme IV-13**) has been prepared while confocal experiments with AMCA derivatives are investigated. The presence of multiple isomeric forms of Alexafluor 568 either greatly reduces the yield (if separated) or prohibits NMR spectral characterization of the products.



**Scheme IV-13:** Alexafluor 568 BCN Synthesis

## Conclusions and Future Studies

A simple and versatile method has been developed for the site-selective modification of apoptolidin with a variety of compounds at a position that has a negligible impact on cytotoxicity in H292 cells. While in these examples, only fluorescent moieties have been attached to apoptolidin, the chemistry is easily modified to incorporate a variety of structures. Furthermore, the bioorthogonality of the click reaction and the apparent cell permeability of conjugates such as **4.24** and **4.29** suggest that these reagents could be used for the in vitro labeling of azides attached to small molecules, natural products or biomolecules within cells.

Experiments utilizing fluorescent apoptolidin A and H conjugates are inconclusive to date, but multiple tools have been prepared yielding two strategies to eliminate non-apoptolidin specific staining observed in control experiments. The use of decoupling agents in addition to Cy3 Apoptolidin A and H conjugates **4.25** and **4.26** may yet allow us to judge the effects of the C27 disaccharide on the cellular transport of apoptolidin A utilizing these compounds. Alternative fluorophores that do not include a cationic moiety have also been prepared that should also eliminate fluorophore specific binding. Finally, should both of these strategies fail, Alexafluor derivative **4.33** could be used to either prepare new fluorescent conjugates of apoptolidin A and H or potentially for in vivo labeling of azido apoptolidins. Results from these experiments will provide novel insight into the importance of sugar moieties in the biological activity of apoptolidin.

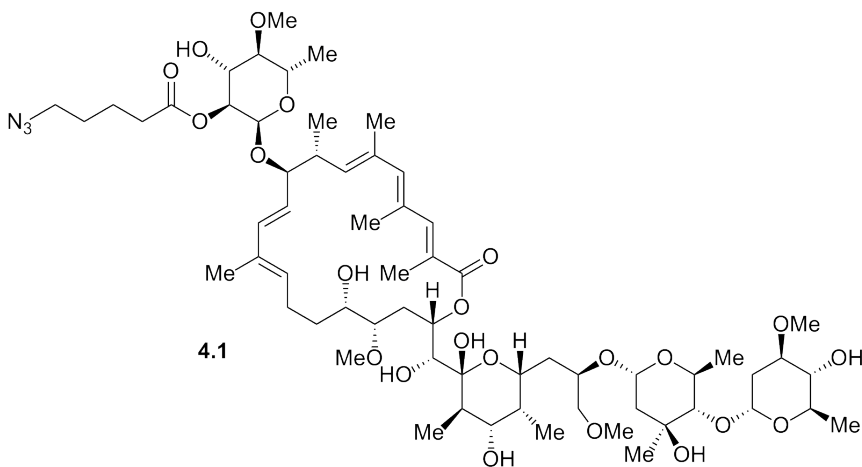
## Experimental Methods

**General Synthetic procedures:** All non-aqueous reactions were performed in flame-dried or oven dried round-bottomed flasks under an atmosphere of argon. Where necessary (so noted) solutions were deoxygenated by alternate freeze (liquid nitrogen)/evacuation/argon-flush/thaw cycles (FPT, three iterations) or degassed by purging with argon for several minutes. Stainless steel syringes or cannulae were used to transfer air- and moisture-sensitive liquids. Reaction temperatures were controlled using a thermocouple thermometer and analog hotplate stirrer. Reactions were conducted at room temperature (rt, approximately 23 °C) unless otherwise noted. Flash column chromatography was conducted as described Still et. al. using silica gel 230-400 mesh.<sup>19</sup> Where necessary, silica gel was neutralized by treatment of the silica gel prior to chromatography with the eluent containing 1% triethylamine. Analytical thin-layer chromatography (TLC) was performed on E. Merck silica gel 60 F254 plates and visualized using UV, ceric ammonium molybdate, potassium permanganate, and anisaldehyde stains. Yields were reported as isolated, spectroscopically pure compounds.

**Materials.** Solvents were obtained from either a MBraun MB-SPS solvent system or freshly distilled (tetrahydrofuran was distilled from sodium-benzophenone; toluene was distilled from calcium hydride and used immediately; dimethyl sulfoxide was distilled from calcium hydride and stored over 4Å molecular sieves). Commercial reagents were used as received with the following exceptions.

**Instrumentation.** Semi-preparative reverse phase HPLC was conducted on a Waters HPLC system using a Phenomenex Luna 5 µm C18(2) 100A Axia 250 x 10.00 mm column or preparative reverse phase HPLC (Gilson) using a Phenomenex Luna column

(100 Å, 50 x 21.20 mm, 5 µm C18) with UV/Vis detection. Infrared spectra were obtained as thin films on NaCl plates using a Thermo Electron IR100 series instrument and are reported in terms of frequency of absorption (cm<sup>-1</sup>). <sup>1</sup>H NMR spectra were recorded on Bruker 300, 400, 500, or 600 MHz spectrometers and are reported relative to deuterated solvent signals. Data for <sup>1</sup>H NMR spectra are reported as follows: chemical shift (δ ppm), multiplicity (s = singlet, d = doublet, t = triplet, q = quartet, p = pentet, m = multiplet, br = broad, app = apparent), coupling constants (Hz), and integration. <sup>13</sup>C NMR spectra were recorded on Bruker 75, 100, 125, or 150 MHz spectrometers and are reported relative to deuterated solvent signals. LC/MS was conducted and recorded on an Agilent Technologies 6130 Quadrupole instrument. High-resolution mass spectra were obtained from the Department of Chemistry and Biochemistry, University of Notre Dame using either a JEOL AX505HA or JEOL LMS-GCmate mass spectrometer or by the Vanderbilt University Center for Neuroscience Drug Discovery (VCNDD) on a Micromass –Q-ToF API-US mass spectrometer.



### Azido Apoptolidin

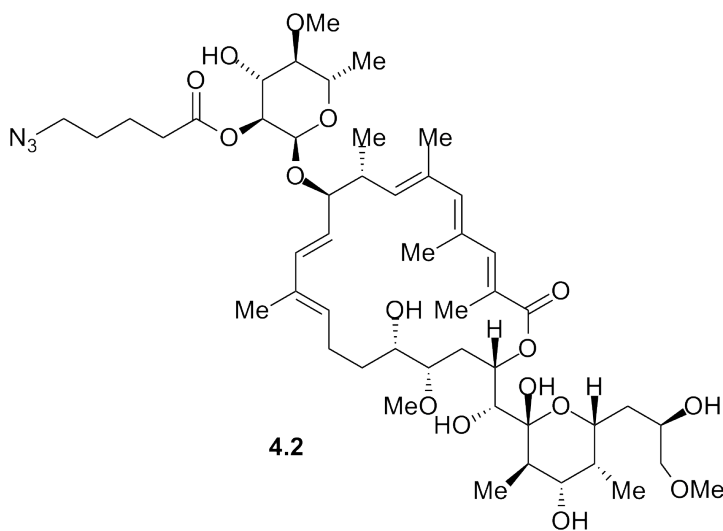
**A 4.1** To a solution of azido pentanoic acid (7.6 mg, 0.053 mmol) in dichloromethane (4.0 mL) at 0°C was

added bromo-tris-pyrrolidino phosphoniumhexafluorophosphate (PyBrop, 25 mg, 0.053 mmol) and diisopropylethyl amine (31 µL, 0.177 mmol) the resulting solution was stirred



at 0 °C for 10 min. Apoptolidin A **2.1** (20 mg, 0.018 mmol) was added to the resulting solution followed by one small crystal of 4-dimethylaminopyridine (DMAP). The resulting solution was warmed to rt and maintained at that temperature for 16 h. Methanol (100  $\mu$ L) was added to the reaction mixture and then concentrated. The resulting residue was diluted in EtOAc (20 mL) and washed with 1 N HCl (5 mL). The aqueous layer was extracted with EtOAc (2 x 10 mL). The combined organic extracts were washed with NaHCO<sub>3</sub> (1x 5mL) and brine (1 x 5 mL) and dried (Na<sub>2</sub>SO<sub>4</sub>) and concentrated in vacuo. The resulting residue was dissolved in 1.2 mL of DMSO, filtered through a 0.2  $\mu$ m polytetrafluoroethylene PTFE syringe tip filter and purified by preparative reversed phase HPLC with a 4 minute gradient from 45% to 75% MeCN in H<sub>2</sub>O in four 300  $\mu$ L injections. Fractions containing desired product (r.t. 2.68 min) were combined and concentrated to remove acetonitrile only (T < 31°C) and the resulting aqueous solutions were frozen at -80°C. Water was removed by lyophilization to afford 7.0 mg (31%) of **4.1** as a white solid: IR (neat) 3436, 2930, 2098, 1668, 1381, 1256 cm<sup>-1</sup>; <sup>1</sup>H NMR (600 MHz, CD<sub>3</sub>OD)  $\delta$  7.38 (s, 1H), 6.19 (s, 1H), 6.15 (d, *J* = 15.7 Hz, 1H), 5.65 (dd, *J* = 7.9, 8.0 Hz, 1H), 5.29 (d, *J* = 11.4 Hz, 1H), 5.21 (d, *J* = 10.0 Hz, 1H), 5.05 (dd, *J* = 8.9, 15.8 Hz, 1H), 4.98 (d, *J* = 3.8 Hz, 1H), 4.94 (d, *J* = 4.1 Hz, 1H), 4.82 (d, *J* = 1.7 Hz, 1H), 4.56 (dd, *J* = 3.9, 10.1 Hz, 1H), 3.95 (m, 1H), 3.91 (dd, *J* = 9.1, 9.9 Hz, 1H), 3.83 (dd, *J* = 8.9, 8.9 Hz, 1H), 3.78 (dd, *J* = 6.3, 9.5 Hz, 1H), 3.71 (dd, *J* = 4.6, 11.1 Hz, 1H), 3.67 (dd, *J* = 6.2, 9.7 Hz, 1H), 3.60 (s, 3H), 3.53 (d, *J* = 1.3 Hz, 1H), 3.45 (m, 1H), 3.43 (s, 3H), 3.41 (m, 1H), 3.37 (s, 3H), 3.34 (m, 1H), 3.33 (m, 5H), 3.27 (s, 3H), 3.21 (dd, *J* = 6.2, 9.2 Hz, 1H), 3.17 (m, 1H), 2.97 (dd, *J* = 8.9, 9.0 Hz, 1H), 2.82 (dd, *J* = 9.2, 9.2 Hz, 1H), 2.72 (dd, *J* = 4.6, 9.8 Hz, 1H), 2.67 (m, 1H), 2.40-2.48 (m, 4H), 2.19 (s, 3H), 2.16

(m, 1H), 2.11 (s, 3H), 2.08 (m, 1H), 2.05 (m, 1H), 1.95 (s, 3H), 1.92 (d,  $J = 12.7$  Hz, 1H), 1.80 (dd,  $J = 4.4, 13.5$  Hz, 1H), 1.74 (m, 1H), 1.73 (m, 1H), 1.69 (m, 2H), 1.66 (s, 3H), 1.65 (m, 2H), 1.57 (m, 1H), 1.48 (m, 2H), 1.32 (s, 3H), 1.30 (m, 2H), 1.29 (m, 1H), 1.25-1.30 (m, 12H), 1.22 (d,  $J = 6.2$  Hz, 3H), 1.13 (d,  $J = 6.6$  Hz, 3H), 1.02 (d,  $J = 6.7$  Hz, 3H), 0.89 (d,  $J = 6.9$  Hz, 3H);  $^{13}\text{C}$  NMR (150 MHz,  $\text{CD}_3\text{OD}$ )  $\delta$ : 174.5, 172.7, 149.3, 146.9, 142.7, 141.3, 134.6, 133.9, 133.7, 133.1, 125.5, 123.8, 101.9, 101.3, 99.5, 93.6, 87.4, 87.4, 85.9, 84.4, 83.9, 82.0, 77.1, 76.9, 76.8, 75.4, 75.1, 74.6, 73.9, 73.2, 73.0, 72.5, 72.3, 69.4, 68.2, 67.4, 61.3, 61.3, 59.5, 57.3, 52.2, 45.5, 40.6, 39.1, 38.4, 37.2, 36.4, 34.4, 33.1, 30.8, 29.4, 24.7, 23.3, 22.8, 18.9, 18.3, 18.2, 18.1, 17.9, 16.5, 14.2, 12.2, 12.1, 5.2; HRMS (ESI-TOF MS)  $m/z$  1276.6925 ( $\text{M}+\text{Na}$ ) $^+$  calculated for  $\text{C}_{63}\text{H}_{103}\text{N}_3\text{NaO}_{22}$ , measured 1276.6940.

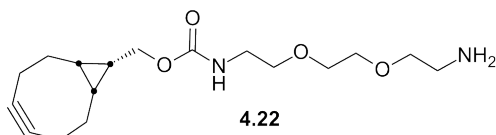


**Azido Apoptolidin H 4.2** To a solution of azido pentanoic acid (10 mg, 0.071 mmol) in dichloromethane (5.0 mL) at  $0^\circ\text{C}$  was added PyBrop (33 mg, 0.071 mmol) and diisopropylethyl amine (41  $\mu\text{L}$ , 0.238 mmol) the resulting

solution was stirred at  $0^\circ\text{C}$  for 10 min. Apoptolidin H **2.11** (20 mg, 0.024 mmol) was added to the resulting solution followed by one small crystal of DMAP. The resulting solution was warmed to rt and maintained at that temperature for 16 h. Methanol (100  $\mu\text{L}$ ) was added to the reaction mixture and then concentrated. The resulting residue was

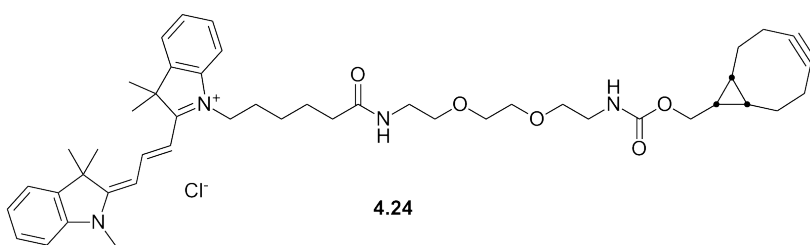
diluted in EtOAc (20 mL) and washed with 1 N HCl (5 mL). The aqueous layer was extracted with EtOAc (2 x 10 mL). The combined organic extracts were washed with NaHCO<sub>3</sub> (1x 5mL) and brine (1 x 5 mL) and dried (Na<sub>2</sub>SO<sub>4</sub>) and concentrated in vacuo. The resulting residue was dissolved in 1.2 mL of DMSO, filtered through a 0.2 μm polytetrafluoroethylene PTFE syringe tip filter and purified by preparative reversed phase HPLC with a 4 minute gradient from 35% to 75% MeCN in H<sub>2</sub>O (r.t. of desired product 3.23 min) in four 300 μL injections. Fractions containing desired product were combined and concentrated to remove acetonitrile only (T < 31°C) and the resulting aqueous solution was frozen at -80°C. Water was removed by lyophilization to afford 5.5 mg (24%) of **4.2** as a white solid.: IR (neat) 3425, 2928, 2098, 1669, 1385, 1257 cm<sup>-1</sup>; <sup>1</sup>H NMR (600 MHz, CDCl<sub>3</sub>) δ 7.28 (s, 1H), 6.15 (s, 1H), 6.11 (d, *J* = 15.7 Hz, 1H), 5.61 (dd, *J* = 6.3, 9.8 Hz, 1H), 5.25 (d, *J* = 5.25 Hz, 1H), 5.16 (d, *J* = 10.0 Hz, 1H), 5.00 (d, *J* = 3.5 Hz, 1H), 4.99 (dd, *J* = 9.6, 15.2 Hz, 1H), 4.71 (dd, *J* = 3.8, 10.2 Hz, 1H), 4.19 (d, *J* = 8.5 Hz, 1H), 4.00 (dd, *J* = 9.5, 9.5 Hz, 1H), 3.86 (dd, *J* = 4.7, 10.7 Hz, 1H), 3.79 (m, 1H), 3.77 (m, 1H), 3.61 (s, 3H), 3.56 (m, 1H), 3.51 (m, 1H), 3.47 (m, 1H), 3.37 (s, 3H), 3.31 (s, 3H), 3.30 (m, 2H), 3.22 (dd, *J* = 3.3, 9.3 Hz, 1H), 3.11 (dd, *J* = 7.7, 9.1 Hz, 1H), 2.86 (dd, *J* = 9.3, 9.3 Hz, 1H), 2.74 (dd, *J* = 5.8, 9.6 Hz, 1H), 2.62 (m, 1H), 2.41 (m, 2H), 2.15 (s, 3H), 2.10 (s, 3H), 2.01 (m, 1H) 1.90 (s, 3H), 1.82 (m, 1H), 1.72 (m, 2H), 1.64 (m, 3H), 1.63 (s, 3H), 1.43 (m, 2H), 1.32 (d, *J* = 6.24 Hz, 3H), 1.25 (m, 2H) 1.12 (d, *J* = 6.4 Hz, 3H), 1.05 (d, *J* = 6.4 Hz, 3H), 0.86 (d, *J* = 6.9 Hz, 3H); <sup>13</sup>C NMR (150 MHz, CDCl<sub>3</sub>) δ;172.8, 171.7, 148.1, 146.6, 141.6, 140.1, 133.3, 133.2, 132.3, 132.2, 124.7, 122.7, 99.9, 92.8, 86.2, 83.9, 82.4, 73.6, 71.4, 67.5, 67.1, 61.2, 61.0, 59.2, 51.2, 38.9, 37.9, 37.0, 36.4, 35.9, 34.7, 33.7, 33.6, 32.1, 29.8, 29.7, 29.5, 28.3, 24.6, 22.8, 22.3, 18.2, 18.0, 17.4, 16.3,

14.3, 13.7, 12.1, 5.0; HRMS (ESI-TOF MS)  $m/z$  988.5353 ( $M+Na$ )<sup>+</sup> calculated for  $C_{49}H_{79}N_3NaO_{16}$ , measured 988.5381.



**Bicyclononyne Amine 4.22** Carbonate **4.20** (36 mg, 0.114 mmol) was dissolved in DMF (1.0

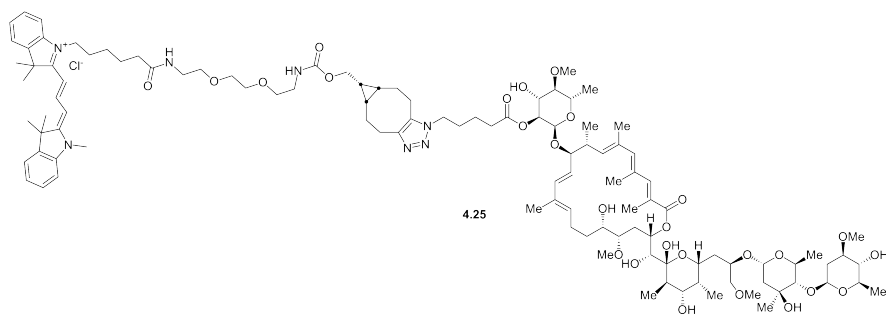
mL). Triethylamine (48  $\mu$ L, 0.685 mmol) was added to the resulting solution. Diamine **4.21** was added at once resulting in an immediate color change of the solution to bright yellow. After 45 minutes, the DMF was removed on high vacuum overnight. The resulting yellow residue was dissolved in 30 mL DCM and washed with 1 N NaOH (2 x 5 mL) and H<sub>2</sub>O (1 x 5 mL). The combined aqueous layers were back extracted with DCM (1 x 10 mL). Combined organics were washed again with H<sub>2</sub>O (1 x 5 mL), dried (Na<sub>2</sub>SO<sub>4</sub>) and concentrated to yield a colorless oil. Flash column chromatography (30 % 80:18:2<sup>20</sup> in DMC) yielded 34.6 mg (94%) of amine **4.22** as a colorless oil. Spectral data for this compound was identical to that reported in the literature.<sup>13</sup>



**Bicyclononyne Cy3 Conjugate 4.24** To a solution of amine **4.22** (24.0 mg, 0.074 mmol)

in DMF (1.0 mL) was added Cy3 NHS **2.23** as a solution in DMF (0.5 mL). After six hours, the DMF was removed on high vacuum overnight. The resulting purple residue was dissolved in methanol (1.0 mL) and purified on semipreparative reverse phase HPLC (30 minute gradient from 35% strong to 100% strong buffer in weak buffer where strong is 95% MeCN in H<sub>2</sub>O + 10 mM NH<sub>4</sub>OAc and weak buffer is 5% MeCN in H<sub>2</sub>O + 10 mM NH<sub>4</sub>OAc). The conical reaction flask was rinsed with an additional 0.5 mL of methanol

and this solution was purified as well. Fractions containing the desired product (r.t. 22.50 min) were combined and concentrated to remove acetonitrile only ( $T < 31^{\circ}\text{C}$ ). The resulting aqueous solution was frozen at  $-80^{\circ}\text{C}$ . Water was removed by lyophilization to yield 4.29 mg (63%) of bicyclononyne Cy3 conjugate **4.24** as a deep red solid.  $^1\text{H}$  NMR (600 MHz,  $\text{CD}_3\text{OD}$ )  $\delta$  8.55 (t,  $J = 13.5$ , 1H) 7.55 (d,  $J = 7.5$ , 2H), 7.45 (m, 2H), 7.36 (dd,  $J = 4.1$ , 8.0, 2H), 7.32 (m, 2H), 6.45 (dd,  $J = 8.4$ , 13.5 Hz, 2H), 4.15 (dd,  $J = 7.5$ , 7.5 Hz, 2H), 4.11 (d,  $J = 8.1$  Hz, 2H), 3.69 (s, 3H), 3.59 (s, 4H), 3.52 (t,  $J = 5.6$  Hz, 4H), 3.34 (t,  $J = 5.6$  Hz, 2H), 3.26 (t,  $J = 3.3$  Hz, 2H), 2.23 (t,  $J = 7.3$  Hz, 2H), 2.1-2.25 (m, 4H), 1.85 (m, 2H), 1.77 (s, 12 H), 1.71 (m, 2H) 1.58 (m, 2H), 1.51 (m, 2H), 1.33 (m, 1H), 1.29 (s, 4H) 0.91 (m, 2H);  $^{13}\text{C}$  NMR (150 MHz,  $\text{CD}_3\text{OD}$ )  $\delta$  179.2, 176.7, 176.0, 175.9, 159.2, 152.1, 144.1, 143.4, 142.2, 142.1, 130.0, 129.9, 126.8, 126.8, 123.5, 123.4, 112.5, 112.3, 103.8, 103.6, 99.5, 71.3, 71.3, 71.0, 70.6, 63.7, 50.7, 50.6, 45.1, 41.6, 40.3, 36.6, 31.8, 30.1, 28.3, 28.2, 28.1, 27.3, 26.5, 23.4, 21.9, 21.4, 18.9; HRMS (ESI-TOF MS)  $m/z$  763.4798 (M-Cl) $^+$  calculated for  $\text{C}_{47}\text{H}_{63}\text{N}_4\text{O}_5$ , measured 763.4794.



**Cy3 Apoptolidin**

**A Conjugate 4.25**

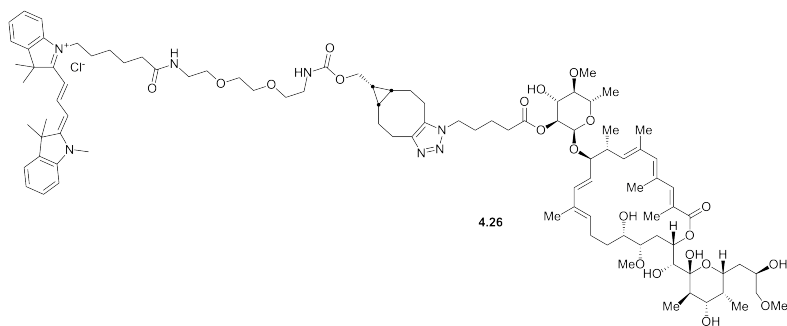
To a solution of

**Cy3** **BCN**

conjugate **4.24**

(2.6 mg, 0.0033 mmol) in methanol (0.5 mL) was added azido apoptolidin A **4.1** (2.05 mg, 0.0016 mmol) as a solution in 0.5 mL methanol. The resulting solution was stirred at  $37^{\circ}\text{C}$  for 4 hours, removed from the bath and concentrated. The resulting residue was

dissolved in methanol (0.5 mL) and purified on semipreparative reverse phase HPLC (30 minute gradient from 35% strong to 100% strong buffer in weak buffer where strong is 95% MeCN in H<sub>2</sub>O + 10 mM NH<sub>4</sub>OAc and weak buffer is 5% MeCN in H<sub>2</sub>O + 10 mM NH<sub>4</sub>OAc). The conical reaction flask was rinsed with an additional 0.5 mL of methanol and this solution was purified as well. Fractions containing the desired product (r.t. 28.10 min) were combined and concentrated to remove acetonitrile only (T<31°C). The resulting aqueous solution was frozen at -80°C. Water was removed by lyophilization to yield 1.29 mg (39%) of Cy3 apoptolidin A conjugate **4.25** as a deep red solid. (600 MHz, CD<sub>3</sub>OD)  $\delta$  8.55 (t,  $J$  = 13.5, 1H) 7.55 (d,  $J$  = 7.5, 2H), 7.45 (m, 2H), 7.36 (dd,  $J$  = 3.6, 8.0, 2H), 7.32 (m, 3H), 6.44 (dd,  $J$  = 8.7, 13.4 Hz, 2H), 6.17 (s, 1H), 6.12 (d,  $J$  = 15.7 Hz, 1H), 5.62 (m, 1H), 5.4 (m, 1H), 5.34 (m, 1H), 5.29 (d,  $J$  = 11.3 Hz, 1H), 5.19 (d,  $J$  = 10.0 Hz, 1H), 5.00 (m, 1H), 4.9 (m, 2H), 4.82 (m, 1H), 4.54 (m, 1H), 4.30 (dd,  $J$  = 7.1, 7.1 Hz, 2H), 4.15 (dd,  $J$  = 7.5, 7.5 Hz, 2H), 4.11 (m, 2H), 3.95 (m, 2H), 3.89 (m, 1H), 3.80 (m, 2H), 3.69 (s, 3H), 3.65 (m, 2H), 3.60 (s(br), 4H), 3.58 (m, 3H), 2.52 (dd,  $J$  = 5.5, 5.5 Hz, 4H), 3.42 (s, 3H), 3.41 (m, 2H), 3.35 (m, 4H), 3.26 (m, 2H), 3.14-3.21 (m, 3H), 2.97 (dd,  $J$  = 9.0, 9.0 Hz, 1H), 2.67-2.88 (m, 5H), 2.63 (m, 1H), 2.29-2.49 (m, 7H), 2.23 (t,  $J$  = 7.3 Hz, 2H), 2.11-2.27 (m, 8H), 2.00-2.11 (m, 8H), 1.9-1.98 (m, 5H), 1.85 (m, 6H), 1.77 (s, 12H), 1.71 (m, 2H), 1.54-1.67 (m, 6H) 1.51 (m, 4H), 1.19-1.36 (m, 13 H), 1.11 (d,  $J$  = 6.6 Hz, 3H), 1.02 (d,  $J$  = 6.7 Hz, 3H), 0.97-1.07 (m, 2H), 0.90 (d,  $J$  = 7.2 Hz 3H), 0.83-0.93 (m, 1H). HRMS (ESI-TOF MS)  $m/z$  2017.1832 (M-Cl)<sup>+</sup> calculated for C<sub>110</sub>H<sub>166</sub>N<sub>7</sub>O<sub>27</sub>, measured 2017.1821.

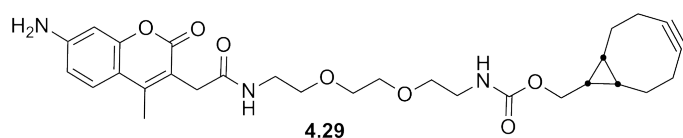


### Cy3 Apoptolidin H

**Conjugate 4.26** To a solution of Cy3 BCN conjugate **4.24** (2.03 mg, 0.0025 mmol) in methanol

(0.5 mL) was added azido apoptolidin H **4.2** (2.45 mg, 0.0025 mmol) as a solution in 0.5 mL methanol. The resulting solution was stirred at 37 °C for 4 hours, removed from the bath and concentrated. The resulting residue was dissolved in methanol (0.5 mL) and purified on semipreparative reverse phase HPLC (30 minute gradient from 35% strong to 100% strong buffer in weak buffer where strong is 95% MeCN in H<sub>2</sub>O + 10 mM NH<sub>4</sub>OAc and weak buffer is 5% MeCN in H<sub>2</sub>O + 10 mM NH<sub>4</sub>OAc). The conical reaction flask was rinsed with an additional 0.5 mL of methanol and this solution was purified as well. Fractions containing the desired product (r.t. 27.35 min) were combined and concentrated to remove acetonitrile only (T<31°C). The resulting aqueous solution was frozen at -80°C. Water was removed by lyophilization to yield 1.38 mg (32%) of Cy3 apoptolidin H conjugate **4.26** as a deep red solid. (600 MHz, CD<sub>3</sub>OD) δ 8.55 (t, *J* = 13.5, 1H) 7.55 (d, *J* = 7.4, 2H), 7.45 (m, 2H), 7.36 (dd, *J* = 3.5, 8.0, 2H), 7.32 (m, 3H), 6.44 (dd, *J* = 8.6, 13.5 Hz, 2H), 6.17 (s, 1H), 6.12 (d, *J* = 15.7 Hz, 1H), 5.64 (m, 1H), 5.57 (m, 1H), 5.40 (m, 1H), 5.30 (d, *J* = 11.2 Hz, 1H), 5.19 (d, *J* = 10.0 Hz, 1H), 5.00 (ddd, *J* = 8.2, 8.2, 16.0 Hz, 1H), 4.95 (m, 1H), 4.54 (ddd, *J* = 2.0, 3.8, 10.2 Hz, 1H), 4.51 (m, 1H), 4.30 (dd, *J* = 7.2, 7.2 Hz, 2H), 4.15 (dd, *J* = 7.5, 7.5 Hz, 2H) 4.00-4.10 (m, 3H), 3.96 (dd, *J* = 9.5, 9.5 Hz, 1H), 3.98 (m, 1H), 3.81 (dd, *J* = 8.9, 8.9 Hz, 1H), 3.72-3.78 (m, 2H), 3.69 (s, 3H), 3.65 (m, 1H), 3.60 (m, 4H), 3.54 (m, 1H), 3.52 (t, *J* = 5.6 Hz, 4H), 3.42 (m, 2H),

3.25-3.72 (m, 2H), 3.24-3.29 (m, 2H), 3.14-3.22 (m, 3H), 3.02 (m, 2H), 3.69-3.87 (m, 3H), 2.63 (m, 1H), 2.29-2.50 (m, 4H), 2.24 (t,  $J = 7.3$  Hz, 4H), 2.12-2.20 (m, 4H), 1.97-2.08 (m, 4H), 1.89-1.95 (m, 2H), 1.86 (m, 4H), 1.74 (s, 12H), 1.71 (m, 4H), 1.55-1.68 (m, 6H), 1.50 (m, 5H), 1.22-1.35 (m, 10H), 1.11 (d,  $J = 6.6$  Hz, 3H), 1.02 (d,  $J = 6.8$  Hz, 3H), 0.97-1.07 (m, 2H), 0.83-0.93 (m, 4H). HRMS (ESI-TOF MS)  $m/z$  1729.0259 (M-Cl)<sup>+</sup> calculated for C<sub>96</sub>H<sub>142</sub>N<sub>7</sub>O<sub>21</sub>, measured 1729.0250.

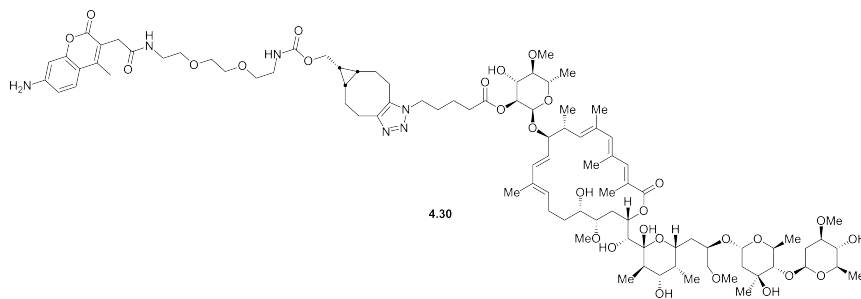


**Bicyclononyne**                      **AMCA**  
**Conjugate 4.29** To a solution of

amine **4.22** (10.0 mg, 0.031 mmol) in DMF (0.25 mL) was added AMCA NHS **2.28** (5.0 mg, 0.015 mmol) as a solution in DMF (0.5 mL). After two hours, the DMF was removed on high vacuum. The resulting residue was dissolved in methanol (0.3 mL) and purified on semipreparative reverse phase HPLC (30 minute gradient from 35% strong to 100% strong buffer in weak buffer where strong buffer was 95% MeCN in H<sub>2</sub>O + 10 mM NH<sub>4</sub>OAc and weak buffer was 5% MeCN in H<sub>2</sub>O + 10 mM NH<sub>4</sub>OAc). The conical reaction flask was rinsed with an additional 0.3 mL of methanol and this solution was purified as well. Fractions containing the desired product (r.t. 10.5 min) were combined and concentrated to remove acetonitrile only (T < 31°C). The resulting aqueous solution was frozen at -80°C. Water was removed by lyophilization to yield 2.83 mg (35%) of bicyclononyne AMCA conjugate **4.29** as a deep white solid. <sup>1</sup>H NMR (600 MHz, CDCl<sub>3</sub>) δ 7.41 (d,  $J = 8.6$  Hz, 1H), 6.76 (s (br), 1H), 6.59 (dd,  $J = 2.2, 8.5$  Hz, 1H), 6.54 (d,  $J = 2.2$  Hz, 1H), 5.46 (s (br), 1H), 4.19 (s (br), 2H), 4.14 (d,  $J = 8.0$  Hz, 2H), 3.5-3.6 (m, 10H), 3.35-3.43 (m, 4H), 2.49 (s, 3H), 2.23 (m, 4H), 1.56 (m, 2H), 1.32 (ddd,  $J = 8.4, 8.4, 17.1$  Hz, 2H), 1.18 (dd,  $J = 7.0, 7.0$  Hz, 1H), 0.89 (m, 2H); <sup>13</sup>C NMR (150 MHz, CDCl<sub>3</sub>) δ



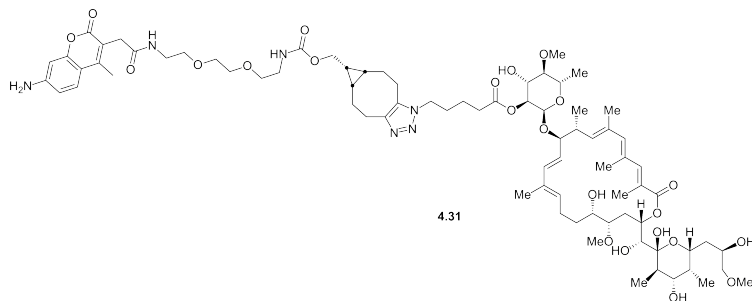
170.3, 163.3, 157.1, 154.3, 150.5, 150.1, 126.4, 112.3, 100.9, 99.0, 70.5, 70.4, 70.3, 69.8, 62.8, 41.0, 39.5, 35.8, 29.8, 29.2, 21.6, 20.2, 17.9, 15.6; HRMS (ESI-TOF MS)  $m/z$  540.2710 (M+H)<sup>+</sup> calculated for C<sub>29</sub>H<sub>38</sub>N<sub>3</sub>O<sub>7</sub>, measured 540.2708.



**AMCA**  
**Apoptolidin A**  
**Conjugate 4.30** To  
a solution of  
**AMCA** **BCN**

conjugate **4.29** (1.05 mg, 0.0029 mmol) in methanol (0.5 mL) was added azido apoptolidin A **4.1** (7.0 mg, 0.0056 mmol) as a solution in 0.5 mL methanol. The resulting solution was stirred at 37 °C for 4 hours, removed from the bath and concentrated. The resulting residue was dissolved in methanol (0.3 mL) and purified on semipreparative reverse phase HPLC (30 minute gradient from 35% strong to 100% strong buffer in weak buffer where strong is 95% MeCN in H<sub>2</sub>O + 10 mM NH<sub>4</sub>OAc and weak buffer is 5% MeCN in H<sub>2</sub>O + 10 mM NH<sub>4</sub>OAc). The conical reaction flask was rinsed with an additional 0.3 mL of methanol and this solution was purified as well. Fractions containing the desired product (r.t. 13.0 min) were combined and concentrated to remove acetonitrile only (T < 31°C). The resulting aqueous solution was frozen at -80°C. Water was removed by lyophilization to yield 3.6 mg (71%) of AMCA apoptolidin A conjugate **4.30** as a white solid. (600 MHz, CD<sub>3</sub>OD) δ 7.50 (d, *J* = 8.7 Hz, 1H), 7.37 (s, 1H), 6.66 (dd, *J* = 2.2, 8.7 Hz, 1H), 6.50 (d, *J* = 2.2 Hz, 1H), 6.16 (s, 1H), 6.12 (d, *J* = 15.7 Hz, 1H), 5.63 (dd, *J* = 7.7, 8.1 Hz, 1H), 5.29 (d, *J* = 11.4 Hz, 1H), 5.19 (d, *J* = 10.0 Hz, 1H), 5.00 (ddd, *J* = 6.7, 8.9, 15.7 Hz, 1H), 4.95 (m, 2H), 4.82 (d, *J* = 1.7 Hz, 1H), 4.58 (s (br), 2H),

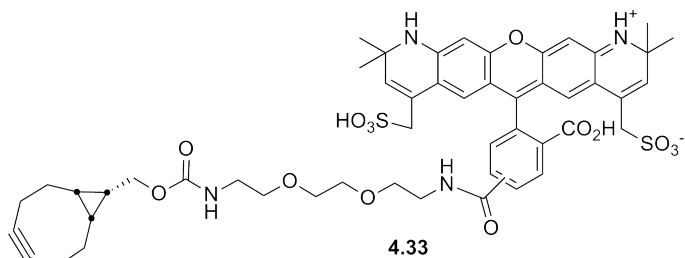
4.55 (ddd,  $J = 1.3, 3.8, 10.2$  Hz, 2H), 4.29 (dd,  $J = 7.0, 7.0$ , 2H), 4.13 (m, 3H), 3.95 (m, 1H), 3.89 (m, 1H), 3.80 (dd,  $J = 8.9, 8.9$  Hz, 1H), 3.78 (dd,  $J = 6.2, 9.5$  Hz, 1H), 3.71 (dd,  $J = 4.7, 11.0$  Hz, 1H), 3.67 (dd,  $J = 6.3, 9.8$  Hz, 1H), 3.66 (m, 1H), 3.61 (s, 4H), 3.59 (s, 2H), 3.58 (s, 2H), 3.51-3.56 (m, 5H), 3.42 (s, 3H), 3.38 (dd,  $J = 5.5, 5.5$  Hz, 1H), 3.36 (s, 2H), 3.34 (m, 2H), 3.29 (m, 2H), 2.36 (m, 2H), 3.21 (dd,  $J = 6.2, 9.3$  Hz, 1H), 3.17 (m, 1H), 2.97 (dd,  $J = 9.0, 9.0$  Hz, 1H), 2.82 (m, 1H), 2.81 (dd,  $J = 9.2, 9.2$  Hz, 1H), 2.74 (m, 1H), 2.71 (dd,  $J = 4.8, 9.9$  Hz, 1H), 2.63 (m, 1H), 2.39 (s, 3H), 2.34-2.50 (m, 4H), 2.22 (m, 2H), 2.17 (s, 2H), 2.14 (m, 1H), 2.09 (s, 2H), 2.06 (m, 3H), 1.93 (s, 1H), 1.91 (s (br), 5H), 1.86 (m, 3H), 1.80 (m, 2H), 1.74 (m, 2H), 1.53-1.78 (m, 8H), 1.44-1.52 (m, 2H), 1.36-1.44 (m, 2H), 1.31 (d,  $J = 6.1$  Hz, 3H), 1.22 (d,  $J = 6.1$  Hz, 3H), 1.20-1.36 (m, 9H), 1.17 (dd,  $J = 7.0, 7.0$  Hz, 1H), 1.11 (d,  $J = 6.6$  Hz, 3H), 1.02 (d,  $J = 6.6$  Hz, 3H), 0.89 (d,  $J = 6.9$  Hz, 1H) 0.81-0.94 (m, 2H). HRMS (ESI-TOF MS)  $m/z$  1793.9743 (M+H)<sup>+</sup> calculated for C<sub>92</sub>H<sub>141</sub>N<sub>6</sub>O<sub>29</sub>, measured 1793.9747.



**AMCA Apoptolidin H Conjugate 4.31** To a solution of AMCA BCN conjugate **4.29** (4.4 mg, 0.0082 mmol) in methanol

(0.5 mL) was added azido apoptolidin H **4.2** (5.5 mg, 0.0057 mmol) as a solution in 0.5 mL methanol. The resulting solution was stirred at 37 °C for 4 hours, removed from the bath and concentrated. The resulting residue was dissolved in methanol (0.5 mL) and purified on semipreperative reverse phase HPLC (30 minute gradient from 35% strong to 100% strong buffer in weak buffer where strong is 95% MeCN in H<sub>2</sub>O + 10 mM

NH<sub>4</sub>OAc and weak buffer is 5% MeCN in H<sub>2</sub>O + 10 mM NH<sub>4</sub>OAc). The conical reaction flask was rinsed with an additional 0.5 mL of methanol and this solution was purified as well. Fractions containing the desired product (r.t. 11.35 min) were combined and concentrated to remove acetonitrile only (T < 31°C). The resulting aqueous solution was frozen at -80°C. Water was removed by lyophilization to yield 2.0 mg (24%) of AMCA apoptolidin H conjugate **4.31** as a white solid. (600 MHz, CD<sub>3</sub>OD) δ 7.50 (d, *J* = 8.7 Hz, 1H), 7.35 (s, 1H), 6.66 (dd, *J* = 2.2, 8.7 Hz, 1H), 6.50 (d, *J* = 2.1 Hz, 1H), 6.16 (s, 1H), 6.12 (d, *J* = 15.7 Hz, 1H), 5.64 (dd, *J* = 7.8, 7.8 Hz, 1H), 5.30 (d, *J* = 11.3 Hz, 1H), 5.18 (d, *J* = 10.0 Hz, 1H), 5.00 (ddd, *J* = 8.0, 8.0, 15.8 Hz, 1H), 4.95 (m, 1H), 4.58 (s (br), 2H), 4.55 (ddd, *J* = 1.6, 3.8, 10.1 Hz, 2H), 4.29 (dd, *J* = 7.0, 7.0, 2H), 4.13 (m, 3H), 4.09 (m, 1H), 3.89 (dd, *J* = 8.9, 10.0 Hz, 1H), 3.80 (dd, *J* = 9.0, 9.0 Hz, 1H), 3.77 (m, 1H), 3.75 (dd, *J* = 4.8, 11.1 Hz, 1H), 3.65 (m, 1H), 3.61 (s, 4H), 3.59 (s, 2H), 3.58 (s, 2H), 3.51-3.56 (m, 5H), 3.38 (dd, *J* = 5.4, 5.4 Hz, 1H), 3.36 (s, 2H), 3.34 (m, 2H), 3.29 (m, 2H), 3.21 (dd, *J* = 4.7, 9.4 Hz, 1H), 3.16 (dd, *J* = 6.3, 9.4 Hz, 1H), 2.95-3.08 (m, 4H), 2.81 (dd, *J* = 8.2, 8.2 Hz, 1H), 2.74 (m, 1H), 2.72 (dd, *J* = 4.3, 9.9 Hz, 1H), 2.63 (m, 2H), 2.39 (s, 3H), 2.34-2.50 (m, 3H), 2.22 (m, 2H), 2.18 (s, 2H), 2.14 (m, 1H), 2.10 (s, 2H), 2.03 (m, 3H), 1.93 (s, 1H), 1.91 (s, 2H), 1.86 (m, 3H), 1.76 (m, 2H), 1.53-1.78 (m, 8H), 1.44-1.52 (m, 2H), 1.36-1.44 (m, 2H), 1.27 (d, *J* = 6.3 Hz, 3H), 1.20-1.36 (m, 9H), 1.16 (dd, *J* = 7.0, 7.0 Hz, 1H), 1.11 (d, *J* = 6.6 Hz, 3H), 1.02 (d, *J* = 6.4 Hz, 3H), 0.88 (d, *J* = 7.0 Hz, 1H), 0.81-0.94 (m, 2H). HRMS (ESI-TOF MS) *m/z* (M-H)<sup>+</sup> 1505.8170 calculated for C<sub>78</sub>H<sub>117</sub>N<sub>6</sub>O<sub>23</sub>, measured 1505.8182.



### Bicyclononyne Alexafluor 568

**Conjugate 4.33** To a solution of amine **4.22** (6.0 mg, 0.0189 mmol) in DMF (0.25 mL) was

added Alexafluor 568 NHS **2.32** (5.0 mg, 0.0063 mmol). After five hours, the DMF was removed on high vacuum. The resulting residue was dissolved in methanol (0.3 mL) and purified on semipreparative reverse phase HPLC (30 minute gradient from 0% strong to 50% strong buffer in weak buffer where strong buffer was 95% MeCN in H<sub>2</sub>O + 10 mM NH<sub>4</sub>OAc and weak buffer was 5% MeCN in H<sub>2</sub>O + 10 mM NH<sub>4</sub>OAc). The conical reaction flask was rinsed with an additional 0.3 mL of methanol and this solution was purified as well. Fractions containing the desired product (r.t. 21.5 min) were combined and concentrated to remove acetonitrile only (T < 31°C). The resulting aqueous solution was frozen at -80°C. Water was removed by lyophilization to yield bicyclononyne alexafluor 568 conjugate **4.33** as a purple solid.

**Confocal Microscopy Studies:** Low passage (P < 25) H292 human lung carcinoma cells were plated in MaTek dishes at 15% confluence in 2.0 mL of RPMI 1640 medium containing 10% fetal bovine serum and allowed to attach and grow for 40 hours. 200 μM stock solutions of carboxylic acid **4.27**, Cy3 apoptolin A **4.25**, Cy3 apoptolidin H **4.26**, or Cy3 BCN **4.24** in DMSO was prepared. Each dish was treated by the following protocol. Media was removed by aspiration and replaced with 2.0 mL serum free RPMI 1640 media. 2.0 μL of the appropriate DMSO stock solution was added to the dish and cells were returned to the incubator for 15 min. Media containing fluorophores was removed by aspiration followed by a wash with serum free RPMI 1640 media (3 x 2.0

mL) followed by a final addition of 2.0 mL of serum free media. After incubation for 30 min, media was removed and replaced by a freshly sonicated (important for mitotracker solubility) 30 nM solution of Mitotracker Green FM. After an additional incubation of 30 min in the incubator, media was removed by aspiration, (PBS, 2 x 2.0 mL) and replaced with 2.0 mL PBS. Each dish was then imaged at ten random fields by confocal microscopy. Confocal microscopy was performed on a LSM780 (Zeiss) using a c-Apochromat 40x 1.2 W Corr M27 oil immersion objective. Cy3 fluorescence was excited using 488 nm laser (2%) and emission was measured with a 492-542 nm bandpass. Mitotracker Green FM fluorescence was excited with a 488 nm laser (2%) and emission as measured with a bandpass of 552-683 nm. All images were acquired using 512x512, 0.14  $\mu\text{m}$  diameter pixels, a 12.6  $\mu\text{s}$  pixel dwell time, 12-bit gray levels and a 2.4  $\mu\text{m}$  optical section. Each compound was tested in 3 dishes of cells. Pearson's coefficients were calculated using the JACoP plugin<sup>8</sup> for ImageJ<sup>21</sup> 1.46r software for each field from each dishes and are reported as the average of the 30 calculations.

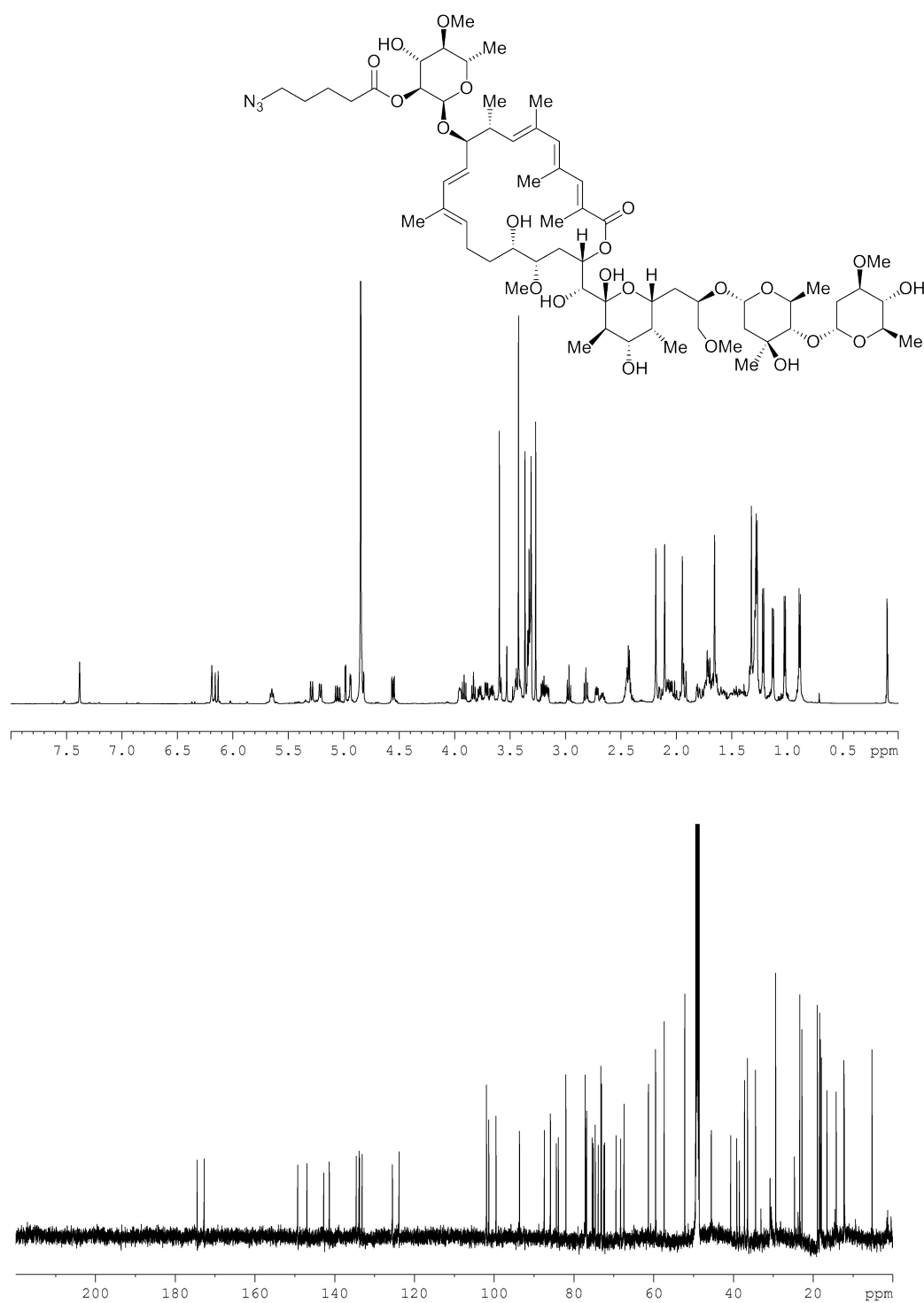
## References

1. Salomon, a R.; Voehringer, D. W.; Herzenberg, L. a; Khosla, C. Apoptolidin, a selective cytotoxic agent, is an inhibitor of F0F1-ATPase. *Chem. Biol.* **2001**, *8*, 71–80.
2. Salomon, a R.; Voehringer, D. W.; Herzenberg, L. a; Khosla, C. Understanding and exploiting the mechanistic basis for selectivity of polyketide inhibitors of F(0)F(1)-ATPase. *Proc. Nat. Acad. Sci. USA* **2000**, *97*, 14766–71.
3. Kolb, H. C.; Finn, M. G.; Sharpless, K. B. Click Chemistry: Diverse Chemical Function from a Few Good Reactions. *Angew. Chem. Int. Ed.* **2001**, *40*, 2004–2021.
4. Wender, P. A.; Jankowski, O. D.; Longcore, K.; Tabet, E. A; Seto, H.; Tomikawa, T. Correlation of F0F1-ATPase inhibition and antiproliferative activity of apoptolidin analogues. *Org. Lett.* **2006**, *8*, 589–92.

5. Lewis, C. A.; Longcore, K. E.; Miller, S. J.; Wender, P. A. An approach to the site-selective diversification of apoptolidin A with peptide-based catalysts. *J. Nat. Prod.* **2009**, *72*, 1864–9.
6. Wender, P. A.; Jankowski, O. D.; Tabet, E. A.; Seto, H. Toward a structure-activity relationship for apoptolidin: selective functionalization of the hydroxyl group array. *Org. Lett.* **2003**, *5*, 487–90.
7. Special thanks to Jashim Uddin M.D. of the Marnett laboratory, Vanderbilt University for both providing Rhox NHS.
8. Bolte, S.; Cordelières, F. P. A guided tour into subcellular colocalization analysis in light microscopy. *J. Microsc.* **2006**, *224*, 213–32.
9. Agard, N. J.; Prescher, J. a; Bertozzi, C. R. A strain-promoted [3 + 2] azide-alkyne cycloaddition for covalent modification of biomolecules in living systems. *J. Am. Chem. Soc.* **2004**, *126*, 15046–7.
10. Joce, C.; Caryl, J.; Stockley, P. G.; Warriner, S.; Nelson, A. Identification of stable S-adenosylmethionine (SAM) analogues derivatised with bioorthogonal tags: effect of ligands on the affinity of the E. coli methionine repressor, MetJ, for its operator DNA. *Org. Biomol. Chem.* **2009**, *7*, 635–8.
11. The cyclooctyne amine was prepared by S.D. as reported in the literature. Special thanks to Jashim Uddin M.D. for preparing and characterizing the conjugate **4.11**. Characterization data is not shown but available from Jashim Uddin of the Marnett Group, Vanderbilt University.
12. Jewett, J. C.; Bertozzi, C. R. Cu-free click cycloaddition reactions in chemical biology. *Chem. Soc. Rev.* **2010**, *39*, 1272.
13. Dommerholt, J.; Schmidt, S.; Temming, R.; Hendriks, L. J. a; Rutjes, F. P. J. T.; van Hest, J. C. M.; Lefeber, D. J.; Friedl, P.; van Delft, F. L. Readily accessible bicyclononynes for bioorthogonal labeling and three-dimensional imaging of living cells. *Angew. Chem. Int. ed. Engl.* **2010**, *49*, 9422–5.
14. Tsien, R.; Ernst, L.; Waggoner, A. Fluorophores for Confocal Microscopy: Photophysics and Photochemistry. In *Handbook of biological confocal microscopy*; 2006; pp. 338–352.
15. Liu, Z.; Bushnell, W. R.; Brambl, R. Potentiometric cyanine dyes are sensitive probes for mitochondria in intact plant cells: kinetin enhances mitochondrial fluorescence. *Plant Physiol.* **1987**, *84*, 1385–90.

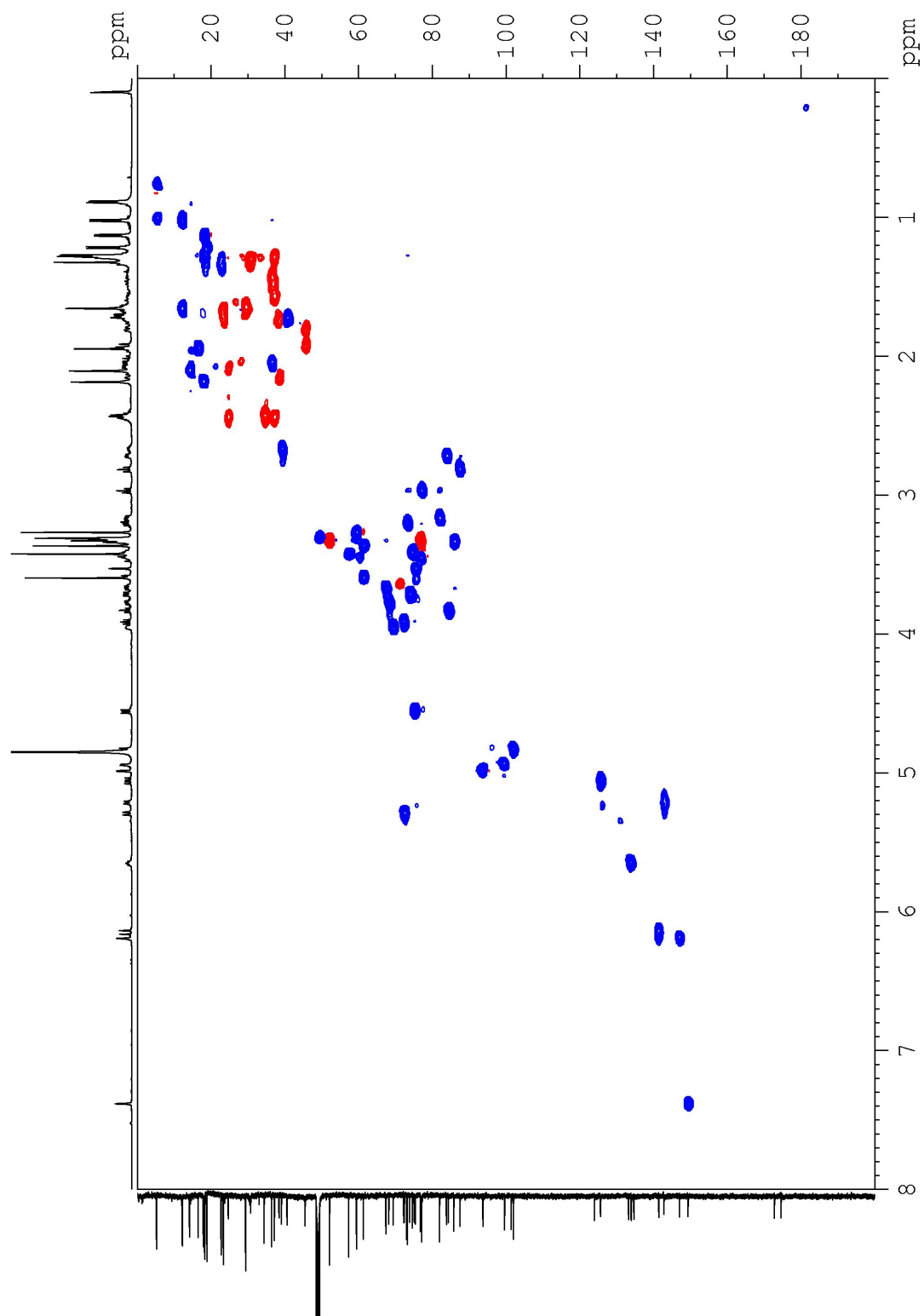
16. Ehrenberg, B.; Montana, V.; Wei, M. D.; Wuskell, J. P.; Loew, L. M. Membrane potential can be determined in individual cells from the nernstian distribution of cationic dyes. *Biophys J.* **1988**, *53*, 785–94.
17. Scaduto, R. C.; Grotyohann, L. W. Measurement of mitochondrial membrane potential using fluorescent rhodamine derivatives. *Biophys. J.* **1999**, *76*, 469–77.
18. Perry, S. W.; Norman, J. P.; Barbieri, J.; Brown, E. B.; Gelbard, H. a Mitochondrial membrane potential probes and the proton gradient: a practical usage guide. *Biotechniques* **2011**, *50*, 98–115.
19. Still, W. C.; Kahn, M.; Mitra, A. Rapid chromatographic technique for preparative separations with moderate resolution. *J. Org. Chem.* **1978**, *43*, 2923–2925.
20. 80:18:2 refers to a premade mixture of 80% DCM, 18% MeOH, and 2% NH<sub>4</sub>OH.
21. Schneider, C. a; Rasband, W. S.; Eliceiri, K. W. NIH Image to ImageJ: 25 years of image analysis. *Nature Methods* **2012**, *9*, 671–675.

## Spectra Relevant to Chapter Four

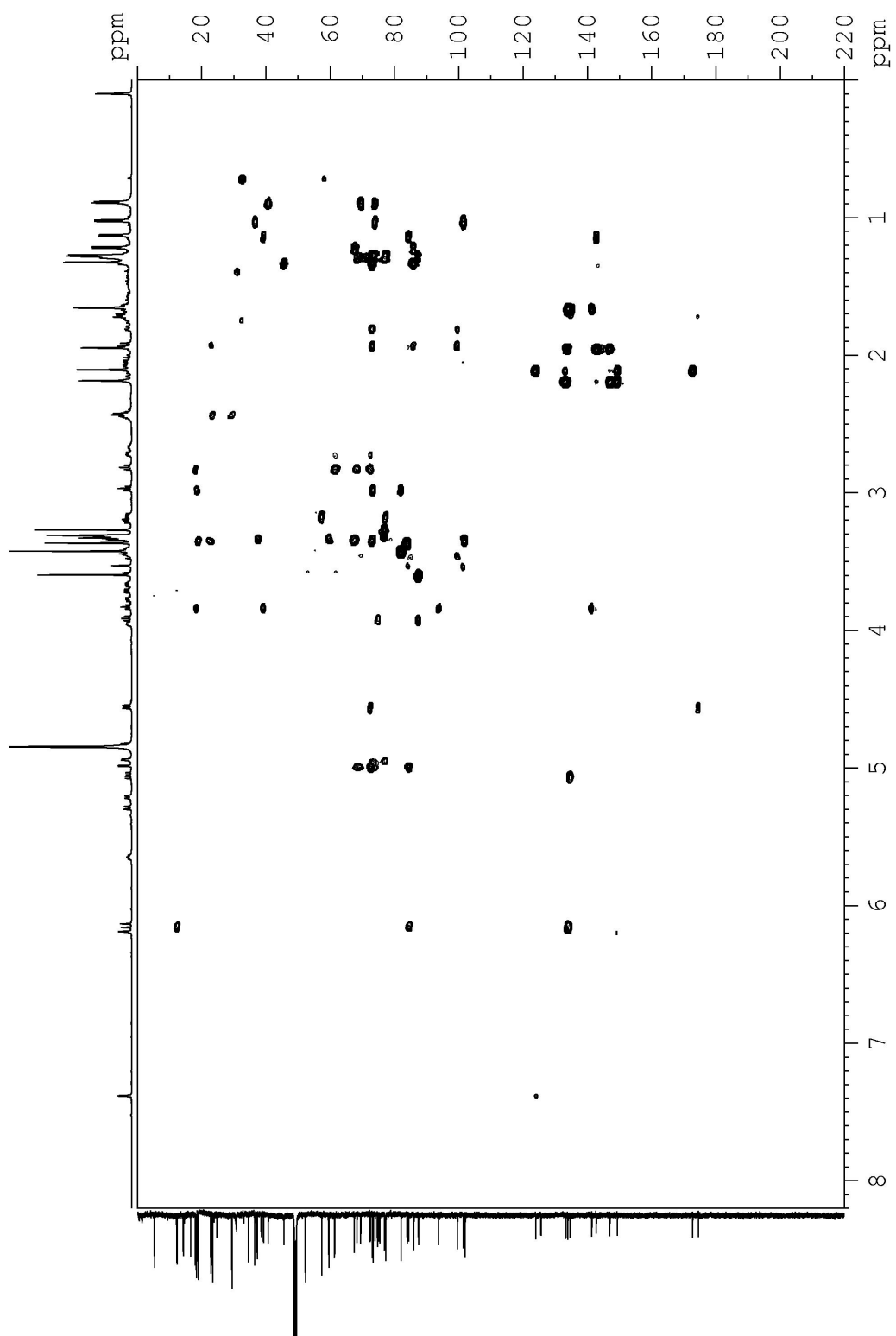


**Spectra IV-1:** The 600 MHz  $^1\text{H}$  and 150 MHz  $^{13}\text{C}$  NMR spectra of **2.1** in  $\text{CD}_3\text{OD}$ .

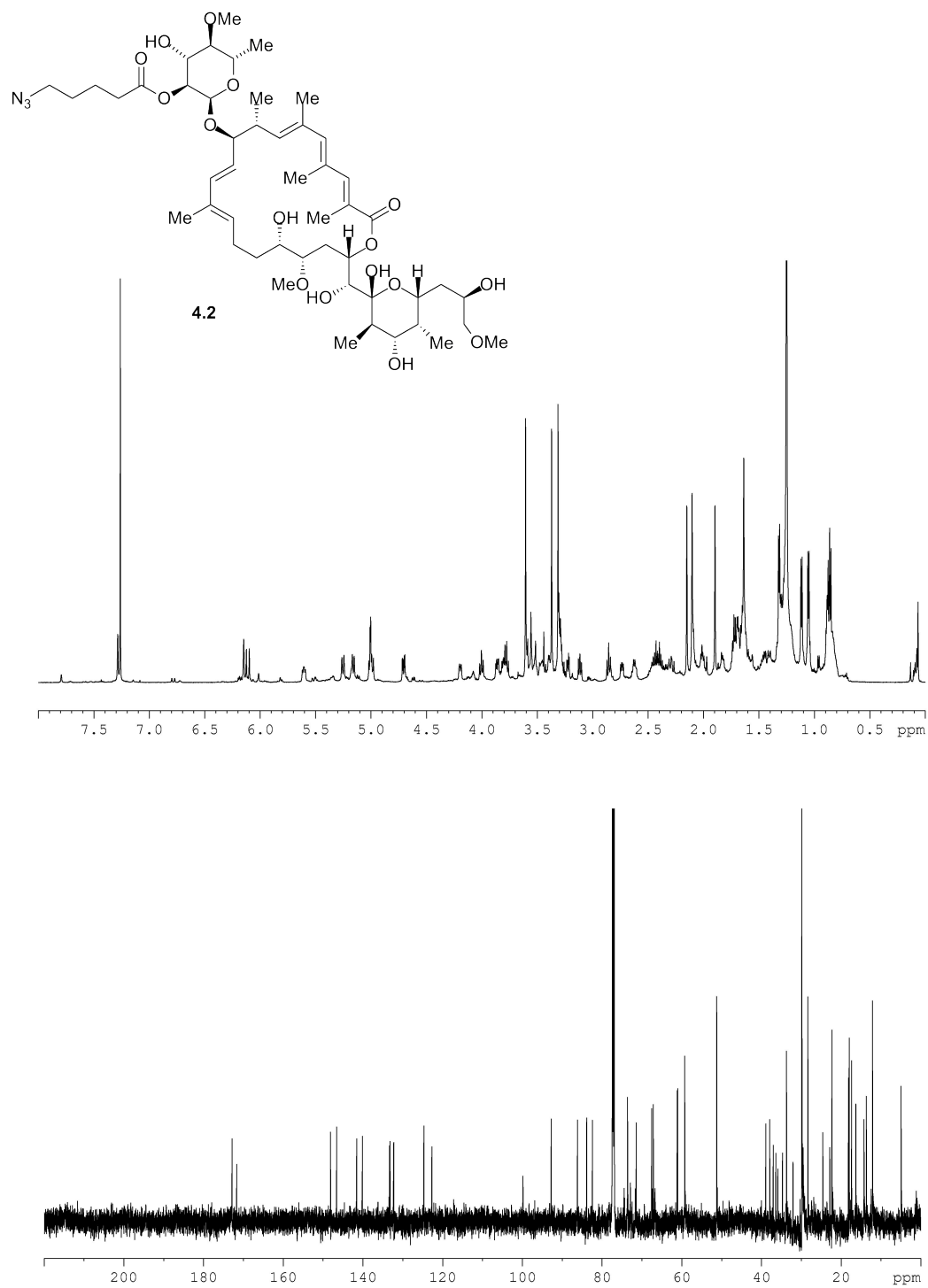




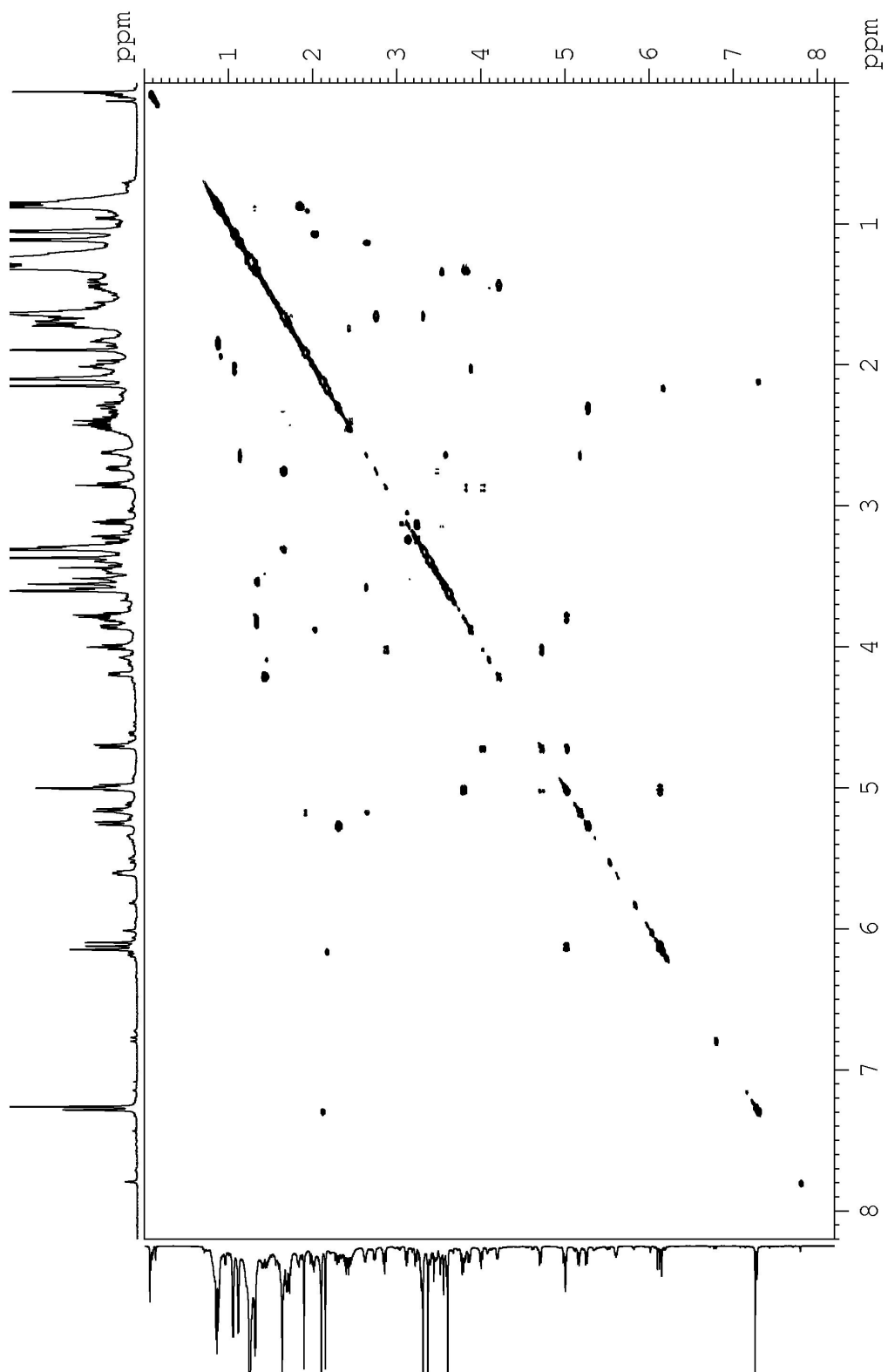
Spectra IV-2: The 500 MHz HSQC NMR spectrum of **4.1** in CD<sub>3</sub>OD.



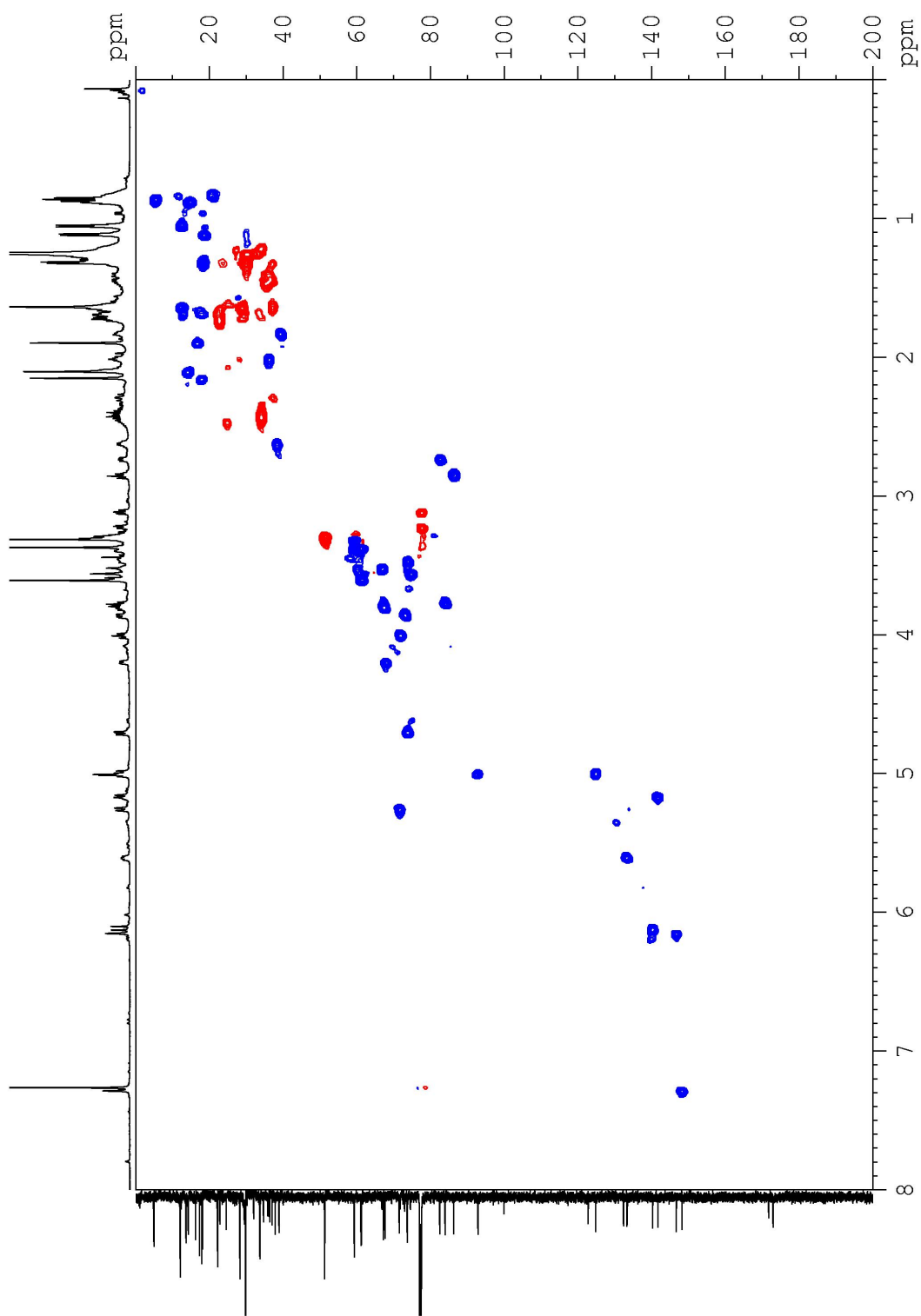
Spectra IV-3: The 500 MHz CIGAR HMBC NMR spectrum of **4.1** in  $\text{CD}_3\text{OD}$ .



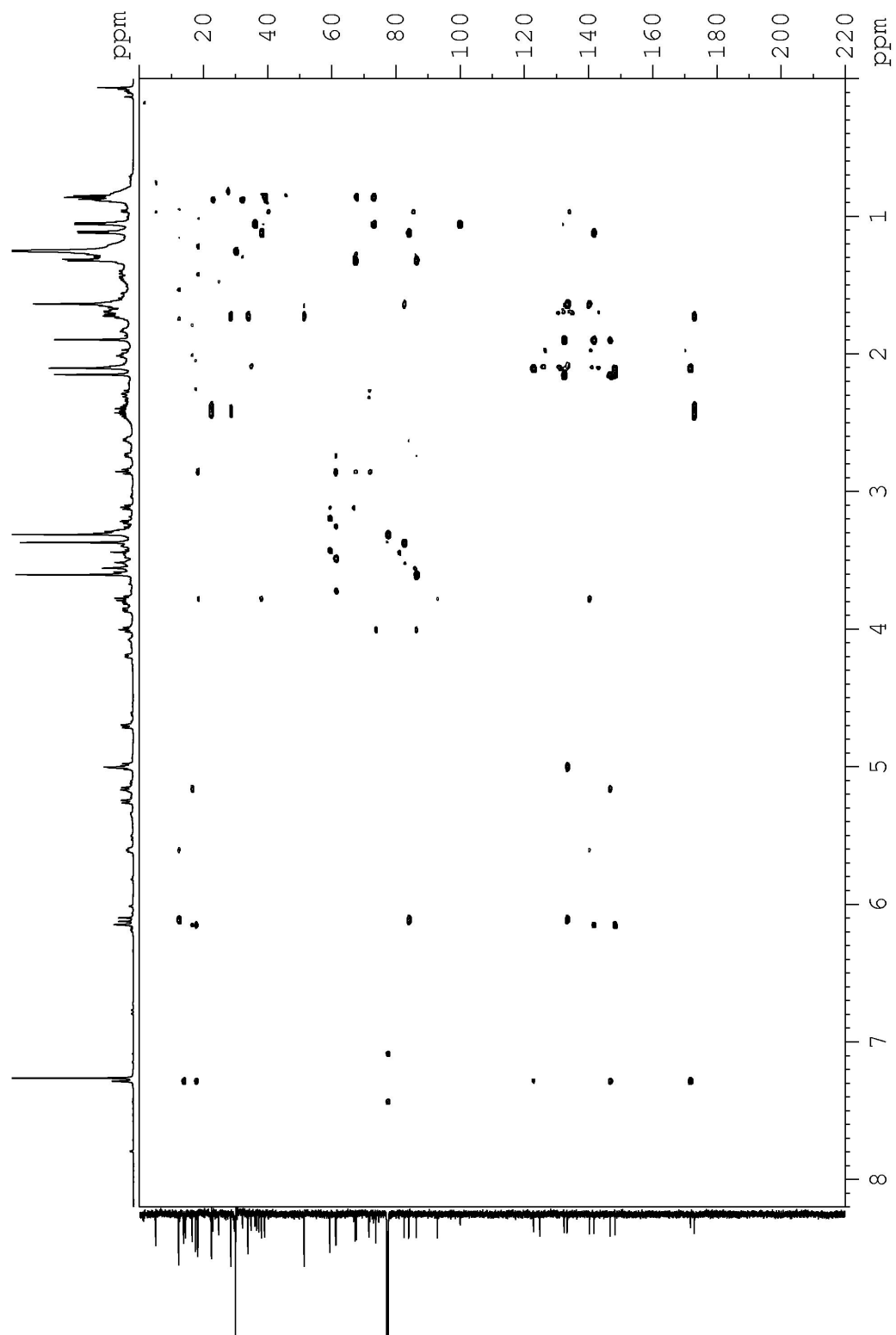
**Spectra IV-4:** The 600 MHz  $^1\text{H}$  and 150 MHz  $^{13}\text{C}$  NMR spectra of **4.2** in  $\text{CDCl}_3$ .



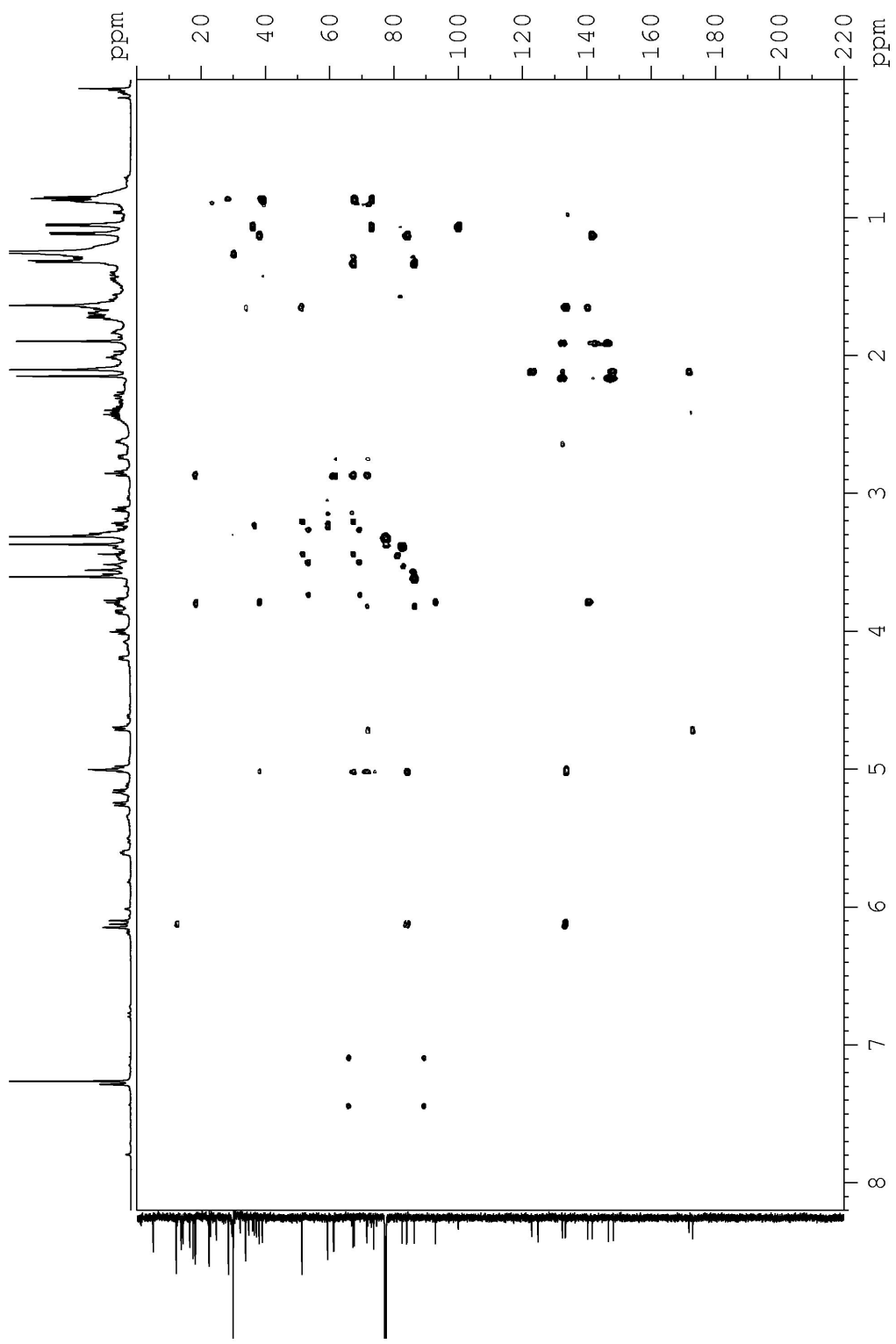
Spectra IV-5: The 600 MHz COSY NMR spectrum of **4.2** in CDCl<sub>3</sub>.



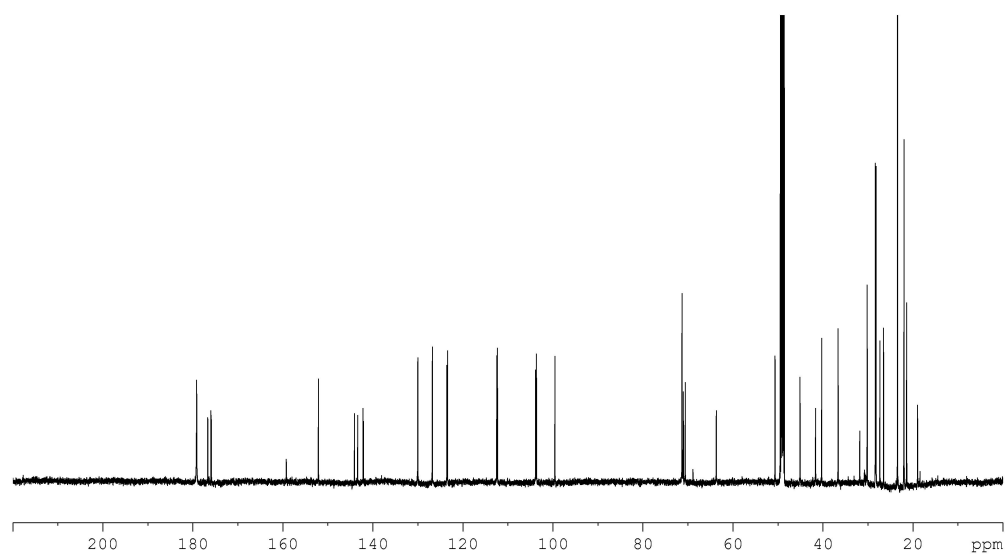
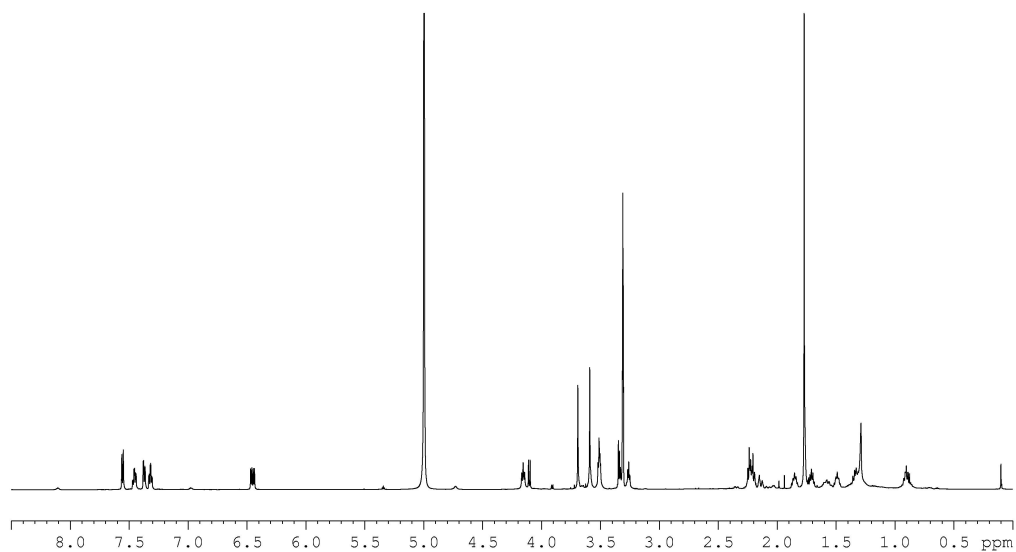
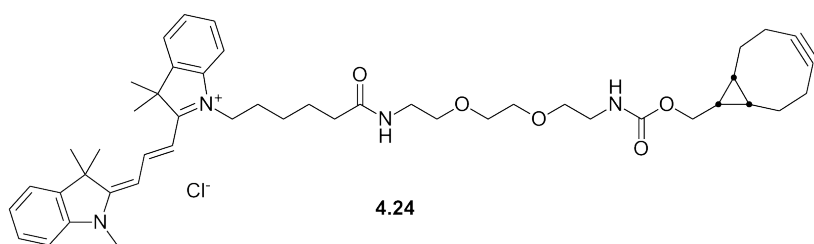
Spectra IV-6: The 600 MHz HSQC NMR spectrum of **4.2** in  $\text{CDCl}_3$ .



Spectra IV-7: The 600 MHz HMBC NMR spectrum of **4.2** in  $\text{CDCl}_3$ .

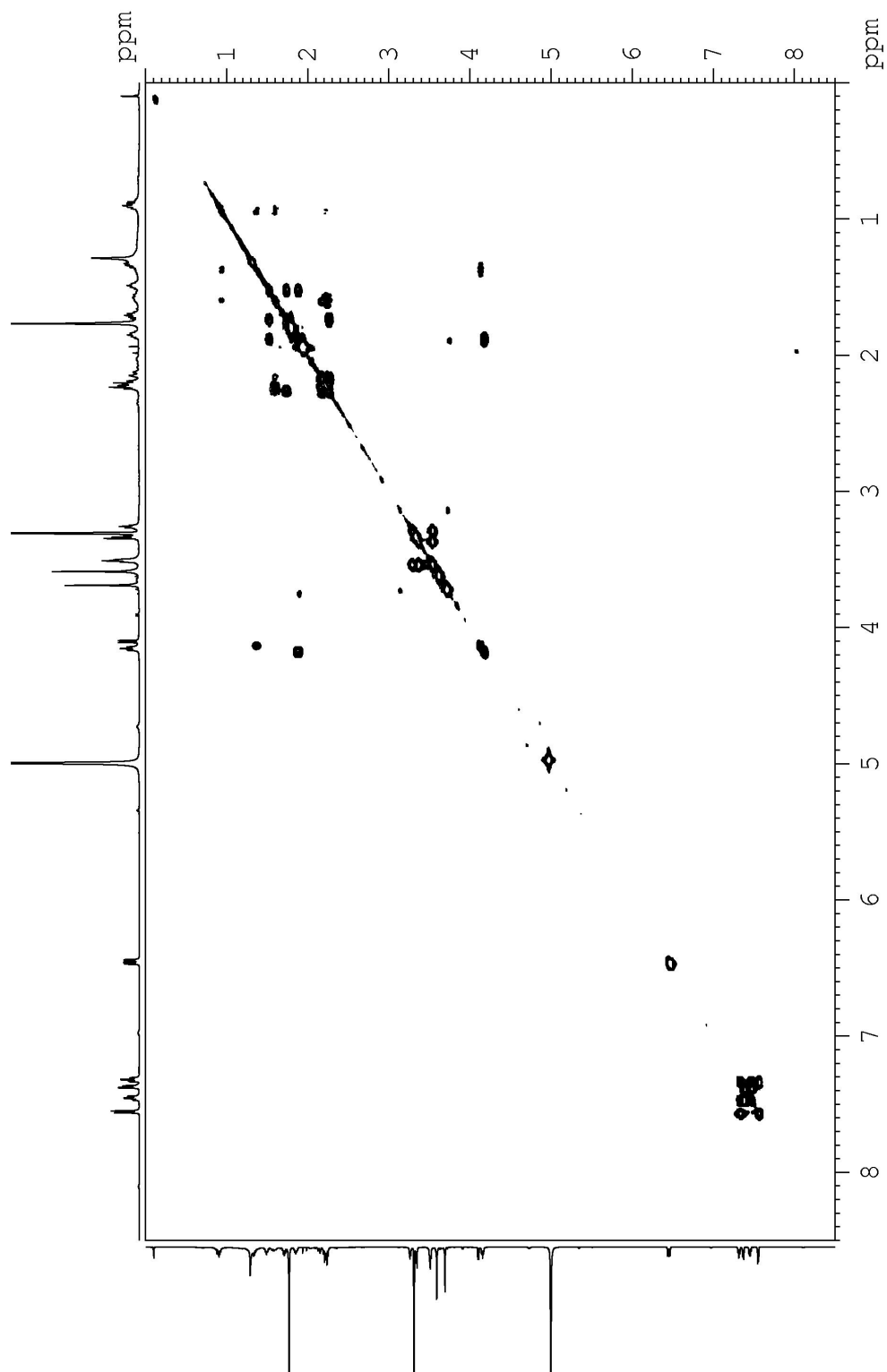


**Spectra IV-8:** The 600 MHz CIGAR HMBC NMR spectrum of **4.2** in  $\text{CDCl}_3$ .

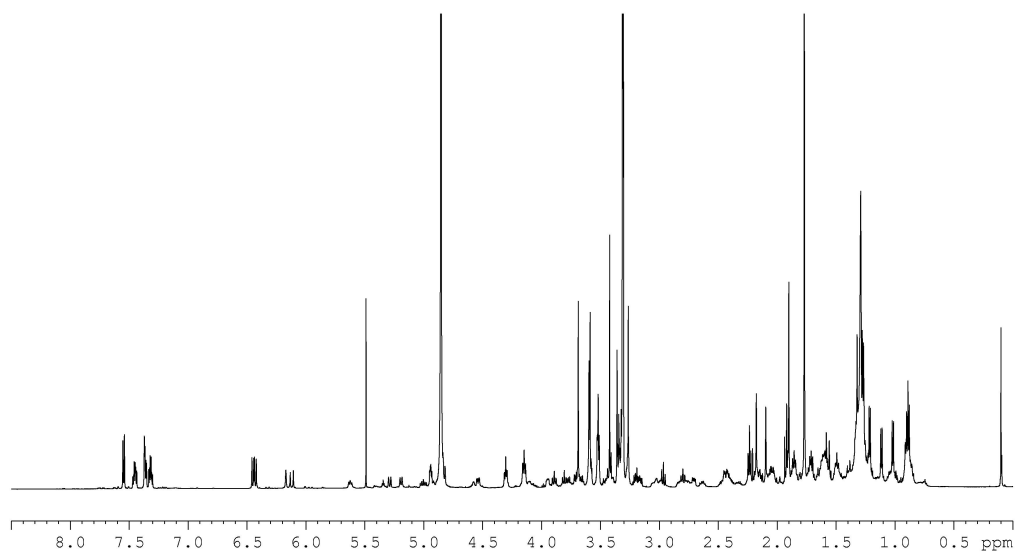
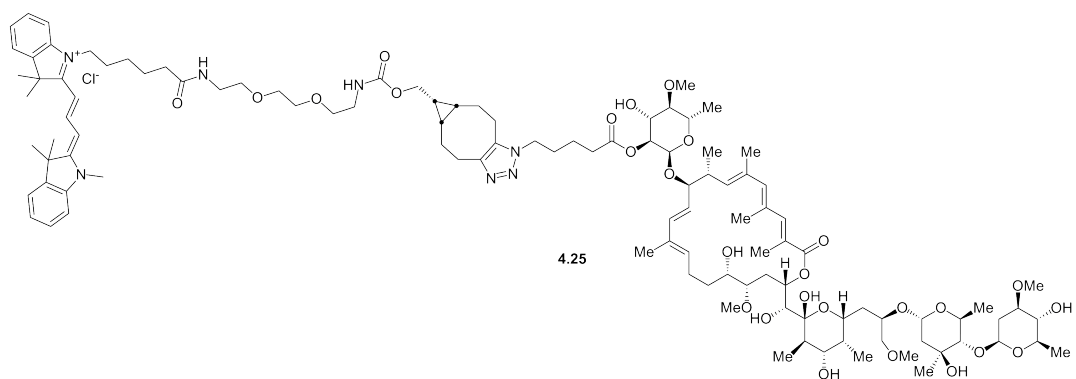


**Spectra IV-9:** The 600 MHz  $^1\text{H}$  and 150 MHz  $^{13}\text{C}$  NMR spectra of **4.24** in  $\text{CD}_3\text{OD}$ .

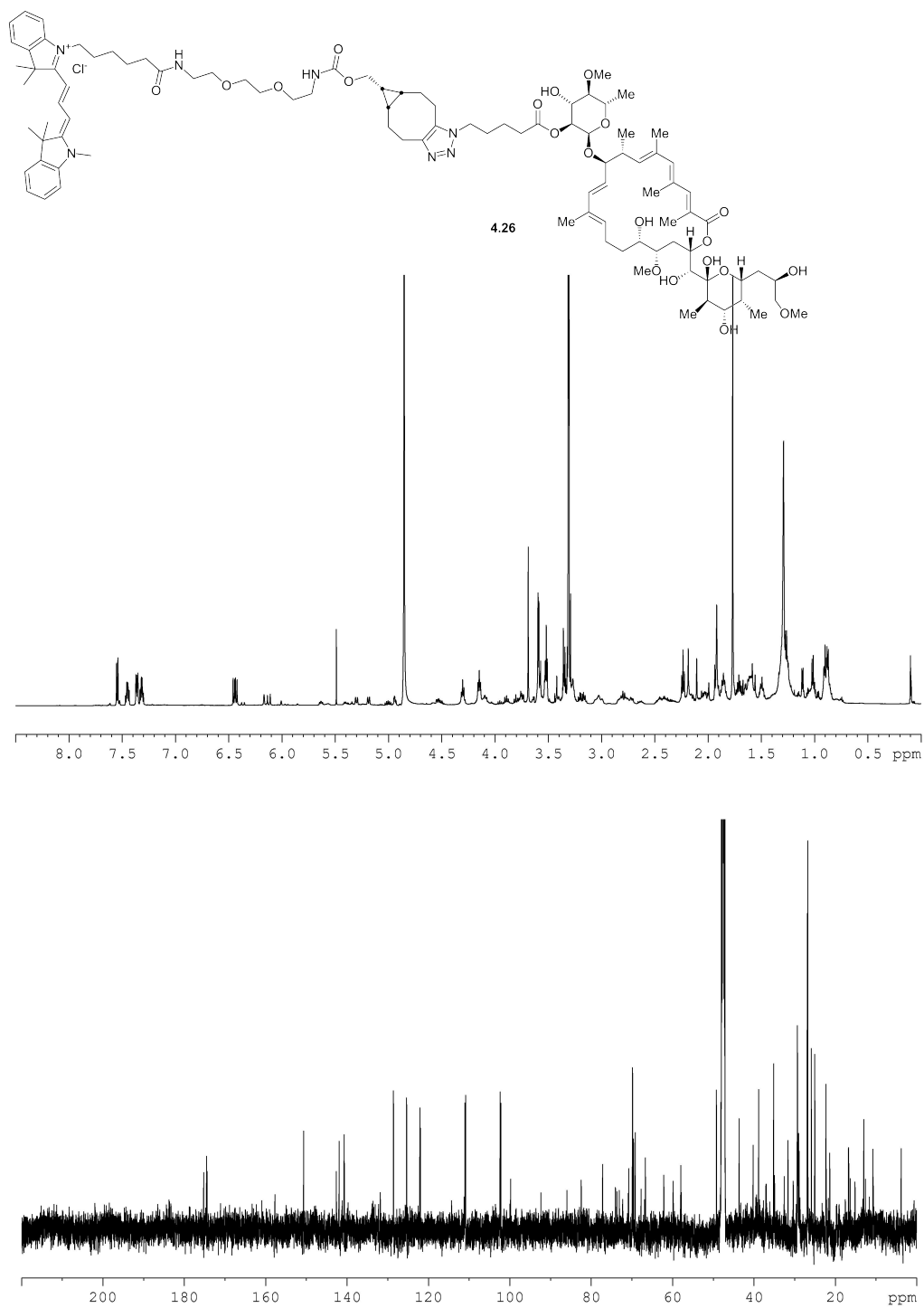




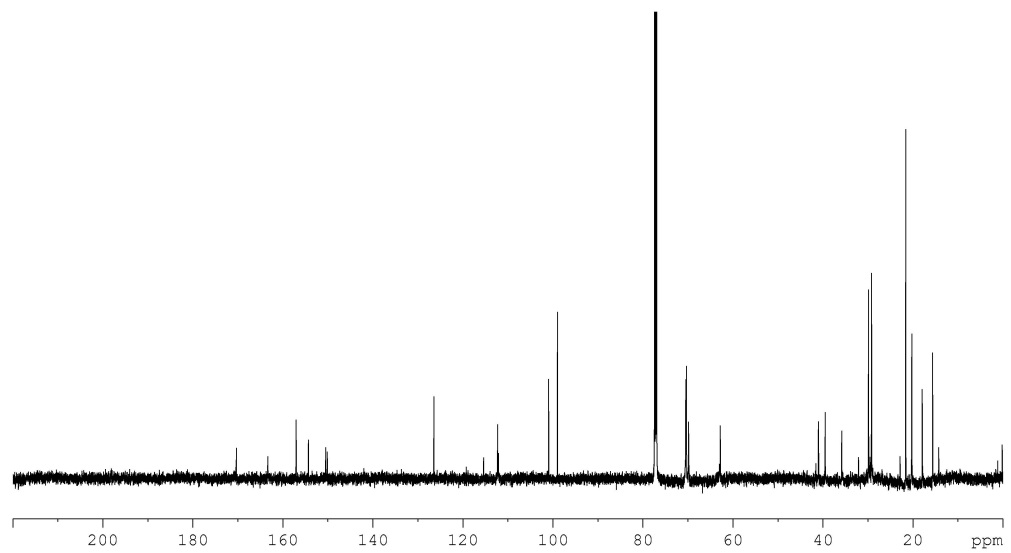
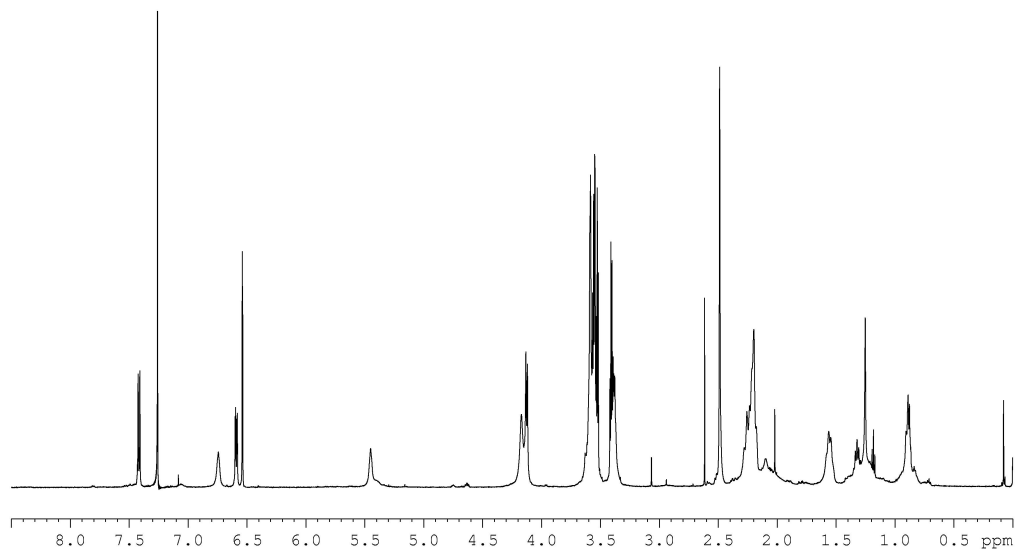
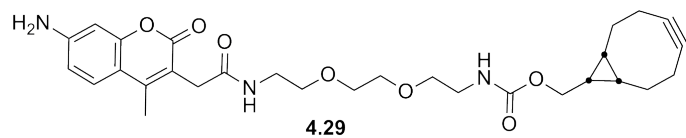
**Spectra IV-10:** The 600 MHz COSY NMR spectrum of **4.24** in CD<sub>3</sub>OD.



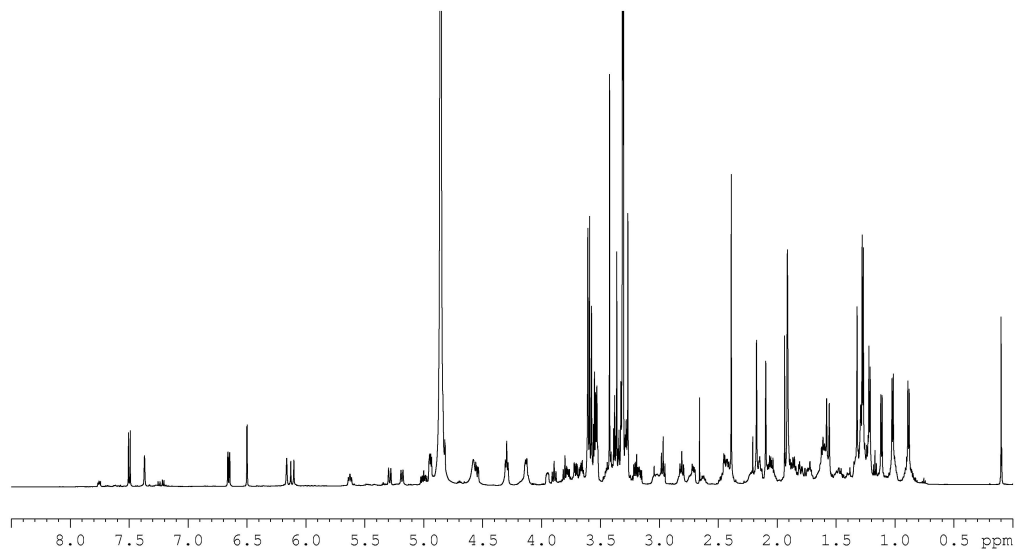
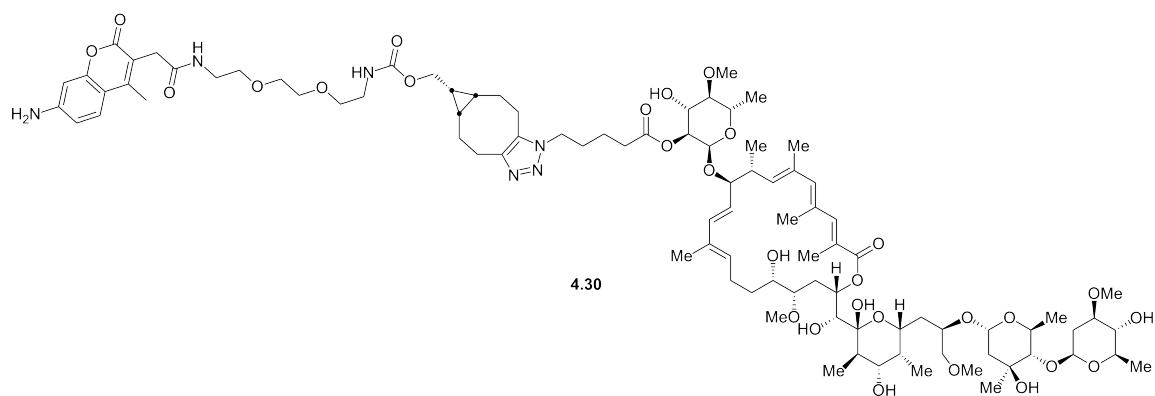
**Spectra IV-11:** The 600 MHz  $^1\text{H}$  NMR spectrum of **4.25** in  $\text{CD}_3\text{OD}$ .



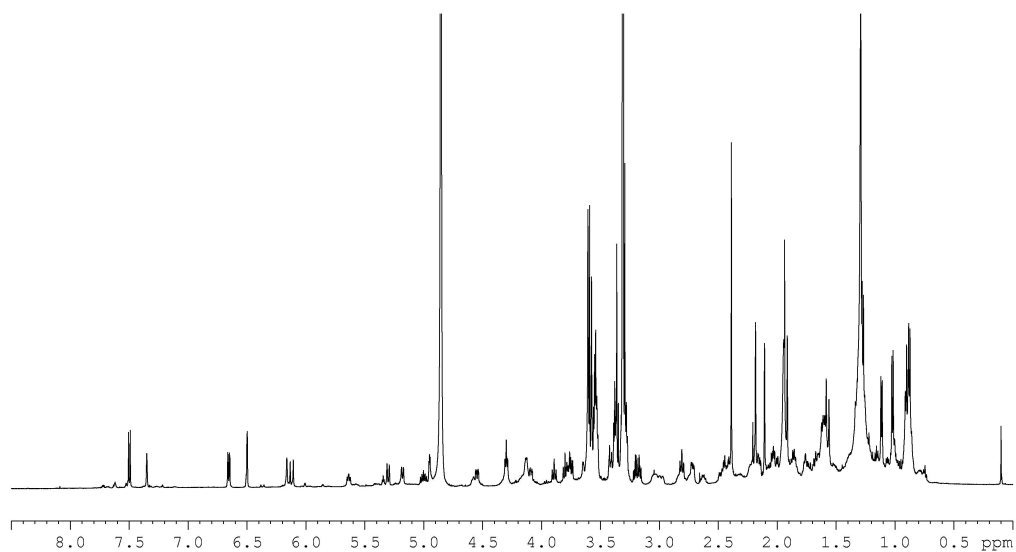
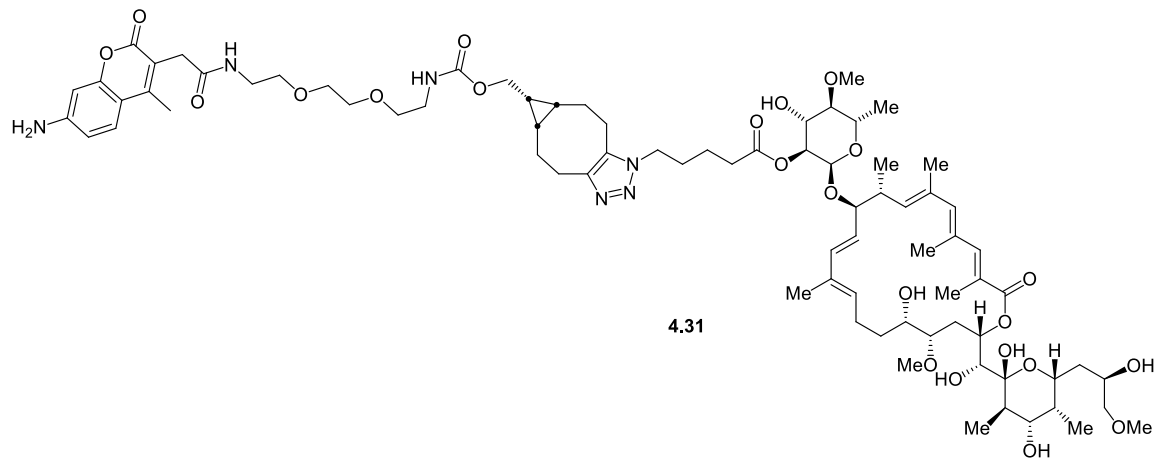
**Spectra IV-12:** The 600 MHz <sup>1</sup>H and 150 MHz <sup>13</sup>C NMR spectra of **4.26** in CD<sub>3</sub>OD.



**Spectra IV-13:** The 600 MHz  $^1\text{H}$  and 150 MHz  $^{13}\text{C}$  NMR spectra of **4.29** in  $\text{CDCl}_3$ .



**Spectra IV-14:** The 600 MHz  $^1\text{H}$  NMR spectrum of **4.30** in  $\text{CD}_3\text{OD}$ .



**Spectra IV-15:** The 600 MHz  $^1\text{H}$  NMR spectrum of **4.31** in  $\text{CD}_3\text{OD}$ .

## CHAPTER V

### Conclusions and Future Directions for Apoptolidin Biological Target Studies

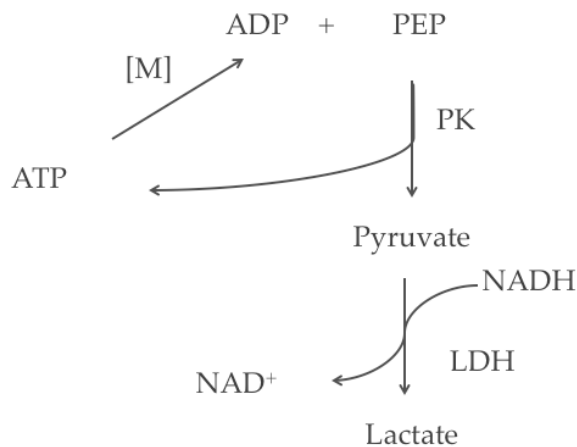
#### **Ongoing Investigations of the Biological Target of Apoptolidin**

The cancer cell line selective cytotoxicity of apoptolidin was attributed to inhibition of the  $F_1F_0$ ATPase in cancer cell lines that rely heavily on mitochondrial respiration for ATP synthesis, but no rationale exists to describe selectivity for cancer cells over “normal” cells that also primarily utilize oxidative phosphorylation for ATP production. The nearly two orders of magnitude difference between the phenotypic  $EC_{50}$  for cytotoxicity (~13 nM) and the concentration required for inhibition of this enzyme in solution (~1  $\mu$ M) further casts doubt on the identification of  $F_1F_0$ ATPase as the significant biological target of apoptolidin. Given the diverse mechanisms by which apoptotic and necrotic cell death can be initiated, it is possible that a different target is responsible for the observed cytotoxicity. In order to fully understand the activity of this natural product, we are currently working to measure the inhibition of the  $F_1F_0$ ATPase and identify novel targets of apoptolidin.

#### *Measuring Inhibition of $F_1F_0$ ATPase*

In order to complete the biological activity characterization of newly isolated apoptolidin congeners from mutasynthesis and apoptolidin analogues prepared through chemical synthesis, we are currently working on the measurement of  $F_1F_0$ ATPase.

ATPase inhibition is easily measured through a pyruvate kinase (PK) coupled assay (Scheme V-1).<sup>1</sup>



**Scheme V-1:** The pyruvate kinase coupled ATPase assay

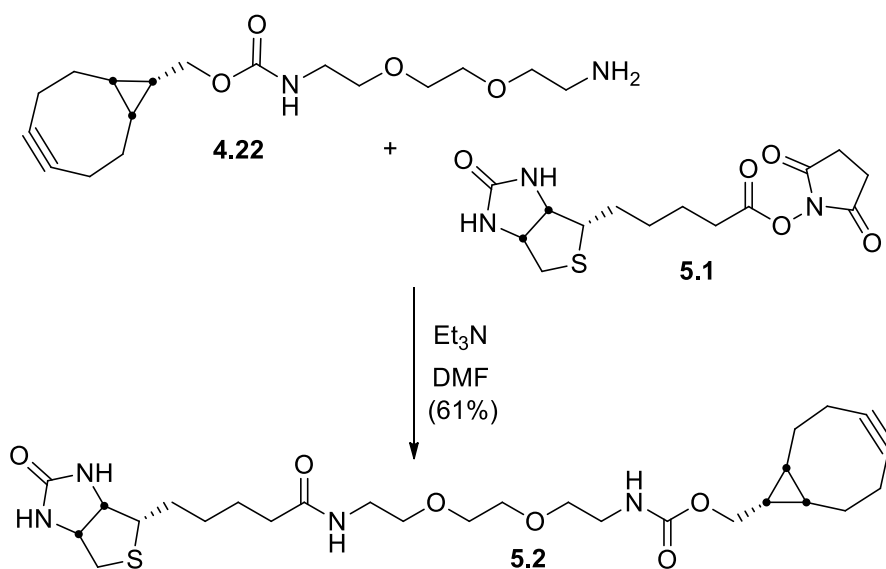
Previous measurements of  $F_1F_0$ ATPase inhibition by apoptolidin have used yeast mitochondrial preparations or solubilized  $F_1F_0$ ATPase derived from yeast. Structural differences between yeast and mammalian  $F_1F_0$ ATPase have been cited as a possible explanation for the large difference between the concentrations required for cytotoxicity and that required for enzyme inhibition.<sup>2</sup> To investigate this, we have attempted to isolate mitochondria from H292 cells using a method designed to isolate mitochondria from eukaryotic cells. Unfortunately, mitochondria isolated using this method were inactive in the ATPase assay. Currently, we are attempting to isolate active mitochondrial preparations from yeast to minimally allow for the characterization of apoptolidin derivatives in the same assay as used by the Stanford group. Future work in understanding the significance of  $F_1F_0$ ATPase inhibition in apoptolidin cytotoxicity



should involve the isolation of active mitochondrial preparations or sub-mitochondrial particles from mammalian cells for the use in ATPase assays.

### *Identifying Novel Targets of Apoptolidin*

The ultimate goal of our investigations into the biological activity of apoptolidin is the identification of a novel biological target that can fully explain the potent and selective nature of the observed cytotoxicity of this compound. To that end, we have prepared affinity purification probes that allow access to multiple strategies for target identification.



**Scheme V-2:** Preparation of biotinyl bicyclononyne conjugate\

To prepare affinity probes of apoptolidin, we utilized the strategy developed for the preparation of fluorescent conjugates. Treatment of the N-hydroxysuccinimide ester of D-biotin **5.1** with bicyclononyne amine **4.22** affords the bicyclononyne biotin

conjugate **5.2** in modest yield. Furthermore, we have been able to successfully couple this compound to azido apoptolidins to provide biotinyl apoptolidin A **5.3** (Scheme V-3). Testing of this compound in our H292 cell viability (Figure V-1) showed an approximate 10 fold loss in activity compared with apoptolidin A **2.1** or azido apoptolidin A **4.1**.

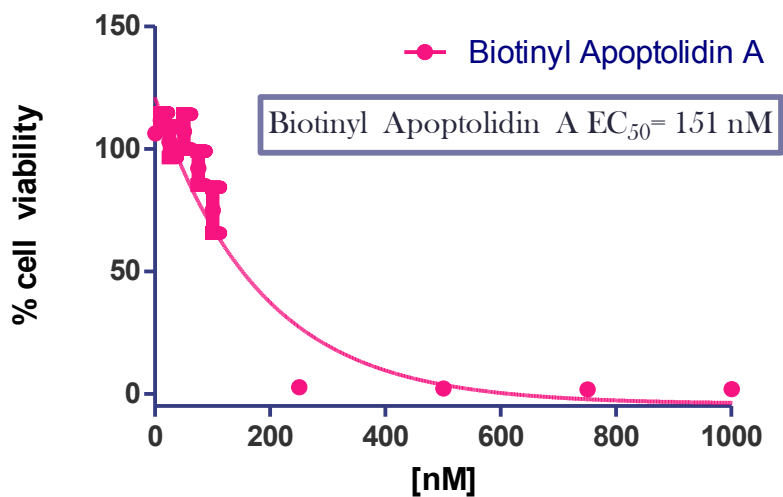
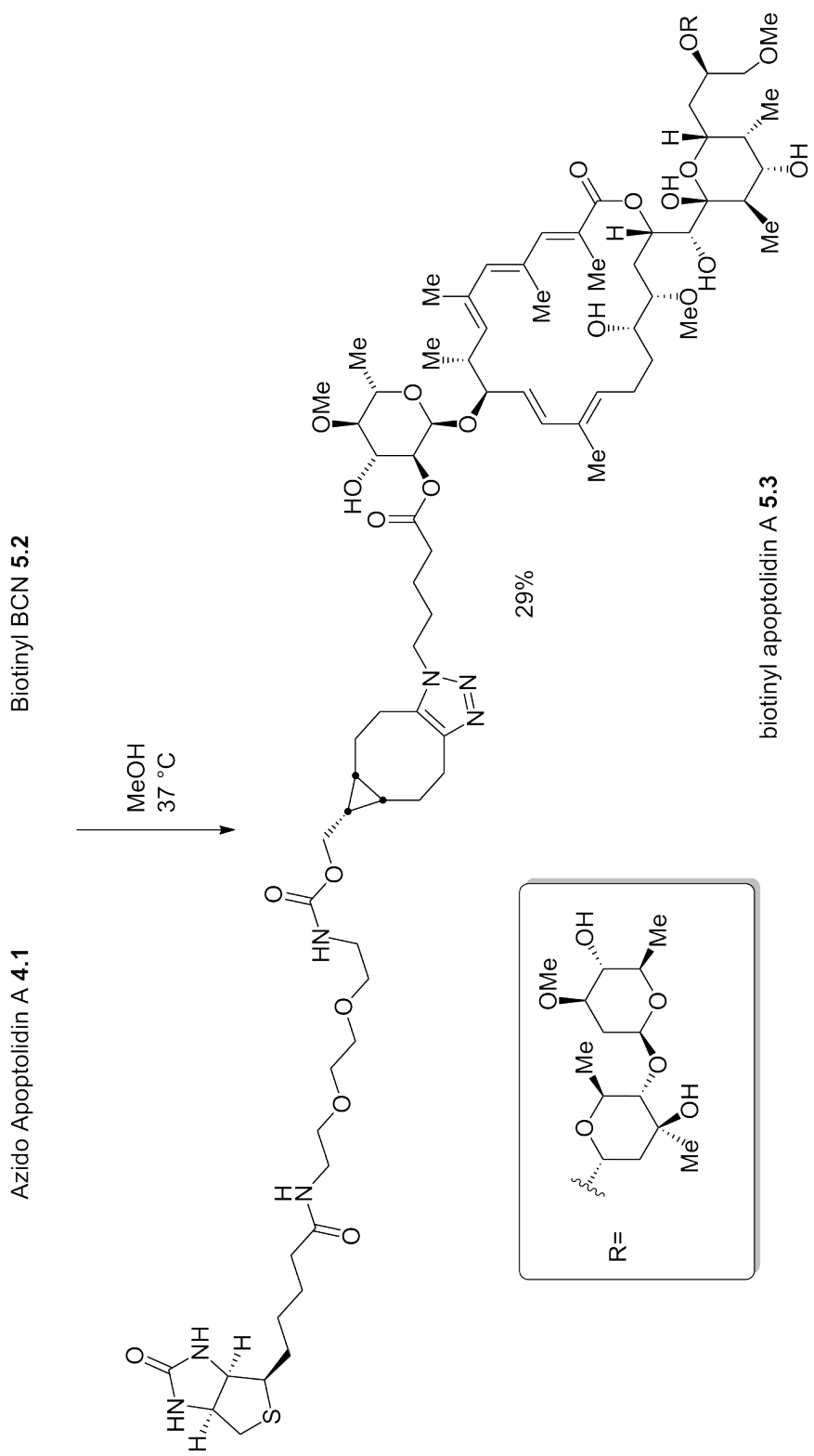


Figure V-1: Biotinyl apoptolidin A H292 cell viability assay



**Scheme V-3: Preparation of biotinyl apoptolidin A 5.3**

With these compounds in hand, multiple strategies can be investigated to identify biological targets of apoptolidin.<sup>3</sup> Whole cells or cell lysates could be treated with **5.3** followed by affinity purification using streptavidin coated beads. Due to the reduced potency of **5.3** compared to apoptolidin A **2.1**, a competitive target binding strategy could also be implemented in quantitative proteomics experiments to aid in the identification of *bona fide* biological targets. Alternatively, biotin BCN conjugate **5.2** could be used with azido apoptolidin **4.1** by either *in vivo* “click” reactions or used to extract protein targets from cell lysates by pre-conjugation onto streptavidin coated beads. Validation of candidate biological targets of apoptolidin identified in such studies through biochemical or genetic strategies will either confirm inhibition of the F<sub>1</sub>F<sub>0</sub>ATPase as the mechanism of action or provide an alternative mechanism.

### **Overview of Apoptolidin Project Results**

Utilizing a high yielding production fermentation protocol of *Nocardiosis* sp. FU40, apoptolidin A based chemical probes have been designed and synthesized for use in experiments to gain insight on the mechanism of the potent, cell-line selective cytotoxicity of this natural product. Furthermore, utilizing a productive mutant producer resulting from selective genetic disruption,<sup>4</sup> analogous probes of apoptolidin H have been prepared to shed light on the biological role of the C27 disaccharide moiety of apoptolidin A in cytotoxicity assays. Conditions required to observe the reported potent cytotoxicity in H292 human lung carcinoma cells were determined that indicate a cell density dependent shift in glucose metabolism resulting in sensitization to apoptolidin at confluence. Experiments aimed at determining the mechanism of cytotoxicity induced by

apoptolidin in H292 cells were unable to confirm an apoptotic mechanism as reported in non-human models.

The prepared apoptolidin derivatives were tested in the H292 cell viability assay and determined to each retain similar biological activity to apoptolidin A or H despite significant and variable structural modifications. While initial experiments utilizing fluorescent apoptolidin probes to determine sub-cellular localization were inconclusive due to unanticipated results in a control experiment, multiple approaches to overcome this complication are currently being pursued. Current results indicate but do not confirm that the C27 disaccharide of apoptolidin A is important for target binding and not for cellular transport as previously hypothesized. Ongoing microscopy studies will either confirm or refute this initial interpretation. Finally, future target identification studies have been made possible by the synthesis of several tools to be used in protein affinity purification experiments. Experiments utilizing tools developed in these studies and building upon results from biological assays described herein may allow for the understanding of the mechanism of action of this highly selective cytotoxin and the advantageous application of this knowledge in new therapeutic strategies.

### **Experimental Methods**

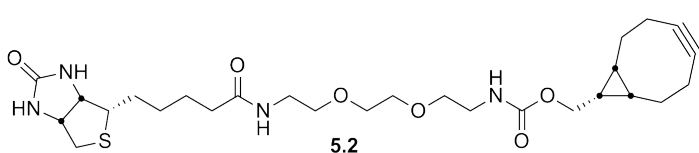
**General procedure:** All non-aqueous reactions were performed in flame-dried or oven dried round-bottomed flasks under an atmosphere of argon. Where necessary (so noted) solutions were deoxygenated by alternate freeze (liquid nitrogen)/evacuation/argon-flush/thaw cycles (FPT, three iterations) or degassed by purging with argon for several

minutes. Stainless steel syringes or cannulae were used to transfer air- and moisture-sensitive liquids. Reaction temperatures were controlled using a thermocouple thermometer and analog hotplate stirrer. Reactions were conducted at room temperature (rt, approximately 23 °C) unless otherwise noted. Flash column chromatography was conducted as described Still et. al. using silica gel 230-400 mesh.<sup>5</sup> Where necessary, silica gel was neutralized by treatment of the silica gel prior to chromatography with the eluent containing 1% triethylamine. Analytical thin-layer chromatography (TLC) was performed on E. Merck silica gel 60 F254 plates and visualized using UV, ceric ammonium molybdate, potassium permanganate, and anisaldehyde stains. Yields were reported as isolated, spectroscopically pure compounds.

**Materials.** Solvents were obtained from either a MBraun MB-SPS solvent system or freshly distilled (tetrahydrofuran was distilled from sodium-benzophenone; toluene was distilled from calcium hydride and used immediately; dimethyl sulfoxide was distilled from calcium hydride and stored over 4Å molecular sieves). Commercial reagents were used as received with the following exceptions.

**Instrumentation.** Semi-preparative reverse phase HPLC was conducted on a Waters HPLC system using a Phenomenex Luna (5 µm C18(2) 100A Axia 250 x 10.00 mm) column or preparative reverse phase HPLC (Gilson) using a Phenomenex Luna column (100 Å, 50 x 21.20 mm, 5 µm C18) with UV/Vis detection. Infrared spectra were obtained as thin films on NaCl plates using a Thermo Electron IR100 series instrument and are reported in terms of frequency of absorption (cm<sup>-1</sup>). <sup>1</sup>H NMR spectra were recorded on Bruker 300, 400, 500, or 600 MHz spectrometers and are reported relative to deuterated solvent signals. Data for <sup>1</sup>H NMR spectra are reported as follows: chemical

shift ( $\delta$  ppm), multiplicity (s = singlet, d = doublet, t = triplet, q = quartet, p = pentet, m = multiplet, br = broad, app = apparent), coupling constants (Hz), and integration.  $^{13}\text{C}$  NMR spectra were recorded on Bruker 75, 100, 125, or 150 MHz spectrometers and are reported relative to deuterated solvent signals. LC/MS was conducted and recorded on an Agilent Technologies 6130 Quadrupole instrument. High-resolution mass spectra were obtained from the Vanderbilt University Center for Neuroscience Drug Discovery (VCNDD) on a Micromass Q-ToF API-US mass spectrometer.

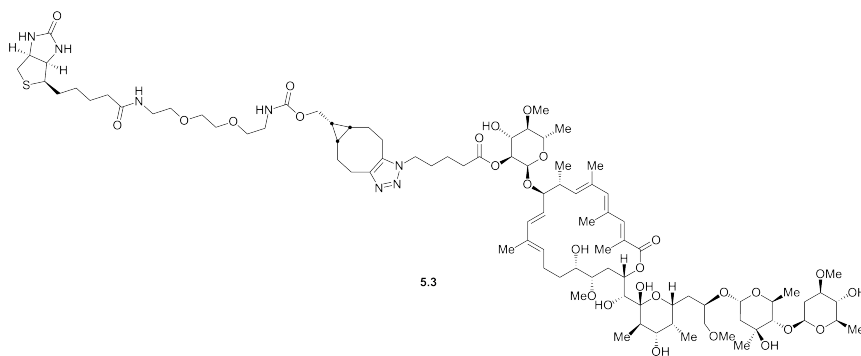


**Bicyclononyne**

**Biotin**

**Conjugate 5.2** To a solution of amine **4.22** (34.0 mg, 0.105

mmol) in DMF (1.0 mL) was added Biotin NHS **5.1** (71 mg, 0.210 mmol). After 16 hours, the DMF was removed on high vacuum. Flash column chromatography (30 % 80:18:2<sup>6</sup> in DMC) yielded 35.0 mg (61%) of bicyclononyne biotin conjugate **5.2** as a pale yellow oil.  $^1\text{H}$  NMR (400 MHz,  $\text{CDCl}_3$ )  $\delta$  6.66 (s (br), 2H), 5.77 (s(br), 1H), 5.40 (s (br), 1H), 4.48 (t,  $J = 6.0$  Hz, 1H), 4.29 (t,  $J = 5.9$  Hz, 1H), 4.13 (d,  $J = 7.8$  Hz, 2H) 3.59 (s (br), 4H), 3.55 (m, 4H), 3.43 (m, 3H), 3.35 (m, 2H), 3.12 (dd,  $J = 6.9, 11.6$  Hz, 1H), 2.88 (dd,  $J = 4.7, 12.7$  Hz, 1H), 2.72 (d,  $J = 12.8$  Hz, 1H), 2.11-2.34 (m, 6H), 1.48-1.76 (m, 6H), 1.28-1.48 (m, 4H), 1.23 (s, 1H), 0.92 (m, 2H).  $^{13}\text{C}$  NMR (100 MHz,  $\text{CDCl}_3$ )  $\delta$  173.3, 164.1, 156.8, 98.7, 70.0, 62.7, 61.7, 60.1, 55.6, 40.7, 40.1, 39.0, 35.9, 33.2, 29.6, 29.0, 28.2, 28.0, 25.5, 22.8, 21.3, 20.0, 17.7; HRMS (ESI-TOF MS)  $m/z$  551.2903 ( $\text{M}+\text{H}$ )<sup>+</sup> calculated for  $\text{C}_{27}\text{H}_{43}\text{N}_4\text{O}_6$ , measured 551.2900.



## Biotin Apoptolidin

### A Conjugate **5.3**

To a solution of Biotin BCN conjugate **5.2** (2.6 mg, 0.0033 mmol)

in methanol (0.5 mL) was added azido apoptolidin A **4.1** (2.05 mg, 0.0016 mmol) as a solution in 0.5 mL methanol. The resulting solution was stirred at 37 °C for 14 hours, removed from the bath and concentrated. The resulting residue was dissolved in methanol (0.5 mL) and purified on semipreparative reverse phase HPLC (30 minute gradient from 35% strong to 100% strong buffer in weak buffer where strong is 95% MeCN in H<sub>2</sub>O + 10 mM NH<sub>4</sub>OAc and weak buffer is 5% MeCN in H<sub>2</sub>O + 10 mM NH<sub>4</sub>OAc). The conical reaction flask was rinsed with an additional 0.5 mL of methanol and this solution was purified as well. Fractions containing the desired product (r.t. 10.5 min) were combined and concentrated to remove acetonitrile only (T<31°C). The resulting aqueous solution was frozen at -80°C. Water was removed by lyophilization to yield 2.63 mg (29%) of biotin apoptolidin A conjugate **5.3** as a white solid. (600 MHz, CD<sub>3</sub>OD) δ 3.73 (s, 1H), 6.18 (s, 1H), 6.13 (d, *J* = 15.8 Hz, 1H), 5.64 (dd, *J* = 7.9, 7.9 Hz, 1H) 5.29 (d, *J* = 11.3 Hz, 1H), 5.20 (d, *J* = 10.1 Hz, 1H), 5.00 (m, 1H), 4.94 (m, 3H), 4.83 (dd, *J* = 1.8, 9.9 Hz, 1H), 4.54 (m, 2H), 4.49 (dd, *J* = 4.9, 7.8 Hz, 1H), 4.31 (m, 5H), 4.17 (m, 3H), 3.95 (m, 1H), 3.90 (m, 3H), 3.81 (dd, *J* = 8.8, 8.8 Hz, 1H), 3.78 (dd, *J* = 6.3, 9.4 Hz, 1H), 3.71 (dd, *J* = 4.6, 11.0 Hz, 1H), 3.67 (dd, *J* = 6.3, 9.7 Hz, 1H), 3.65-3.86 (m, 3H), 3.62 (s(br), 4H), 3.59 (s, 3H), 3.58 (m, 1H), 3.52-3.57 (m, 5H), 3.42 (s, 3H), 3.41 (m, 3H), 3.37 (m, 3H),

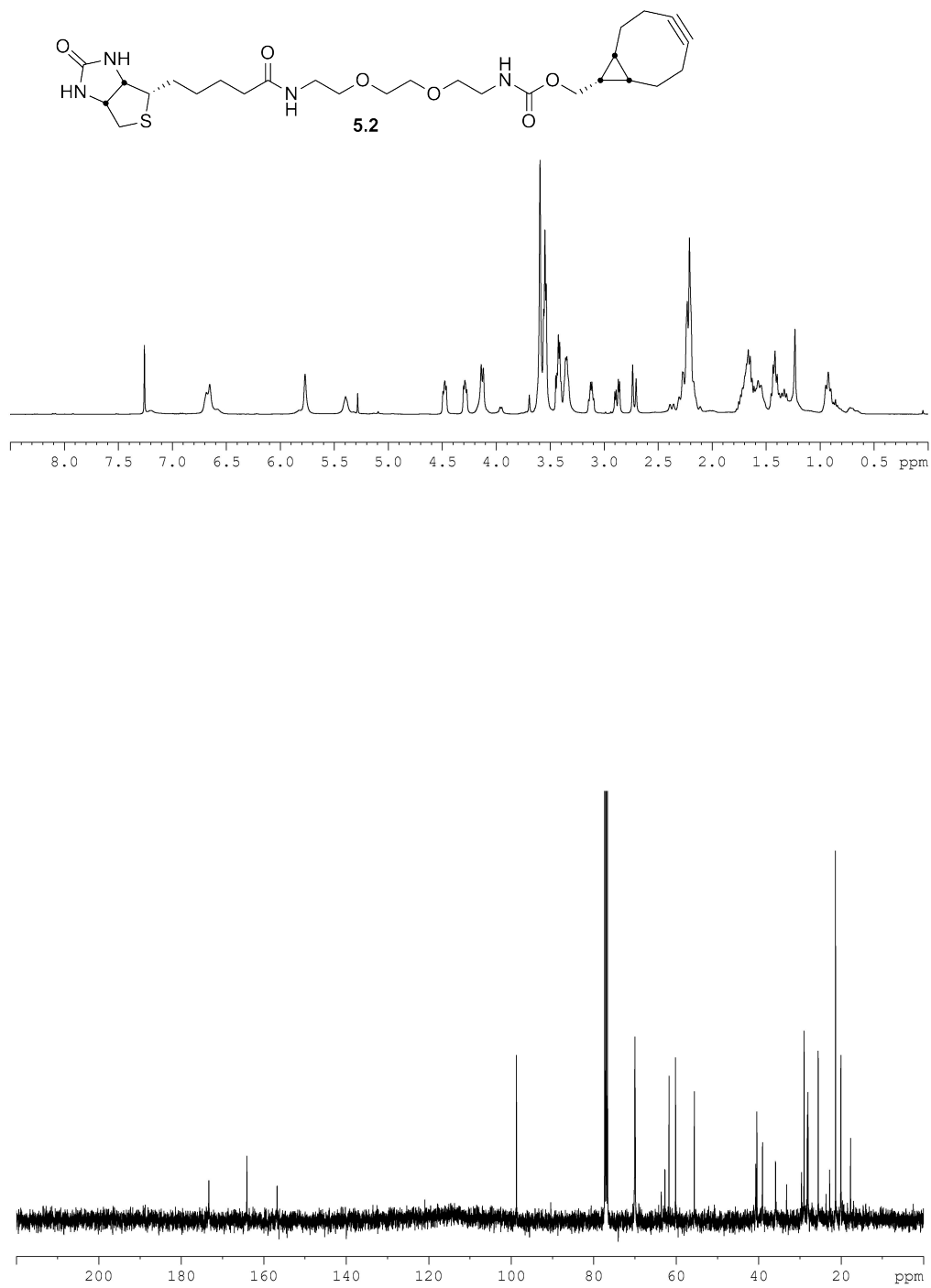


3.36 (s, 3H), 3.32 (m, 1H), 3.27 (s, 3H), 3.21 (dd,  $J = 6.0, 9.2$  Hz, 1H), 3.17 (m, 2H), 3.06 (m, 1H), 2.97 (dd,  $J = 9.0, 9.0$  Hz, 1H), 2.92 (dd,  $J = 5.0, 12.8$  Hz, 1H), 2.81 (dd,  $J = 9.3, 9.3$  Hz, 1H), 2.71 (m, 2H), 2.64 (m, 1H), 2.43 (m, 4H), 2.21 (m, 6H), 2.18 (s, 3H), 2.14 (m, 1H), 2.10 (s, 3H), 1.97-2.08 (m, 4H), 1.92 (m, 1H), 1.89 (s, 3H), 1.50-1.82 (m, 18H), 1.32 (s, 3H), 1.28-1.48 (m, 9 H), 1.25-1.28 (m, 13H), 1.22 (d,  $J = 6.3$  Hz, 3H), 1.12 (d,  $J = 6.5$  Hz, 3H), 1.02 (d,  $J = 6.7$  Hz, 3H), 0.90 (m, 2H), 0.89 (d,  $J = 6.9$  Hz, 3H); HRMS (ESI-TOF MS)  $m/z$  1804.9937 (M+H)<sup>+</sup> calculated for C<sub>90</sub>H<sub>146</sub>N<sub>7</sub>O<sub>28</sub>S, measured 1804.9946.

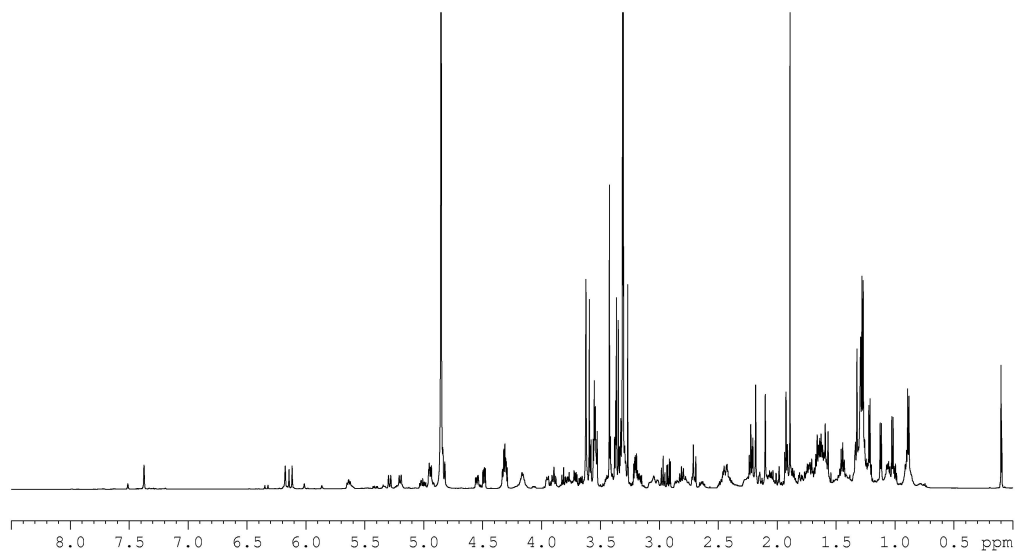
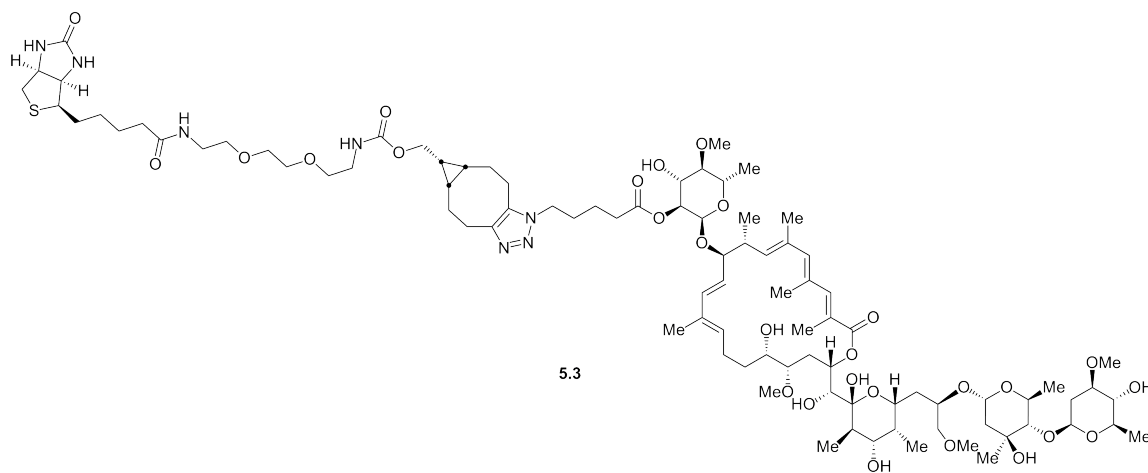
## References

1. Jenkins, W. T. The pyruvate kinase-coupled assay for ATPases: A critical analysis. *Anal. Biochem.* **1991**, *194*, 136–139.
2. Salomon, a R.; Voehringer, D. W.; Herzenberg, L. a; Khosla, C. Apoptolidin, a selective cytotoxic agent, is an inhibitor of F<sub>0</sub>F<sub>1</sub>-ATPase. *Chem. Biol.* **2001**, *8*, 71–80.
3. Cheng, K.-W.; Wong, C.-C.; Wang, M.; He, Q.-Y.; Chen, F. Identification and characterization of molecular targets of natural products by mass spectrometry. *Mass Spec. Rev.* **2010**, *29*, 126–55.
4. Du, Y.; Derewacz, D. K.; Deguire, S. M.; Teske, J.; Ravel, J.; Sulikowski, G. a; Bachmann, B. O. Biosynthesis of the Apoptolidins in *Nocardopsis* sp. FU 40. *Tetrahedron* **2011**, *67*, 6568–6575.
5. Still, W. C.; Kahn, M.; Mitra, A. Rapid chromatographic technique for preparative separations with moderate resolution. *J. Org. Chem.* **1978**, *43*, 2923–2925.
6. 80:18:2 refers to a premade mixture of 80% DCM, 18% MeOH, and 2% NH<sub>4</sub>OH.

## Spectral Data Relevant to Chapter 5



**Spectra V-1:** The 400 MHz  $^1\text{H}$  and 100 MHz  $^{13}\text{C}$  NMR spectra of **5.2** in  $\text{CDCl}_3$ .



**Spectra V-2:** The 600 MHz  $^1\text{H}$  NMR spectrum of **5.3** in  $\text{CD}_3\text{OD}$